Linking the structure of alpha-synuclein oligmers to function in Parkinson's disease.

ILLES-TOTH, Timea E.

REFERENCE

Linking the structure of alpha-synuclein oligomers to function in Parkinson's disease

Timea Eva Illes-Toth

A thesis submitted in partial fulfilment of the requirements of Sheffield Hallam University for the Degree of Doctor of Philosophy

Faculty of Health and Wellbeing

Nov 2013

Acknowledgements

I am grateful to the Biomedical Research Centre at Sheffield Hallam University for the funding of my project and for enabling me to attend several conferences and short-courses.

A number of people have helped me in many different ways during my project, therefore I would like to acknowledge those who contributed to it:

Dr David Smith my Director of Studies who has given me an opportunity to pursue a PhD. Many thanks for introducing me to the field of alpha-synuclein research and native mass spectrometry and for giving me continued guidance throughout the entire course of this project. I am thankful for the valuable modelling data that has been added to this thesis.

I would like to thank Dr Caroline Dalton my Co-supervisor for her advice on the cell culture experiments and other insightful comments on the development and write-up of this work.

I would like to thank members of the Neuroimmunology, Biochemistry and Bioanalytical group for their practical help and discussions during our meetings. Special thanks to Rachel, Leesa, Marina, Jen, Sara, Melanie, Philippa, Nat, Claire, Boom, Callie, Hannan, Mafalda, Mowfag, Yasin, Patrick, Rich and David Moore for sharing the joys and and less memorable parts of the PhD.

A number of friends from Sheffield, London and Hungary have been essential in keeping me happy and providing company for me whilst initiating conversations of non-scientific nature. I would like to thank my former science and PE teachers and Susan Bowie for inspiring me as a young girl, Michelle for giving me a bandana at the start reminding me of our frantic times of revision, all of my past colleagues, in particular Neghat and Viki who have shown so much care

even after moving away. I am thankful to Albert, Hiroko and Funso and all the guys from Crookes who have seen me through in the last three years and shared so much with me. I thank Pam and Douglas for all the walks exploring the Peak District and for the invites to Sunday lunches.

I would like to express my gratitude to my family, especially to my mum who is such a role model for me, my brother, Aniko and Gabi who have always been supportive of me.

Without all of these people listed here and many more who remained unmentioned I would have not been able to complete my PhD.

Abstract

Misfolding and aggregation of alpha-synuclein (α-syn) are associated with a range of neurological disorders, including Parkinson's disease (PD). Fibrillar, insoluble aggregates of α-syn, known as Lewy bodies (LBs) are deposited in the *substantia nigra* and are a pathological hallmark of PD. α-syn is a natively unstructured protein, co-populating extended and more compact conformational forms under equilibrium. The fine balance of this equilibrium can be shifted due to changes in its environment such as alterations in metal content, ionic strength, free dopamine or others, promoting the assembly of α-syn into toxic conformations. Small, soluble oligomers preceding LB formation are thought to be causative. *In vitro*, different α-syn oligomers have been produced with alternate biochemical properties. Here the primary objective was to uncover the link between conformation and toxic gain of function by the use of functional assays in combination with ESI-IMS-MS. Epitope mapping procedures indicated that different α-syn oligomers have unique epitope features. Dye binding assays such as ThT and ANS fluorescence inferred that the various oligomer types differ in their amyloidogenicity and hydrophobicity. Furthermore, intracellular aggregation assays, MTT cell proliferation and Ca(II) influx analysis in SH-SY5Y neuroblastoma cells showed that cellular effects correlated with structural features. ESI-IMS-MS spectra of the different oligomers have been acquired and allowed the conformations of the oligomer subsets to be determined. The oligomers assembled up to a hexameric form with a closed ring-like conformation. These results demonstrated that unique structural features are required for toxicity and that a subset of oligomers with characteristic structures may be pivotal in PD.

Abbreviations

A: correction factor for electric field parameters

AA: ammonium acetate

Aβ: Alzheimer β

AD: Alzheimer's disease

AD: autosomal dominant

AFM: atomic force microscopy

alpha-synuclein: α-syn

ANS: 1-Anilinonaphtalane-8-sulphonic acid

APIMS: ambient pressure ion mobility

AR: autosomal recessive

Asp: aspartic acid

ATD: arrival time distribution

B: correction factor for non-linear effects of triwave

BCA: bicinchronic acid

CaN: calcineurin

CD: circular dichroism

CID: collision induced dissociation

CMF-DA: 2,7-dichloromethylfluorescein diacetate

CREB: cAMP response element binding

CSD: charge state distribution

CSF: cerebrospinal fluid

D: dimer

DA: dopamine

DAPI: 4'6-diamidine-2'-phenylindole dihydrochloride

DAT: dopamine transporter

DC: direct current

DLB: dementia with Lewy bodies

DMEM: Dulbecco's modified Eagle medium

DMSO: dimethyl sulfoxide

DOPAL: 3,4-dihydroxyphenylacetaldehyde

ε_0: empirical permittivity of vacuum

e: charge of electron

EDTA: ethylenediaminetetra-acetic acid

EGCG: catechin epigallocatechin gallate

EHSS: exact hard sphere scattering

EM: electron microscopy

EPR: electron paramagnetic resonance

ER: endoplasmic reticulum

ESI-ECD-FT-ICR: Electrospray Ionisation- Electron Capture Dissociation- Fourier Transform Ion Cyclotron Resonance

ESI-ECD-MS/MS: Electrospray Ionisation- Electron Capture Dissociation- Mass Spectometry/ Mass Spectrometry

ESI-IMS-MS: electrospray ionisation ion mobility spectrometry- mass spectrometry

ETD: electron transfer dissociation

FRET: fluorescence resonance energy transfer

FTIR: Fourier transformed infrared spectra typing

GAGs: glycosaminoglycans

Gly: glycine

Gln: glutamine

γ: surface tension

H: hexamer

HFIP: hexafuoro- 2- propanol

His: histidine

HPLC: high performance liquid chromatography

IAPP: islet amyloid precursor protein

IC: intracellular

IDP: intrinsically disordered proteins

IPD: idiopathic Parkinson's disease

IPTG: isopropyl β-D-1-thiogalactopyranoside

K: ion mobility constant

K_0: reduced mobility

K_b: Boltzmann constant

L: length

LB: Lewy body

LB: Luria Broth

Leu: leucine

LS: long, straight

Lys: lysine

m: mass of buffer gas

M: mass of an ion

M: monomer

MALDI-MS: matrix assisted laser desorption ionisation- mass spectrometry

MAO: monomamine oxidase

Met: Methionine

MHC: major histocompatibility complex

MPP: 1-methyl-4-phenylpyridinium

MSA: multiple system atrophy

mtDH: mitochondrial dehydrogenase

MTT: 3-(4,5-dimethylthiaziazol-2-yl)-2,5-diphenyl-2H-tetrazolium bromide

MW: molecular weight

m/z: mass-to-charge ratio

N: number density of buffer gas

NAC: non-Aβ component of Alzheimer's amyloid

nESI-IMS-MS: nano electrospray ionisation ion mobility spectrometry- mass spectrometry

NMR: nuclear magnetic resonance

p: buffer gas pressure

P: pentamer

PA: projection approximation

PA: phosphatidic acid

PC: phosphatidylcholine

PD: Parkinson's disease

PDB: protein data bank

PFA: paraformaldehyde

PG: phosphatidylglycerol

PMSF: phenylmethylsulphonyl fluoride

POPC: 1-palmitoyl-2-oleoyl-sn-glycero-3-phosphocholine

PS: phosphatidylserine

PSP: progressive supranuclear palsy

Q: tetramer

QTOF: quadrupole time-of flight

R: radius of droplet

RF: radio frequency

R_g: radius of gyration

ROS: reactive oxygen species

SAA: serum amyloid A

SAXS: small angle X-ray scattering

SD: standard deviation

SEC: size exclusion chromatography

SELDI: Surface enhanced laser desorption ionisation

SNPc: substantia nigra pars compacta

SP: sodium phosphate

STEM: scanning transmission electron microscopy

SVAU: sedimentation velocity analytical ultracentrifugation

T: temperature

T: trimer

TAE: Tris acetate EDTA

tD: drift time

TFE: trifluoroethanol

ThT: Thioflavin T

TM: trajectory method

TRAP: trp RNA binding complex

Trp: tryptophan

Tyr: tyrosine

UPLC: ultra performance liquid chromatography

UPS: ubiquitin proteasome system

v: velocity

v_D: drift velocity

WT: wild type

ze: absolute charge

z_R: calculated charge of protein

Ω: collisional cross section

Ω': reduced collisional cross section

Contents

List of Tables

Table of Figures

1 Chapter 1

Introduction

1.1 Amyloid disease states

1.1.1 Misfolding and toxic conformations

The propensity of proteins to fold properly and adopt appropriate tertiary structures is essential to their function and localisation. A group of proteins called intrinsically disordered proteins (IDPs) e.g. alpha-synuclein (a-syn) and p53 do not adopt well defined 3 D structures but are very dynamic and sample numerous conformational states to perform varied biological functions (Forman-Kay *et al.* 2013).

The failure of proteins to fold or to fold correctly can cause disease states hence misfolding and aggregation are of paramount importance *in vivo.* The consequences of misfolding are protein aggregation, fibril formation, loss of function or toxic gain of function. A significant proportion of the protein misfolding diseases can be accounted for by the appearance of filamentous, insoluble protein aggregates, called amyloid that can be deposited into a variety of organs and tissue types either locally or systematically as shown in Table **1.1.** below (Uversky 2008).

Amyloidogenic protein	Type of structure	Disease
Immunoglobulin light chain (kappa or lambda)	Folded	Primary amyloidosis (AL); Associated with plasma cell dyscrasia and multiple myeloma
Serum amyloid A	Folded	Secondary systematic amyloidosis; Associated with chronic infections and inflammatory diseases such as rheumatoid arthritis, familial Mediterrenean fever, osteomyelitis and granulomatous ileitis, inflammatory bowel disease
α-syn	Natively unfolded	Parkinson's disease (PD), Diffuse Lewy bodies disease (DLB), Lewy body variant of Alzheimer's disease (LBVAD), Dementia with Lewy bodies (DLB), Multiple system atrophy (MSA), Hallervoden-Spatz disease
Amyloid β and its fragments	Natively unfolded	Alzheimer disease (AD), Dutch hereditary cerebral hemorrhage with amyloidosis (HCHWA) also known as cardiovascular amyloidosis, Congophilic angiopathy
Tau protein	Natively unfolded	Alzheimer's disease (AD), Pick's disease, Progressive supranuclear palsly (PSP)
ABri& ADan	Natively unfolded	Familial British Dementia& Familial Danish Dementia
Prion protein and its fragments	N-terminal fragement (23-121) is natively unfolded, C-terminal domain (121-230) is predominantly α-helical	Creutzfeld-Jacob disease (CJD), Gertsmann-Straussler-Scheineker Syndrome (GSS), Fatal familial insomnia (FFI), Kuru, Bovine spongiform encelopathy (BSE) and scrapie
Huntingtin	Exon 1 is unfolded	Huntington disease
Ataxin-1	Unknown (natively unfolded)	Spinocerebellar ataxia (SCA), Neuronal intracellular inclusion disease (NIID)
Androgen receptor protein	Ligand binding (LBD) and DNA binding domains (DBD) are all α-helical, amino terminal domain (NTD) is natively unfolded	Spinal and bulbar muscular atrophy (SMBA)
DRPLA protein (atropin-1)	Unknown (probably natively unfolded)	Hereditary dentatorubral-pallidoluysian atrophy (DRPLA)
Nuclear poly(A) binding protein	Natively unfolded	Oculopharyngeal muscular dystrophy
Calcitonin	Natively unfolded	Medullary carcinoma of the thyroid (MCT)
Gelsolin	Amyloidogenic fragment 173-243 is natively unfolded	Finnish-Type Familal Amyloidosis
β2 microglobulin	β-sheet	Hemodialyis related amyloidosis

Table 1.1. *Some amyloid diseases and their associated proteins. Protein misfolding and aggregation are a common theme in amyloidogenic disorders of structurally distinct amyloid proteins* (Adapted from Uversky 2008).

In the case of neurodegenerative diseases, for example new variant Creutzfeld-Jacob disease, the prion protein (PrP) assembles and forms extracellular aggregates including amyloid fibrils (Prusiner 2012; Kraus *et at.* 2013). In Alzheimer's disease (AD) the characteristic senile plaques are composed of the amyloid beta-peptide (Ap) and neurofibrillary tangles containing Tau protein (Hardy *et at.* 1991; Allsop 2000; Selkoe 2011), whereas in Parkinson's disease (PD) the principal component of proteinaceous intracellular inclusions, termed Lewy bodies (LB), is a-syn (Jellinger 2011). These amyloid plaques are diagnostic hallmarks of the disease states and share a common cross-p structure. It is known that amyloid fibrils share common structural features despite each disease being characterised by the deposition of a unique protein or peptide (Westermark *et al.* 2005). Amyloid is described as "an *in vivo* deposited material, which can be distinguished from non-amyloid deposits by characteristic fibrillar electron microscopic appearance, typical X-ray diffraction pattern and histological staining reactions, particularly affinity for the dye Congo red with resulting birefringence" (Westermark *et al.* 2007). Amyloid fibrils of unrelated proteins and peptides share a common core structure in that they are unbranching macromolecular assemblies many pm in length, having a regular cross-p structure in which p-sheets are stacked parallel to the fibril axis *(Jahn et al.* 2010).

1.1.2 Synucleinopathies

In 1817, James Parkinson released an essay entitled "An essay of the shaking palsy", summarising his clinical observations of six individuals and providing impetus for the diagnosis and terminology of PD. Another milestone was the isolation of levodopa and its move to become a therapeutic agent for "dopamine

replacement" ~1960's, alleviating the symptoms of PD (Hornykiewicz 2010). Meanwhile, Friedrich Henry Lewy first described the Lewy bodies containing abrnormal intracellular protein inclusions in 1912 (Holdorff 2002). Thereafter, Spillantini found that these filamentous protein inclusions contain predominantly α-syn and that this brain pathology is shared between PD, Dementia with Lewy bodies (DLB) and Multiple System Atrophy (MSA), commonly termed as synucleopathies (Spillantini *et al.* 1997; Spillantini 1999).

α-syn is associated with number of diseas i.e. PD, DLB, MSA and Lewy body variant of AD. Early differential diagnosis and identification of neurodegenerative synucleopathies would be particularly useful involving reliable diagnostic biomarkers (Eller *et al.* 2009). Markers of CSF and plasma hold the greatest promise (Foulds *et al.* 2012) or as another avenue skin fibroblasts could perhaps be explored (Hoepken *et al.* 2008). To date, clinical diagnosis is made based on development of special symptoms as listed below in **Table 1.2.** (Eller *et al.* 2011).

Idiopathic Parkinson's disease (IPD)

- Essential inclusion criteria: bradykinesia plus muscular rigidity, resting tremor and/or postural instability
- Exclusion criteria: sustained remission, supranuclear palsy, upper motor neuron signs
- Supportive criteria (three required): excellent response to levodopa, progressive disorder, unilateral onset

Multiple System Atrophy (MSA)

MSA-parkinsonism

- Parkinsonism (bradykinesia, rigidity and tremor)
- Early, severe autonomic disturbance (postural hypotension, sweating abnormalities, severe constipation, urinary disturbance, male impotence, Raynaud phenomena), upper motor neuron signs, sometimes cerebellar signs

MSA-cerebellar

Idiopathic late onset cerebellar syndrome

Early, severe autonomic disturbance, varying degrees of upper motor neuron signs, parkinsonism

Dementia with Lewy bodies (DLB)

1. Central feature (essential diagnosis for possible or probable DLB)

Dementia defined as progressive cognitive decline of sufficient magnitude to interfere with normal social or occupational function. Prominent or persistent memory impairment may not necessarily occur in the early stages but is usually evident with progression. Deficits on test of attention, executive function, and visuospatial ability may be especially prominent.

2. Core features (two core features are sufficient for diagnosis of probable DLB, one for possible DLB)

Fluctuating cognition with pronounced variations in attention and alertness

Recurrent visual hallucinations that are well formed and detailed

Spontaneous features of Parkinsonism

3. Suggestive features (if one or more of these present in the presence of one or more core features, a diagnosis of probably DLB can be made. In the absence of any core features, one or more suggestive feature is sufficient for possible DLB. Probable should not be diagnosed on the basis of suggestive features alone.)

REM sleep behaviour disorder

Severe neuroleptic sensitivity

Low dopamine transporter uptake in basal ganglia demonstrated by PET imaging

Table 1.2. *The typical clinical features of IPD, MSA and DLB. Table adapted from Eller and Williams* (Eller *et al.* 2011).

1.2 a-syn is associated with Parkinson's disease (PD)

1.2.1 PD

PD has a prevalence of approximately 0.5 to 1 % in the age group of 65-69, rising to 1 to 3 % over the age of 80 (Marder *et al.* 1996; de Lau *et al.* 2006). The clinical symptoms of the disease include resting tremor on one or both side(s) of the body, stiffness of the limbs (rigidity), generalised slowness of movement (bradykinesia) and gait or balance problems (postural dysfunction) and non-motor symptoms including cognitive abnormalities and sleep disorders (Jankovic 2008). A key finding in PD is the selective and gradual degeneration of dopaminergic neurons in the *substantia nigra pars compacta (SNPc*), yet the precise mechanisms of neuronal death are not fully understood. Surviving neurons in PD post-mortem brains display abnormal intracellular protein aggregates called Lewy bodies (Forno 1996; Shults 2006). The main constituent of Lewy bodies and Lewy-neurites found within these cells is the protein a-syn (Wakabayashi *et al.* 2013). Approximately 5-10 % of PD cases have a genetic cause with both recessive and dominant modes of inheritance as shown in Table 1.3.. The autosomal recessive (AR) genes that cause a loss-of-function phenotype include *parkin, DJ-1* and *PINK1,* whereas *SNCA* and *LRRK-2* are inherited in autosomal dominant (AD) fashion. Ubiqutin carboxyl terminal esterase L-1 (*UCLH-1*) has recently been identified and its role is not well understood.

Locus	Inheritance	Gene (protein)	Protein function	Clinical presentation	Neuropathology	Age at onset
PARK1 (PARK4)	AD	*SNCA* (α-syn)	poorly characterised synaptic function	Duplications: IPD; some postural tremor, slow progression. Triplications: PD; PD with dementia: diffuse LB disease; aggressive course mutations: A53T, A30P, E46K: Idiopathic PD; H50Q and G51D; parkinsonism and diffuse LBs	LBs	Mid 30-60
PARK2	AR	*Parkin*	E3 ubiqutin ligase	Parkinsonism; slow progression	Variable presence of LBs	Juvenile to 40
PARK5	AD	*UCLH-1*	Ubiquitin hydrolase and ligase	PD	unknown	30-50
PARK6	AR	*PINK1*	Mitochondrial Ser-Tyr kinase	Parkinsonism	unknown	30-50
PARK7	AR	*DJ-1*	Oxidative stress response	Parkinsonism	Unknown	30-50
PARK8	AD	*LRRK2* (dardarin)	poorly characterised protein kinase	PD	Diffuse LBs; Lewy Neurites; ±Tau inclusions; ± amyloid plaques	40-60

Table 1.3. *Mendelian PD genes. Adapted by permission from Elsevier: Trends in Molecular Medicine, (Wood-Kaczmar et al. 2006).*

More recent genetic linkage analysis and genome-wide association studies identified more than 11 loci and 9 genes responsible for the disease (International Parkinson Disease Genomics Consortium *et al.* 2011).

The most compelling evidence for the direct role of α-syn in PD has been provided by three known missense mutations Ala30Pro(A30P) (Kruger *et al.* 1998), Ala53Thr (A53T) (Polymeropoulos *et al.* 1997) and Glu46Lys (E46K) (Zarranz *et al.* 2004) in the *SNCA* gene that have been linked with the autosomal dominant early-onset PD. α-syn containing these mutations is thought to have higher propensity to aggregate *in vitro*, however evidence regarding the ability of A30P α-syn to accelerate the rate of fibrillation is inconclusive (Conway *et al.* 1998; Greenbaum *et al.* 2005; Fredenburg *et al.* 2007). Furthermore, duplications (Chartier-Harlin *et al.* 2004) and triplications (Singleton *et al.* 2003) of the *SNCA* gene have also been detected in familial forms of PD. However, most forms of PD classed as sporadic and appear to be not strictly genetic in nature but arise from a number of factors acting in conjunction with each other during the life time of an individual (Irwin *et al.* 2013). A recent two-hit animal model incorporating neuroinflammation induced by lipopolysaccharide treatment and human A53T mutant α-synuclein overexpression demonstrated the synergistic effects of genetic predisposition and environmental exposures in the development of PD (Gao *et al.* 2011). In addition to the three well described familial mutations A53T, A30P and E46K two probable pathogenic mutations, His50Gln (H50Q) and Gly51Asp (G51D) and two possible missense mutations, Ala18Thr (A18T) and Ala29Ser (A29S) have recently been identified (Fujioka *et al.* 2014). The H50Q point mutation was identified in a single PD patient using Sanger sequencing of *SNCA* coding exons, who showed responsiveness to levodopa treatment, had cognitive impairment, apathy and dementia (Appel-Cresswell *et al.* 2013). Another case of the H50Q missense mutation has been reported by Proukakis *et al.* (Proukakis *et al.*, 2013). The pathogenic G51D mutation was found both in a

French (Lesage *et al.* 2013) and in a British family (Kiely *et al.* 2013). The clinical manifestation of this mutation is characterised by early onset, rapidly progressive PD, displaying pyramidal signs and psychiatric symptoms with the absence of cognitive impairment (Fujioka *et al.* 2014). The A18T and A29S mutations were identified in Polish patients with characteristic clinical features of PD (Hoffman-Zacharska *et al.* 2013).

Indications for the role of α-syn in the disease state have been highlighted through transgenic adenoviral, lenti-viral based animal models. In these systems, overexpression of α-syn recapitulated signs of neurodegeneration and Lewy-body like inclusions (Lo Bianco *et al.* 2002; Masliah *et al.* 2000; Martin *et al.* 2006). In contrast, dopaminergic cells have been rescued with down-regulation of α-syn expression in an 1-methyl-4-phenylpyridinium (MPP) (+) PD rat model (Hayashita-Kinoh *et al.* 2006). Yet, the survival of neurons with intracellular Lewy bodies indicates that these aggregates are not explicitly causative in all cases but they might be responsive inclusions that sequester potentially toxic constituents from other cell compartments (Tompkins *et al.* 1997).

Alternatively, it has been proposed that small soluble oligomers, or protofibrils populated prior to fibril formation are responsible for neurotoxicity (Quist *et al.* 2005; Winner *et al.* 2011; Giehm *et al.* 2011). One of the explanations for the toxic effect of amyloid oligomers suggests that some oligomeric species are capable of forming pores or channel-like structures (Lashuel *et al.* 2002) that can cause defects in the control of membrane permeability, may activate pre-existing ion channels or the oligomers may enhance the ability of ions to move through the phospholipid bilayer without the formation of pores (Kim *et al.* 2009;

Malchiodi-Albedi *et al.* 2011). It has been shown that some species of a-syn oligomers resemble annular or pore-like structures with outer diameters of 10-12 nm and inner diameters of 2 nm (Lashuel *et al.* 2002). This concept is analogous to the toxic oligomeric amyloid (3 (Af3) hypothesis proposed in AD where Ca(ll) dysregulation is a central element of neurotoxicity (Quist *et al.* 2005; Demuro *et al.* 2005). The build-up of oligomeric species may cause oxidative stress, disruption of axonal transport, synaptic dysfunction, mitochondrial dysfunction and an overload in the physiological quality control systems (molecular chaperones, ubiquitin-proteasome system (UPS) and phagosome-lysosome system) hindering the elimination and clearance of toxic agents as shown in Figure 1.1. (Irwin *et al.* 2013).

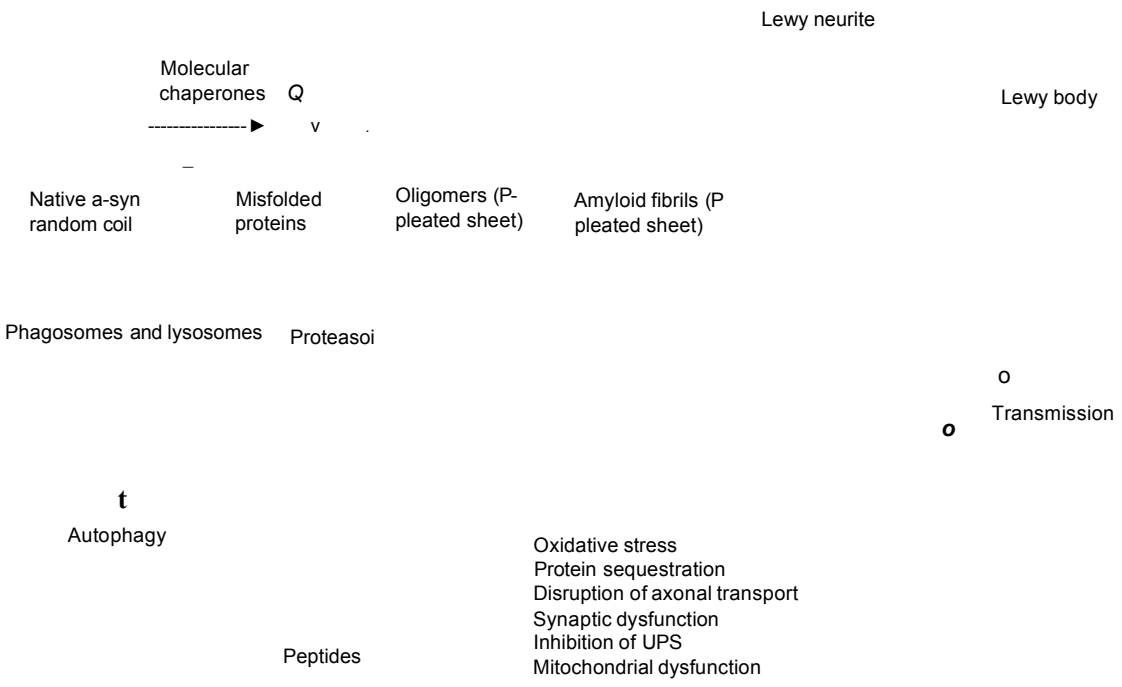

Figure 1.1. *Toxic mode of action of a-syn and its assemblies involving multiple cell components and mechanisms as reviewed by Irwin, Lee and Trojanowski. Adapted by permission from Macmillan Publishers Ltd: Nature Reviews Neuroscience,* (Irwin *et al.* 2013).

Strategies to regulate a-syn synthesis by small interfering RNA or microRNA or hinder self-assembly of the protein by peptides or small molecule inhibitors are in development. Other points for therapeutic intervention are being sought including enhancing disassembly or clearance of aggregates, activating autophagy and the proteasome system, restoring functions of heat shock proteins, using antioxidants, anti-inflammatories and neuroprotective agents (Irwin *et al.* 2013, Lashuel *et al.* 2013).

1.2.2 The role of metal ions in PD

Increased chronic exposure to heavy metals such as manganese, lead, iron and copper acting individually or synergistically has been documented as a potential risk factor in PD and has been underpinned by an array of epidemiological studies (Gorell *et al.* 1999; Gorell *et al.* 2004; Coon *et al.* 2006). In a recent critical review, Santer and Uversky have summarised the progress of research made to date about the interactions of a-syn with metals e.g. aluminium, cobalt, copper, iron, lead, magnesium, manganese, terbium and zinc in relation to binding and aggregation propensities.

Regarding iron, Fe(II) is thought to cause oxidative damage through promoting the formation of reactive oxygen species (ROS) and oxidative stress which is detrimental to cell function. Redox active metal ions such as Fe(II) can react with hydrogen peroxide (H_2O_2) leading to the formation of hydroxyl radicals by Fenton chemistry. Furthermore, Fe(II) can promote aggregation of a-syn which is then deposited in LB and plays a part in the development of nigrostriatal injury and neurodegeneration (Santner *et al.* 2010).

Binolfi *et al.* have investigated the interactions of α-syn with a range of divalent metal ions, namely Fe(II), Mn(II), Co(II), and Ni(II) in comparison to Cu(II) and their influence on its aggregation at the atomic level. The study showed that divalent metal ions bind predominantly to the C-terminal of α-syn. The preferred binding site site is the DPDNEA motif (119-124 aa), where Asp121 serves as an anchoring residue to which they bind with low selectivity and affinity (Kd ~1 mM). The interactions are not only dependent on electrostatic forces but are determined by the residual structure of the C-terminus as well (Binolfi *et al.* 2006). The specificity and high binding affinity of Cu(II) for α-syn in the submicromolar range was highlighted in a further study undertaken by Binolfi *et al.*, where binding of this metal ion was demonstrated using nuclear magnetic resonance (NMR), electron paramagnetic resonance (EPR), circular dichroism (CD) and matrix assisted laser desorption ionisation mass spectrometry (MALDI MS) measurements. Both in the case of α-syn and β-syn, two distinct binding sites of Cu(II) have been identified in the presence of competitive chelators, one in the N-terminus encompassing Met1 and another lower affinity binding site located at the imidazole ring of the unique His residue (Binolfi *et al.* 2008). Further Cu(II) specifics of the His50 residue were reported by Valensin *et al.* who estimated a dissociation constants of 1.5 μM at pH 7.5 for α-syn 44-55 peptide containing either E46K or A53T substitutions, in the pH range of 6.5-7.0, revealing information about co-ordination geometry of Cu(II) and its binding constraints (Valensin *et al.* 2011). In a cellular model, oligomer and aggregate formation was reduced upon lower levels of cellular Cu(II) (~ 10 μM), and α-syn was shown to become more closely associated with the plasma membrane where these changes appeared to be reversible. Deletions of the C or N-terminal residue conferred an inability of the protein to aggregate, and mere C-

teminal truncation reduced susceptibility of cells to Cu(II) induced cytotoxicity, while overexpression of a-syn increased the sensitivity to Cu(II) (Wang *et al.* 2010c).

1.2.3 Posttranslational modifications

Posttranslational modifications of a-syn e.g. phosphorylation, nitration, ubiquitination and truncations can contribute to dramatic biophysical and biochemical changes and are active areas of research (Shults 2006; Oueslati *et al.* 2010; Beyer *et al.* 2013). Lewy bodies in the brain contain phosphorylated a-syn and it has been detected in blood plasma as well (Foulds *et al.* 2012). Investigations into the molecular mechanisms governing phosphorylation at Seri 29 and Ser87 modification sites are underway (Inglis *et al.* 2009). Recently, Ouselati *et al.* reported the relevance of Polo-like kinase 2 enzyme as a regulator of a-syn turnover that is up-regulated in synucleinopathies and co-localised with phosphorylated Ser129 in diseased brains. It has been shown that Polo-like kinase forms a complex with a-syn and phosphorylates it at Seri 29, resulting in an enhanced autophagic degradation of a-syn in an ATP dependent manner. Overexpression of this enzyme in a rat model of PD led to a decreased intraneuronal accumulation of a-syn, less severe dopaminergic neurodegeneration and to reversal of motor impairments (Oueslati *et al.* 2013).

Importantly, the C-terminal domain contains metal binding motifs and phosphorylation sites in close proximity. Some insights into the modulatory effects of phosphorylation dependent metal binding including Al(III), Fe(III) and Tb(III) have emerged (Liu *et al.* 2007) but are not fully conclusive yet. Overproduction of oxygen reactive species and nitration species create nitrating

agents that convert the Tyr residues of a-syn to three nitrotyrosine. A variety of nitration specific antibodies have detected nitrated a-syn in insoluble intracellular deposits of a-syn. It is speculated that nitration of the Tyr residues of a-syn promotes fibrillisation or perhaps nitration occurs after a-syn assembles into fibrils and play a part at the onset of synucleopathies (Giasson *et al.* 2000).

As another posttranslational modification, C-terminal truncation of a-syn has been shown to occur in human brain tissue and neuronal cell culture as demonstrated by immunoblotting procedures. The C-terminal has an essential chaperone activity and cellular processes remain to be identified that cause truncation of full length protein. The C-terminally truncated protein *in vitro* has a propensity to promote the self-assembly of the full length protein. Further evidence has shown that C-terminal truncation, i.e. the loss of at least 17 amino acids was observable both in neuronal cultures and the brain from A53T harbouring human familiar forms of transgenic mice and was not a mere artifact of pathological processing as revealed by utilising a Cipergen Surface Enhanced Laser Desorption and Ionisation(SELDI MS) approach in combination with immunoblotting procedures (Li *et al.* 2005).

1.2.4 Links of a-syn to other disease states

Interestingly, insights obtained from cell culture models and brain extracts strengthen the hypothesis that extracellular a-syn is involved in propagating the LB like pathology by mechanisms described in prion disease. Despalts *et al.* reported that a-syn was transmitted via endocytosis to neighbouring neurons and neuronal cells, forming LB like inclusions when the recepient's lysosomes

were inhibited (Desplats *et al.* 2009). Postmortem examination of two subjects with PD who had long-term survival of transplanted foetal mesencephalic dopaminergic neurons showed that the transplanted cells had developed immunopositive LBs raising a possibility of a host-to-graft disease propagation (Li *et al.* 2008). Since these early reports, an increasing body of evidence for the cell-to-cell propagation of α-syn has been now gathered (Angot *et al.* 2012) which suggests common links between misfolded α-syn and other prion diseases as argued by Prusiner (Prusiner 2012).

α-syn inclusions apprear in numerous taupathies (Mukaetova-Ladinska *et al.* 2006). Equally, a group of PD patients present with strong dementia, clinically classified as Parkinson's disease dementia group (PDD). Symptoms often coincide with the spread of α-syn from the brainstem to limbic and neocortical regions (Braak *et al.* 2003). Of note, 50 % of the affected cells also show amyloid-β plaques and neurofibrillary tangles consisting of Tau that are critical hallmarks of AD. These distinct but converging pathologies and their relationships will require a better understanding in order to develop successful therapies (Irwin *et al.* 2013).

Tsigelny *et al.* have examined the potential interactions of Aβ and α-syn both by analysing immunoblots of brains from patients with AD/PD and amyloid precursor protein/α-syn transgenic mice and by molecular stimulations and other *in vitro* studies. Molecular modelling showed that Aβ binds to α-syn monomers, homodimers and trimers, forming more stable pentamers and hexamers with a ring-like topology. Moreover, membrane docking experiments implied that α-syn and Aβ co-structures docked to a 1-palmitoyl-2-oleoyl-sn-glycero-3-phosphocholine (POPC) membrane have incorporated other α-syn

molecules resulting in a ring-like organisation. In accordance with these findings, cell-free studies highlighted that freshly-solubilised Ap1-42 promoted the aggregation of soluble a-syn in *a* time and dose dependent manner. The hybrid a-syn and Ap complexes formed functional cation nanopores in HEK293T cells potentially leading to increase in the influx of Ca(ll) (Tsigelny *et al.* 2008).

An early indicator of a-syn induced neuronal demise is synaptic dysfunction. Synapse damage was studied by measuring synaptophysin in cultured neurons incubated with overexpressed a-syn, or with amyloid-p 1-42 (Ap 1-42) peptides. Treatment with recombinant human a-syn decreased both the synaptophysin content of cells and synaptic vesicle recycling as indicated by the uptake of the fluorescent dye FM 1-43. While the addition of p-syn moderated the effects of a-syn, Ap 1-42 enhanced the negative effects of a-syn on synaptic vesicle recycling as well as on synapse damage and similarly a-syn accelerated synapse damage provoked by Ap 1-42. Additionally, the synaptophysin content of cortical neurons did not differ when treated with prion-derived peptide PrP 82-146 alone or with the mixture of a-syn/ PrP 82-146. These observations imply that interactions between these proteins or other peptides might influence the manner of synapse degeneration (Bate *et al.* 2010).

1.3 a-syn monomer and its misfolded forms

1.3.1 Physiological roles and structure of human a-syn

a-syn is a 140 amino acid cytosolic protein which was first isolated from synaptic vesicles of *Torpedo californica* and rat brain (Maroteaux *et al.* 1988). It is encoded by chromosome 4 and is abundantly expressed in neurons, mostly

localised at the presynaptic nerve terminals. The physiological functions of α-syn include regulation of vesicle transport (Murphy *et al.* 2000), synaptic plasticity and chaperone activity. It also plays a part in the assembly of SNARE protein complex (Burre *et al.* 2010) that is instrumental in neurotransmitter release, vesicle recycling and synaptic integrity (Chandra *et al.* 2005). Similarly, α-syn is associated with mitogen activated protein kinases (MAPKs) (Iwata *et al.* 2001) and phospholipase D (Ahn *et al.* 2002). Moreover, it plays an important role in the metabolism of dopamine by modulating tyrosine-hydroxylase that is a rate-limiting enzyme in dopamine production (Lotharius *et al.* 2002a; Yavich *et al.* 2004). α-syn is an intrinsically unstructured or natively unfolded protein with a negative net charge. The main domains of α-syn are the N-teminal region (aa 1-37) consisting of imperfect, repetitive tandem motifs that can adopt amphipathic helical structures upon membrane binding (Uversky *et al.* 2009), the central hydrophobic domain (amino acids 61-95) referred to as non-amyloid β-component (NAC) of Alzheimer disease amyloid (Ueda *et al.* 1993), with a tendency to form β-structures and associated with pathological brain lesions (El-Agnaf *et al.* 1998, Uversky *et al.* 2000) inducing apoptotic cell death in culture, and finally the highly acidic, proline rich, C-terminal residue (amino acids 96-140) (Meuvis et al. 2010) with a chaperone-like activity (Burre *et al.* 2010). The domains of human α-syn are shown below (**Figure 1.2.**) (Bisaglia *et al.* 2009).

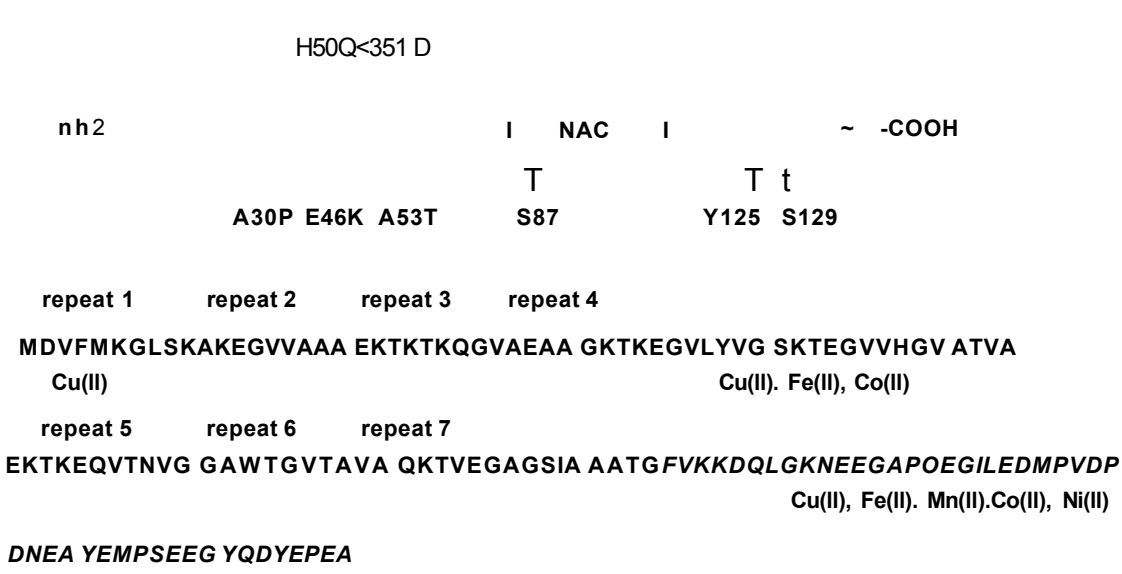

Figure 1.2. *Schematic representation of a-syn domains. The N-terminal (1-60) is denoted by regular capital letters, the NAC region (61-95) by bold capital letters, and the C-terminal region (96-140) by italics. The three well known familial mutations (A30P, E46K and A53T), two recent probable pathogenic substitutions (H50Q and G51D) and the phosphorylation sites (S87, Y125 and S129) of a-syn are marked by arrows, metal interaction sites by italics. Reproduced by permission of Springer, Neuromolecular Medicine, (Bisaglia et al. 2009).*

At neutral pH, far-UV circular dichroism (CD) and Fourier transform infrared (FITR) spectra typing have shown a significantly unfolded polypeptide chain with low content of ordered secondary structure. The reported radius of gyration (Rg) at neutral pH is smaller (40 Å) than that estimated for a random coil (52 Å), indicating that a-syn is more compact than an expected random coil (Uversky *et al.* 2001a). However, Rg of the partially folded conformer (30 Å) is greater than folded globular protein's with the same size (15 Å), suggesting that it is slightly expanded, lacking a tightly packed secondary structure. Nuclear magnetic resonance (NMR) analysis reported that the region of 6-37 amino acids has a

preference for adopting helical conformation. The far-UV CD spectrum of a-syn at neutral pH is typical that of an unfolded polypeptide chain, at acidic pH the natively unfolded a-syn is transformed into a partially folded conformation with substantial amount of ordered p-structure. Changes in temperature can equivocally induce structural changes in the polypeptide chain more likely by a stronger hydrophobic driving force for folding (Uversky *et al.* 2001 a).

Conformational behaviour of a-syn has been extensively investigated under a variety of conditions depending on not only pH and temperature but on organic solvents (Munishkina *et al.* 2003), various salts (Munishkina *et al.* 2009), pesticides (Uversky *et al.* 2002), herbicides (Manning-Bog *et al.* 2002), heparin (Cohlberg *et al.* 2002) polycations (Goers *et al.* 2003), methionine (Met) oxidation (Glaser *et al.* 2005) and metal ions (Uversky *et al.* 2001c; Brown 2007; Bisaglia *et al.* 2009; Lee *et al.* 2008b; Lucas *et al.* 2011) and agrochemicals (Silva *et al.* 2013).

1.3.2 Aggregation of a-syn

As shown by atomic force microscopy (AFM) and electron microscopy, there are distinct final products of a-syn aggregation; soluble oligomers, fibrils and amorphous, large aggregates, occasionally arising from different competing or parallel aggregation pathways driven by their own adequate energetics and kinetics. Aggregation of a-syn starts with a distinct, slow lag phase which is followed by a nucleation step and a growth phase (elongation) until a thermodynamic equilibrium is reached between the aggregate and the monomer, marking the steady state (Wood *et al.* 1999). In the lag phase the saturated protein solutions remains stable and formation of pre-nuclear

oligomers is initiated. Upon the appearance of nuclei, the aggregates elongate rapidly during the growth phase and transition into the steady state, where the so-called growth equilibrium constant describes the solubility of the protein and equates to the critical concentration (Andreu *et al.* 1986).

The critical concentrations do not deviate greatly for the familial mutants of α-syn and the WT protein, implying that accelerated aggregation of the mutants is not a matter of increased solubility of the mutant types but perhaps a result of different nucleation rates. This nucleation-dependent fibrillogenesis of α-syn is similar to that of β-amyloid (Aβ) (Takahashi *et al.* 2008). A common cross β structure is shared between α-syn fibrils and paired helical filaments of Aβ fibrils (Friedhoff *et al.* 1998) that are observed in AD (Wood *et al.* 1999). The nucleation dependent polymerisation is dependent on protein concentration and time, and amyloid fibril formation can be seeded by the addition of preformed fibrils that abolish the lag phase (Harper *et al.* 1997; Jarrett *et al.* 1993).

After a nucleation event the self-assembly proceeds by formation of small soluble oligomers that may further assemble to larger oligomers then to protofibrils (10-50-mers depending on the type of protein) to form large, insoluble amyloid fibrils with a characteristic cross-β structrure as illustrated in **Figure 1.3.** (Takahashi *et al.* 2008). Modifications can stabilise oligomers, for example conversion of the four Met residues to methionine sulfoxide (Glaser *et al.* 2005), nitration of the Tyr residues (Yamin *et al.* 2003), interaction with rifampicin (Li *et al.* 2004), other dopamine analogues (Li *et al.* 2005) and polyphenols. These modifications and the inclusion of co-factors yield hardy oligomers, resistant to dissociation and commonly these oligomers do not rapidly form fibrils (Fink 2006).

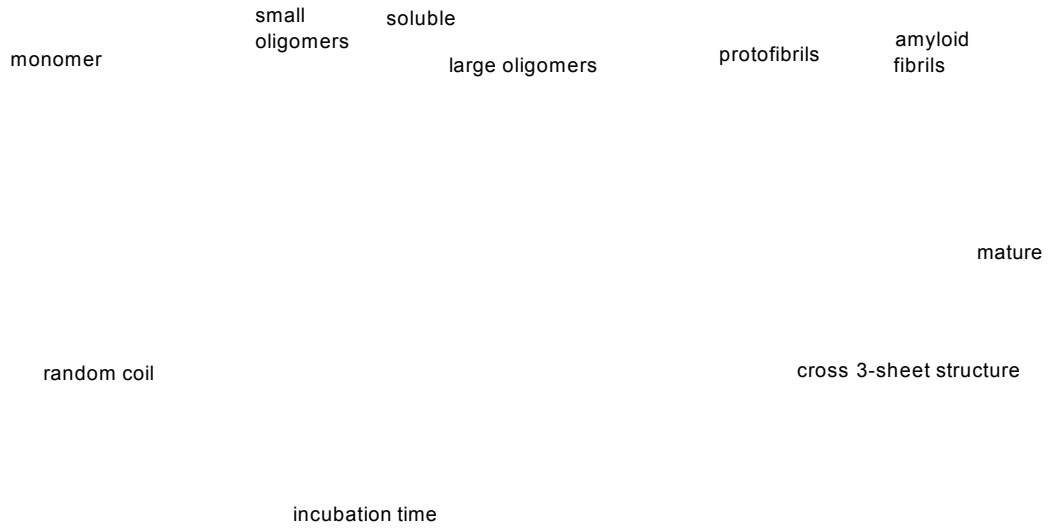

Figure 1.3. *Schematic representation of the aggregation of an unstructured monomer into amyloid fibrils with /3-sheet structures through small and large oligomers and protofibrils. The aggregation kinetics in vitro shows a typical sigmoidal curve that is comprised of a lag phase (nucleation phase), an exponential elongation phase (fibril growth phase) and a plateau phase (steady state). Adapted with permission from (Takahashi et al. 2008), American Chemical Society.*

The successfully formed and mature fibrils of a-syn grown *in vitro* have been demonstrated to display a length from 500 nm to 3 pM. Three ranges of heights were observed with 3.8±0.6 nm for protofilaments, 6.5±0.6 nm for protofibrils and 9.8±1.2 nm for fibrils (Khurana *et al.* 2003). In this study, a "hierarchical assembly model" was described to classify the morphology of different subspecies during aggregation whose formation is driven by nucleated polymerisation kinetics. It was assumed that nascent protofilaments appear at the early phase of fibrillisation and they grow by the recruitment of monomeric, partially folded intermediates to the ends of protofilaments. These

protofilaments (-two or three protofilaments) then associate to yield protofibrils. Subsequently, two protofibrils assemble to form more rigid, mature fibrils (Khurana *et al.* 2003). Glycosaminoglycans (GAGs) such as heparin have been shown to promote the formation of a-syn fibrils that may influence *in vivo* aggregation of a-syn as Lewy bodies were shown to contain GAGs (Cohlberg *et al.* 2002). Interestingly, p- and y-syn which are also abundant in the brain do not form fibrils or form fibrils at a much slower rate, respectively (Uversky *et al.* 2002).

1.3.3 Amyloidogenic a-syn oligomers are toxic species

a-syn has an increased propensity to form morphologically different oligomers and different protocols yield alternate oligomeric forms, where these intermediates are often lowly populated and transient.

Importantly, overexpressed recombinant human a-syn can assemble under certain conditions into soluble oligomers or fibrils *in vitro* that are similar in morphology and staining to filaments extracted from the diseased brain and are toxic to primary neurons and dopaminergic neuronal cell lines (Forloni *et al.* 2000; Seo *et al.* 2002; Danzer *et al.* 2007; Wright *et al.* 2009).

First evidence for presence of significantly elevated levels of oligomeric forms of a-syn was shown in plasma samples obtained from 34 PD patients compared with 27 controls by a novel ELISA method (El-Agnaf *et al.* 2006). A more recent investigation suggested that levels of a-syn oligomers in the CSF and the oligomers/ total-a-syn ratio can be useful biomarkers for diagnostic early detection of PD (Tokuda *et al.* 2010). Moreover, total a-syn, phosphorylated a-syn and oligomeric forms were measured in 76 post mortem samples taken

from patients with PD, DLB progressive supranuclear palsy (PSP) and multiple system atrophy (MSA) besides 20 control samples. Out of the four forms, phosphorylated oligomeric α-syn differed significantly in MSA when comparing to other subgroups, indicating a potentially useful biomarker in differential diagnosis (Foulds *et al.* 2012).

The detailed entities of fibril formation *in vitro* have been reported in equimolar mixtures of A53T/ wild-type (WT), in equimolar mixtures of A30P/ WT and in WT α-syn by Conway and colleagues. In this study, three alternate forms of prefibrillar, oligomeric species with different morphology (spheres, chains and rings) have been detected by using AFM at the early stages of fibril formation following their separation from other fibrillar and monomeric species by sedimentation analysis and size exclusion chromatography (Conway *et al.* 2000).The spheres had a 2-6 nm height, the protofibrils had a height of 4 nm, while the rings comprised of two classes, a circular one with a diameter of 35-55 nm, and an elliptical one with widths between 35-55 nm and lengths of 65-130 nm. Fibrillation of A30P was found to be comparable to the WT α-syn, whereas the monomers were consumed faster in case of A53 during fibril formation. The larger α-syn fibrils similarly to other amyloidogenic species displayed a cross β-sheet structure when stained by Thioflavin T (ThT) and Congo red in agreement with data derived by X-ray diffraction (Serpell *et al.* 2000).

Lashuel *et al.* have shed some light on the structure of protofibrils assembled from A30P, A53T as well as WT α-syn by employing complementary approaches such as analytical gelfiltration, CD, sedimentation velocity analytical ultracentrifugation (SVAU) and scanning transmission electron microscopy (STEM). Electron microscopy images showed that both autosomal dominant

mutants populated three to four classes, most commonly annular protofibrils, although tubular protofibrils appeared only for A53T. Notably, the wild-type protein's ability to form annular protofibrils was less pronounced than its mutants and needed an extended six to eight weeks incubation period (Lashuel *et al.* 2002).

Morphological properties of annular oligomers formed from 10 μM α-syn in the presence of 100 μM di- and trivalent metals at 4 °C was examined in an AFM study as described by Lowe *et al.* (Lowe *et al.* 2004). Cu(II), Fe(III) and Ni(II) produced 0.8-4 nm spherical particles, similar to the ones in the absence of metals, Mg(II), Cd(II) and Zn(II) that produced 5-8 nm spherical oligomers. Addition of Co(II), Ca(II) resulted in annular oligomers, with 70-90 nm diameter for Ca(II) and with 22-30 nm diameter for Co(II). Without metal the protein yielded 45-90 nm annular oligomers in diameter after 10 days incubation and short, branch like structures with extended filaments occurred after 2-3 months. In the absence of the Ca(II) binding C-terminal domain, α-syn did not form annular oligomers following Ca(II) addition (Lowe *et al.* 2004).

Rapidly formed sphere like structures were observed to enable the assembly of annular protofibrils composed of solely from A53T, A30P and WT α-syn or from 1:1 mixture of WT/ A53T upon longer incubation (>2 weeks) as detailed by Ding *et al.* (Ding *et al.* 2002). Spherical structures bound to brain derived membrane fractions better than monomeric or fibrillar α-syn and membrane associated annular protofibrils displayed dimensions with striking similarities to bacterial pore forming toxins. One possibility is that the protofibrils are not participants of the direct monomer-to-fibril pathway but they are more stable and first the need to "reopen" to be converted to fibrils (Ding *et al.* 2002).

The fact that amyloid fibrils of a-syn are sensitive to cold temperatures has been harnessed to produce soluble a-syn oligomers in substantial quantity *in vitro.* Oligomers generated by supercooling dissociation were then examined to reveal any further structure and toxicity relationship by structural spectroscopic methods and electrophysiological measurements. The dynamic radii of these oligomers were determined to be ~35 and 125 nm in solution and had p-structures that were deemed to be different from the fibrillar form. These oligomeric species elicited disturbances in ion channel conductance. The oligomers formed slightly cation selective ion channels in a range of membranes, monomers and fibrils showed minimal or no channel forming activity in synthetic membranes. Green tea cathecin epigallocatechin gallate (EGCG) has anti-oxidant effects and it can also directly bind to a-syn and a-syn oligomers, redirecting their aggregation into non-toxic forms. In this study, the observed pore formation evoked by soluble a-syn oligomers could be inhibited by incubation with EGCG for 2 hr at a 1:10 molar ratio. (Kim *et al.* 2009).

1.4 Biochemical and biological effects of a-syn oligomers and its related species in neuronal models

1.4.1 Complex morphological characteristics and cytotoxic effects through Ca(II) influx and seeding associated with *in vitro* oligomers

The rationale for Ca(II) channel formation of a-syn was demonstrated through collecting several lines of evidence and it has now widely been accepted that a-syn can cause Ca(II) dysregulation (Voiles *et al.* 2001; Lowe *et al.* 2004; Lashuel *et al.* 2002; Quist *et al.* 2005; Danzer *et al.* 2007; Zakharov *et al.* 2007; Kim *et al.* 2009; Winner *et al.* 2011; Malchiodi-Albedi *et al.* 2011; Giehm *et al.*

2011). AFM images seem to suggest annular structures as the pivot for the formation of pore like channels across A(B 1-40, a-syn, ABri, ADan, amylin and serum amyloid A (SAA). However the resolving power did not allow resolution of individual subunits. The dimensions were estimated to be around 25 nm for both Ap 1-40 and a-syn, 35 nm for ADan, 25 nm for amylin and 20 nm for serum amyloid as shown in Figure 1.4..

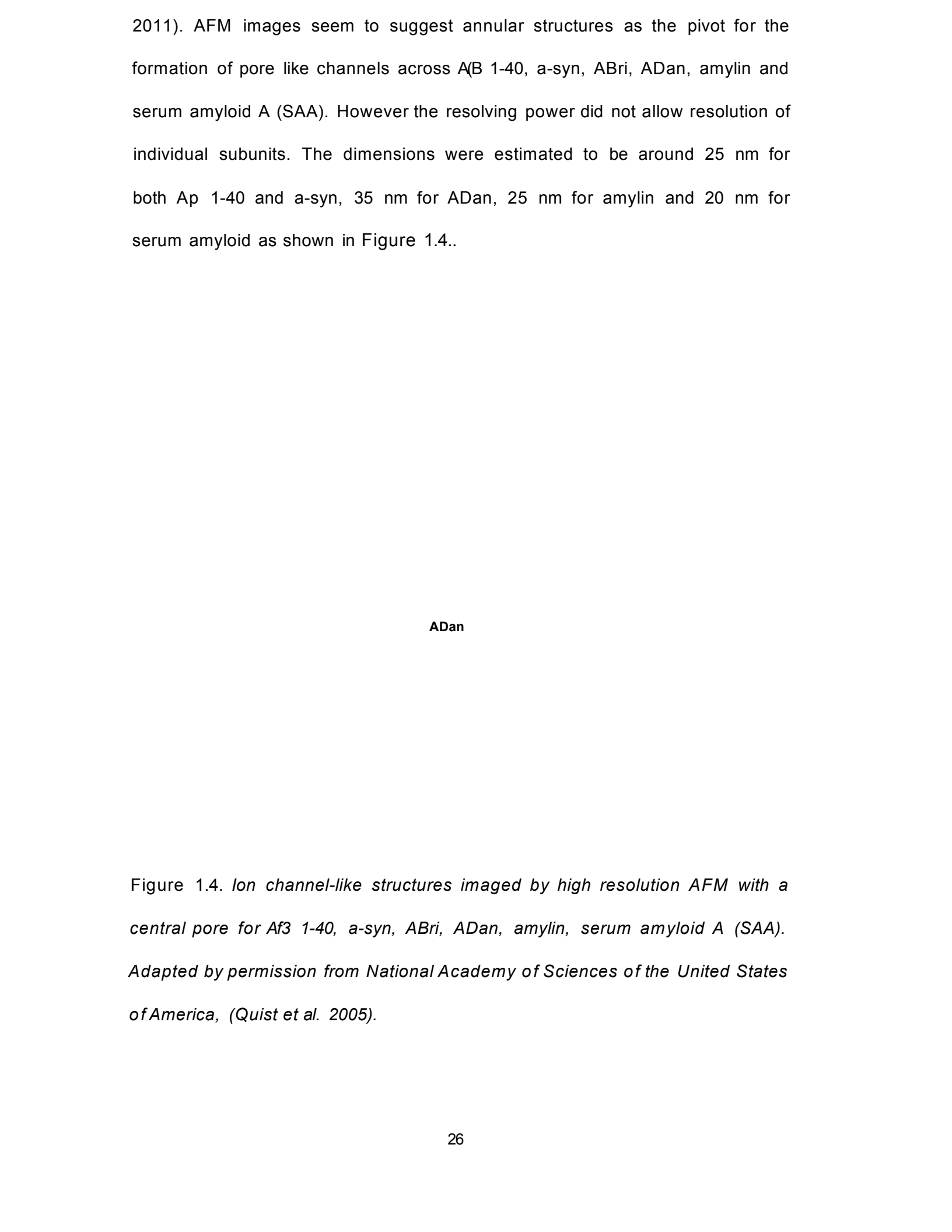

Figure 1.4. *Ion channel-like structures imaged by high resolution AFM with a central pore for Af3 1-40, a-syn, ABri, ADan, amylin, serum amyloid A (SAA). Adapted by permission from National Academy of Sciences of the United States of America, (Quist et al. 2005).*

Danzer *et al.* have described *in vitro* oligomerisation protocols resulting in Type A, B and C toxic, soluble, a-syn oligomers. All three aggregation protocols described in this study with or without the addition of FeCl3 resulted in a heterogeneous population of oligomers. Type A1 and A2 type oligomers evoked an increase in the intracellular Ca(II) levels in support of the previously mentioned pore forming theory, whereas extracellularly added type B oligomers entered the cells and seeded aggregation of cytosolic a-syn. Both type C1 and C2 type oligomers induced punctate aggregate formation in a SH-SY5Y cell line overexpressing A53T a-syn (Danzer *et al.* 2007). A later follow-up study provided further evidence that type C oligomers were capable of inducing transmembrane a-syn seeding in both primary cortical neurons and in BeM17 or SFI-SY5Y cell lines in a time and dose dependent manner when added extracellularly. In addition, *in vitro* type A oligomers could be converted to type C oligomers with corresponding biological effects that indicates the two types of oligomers have dynamic properties (Danzer *et al.* 2009). Overall, these two studies proposed that different physiological conditions will lead to a heterogeneous group of oligomers co-existing under equilibrium and have formed a basis of the preparation protocols adapted here and discussed later on.

1.4.2 Morphology and toxicity of oligomers prepared in the presence of curcumin

Overexpression of a-syn and addition of a-syn oligomers extracellularly have been shown to enhance the formation of reactive oxygen species that induced apoptosis by increasing the activity of caspase-3. When oligomers were co-incubated with curcumin a-syn induced cytotoxicity and oxidative stress were

both attenuated, preventing apoptosis in SH-SY5Y neuroblastoma cells. Co-incubation of monomeric a-syn with curcumin did not alter toxicity and co-incubation of fibrils with curcumin exhibited an increased cytotoxic effect. SH-SY5Y cell treated with oligomeric a-syn extracellularly displayed increased oxidative stress, which was significantly reduced by the addition of curcumin (Wang *et al.* 2010b), supporting the earlier finding that curcumin acts as an antioxidant (Ono *et al.* 2006). It was demonstrated by AFM that curcumin does not change the morphology of the monomeric and preformed oligomeric species but that does destabilise pre-formed a-syn fibrils, consistent with previous findings (Ono *et al.* 2006; Pandey *et al.* 2008). Recent biophysical findings suggest that the beneficial effect of curcumin is due to its ability to modulate the hydrophobic surface exposure of preformed oligomers. 2D-NMR data showed that curcumin binds selectively to the preformed oligomers but not to the monomeric protein. This study however concluded that curcumin did alter the morphology of preformed oligomers by increasing the height of oligomers and making them more elongated (Singh *et al.* 2013). These oligomers were prepared by a different preparation protocol from that reported by Ono *et al.* (Ono *et al.* 2009) limiting direct comparison between the two studies (Singh *et al.* 2013).

1.4.3 Oligomers seeded with Ap are shown to be toxic in ex *vivo* rat brain and mice and neuronal cells

Oligomeric a-syn seeded with a small amount of Ap (1:40) has been applied exogenously in various model systems and found to negatively impact vital neuronal functions such as synaptic plasticity and cognitive function, a-syn

oligomers promoted a rise in intracellular Ca(II) levels, induced calcineurin (CaN) activity, dampened the cAMP response element binding protein (CREB) transcriptional activity, leading to cell death in SH-SY5Y cells. CaN is a protein abundant in the brain and is responsible for synaptic plasticity, learning and short- and long-term memory (Mansuy *et al.* 1998). CaN indirectly regulates the transcription factor CREB (Bito *et al.* 1996). When rat brain slices were treated with oligomeric a-syn, higher CaN activity and inhibition of CREB were similarly observed. In mice following intracerebroventricular injections, oligomeric a-syn elicited an increased CaN activity, inhibited CREB and brought about memory impairments (Martin *et al.* 2012).

1.4.4 Effects of oligomers prepared by metal induced aggregation

As for metal induced cellular aggregation, Wright and colleagues have determined the effects of Cu(II)-induced oligomerisation versus Fe(III) in SH-SY5Y neuroblastoma cells using both WT and missense mutant forms of a-syn (Wright *et al.* 2009). In this cell culture model, the combination of elevated levels of extracellular a-syn oligomers and Cu(II) caused greater toxicity than Fe(III) as suggested by MTT cell viability tests, a-syn oligomers isolated by fractionation techniques resembled small spherical aggregates with the diameter of 15-20 nm, and small fibrils with the length of 50-150 nm and 6-8 nm diameter. Moreover, no significant morphological changes appeared in the a-syn fibrils formed in the presence or absence of metal with missense mutations (Wright *et al.* 2009).

1.4.5 Uptake and clearance of a-syn and its intermediates

Lee and colleagues have noted that protein folding stresses and inhibition of the protein quality systems increase vesicle translocation and secretion of a-syn as a compensatory action to aid the removal of the damaged protein (Lee *et al.* 2008a). The clearance of dysfunctional a-syn from the extracellular space might become increasingly challenging whilst maintaining the brain parenchyma's integrity. To dissect the translocation machinery, the assembly-dependent endocytosis and clearance of extracellular aggregates from oligomeric and fibrillar forms and monomeric a-syn were investigated in SH-SY5Y cells, COS-7 cells and rat primary cortical neurons. It was shown that uptake of fibrillar a-syn could be internalised by receptor mediated endocytosis and proceeded through the endosomal pathway to facilitate clearance of aggregates by the lysosome. The internalisation of non-fibrillar, oligomeric a-syn occurred by endocytosis and became degraded by the lysosome. By contrast, the internalisation of monomeric a-syn was suggested to proceed by direct translocation across the plasma membrane, avoiding any significant proteolysis given its short half-life (Lee *et al.* 2008a).

1.4.6 a-syn fibrils seed intracellular aggregation of endogeneous a-syn that undergoes posttranslational modification

Intracellular aggregation of a-syn has been shown to be induced by treatment with exogeneously produced fibrillar species in QBI-HEK293 cells and SH-SY5Y neuroblastoma cells. These fibrils acted as seeds which then recruited intracellular a-syn to produce hyperphosphorylated and ubiquitinated

aggregates. This resembles Lewy body like pathology observed in PD and other synucleinopathies. The inclusions co-localised with ubiquitin and molecular chaperones e.g. Hsp 70 and Hsp 90 indicating a reactive response for elimination and degradation of misfolded protein and the inclusions also disrupted the Golgi apparatus (Luk *et al.* 2009). It is conceivable that nuclei inititating aggregation in glial and neuronal cells may arise by copy number variations of α-syn, familial mutations (Devine *et al.* 2011, Houlden *et al.* 2012), C-terminal truncation of α-syn (Li *et al.* 2005), due to malfunctions of the protein quality control systems (Emmanouilidou *et al.* 2010b, Mullin *et al.* 2013) or external seeds may enter from surrounding cells (Emmanouilidou *et al.* 2010a). Further evidence for propagation of α-syn involving endocytosis and seeding was obtained in subsequent studies performed in cultured cells and also in *in vivo* animal models grafted with neurons (Angot *et al.* 2012). A working model of aggregation and transmembrane seeding has been outlined by Lashuel *et al.* as shown in **Figure 1.5.** below (Lashuel *et al.* 2013).

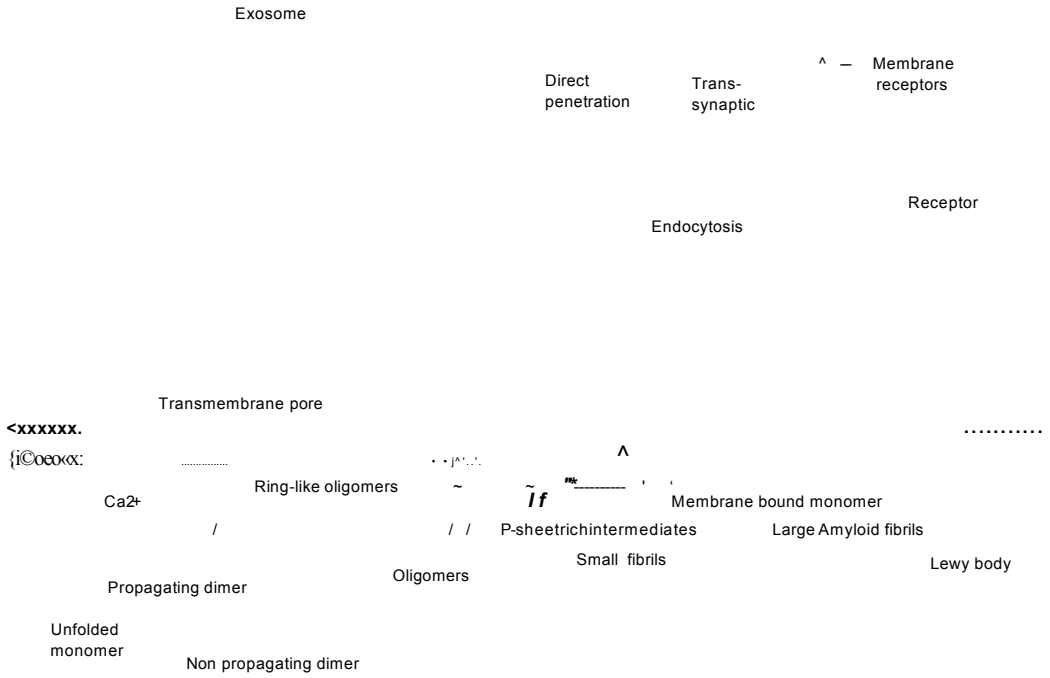

Figure 1.5. *Self-assembly and toxic mode of action of alternate a-syn species including pore formation and transmembrane propagation. Adapted by permission from Macmillan Publishers Ltd: Nature Reviews Neuroscience,* (Lashuel *etal.* 2013).

After a nucleation step, various types of oligomers with alternate morphologies are formed in the cytosol that are capable of converting to amyloid fibrils. Lewy bodies consist mainly of insoluble fibrillar a-syn. Meanwhile, membrane bound a-syn is chiefly a-helical, under certain conditions the protein undergoes a conformational transition that coincides with oligomerisation, yielding (3-sheet rich oligomers. These oligomers may be of several types i.e. transmembrane amyloid pores or ring-like assemblies. The mitochondrial functions, endoplasmic

reticulum (ER) and Golgi-trafficking, protein degradation and synaptic transmission could be affected due to the formation of these toxic, intermediate species. The appearance of ring-like structures results in dysregulation of Ca(II) homeostasis and signalling. Propagation of a-syn can progress via endocytosis, direct penetration, trans-synaptic transmission or by a receptor mediated mechanism of action leading to the spread of pathology (Lashuel *et al.* 2013).

1.5 Electrospray ionisation-ion mobility spectrometry-mass spectrometry (ESI-IMS-MS) for the study of non-covalent complexes

1.5.1 The advantages and utility of ESI-IMS-MS

The knowledge of the tertiary and quaternary structure of proteins and protein complexes is essential to better understand their functions and interactions in biological pathways and disease states. Using ion mobility coupled to mass spectrometry holds a great potential in structural biology due to its ability to interrogate the structure of heterogeneous complexes in near native conditions and to determine the respective overall geometry of individual components (Heck 2008). IMS measurements provide detailed structural information through calculation of rotationally averaged collisional cross sections (Q) (Ruotolo *et al.* 2008; Clemmer, D. E., Indiana University, Cross Section Database) that can be directly compared to NMR structures and crystal structure coordinates (Scarff *et al.* 2008). Thus IMS has recently become a powerful analytical tool well suited to characterising co-populated stereoisomers, chiral enantiomers and alternate protein conformers under varying conditions (Woods *et al.* 2012; El-Hawiet *et al.* 2012a).

An excellent use of this technique has been illustrated in an IMS analysis of the trp RNA binding protein complex (TRAP) that revealed an 11-membered ring morphology which could be maintained in the absence of bulk solvent. Furthermore, binding of tryptophan increased the stability of the ring structure and the structural collapse could be prevented by the binding of a specific mRNA molecule that had stabilised the assembly in solution and showed the largest Q (7400 A2) (Ruotolo *et al.* 2005). Several viral coat proteins self-assemble into capsids *in vitro* that are identical to virions *in vivo* supposedly through smaller transient oligomeric intermediates that might be technically difficult to monitor. Uetrecht *et al.* have successfully demonstrated that native IMS coupled to computational modelling is capable of elucidating the structural features of low abundance oligomers of Hepatitis B virus and norovirus under equilibrium (Uetrecht *et al.* 2011).

1.5.2 Technical considerations of ESI-IMS-MS

Regarding instrumentation, ESI-IMS-MS comprises of a nano-electrospray ionisation source, an ion funnel, a modified drift cell and a quadrupole mass filter. Ions are generated in the nano-spray source which creates a continuous beam of ions that are injected into an ion funnel that serves as an interface to the vacuum system. It is capable of converting the continuous ion beam into short ion pulses for Q measurements. Ions in the modified drift cell are thermalised by collisions with the He or N2 gas. The ions leaving the drift cell are analysed in a hybrid time-of-flight mass analyser by their mass-to-charge ratio (*m/z*) and detected to derive their respective arrival time distributions (ATD). By an equation described below ion mobility can be related to the Q and to the arrival time at the detector in the conventional instruments.

1.6 Drift time IMS-MS

Traditional drift time ion mobility spectrometry measures the time taken for an ion to migrate through buffer a gas in the presence of a low electric field. Ion mobility under low field conditions can be regarded as "directed diffusion" where the velocity of the ion *(v)* is directly proportional to the electric field (E) as follows *v=KE.* This proportionality constant is termed as the ion mobility constant (*K)* and is related to the Q as follows:

i i

Equation 1. *q is the charge on the ion, N is the number density of the buffer gas, k is the Boltzmann's constant, T is the absolute temperature, m is the mass of the buffer gas, M is the mass of the ion and* Q *is the collision cross section of the ion* (Revercomb *et al.* 1975).

The experimental Q which is buffer gas dependent can be compared to theoretical O derived from computational modelling or NMR strucutres and crystal structure coordinates (Scarff *et al.* 2008; Jurneczko *et al.* 2011). The fundamental principles of ion mobility have been laid down by von Helden, Bowers, Shvartsburg and Jarrold who evaluated and contrasted the suitability and limitations of different models for accurate mobility predictions using either the projection approximation, trajectory calculations (von Helden *et al.* 1993; Shvartsburg *et al.* 2008) and hard spheres scattering methods (Shvartsburg et al. 1996). In the travelling wave devices the electric field is not constant and the travelling wave of electric potential changes with both time and the length of the

drift tube, therefore correction parameters have to be adopted to derive the Q (Clemmer *et al.* 1997; Ruotolo *et al.* 2007; Ruotolo *et al.* 2008; Smith *et al.* 2009) as will be described in more detail in Chapter 4. Two types of operation modes have been developed based on the drift time ion mobility spectra: reduced pressure ion mobility spectrometry (RPIMS) and ambient pressure ion mobility (APIMS) (Kanu *et al.* 2008).

1.6.1 Travelling wave ion mobility mass spectrometry

A commercial development of ion mobility, Synapt HDMS, was first launched by Waters Technologies in 2006. This instrument has three stacked ring regions to propel ions through the device, a travelling wave consisting of a series of transient DC voltages is superimposed beyond the RF voltage. A second generation instrument, Synapt G2 HDMS, was launched in 2009 with a series of improved features in terms of sensitivity, mass accuracy, ion resolving power and data acquisition rate (Jurneczko *et al.* 2011).

Further details are discussed in the introduction of Chapter 4.

1.6.2 Field asymmetric waveform ion mobility spectrometry

In field asymmetric waveform ion mobility spectrometry (FAIMS) ions traverse between two electrodes in the presence of a tangential gas flow. The voltages applied to the electrode and the speed of the gas flow can be altered so that ions with a specific mobility transmitted through the device. Thus, one of the strengths of this equipment is that it is capable of separating ions from large proteomic mixtures specifically by their different mobilities at high and low voltage of electric field (Shvartsburg *et al.* 2010).

1.7 Ion mobility of monomeric a-syn

1.7.1 ESI-IMS-MS of a-syn depending on pH, different alcohols and copper in negative ion mode

Numerous recent ion mobility studies have aimed at defining the conformational forms of either WT or mutant a-syn under various conditions. Negative-ion ESI-IMS-MS analysis of a-syn at pH 7 resulted in a charge state distribution of -6 to -16, centered at -11 where ion mobility data suggested an extended morphology. In contrast, a narrow charge distribution was observed at pH 2.5, in the range of -6 to -11, centered at -8 indicating a more compact a-syn structure. Dimer peaks appeared at -17 to -21 with significant intensity when electrosprayed from 5 mM ammonium acetate (AA), pH 7 solution but not from pH 2.5 solution. It is estimated that the average O of a-syn at pH 7 is 2530 A2 corresponding to a relatively open structure, whereas the average Q is 1690 A2 at pH 2.5, corresponding to a more globular, compact structure (Bernstein *et al.* 2009).

Conformational transitions of a-syn induced by a range of alcohols and Cu(II) have been examined by Natalello and co-workers (2001) using a quadrupole time-of flight (QTOF) instrument (QSTAR-Elite, Applied Biosystems, Foster City, CA) equipped with a nano-ESI sample source in negative-ion mode. At pH 7.4, 12 pM a-syn dissolved in 10 mM AA showed a bimodal charge state distribution, predominantly with two main conformational envelopes, one with highest signals at -14 and -15 charge states corresponding to less compact forms and one with dominant charge states at -7 and -8, being an alternate conformer with a greater degree of compactness. According to previous

observations by far-UV-CD, alcohols can potentially inhibit fibrillisation by the formation of β-structure-enriched oligomers with high concentrations of methanol, ethanol, and propanol and lower concentrations of trifluoroethanol (TFE), or by the presence of a conformation with high α-helix content at high TFE and hexafluoro-2-propanol (HFiP) concentrations (Munishkina *et al.* 2003). This study confirmed that methanol as a co-solvent seemed to stabilise the more compact form in relation to the intermediate form, whereas HFiP promoted the appearance of a partially folded intermediate conformer with a -9 charge state, distinct from the compact and disordered states present at pH 7.4. High concentrations of TFE (~15 %) revealed the accumulation of a partially folded form with a charge of -12, and with further increments of TFE the protein transitioned into a homogeneous intermediate with a charge state centered at -11 charge state ions, which is consistent with earlier far-UV CD data (Munishkina *et al.* 2003).

The ability of metals, in particular Cu(II) to promote oligomerisation (Paik *et al.* 1999) and fibrillisation of α-synuclein has been established by employing several spectroscopic methods including CD, Tyr fluorescence (Uversky *et al.* 2001c) and NMR (Rasia *et al.* 2005). α-syn has multiple binding sites for Cu(II) with different binding constants and stoichiometry that are somewhat argued (Binolfi *et al.* 2006; Binolfi *et al.* 2008; Lee *et al.* 2008b; Hong *et al.* 2009; Valensin *et al.* 2011). In order to further analyse the interaction of α-syn and Cu(II), a titration with a range of 0-80 μM Cu(II) was performed in the presence or absence of glycine (Gly). Binding of Cu(II) resulted in the appearance of metal adducts and in a mass shift by the factor of 61.5 Da, implying that the binding of each Cu(II) ion (63.5 Da) repels two protons from the protein. Only the 1:1 Cu(II) to protein complex accumulated significantly in the presence of

Gly, suggesting the involvement of the more specific, high-affinity binding site for Cu(II). Furthermore, the data presented in this study indicated that the protein folding initiated by Cu(II) decreased the amount of the disordered conformer and caused a shift towards a highly compact, partially folded conformer (Natalello *et al.* 2011). The effect of Cu(II) was very substantial regarding both the shift of the dominant charge state from -15 to -8 and the stability of the more compact, bound protein (-45 %) as indicated by quantitation with Gaussian fitting (Dobo *et al.* 2001).

1.7.2 ESI-IMS-MS of WT and autosomal, dominant mutant forms of a-syn in negative mode

WT a-syn and its A53T mutant exhibited the existence of a compact, partially-folded family of structures with charges -6, -7 and -8. For the A30P mutant, this compact form was only apparent when the protein possessed a net charge of -6 (Grabenauer *et al.* 2008). Spermine is a naturally present polyamine involved in neuronal cell proliferation, differentiation, and modulation of ion channel receptors (Gilad *et al.* 1991). It forms a complex with a-syn under physiological conditions without significantly affecting the secondary structure and enhances the rate of fibrillation of a-syn (Antony *et al.* 2003). Evidence from NMR data suggested that although spermine binds specifically to the C-terminal of the a-syn (aa109-110), it induces changes in the N-terminal in the proximity of Gly and Tyr residues in the region of aa 22-93 and it leads to adoption of a (3-sheet conformation (Fernandez *et al.* 2004) typical of fibrillar a-syn. Notably, these two mutant forms harbour an amino acid substitution in the latter region and were therefore chosen to be subjected to investigations. Upon binding to spermine, all three proteins experienced a structural collapse, causing a charge state

reduction from -10 to -6 at pH 7.5 that indicated a Q reduction from 2600 Å2 to 1430 Å2, respectively. It appears possible that spermine increases the aggregation rate of a-syn by a structural collapse as observed with metals which subsequently gave rise to formation of aggregates (Grabenauer *et al.* 2008).

1.7.3 ESI-MS acquisitions at various pH and alcohol contents reveal four conformational families of monomeric a-syn

ESI-MS data has indicated that a-syn populates four different conformations characterised by varying degree of compactness that co-exist under equilibrium (Frimpong *et al.* 2010). Charge state distribution analysis under various conditions demonstrated distinct, partially folded forms that accumulated in response to environmental conditions. For example, the most compact form, was represented under all conditions examined in this work including pH from 2.5 to 10 and its presence was exceptionally abundant at low pH and upon addition of 10 % to 60 % alcohol. Its solvent-accessible surface area is approximately 7.3x 10 Å2 using estimates developed by the Kalthasov laboratory (Kaltashov *et al.* 2005). A further intermediate conformer was also found to populate all conditions assessed. Another, second intermediate conformation showed a moderate contribution under most conditions but was pronounced at high concentrations of ethanol and presumed to have folded p-strands. The unstructured conformation was not prominent but became observable as the pH increased, then in the presence of ethanol but not TFE its population decreased at high pH. Beside the monomeric features, the ESI spectra was comprised of non-covalent features, a-syn dimers that displayed a narrow charge state distribution clustering around +11 charge state ion at pH

2.5, in contrast at higher pH >4, the charge state distribution became broad with ions from +13 to +26. This study demonstrated the enrichment of particular conformational forms of a-syn in response to alternate concentrations of alcohols and pH (Frimpong *et al.* 2010).

1.8 Ion mobility to study amyloid formation

1.8.1 Collisional cross section and *in silico* calculations aid structural determination of heterogeneous assemblies

Understanding the morphological and biochemical properties of soluble protein or peptide aggregates is critical to developing rational diagnostic and therapeutic strategies for amyloid disease. The transition of globular conformations into (3-sheet is closely linked to cytotoxicity. However, details of the folding pathways that govern the assembly of soluble oligomers indicated in the pathogenesis of amyloid diseases including PD, AD or Type 2 diabetes have only started to be unravelled within the last decade. IMS-MS allows the isolation and study of transient and dynamic oligomers at an early stage in the gas phase. This is permitted only to a limited extent by using traditional biophysical methods due to the low concentrations of these small, heterogeneous species that are often transient in nature and co-exist in solution (Figure 1.6.). Key to the usefulness of the system is the ability to determine both the mass of a given protein or complex as well as its conformational states through calculation of its *Ω*. The development of ESI-IMS-MS and its applications to a range of biomolecular molecules and complexes have recently been reviewed by Uetrecht *et al.* (Uetrecht *et al.* 2010) and instrumentation reviewed by Kanu and Hill (Kanu *et al.* 2008). Where the structure of the protein

or complex is unknown as in the case of the amyloid oligomers, *in silico* algorithms have been developed to predict the O from model protein structures allowing the 3 D conformation of known protein complexes to be determined (Ruotolo *et al.* 2005; Ruotolo *et al.* 2005; Bernstein *et al.* 2009; Smith *et al.* 2010; Politis *et al.* 2013). In order to obtain this structural information intuitive models guided by experimental data or molecular structures obtained from molecular dynamics simulations are created and the theoretical Q determined. This value is then compared with the experimentally determined Q. Fragmentation techniques of selected ions such as Collision Induced Dissociation (CID) and Electron Transfer Dissociation (ETD) are also proving to be invaluable methods to gain topological information (Beardsley *et al.* 2009).

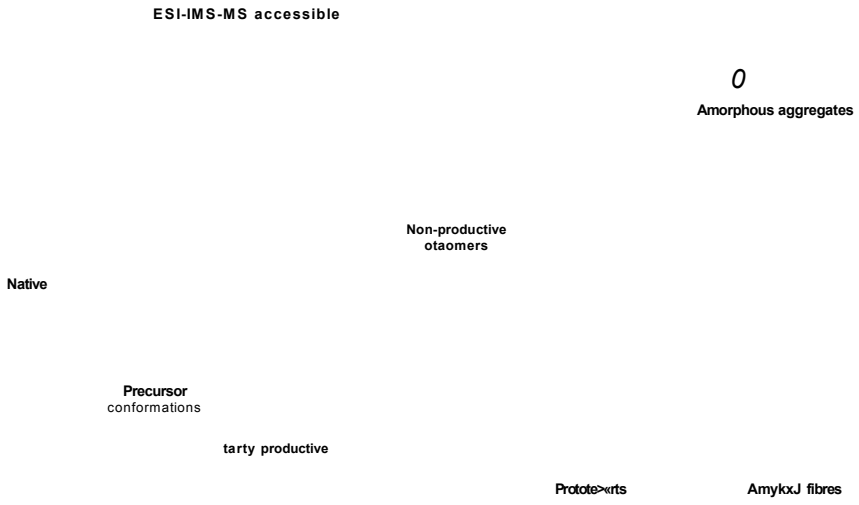

Figure 1.6. *A simplified schematic representation of amyloid formation and the role of early precursor conformations and oligomeric states in assembly. A number of possible aggregation pathways of the native monomer are shown, leading to the formation of amorphous aggregates (green), non-productive off pathway oligomers (blue), amyloid fibrils with alternate morphology assembled from differing intermediates (orange and red). Image adapted from Chiti and Dobson* (Chiti *et al.* 2006).

The area shaded in Figure 1.6. (Chiti *et al.* 2006) with grey colour is readily available to ESI-IMS-MS based experimentation. Conformational change within the monomer leads to a range of precursor conformations. The conformation of these precursors dictates the assembly pathway leading to soluble oligomers and larger order insoluble aggregates.

1.8.2 ESI-IMS-MS study of synthetic amyloidogenic peptides

Bleiholder and colleagues have demonstrated that globular peptide oligomers convert into peptide fibrils rich in (3-sheet contents as analysed by ESI-IMS and AFM (Bleiholder *et al.* 2011). This study examined the structural transitions of a selection of peptides such as NNQQNY from amyloid-forming yeast prion protein Sup35, VEALYL from insulin and SSTNVG from IAPP with known X-ray structures that in addition to an internal control Leu-enkephalin (YGGFL). Macroscopic granular aggregates were seen for NNQQNY and SSTNVG, whereas fibril formation was observed for VEALYL, NNQQNY and SSTNVG. YGGFL formed only granular structures and no fibrils as judged by AFM microscopy. All the amyloid-forming peptides clipped from larger peptides or proteins showed pronounced oligomerisation under the IMS-MS conditions. IMS-MS experiments performed on the NNQQNY peptide gave a direct demonstration of how a globular peptide converts into (3-strand conformation. IMS-MS analysis demonstrated that single strand fibril growth proceeded isotropically from dimer to pentamer which then transitioned near the nonadecamer stage into a more ordered (3-pleated sheet. The *Q* obtained during ESI-IMS experiments helped to discern significant differences in the

early growth phase of these peptides at the level of one monomer addition at a time (Bleiholder *et al.* 2011).

1.8.3 ESI-IMS-MS analysis of p2 microglobulin

p2 microglobulin is a 99-residue protein that forms the light-chain of the class-I major histocompatibility complex (MHC-I). It is constantly shed from cells displaying MHC-I and carried by the bloodstream to the kidney to become finally degraded (Saper *et al.* 1991). In case of renal failure, the clearance of p_2 microglobulin is impaired and its level can be up to 50 fold elevated in the plasma. The aggregation of p2 microglobulin into amyloid material is closely associated with dialysis-related amyloidosis (Gorevic *et al.* 1986). P_2 microglobulin accumulates in skeletal joints, collagen-rich tissues, attracting monocytes and macrophages, subsequently leading to destructive athropathy, bone destruction and carpal tunnel syndrome as unwanted complications of long-term hemodialysis (Heegaard 2009). *In vitro,* P_2 microglobulin assembles in a nucleation-dependent fashion under acidic conditions, at pH 2.5 and low ionic strength, giving rise to long straight (LS), fibrils (McParland *et al.* 2000). Analysis of p2 microglobulin oligomers at acidic conditions has been undertaken by Smith *et al.* (Smith *et al.* 2010). The in-depth characterisation of different species by ESI-IMS-MS revealed that monomers to tetramers were populated through the lag phase of fibril growth with no apparent higher order conformers under the conditions employed as displayed in Figure 1.7.,

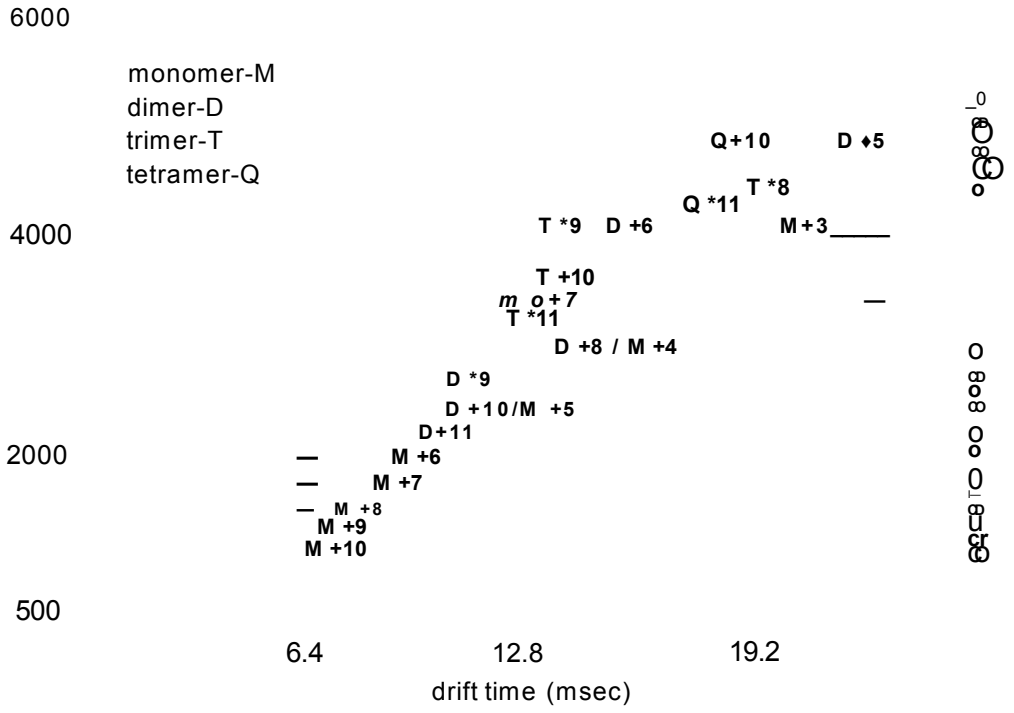

Figure 1.7. *Mobility plot and mass spectrum (on the right) of p2m (pH 2.5) at 1 min into lag time of fibril assembly. M-monomer, D-dimer, T-trimer, and* Q-*tetramer with associated charge states. The scaling is shown in square root and log as marked. The x axis represents drift time (msec) and on the y axis m/z is shown. Adapted by permission from National Academy of Sciences of the United States of America,* (Smith *et al.* 2010).

The dimers observed here appeared to be compact species when compared to theoretical structures with smaller Qs than predicted for elongated features. Experimental Os of trimers and tetramers were larger than would be expected for globular proteins of the same mass as the oligomers, suggesting they were not spherical but rather stacked, elongated assemblies. The dynamics of each oligomeric species in the ensembles were also examined by monitoring the subunit exchange of ^{14}N- and ^{15}N labelled oligomers. This showed a decrease in oligomer dynamics concomitant with increasing oligomer size. Differences in

the behaviour displayed by the trimer ions of different charge states indicated the presence of two populations: a more highly charged, faster exchanging conformer populated at the early stages of aggregation and a less charged, more stable conformer that became prevalent later on. These trimeric forms preceded tetramer formation and no higher order oligomers were observed during the lag phase of assembly. These results have shed light on the size, mass, molecular organisation and stability of of p2 microglobulin oligomers. It has been also shown that oligomerisation of p2 microglobulin progressed by stacked oligomer addition at the early phase of aggregation (Smith *et al.* 2010).

1.8.4 ESI-IMS-MS analysis of Ap

Alzheimer's disease (AD) is the most common neurodegenerative disorder in which amyloid plaques of Ap and the neurofibrillary tangles of Tau are cardinal features. Soluble oligomers of Ap have been associated with synaptic dysfunction and neuronal loss (Lesne 2013). Ap40 and Ap42 peptides arise due to alternate proteolytic cleavage of the amyloid precursor protein (APP) by gamma-secretases (Sinha *et al.* 1999). The balance of Ap40 to Ap42 has been demonstrated to be critical to the progression of AD. Ap42 is predominately linked to the disease state and has a higher tendency to aggregate (Mondragon-Rodriguez *et al.* 2010). Identification and characterisation of Ap oligomers has been an active area of research in which ESI-IMS-MS has made a significant contribution (Bernstein *et al.* 2009; Gessel *et al.* 2012; Hyung *et al.* 2013). One of the first ion mobility experiments gave insights into the structural differences of Ap40 and Ap42 oligomers. Arrival time distributions (ATD) for solutions where Ap40 and Ap42 were co-populated suggested that the AP40 form of the peptide may inhibit amyloid formation of the Ap42 form (Jan *et al.*

2008). Analysis of the -5 dimer peak for A(340 showed that this charge state was co-populated by both dimeric and tetrameric forms, whereas the same charge state for Ap42 populated di-, tetra-, hexa- and dodecameric forms as shown in Figure 1.8. (Murray *et al.* 2009a).

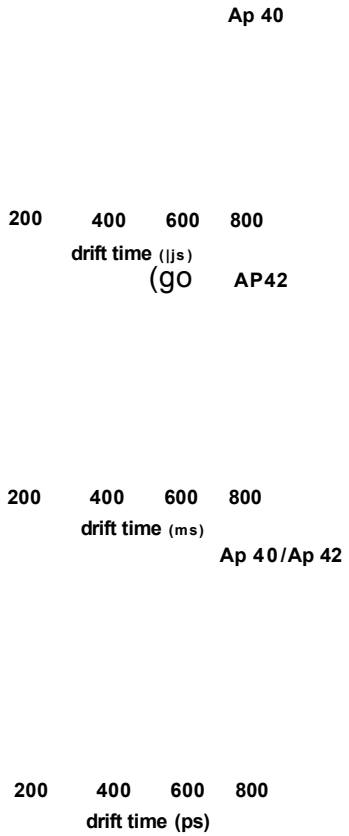

Figure 1.8. *ATDs (in IJS) of the -5 charge state of various A/3 peptides; (predominantly dimeric peak co-populated with higher order oligomers). A: A/340 (dimeric and tetrameric populations present), B: A/342 (dimeric, tetrameric, hexameric and dodecameric forms are observed) and C: A/340/A/342 (dimers and tetramers are seen). Adapted with permission from (Murray et al. 2009a), American Chemical Society.*

The ATDs for the dimeric and tetrameric forms of the two peptide forms differed in that the A(342 forms had taken longer to traverse the drift tube, indicating more expanded conformations. Notably, a mixture of dimers (-5 charge state) and tetramers (-10 charge state) could be observed only at the 1:1 ratio of Ap40/Ap42 and not for the 3:1 and 1:3 ratios, indicating that oligomer formation proceeded by dimer condensation rather than sequential monomer addition and that Ap40 can theoretically prevent aggregation at the tetrameric stage. Interestingly, trimers of Ap were not reported in this study (Murray et al. 2009a). Bernstein *et al.* have speculated that tetramers of Ap40 and AP42 determine the dynamics of assembly. Moreover, one of the larger, dodecameric (12-mer) species of 55.2 kDa that is a stack of two hexamers may be a previously identified neurotoxic species (Bernstein *et al.* 2009). This was observed in middle aged Tg2576 transgenic mice, had a corresponding mass and was referred to as Ap*56. It was shown to cause memory deficits when administered to young rats (Lesne *et al.* 2006).

1.9 Main objectives

Overall aim

The hypothesis was that alternate oligomeric forms of a-syn with toxic gain of function have alternate structures. The main interest was focused on the formation of small, toxic oligomers that still lack detailed structural determination regarding their size, shape and compactness. Here, previously described *in vitro* a-syn oligomeric preparation protocols have been modified to make oligomers suitable for ESI-IMS-MS analysis. Structural characterisation was then undertaken through determination of their respective subunit sizes and

assignment of their molecular organisation via Ω measurements. In conjunction with the native mass spectrometry measurements, the biochemical and functional properties of these oligomers were elucidated by using a variety of biochemical and cell culture based assays.

The specific goals were:

i. to investigate the biochemical characteristics and biological properties of alternate oligomeric forms by using an array of biochemical methods and assays in a SH-SY5Y cell culture model.

ii. to develop methods for the production of oligomers suitable for ESI-IMS-MS investigation by altering previously published *in vitro* oligomerisation methods of recombinant α-syn either in the presence or absence of metal ions.

iii. to ascertain the size, shape and foldedness of the pre-fibrillar oligomeric species using native mass spectrometry and to view these findings in the context of biophysical and biochemical characteristics to reveal structure and function relationships of α-syn oligomers.

iv. to address the immediate effects of binding partners on the conformational forms of natively unstructured monomeric protein by ESI-IMS-MS with potential implications in its self-assembly.

2 Chapter 2

Materials and Methods

2.1 Protein biochemistry and spectroscopy

2.1.1 Transformation of competent BL21 DE(3) cells with pET23a+ containing WT a-syn and preparation of glycerol stock

Luria Broth (LB) media was made by dissolving 10 g Bactotryptone (Fisher, BPE1421-500), 5 g yeast extract (Oxoid, LP0021) and 10 g NaCl (Fisher, S/3120/60) in 1 L ultrapure water and sterilised. BL21 (DE3) competent cells (Agilent, 200121) were thawn out on ice. Three reactions were set up: 2 pL of the plasmid containing WT a-syn insert was added to 50 pL of the cells, 1 pL of the plasmid DNA with a-syn added to 50 pL competent cells and 50 pL competent cells only. The reaction mixtures were agitated gently a few times over a 30 min incubation period at room temperature. After this step, the different samples were exposed to 45 sec heat shock in a 42 °C water bath and returned to ice for 5 min. 500 pL sterile LB media was added to each tube and incubated for 1 hr at 37 °C 200 rpm shaking to allow the bacteria to express antibiotic resistance. After 1 hr growth, the cells were centrifuged at 10, 000 rpm for 5 min and the supernatant was removed. The -100 pL pellet was resuspended and split into two halves, -20 pL and the remainder -80 pL of each reaction mix were spread out on agar plates containing 100 mg/mL ampicillin (Fisher, FL-04-0406) for selection. The plates were placed into 37 °C

incubator overnight and colonies were observed the next day after transformation apart from control plates inoculated with competent cells only.

Subsequently, single colonies were picked and inoculated into 50 mL LB media containing 50 pL of 100 mg/mL ampicillin solution and grown overnight at 37 °C at 200 rpm shaking. 10 mL of overnight culture was then used to seed 100 mL LB supplemented with 100 mg/mL ampicillin and the OD_{600} was monitored by the Jenway 6715 UV/Vis Spectrophotometer and bacterial culture was grown until it reached an OD_{600}~ 0.40-0.45 value. Cells were then harvested at 4, 000 rpm and 4 °C for 10 min and the resultant pellet was resuspended in 10 mL sterile, prechilled 100 mM M $CaCl_2$ (BDH, 275844L). Tubes were incubated on ice for 10 min and centrifuged again as before followed by resuspension of the pellet in 2 mL 100 mM $CaCl_2$ and 30 % v/v glycerol (Sigma, G5516) and division into 100 pL aliquots, snap freezing at -80 °C for further long term storage.

2.1.2 Qiagen plasmid miniprep kit

Plasmids from overnight cultures were extracted by using the QIAgen Midiprep kit (Qiagen, 12143). The procedure was carried out following the manufacturer's recommendations. The plasmid maintaining a-syn was aliquoted out and frozen down at -20 °C for further use. The plasmid containing the insert was sent for sequencing for confirmation of the open reading frame. The size of the extracted plasmid was also assessed by 1 % agarose gel electrophoresis and and purity was estimated by calculating the OD_{260} and OD_{280} ratio (ideally between 0.1-1.0) from values measured on the NanoDrop spectrophotometer.

2.1.3 Agarose gel electrophoresis

10x TAE buffer was prepared by mixing and dissolving 24.2 g Tris base (Sigma, T1503), 5.71 mL glacial acetic acid (Sigma, A6283), 10 mL 0.5 M ethylenediaminetetra-acetic acid (EDTA) (Sigma, ED S) in 500 mL total volume of distilled water. 1 % agarose gels were prepared by mixing 1 g agarose (Fisher, BP1356-1 OOg), 49 mL ultrapure water, 1 mL 1x TAE buffer, microwaved to dissolve the solution and after it cooled down ethidium bromide (Sigma, E7637) was added to a 5 pg/mL final concentration from a 10 mg/mL stock and poured to cast 10-12 mm thick gels. DNA samples were diluted into a 6x gel loading buffer (Thermo Scientific, R0611). 5 pL of 1 Kb GeneRuler™ DNA ladder (Thermo Scientific, SM0314), 100 bp GeneRuler™ marker (Thermo Scientific, SM0241) and samples with a DNA content of 100 ng- 1 pg per lane were loaded for electrophoresis. The agarose electrophoresis tank was filled with 1X TAE buffer containing and ran at 100 V for 1 hr.

2.1.4 a-syn protein overexpression in *E. coli* and purification by anion exchange and size exclusion

BL21 (DE3) *Escherichia coli* competent cells (Agilent Technologies, 200121) were transformed with pET 23 a+ vector containing the human WT a-syn sequence. A 50 mL culture was grown overnight and 10 mL of that was inoculated into 1 L LB containing 100 mg/mL ampicillin for large scale expression. Protein expression was induced at OD_{600} 0.6 with 1 M isopropyl (3-D-1-thiogalactopyranoside (IPTG) (Fisher, BP1755) for 3 hr. Cells were harvested by centrifugation at 10,000 rpm at -20 °C and the pellet was

resuspended in a lysis buffer containing 10 mM Tris-HCl, pH 8.0, lysozyme (100 µg/mL) (Sigma, L6876), 1M phenylmethylsulphonyl fluoride (PMSF), DNase (20 µg/mL) (Sigma, D4263), RNase (20 µg/mL) (Sigma, R6512) and incubated for 30 min before the addition of 1 mM EDTA. Cells were further lysed by sonication. The lysate was centrifuged at 10, 000 xg for 40 min to remove debris and the supernatant was acidified to pH 4.5, centrifuged again at 10, 000 xg for 30 min to remove the aggregated protein that was followed by a final neutralisation step at pH 8.0. The crude lysate was injected onto a 50 mL Q-Sepharose column (GE Healthcare) for anion exchange at 4 ^{0}C. Prior to that the column was equilibrated with two column volume of buffer A (25 mM Tris-HCl, pH 8.0), then the protein was eluted with a 0-100 % linear gradient of buffer B (25 mM Tris-HCl with 1 M NaCl, pH 8.0). α-syn eluted at ~ 300 mM NaCl concentration point of the gradient. SDS-PAGE analysis of Q-Sepharose fractions was performed and the fractions enriched for α-syn were pooled. The collected fractions were dialysed extensively at 4 ^{0}C in ultrapure water and the freeze-dried. The lyophilised protein was redissolved and passed over a High Load 26/90 SuperdexTM 75 Prep Grade size exclusion column (Amersham Biosciences) using 20 mM Tris and 25 mM NaCl, pH 8.0 as running buffer. The pooled and purified fractions were dialysed repeatedly, re-lyophilised and stored at -80 ^{0}C for further experiments. Protein concentration was measured by absorbance at 280 nm with extinction coefficient 5960 $M^{-1}cm^{-1}$ on a Jenway 6715 UV/Vis Spectrophotometer. Samples of the protein were analysed by ESI-MS to ensure the correct mass.

2.1.5 Production of a-syn oligomers

All oligomers were prepared as described by Danzer *et al.* previously (2007) unless otherwise stated (Danzer *et al.* 2007). To make oligomers suitable for ESI-IMS-MS analysis sodium phosphate (SP) buffer has been replaced with 50 mM AA (Fisher, A/3440/50), pH 7.0.

Type A oligomers were prepared by dissolving lyophilised protein in 50 mM SP (500 mL 50 mM SP buffer was prepared by mixing 1.038 g sodium phosphate monobasic (Sigma, S1001) and 2.3 sodium phosphate dibasic (Sigma, S2002) in deionised water) or AA, containing 20 % ethanol to a final concentration of 7 pM. In case of type A2 oligomers, 10 pM $FeCl_3$ (Sigma, F7134) were additionally added, whereas type A1 oligomers were prepared without addition of $FeCl_3$. After 4 hr of shaking, both types of oligomers were re-lyophilised and resuspended with one-half of starting volume in 50 mM SP or AA buffer, pH 7.0, containing 10 % ethanol (Fisher, M/4450/17). This was followed by shaking for 24 hr (Thermomixer, Eppendorf, Germany) at 21 °C with open lids to evaporate residual ethanol. After 6 day incubation of both oligomers types with closed lids at 21 °C, oligomers were used for characterisation by a combination of techniques.

Type C oligomers were (spin concentration protocol) also prepared similarly to type A oligomers by dissolving lyophilised protein in 50 mM SP or AA, pH 7.0, containing 20 % ethanol to a final concentration of 7 pM. In case of type C2 oligomers, 10 pM $FeCl_3$ was added, whereas type C1 oligomers were prepared without addition of $FeCl_3$. After overnight incubation at 21 °C under continuous shaking (Thermomixer, Eppendorf, Germany), the oligomers were concentrated

and separated from monomer using a MWCO 30 kDa filter (VivaSpin500 30,000 MWCO columns; Sartorius). In an attempt to make Cu(II) induced oligomers 10 pM $FeCl_3$was replaced with 10 pM $CuCl_2$for both type A and C oligomers.

2.1.6 Size exclusion chromatography

For size exclusion chromatography the GE Healthcare 10/300 GL column was used (Amersham Biosciences). Instrument was operated by the Unicorn software. Separation of different components were achieved by flushing the column with either degassed 50 mM AA or SP followed by direct injection of samples (30-100 pL) into the injection port and by elution at 0.100 mL/min flow rate. 500 pL samples of fraction of interest were collected and solvent evaporated under a SpeedVac freeze drier. Typically, oligomeric peaks were eluted in 2 or 3x 500 pL fractions per 50-100 pL injection. For an estimation of molecular weight compared to globular proteins in a range of -12.5 kDa- 2000 kDa, a Gel Filtration Molecular Size Standards kit was utilised (Sigma, MWGF-200-1KT) and the elution volumes have been plotted.

2.1.7 SDS PAGE

Running buffer was prepared by mixing 25 mM Tris-HCl (Sigma, T5941), 250 mM glycine (Fisher, BP-381-1), pH 8.3, 0.1 % w/w SDS (Sigma, L3771) in 1 L deionised water. Reagents purchased for SDS gel included tetramethylethylendiamine (TEMED) (Sigma, 9281), ammonium persulfate (APS) (Sigma, A3678) and acrylamide bis acrylamide (Sigma, A2917-1L)

Solution component	Added volume for resolving gel (mL)	Added volume for stacking gel (mL)
30 % acrylamide	3.75	0.415
ultrapure water	1.7	1.7
1.5 M Tris-HCl pH 8.8	1.9	-
1 M Tris-HCl pH 6.8	-	0.315
10 % w/w sodium dodecyl sulfate	0.075	0.025
10 % w/w APS	0.075	0.025
TEMED	0.003	0.0025

Table 2.1. *Components of 10 % SDS gel shown for the resolving and stacking gel.*

Glass plates were assembled according to the manufacturer's instructions. The resolving gel was cast first and allowed to polymerise followed by pouring the stacking gel (**Table 2.1.**) and by inserting a comb for the formation of wells. Samples were diluted 1:5 with 2x NuPage SDS Sample buffer and electrophoresed in 1 x Tris-Glycine running buffer at constant voltage of 150 V. To aid molecular weight determination, 5 µL SeeBlue Plus 2 molecular weight marker (Novex, LC5925) was loaded. Gels were stained in either Instant Blue (Expedeon, ISB01L) for 30 min or in Coomassie stain containing 0.25 % w/v Coomassie Brilliant Blue R250 (Thermo Scientific, 6104-59-2), 50 % v/v methanol (Fisher, M/4056/17), 10 % v/v acetic acid and 40 % v/v ultrapure water for 2 hr. Destaining was performed with ultrapure water for Instant Blue and with a destaining solution comprised of 50 % v/v methanol, 10 % v/v acetic acid and 40 % v/v ultrapure water for Coomassie until background was reduced and bands became visible. Gel images were captured on an Epson flatbed scanner.

2.1.8 Native gels

For clear native electrophoresis, 12 % Tris Glycine gels (EC60052BOX) were electrophoresed in 10-fold diluted Tris-Glycine Native Running Buffer 10x (Novex, LC2672). 5 µL volumes of samples were mixed with 5 µL 2x Native Tris Glycine Sample Buffer that had previously been prepared by mixing 100 mM Tris-HCl, 10 % v/v glycerol, 0.0025 % w/v Bromophenol Blue, pH 8.6. Unstained NativeMark (Invitrogen, LC0725) was loaded for an estimation of molecular weight.

Samples were electrophoresed on Novex NuPAGE® Tris-Acetate gels under native conditions according to the manufacturer's instructions. All samples were loaded in 1X Tris-Glycine Native Sample buffer composed of 100 mM Tris-HCl, 10 % glycerol, 0.0025 % Bromophenol blue at pH 8.6 and electrophoresis was performed in 10x Tris-Glycine Native Running Buffer (Novex, LC2672) diluted to 1x at 150 V constant until the front of the blue dye reached the bottom of the gel.

Blue Native PAGE was performed using 10 % Bis-Tris gels (Novex, NP0302BOX). Samples were prepared in the Native Sample Prep kit (Invitrogen, BN2008) containing G250 additive. Unstained NativeMark (Invitrogen, LC0725) was loaded for an estimation of molecular weight (0.5 µL Unstained NativeMark ladder mixed with 2.5 µL 4x Sample Buffer and 0.5 µL G250 additive and 6.5 µL deionised water). For the outside chamber, Native Page 20X Running Buffer (Invitrogen, Anode Buffer BN2001) diluted to 1X was used, while for the inside chamber the Native Page 20x Cathode Buffer

(Invitrogen, BN2002) was used diluted and prepared according to the manufacturer's instructions and electrophoresed at 150 V constant.

At non-native conditions, 10 % Bis-Tris Novex gels were also electrophoresed using 20x MOPS running buffer (Novex, NP0001) diluted to 1x where samples were prepared in NuPage 4x (Novex, NP0007) Sample Buffer.

2.1.9 Silver staining

Silver staining of both native and non-native gels was performed by using the ProteoSilver TM2 kit (Sigma, Protosilkit2) following the manufacturer's instructions with minor modifications. Images were taken on an Epson flatbad scanner.

2.1.10 Dot blotting procedure

1 pL of each oligomer, a-syn monomer or BSA was pipetted onto nitrocellulose membrane and air dried before the addition of 2 % BSA blocking solution in PBS for 30 min. After blocking an adequate volume of primary antibody was added diluted in PBS-T containing 10 % blocking solution. The PBS-T buffer constituted of 8 g NaCl, 0.2 g KCl, 1.44 g Na_2HPO_4 and 0.24 g KH_2PO_4 and 1 mL Tween 20 (Sigma, P1379) in 1 L, pH 7.2 solution. The range of commercially available antibodies used were: syn 211 anti-a-syn mouse antibody (epitope aa 121-125, Life Technologies, AHB0261) at dilution 1:500, A11 anti-amyloid oligomeric rabbit polyclonal antibody (epitope: n/a; oligomeric; Millipore, AB9234) at dilution of 1:1000. The in-house antibodies used in these experiments were a kind gift from Prof R. Cappai (University of Melbourne) as listed below:

1. anti-a-syn rabbit polyclonal, 3rd bleed, 1:50,000 dilution
2. 45/08 5G7-1 mouse monoclonal, epitope: EAYEMP, 4.0 mg/mL, 1:30, 000 dilution
3. 31/09 4H4-14-27-12 mouse monoclonal, epitope: KKDQLGK, 1.8 mg/, 1: 20, 000 dilution
4. 35/10 7D2 (immunised with AS3X peptide, H-M[Ox]DVFM[Ox]KGLSKAKC-OH; Met 1 and Met 5-oxidised) mouse monoclonal, 1.78 mg/mL, 1:400 dilution

For detection of antibodies raised in mouse, goat anti-mouse IR DyeR 680 LT IgG (H+L) fluorescent secondary antibody (Odyssey, 926-68020) was utilised at 1:20, 000 dilution. For detection of epitopes recognised by the full anti a-syn rabbit polyclonal antibody, goat anti-rabbit IR DyeR 800 CW IgG (H+L) fluorescent secondary antibody (Odyssey, 926-32211) was used at 1:15, 000 dilution.

2.1.11 Western blotting

After electrophoresis, SDS gels or 10 % Bis-Tris non-native precast Novex gels were transferred onto Immobilon FL PVDF membrane, 0.45 pM pore size (Milipore, IPFL20200). SDS PAGE gels were transferred in 1x Tris Glycine transfer buffer consisting of 20 mM Tris-HCI, 150 mM glycine and 20 % v/v methanol and 0.038 % w/v SDS in 1 L deionised water, whereas precast gels were transferred in chilled, 20-fold diluted NuPage Transfer Buffer 20x (NP0006-1) containing 20 % v/v methanol at a constant of 150 V for 90 min. The membrane then was treated with 0.4 % paraformaldehyde (PFA) (Sigma, 441244) for 30 min at room temperature except for membranes probed with

anti-amyloid, A11 antibody (Millipore). The membrane was then blocked with 2 % BSA or 5 % blocking grade blocker (Biorad, 170-6404) in PBS. Blocking was followed by incubation with the appropriate primary antibody in PBS-T with 10 % v/v of blocking solution for 1 hr at room temperature or overnight at 4 °C. As primary antibodies, syn 211 anti-a-syn mouse antibody at dilution 1:500 or A11 anti-amyloid oligomeric rabbit polyclonal antibody at dilution of 1:1000 or full length anti-a-syn rabbit polyclonal antibody at 1:50, 000 (gift of Prof R. Cappai, University of Melbourne) were used. After washing at least 3 times for 10 min with PBS-T, the membrane was incubated for 1 hr with an appropriate secondary antibody for fluorescent detection on the Licor system.

2.1.12 ThT assay and dot blotting to monitor fibril formation

70 pM a-syn (1 mg/mL) was dissolved in 50 mM AA or SP at pH 7.1 and shaken at 200 rpm at 37 °C. Fibril growth was monitored by taking daily aliquots for 7 days. For seeded fibril formation measurements, 10 % or 20 % v/v of oligomers were added to the 70 pM monomeric mixture at day 0 and fibril formation was monitored by taking daily aliquots over 7 days to perform Thioflavin T (ThT) assay. 1000 pM stock solution of ThT (Sigma, T3516) was made fresh in ultrapure water on the day of the assay and diluted to a 100 pM end concentration in either 50 mM AA or SP. To 100 pL of ThT reagent 20 pL sample of the various groups was added in a black 96 well plate and fluorescence intensity was measured between wavelengths of 350-600 nm at 5 sec intervals at 0.5 mm slith width. The fluorescence values from triplicate measurements have been averaged and expressed as a percentage of ThT

buffer only at 382 nm wavelength. For emission scan of only mature fibrils and monomeric protein the samples were dissolved in 20 mM Tris buffer at pH 7.2.

Aliquots were obtained on each day of the experiment to perform dot blotting with anti-amyloid fibrils LOC rabbit polyclonal antibody (Millipore). 1 pL of each sample was spotted onto nitrocellulose membrane and air dried before blocking with 2 % BSA (Fisher, A/1278/46). Following blocking, the rabbit anti-amyloid fibris LOC antibody (Millipore, 2197267) was added at 1:1000 dilution and incubated on a shaker at room temperature for 1 hr. Subsequently, the membrane was rinsed three times for 15 min with PBS-T and then it was incubated with the secondary goat anti-rabbit antibody IR DyeR 800 CW IgG (H+L) (Odyssey, 926-32211). The fluorescence signal was detected by using the Licor system employing the 700 nm, green channel.

2.1.13 1-Anilinonaphtalane-8-sulphonic acid (ANS) fluorescence

ANS (Sigma, A1028) was dissolved to a final concentration of 25 pM in 50 mM AA or 50 mM SP and to 100 pL of ANS solution 20 pL of the respective sample of oligomers or monomeric a-syn was added in a black 96 well plate. For all alternate samples measurements were performed in triplicate. For excitation, 385 nm wavelength was used and the emission scan was recorded between 400-600 nm on the Tecan Infinite M200 plate reader. All values of triplicate measurements were averaged, expressed as mean±standard deviation (SD) and normalised to ANS only.

2.2 Cell culture techniques

2.2.1 Maintaining and cryopreserving SH-SY5Y neuroblastoma cells

SH-SY5Y human neuroblastoma cells were maintained and grown in complete Dulbecco's modified Eagle medium (CDMEM) consisting of 500 mL DMEM+ GlutaMAX™ -II (Gibco, 804781), 50 mL fetal bovine serum (Biosera, heat inactivated, qualified , S06908S1900), 5 mL Pen Strep (Penicillin Streptomycin, 5000 units/mL penicillin, 500 pg/mL streptomycin, Gibco, 15070) up to a maximum of 20 passages. The identity of the cell line was confirmed by a 16 loci Cell Line Authentication certificate. Transient transfection and then a stable transfection with the familial A53T mutant was kindly established by Mafalda Ramos (Erasmus Programme). Overexpression of the A53T mutant was confirmed by immunocytochemistry and Western blotting. SH-SY5Y neuroblastoma cells overexpressing the the A53T a-syn mutant were maintained in CDMEM with 200 pg/mL selective G418 antibiotics (Sigma, G8168-10 mL). A freezer stock of both SH-SY5Y neuroblastoma cells and SH-SY5Y cells overexpressing A53T was deposited for long term storage in liquid nitrogen dewars. The freezing procedure involved obtaining a -300 pL homogeneous cell suspension in CDMEM to which culture media comprising of 30 % v/v dimethyl sulfoxide (DMSO) (Sigma, D8418) and 70 % v/v fetal bovine serum was added with a final cell count of approximately 1 million cells per cryovial. Cells were gradually cooled down on ice to prevent osmotic rupture and stored at -80 °C before filing them in a dewar for replenishment of stock.

2.3 3-3'-diaminobenzidine (DAB) staining

SH-SY5Y cells were cultured in CDMEM and SH-SY5Y neuroblastoma cells overexpressing the familiar mutant A53T were maintained in CDMEM supplemented with 200 pL/mL G418 antibiotics. Both cell line types were seeded in CDMEM in 8 well Lab-Tek II chamber slides (Nunc, 154534) at 0.5x105 cells/mL and 600 pL cell suspension was added for each chamber and grown to -70 % confluence. Thereafter, the media was removed from the chambers and the cells were fixed with ice cold methanol for 15 min, followed by three 3 min washes in PBS-T and 5 min incubation with 0.5 % Triton-X100 (Sigma, X-100) in PBS to permeabilise cells. An incubation step with 3 % H20 2 for 10 min followed the permeabilisation. Then another three 3 min washes were carried out in PBS-T before blocking with 2 % horse serum provided in the VECTASTAIN® kit (Vector Laboratories, PK-4000) and syn 211 mouse monoclonal anti-a-syn primary antibody was added for 1 hr incubation at 1:1000 dilution at room temperature that was followed another three 3 min washes with PBS-T. The secondary biotinylated antibody (1:1000 dilution) was incubated for 1 hr at room temperature and two 3 min washes followed the secondary incubation step before adding the avidin containing ABC Reagent from the VECTASTAIN® kit for 30 min prepared according to the manufacturer's instructions. Then the chromogen DAB was added for 20 min according to the manufacturer's instructions and the chambers were protected from light, followed by one 5 min wash in deionised water. Then 4'6-diamidine-2'-phenylindole dihydrochloride (DAPI) (Sigma, D8417) was used for counterstaining the nuclei followed by one more wash with PBS-T. Mounting was carried out by using two drops of Fluoromount-G water soluble mounting

agent (SouthernBiotech, 0100-01) for each chamber which were covered by glass coverslips for visualisation by fluorescent microscopy on an Olympus BX60 microscope. To assess background staining, primary antibody was omitted in a designated chamber. Acquisition settings of Capture Pro6 software were on an Olympus BX60 microscope using light microscopy at 40x magnification.

2.3.1 Cell lysis of SH-SY5Y cells for Western blotting

SH-SY5Y cells were grown to -80-90 % confluency in a T75 flask and rinsed with PBS twice. To one T75 flask of neuroblastoma cells 1 mL lysis buffer was added, consisting of 0.9 mL RIPA buffer (Sigma, R0278) and 0.1 mL mammalian protease inhibitor cocktail (Sigma, P830) for 2 min at 37 °C at 5 % C02. The cells were then scraped off with a cell scraper and collected into an Eppendorf tube and incubated on ice for 30 min. Incubation was followed by a centrifugation step at 15, 000 xg for 10 min and the supernatant aspirated and analysed by bicinchronic acid (BCA) assay and Western blotting.

2.3.2 MTT cell viability assay

SH-SY5Y neuroblastoma cells and SH-SY5Y cells overexpressing A53T a-syn were seeded in a 96-well plate at a density of 1x105 cells/well and cultured overnight. Next day the cells were treated with a-syn oligomers at 10 % v/v (0.01 mg/mL) or 20 % v/v (0.02 mg/mL) or 7 pM monomer in the presence of appropriate solvent and positive controls and incubated for 4 hr, 24 hr and 48 hr at 37 °C, 5 % C02. Subsequently, 20 pL of 0.5 mg/mL 3-(4,5-dimethylthiaziazol-2-yl)-2,5-diphenyl-2H-tetrazolium bromide (MTT) (Sigma, M2128) was added to

each well and incubated for a further 4 hr. The medium was then removed followed by the addition of 150 pL of DMSO to dissolve the purple formazan crystals. After 15 min agitation, the colour intensity was read at 570 nm and 650 nm on the Tecan Infinite M200 plate reader. The data was analysed by the GraphPadPrism software to evaluate the statistical difference. One-way Anova followed by Bonferroni post-hoc test was used to establish whether significant differences existed among various treatment groups. The cell viability of untreated cells is considered as 100 %, all treatments are expressed in relation to that. Mean cell viability (%) and standard error of measurement (SEM) are shown for each group.

2.3.3 Measurement of intracellular Ca(ll) influx

For the initial experiments to evaluate intracellular Ca(ll) influx, the fluorescent blue dye Mk-1 (Molecular Devices) reconstituted with Krebs Ringer buffer (Sigma, K4002) supplemented with 1 mM CaCI2 and 20 mM HEPES to 2X working strength and used to replace the medium of the SH-SY5Y cells seeded in CDMEM into 96 well black wall, flat clear bottom fluorescent plates at 1x105 cells/well density one day prior to the assay. After 60 min loading time at 37 °C at 5 % C02 in dark conditions, the previously prepared 50 pL fixed aliquots of alternate treatment groups dissolved in modified Krebs Ringer buffer were directly injected onto the loaded cells cultured in the fluorescent imaging plates and fluorescent intensities were read at 485 nm and 535 nm. Fluorescence intensities were monitored immediately after the addition of treatment groups and every 10 min up to 60 min. All measured values were averaged and matched solvent controls were subtracted. To determine statistical significance, one-way Anova was used combined with Bonferroni post-hoc test of selected

pairs and all values were expressed as mean±SEM of relative fluorescence units. The dye has been discontinued and a new generation, higher sensitivity fluorescent marker was used as follows: SH-SY5Y cell were cultured and seeded the day before the assay at 1x105 cells/well density in CDMEM in 96 well black/clear, tissue culture treated, flat bottom fluorescent imaging plates (BD Biosciences, 353219). Next day the media was removed and the cells were rinsed with 100 pL Krebs Ringer buffer for each well and loaded with 50 pL of 2X FLIPR Fluo6 dye (Molecular Devices, Calcium 6-QF Assay, R8192) dissolved in modified Krebs buffer (50 pL/well). The plate was then incubated for 120 min at 37 °C at 5 % C02 in dark conditions.The various oligomers were prepared to a 10 % v/v or 20 % v/v end concentration (for oligomers 0.01 mg/mL or 0.02 mg/mL referring to the monomer's concentration) and ionomycin (Sigma, I0634) positive control to a 5 pM final concentration in modified Krebs Ringer buffer and equal volumes (50 pL) of the various oligomers, vehicles and controls were pipetted directly onto the cells before measurement. The fluorescent intensity was measured at 485 nm and 535 nm. At regular time intervals, the intensities were collected and the 60 min after injection readings were stopped. After appropriate solvent subtraction values were analysed by one-way Anova using Bonferroni multiple comparison test for selected pairs and expressed as mean±SEM.

2.3.4 Measurement of intracellular ROS formation by using CMF-DA fluorescence

SH-SY5Y cells and SFI-SY5Y cells harbouring the A53T mutant were cultured and seeded in a 96 well plate the day before the assay in CDMEM. For SH-SY5Y cells overexpressing A53T a-syn, 200 pg/mL G418 was included as a

selective antibiotics. The media was removed next day and cells were rinsed with 100 pL/well PBS 1X and loaded with 10 |jM 2,7-dichloromethylfluorescein diacetate fluorescent dye (CMF-DA, Molecular Probes, C2925) dissolved in DMEM-Glutamax II (50 |jL/well) and incubated at 37 °C at 5 % CO_2 for 45 min in dark conditions. After the incubation the alternate treatments were added to the plate at 10 % or 20 % v/v (for oligomers 0.01 mg/mL or 0.02 mg/mL) including hydrogen peroxide (Sigma, H3410) as positive control and incubated for various lengths of time (4 hr, 8 hr and overnight treatment). The wells were then emptied and 100 pL/mL PBS was added to the plate to measure the generated intracellular oxidative species at wavelengths of 485 nm of excitation and 530 nm of emission. After solvent subtraction the values were analysed by one-way Anova followed by Bonferroni post-hoc test for selected pairs and expressed as mean±SEM.

2.3.5 Immunocytochemistry

2.3.6 Assessing intracellular aggregation

SH-SY5Y cells were cultured in CDMEM and the same cell line containing the familial mutant A53T was maintained in CDMEM supplemented with 200 pL/mL G418 antibiotics. For seeding, both cell line types were seeded in CDMEM in an 8 well Lab-Tek II chamber slides (Nunc, 154534) at 0.5x105 cells/mL and 600 pL cell suspension was added to each chamber and grown to ~70 % confluence. Treatment groups were added in the presence of appropriate vehicle controls at 10 % or 20 % v/v (0.01 mg/mL or 0.02 mg/mL concentrations referring to the monomer's concentration) for 8 hr treatment. Thereafter, the media was removed from the chambers and the cells were fixed with ice cold

methanol for 15 min, followed by three 3 min washes in PBS-T and 5 min incubation with 0.5 % Triton–X100 (Sigma, X-100) in PBS to permeabilise cells. Then another three 3 min washes were carried out in PBS-T before blocking with 2 % horse serum (VECTASTAIN®, PK-4002) and the appropriate primary antibody (syn 211, monoclonal antibody, or anti-α-syn rabbit polyclonal antibody, a gift from Prof R. Cappai, University of Melbourne) was added for overnight incubation at 4 ^{0}C or for 1 hr incubation at 1:1000 dilution or 1:5000 dilution respectively at room temperature that was followed another 3 washes with PBS-T. The secondary fluorescent antibody, either Alexa Fluor 594 conjugated goat anti-mouse antibody or Alexa Fluor 488 conjugated goat anti-rabbit antibody at 1:1000 dilution (Molecular Probes, Invitrogen, A11008) was incubated for 1 hr and two 3 min washes followed the secondary incubation step before adding 0.5 mg/mL DAPI (Sigma, D8417) for counterstaining the nuclei. After DAPI staining one more wash with PBS-T was performed and mounting was carried out by using two drops of Fluoromount-G water soluble mounting agent (SouthernBiotech, 0100-01) for each chamber which were covered by glass coverslips for visualisation by fluorescent microscopy on an Olympus BX60 microscope. To assess background fluorescence, primary antibody was omitted in a designated chamber and all other stages were the same as described above. Acquisition settings of Capture Pro6 software were on an Olympus BX60 microscope: gamma 1.23, gain 0.850, auto white balance red 0.9960, green 1, blue 0.9960, 680x480 FF, RTV power resolution, 2560x1920 FF, Bin1 acquisition resolution, exposure power 1.800 except DAPI (exposure power 1.00) at 40x magnification. Pseudo-colours were extracted and recombined after acquisition to obtain merged images.

2.3.7 Neurofilament immunostaining

Neurofilament mouse, monoclonal antibody was purchased from Abeam (Ab7255 DA2) and used at 1:500 dilution. For immunostaining of cells, the same protocol was performed but microscopic visualisation was undertaken using a x100 oil immersion objective.

2.4 ESI-IMS-MS experiments

2.4.1 Needle puller

10 cm, 1 mm diameter borosilicate thin wall glass capillaries (Harvard Apparatus, GC100T-10) were pulled to optimal shape by a Sutter Instrument Co. P-97 Needle Puller. Tips were visualised and trimmed to size with tweezers directly before acquisition on an Olympus, Zeiss light microscope. The adjusted settings of the needle puller for attaining a stable spray were as follows in Table **2.2**.:

Parameter	Round 1	Round 2	Round 3
Heat	246	224	250
Pull	-	-	250
Velocity	18	15	40
Time	100	75	90

Table 2.2. *Parameters of heat, pull, velocity and time used for needle pulling at various cycles.*

2.4.2 Sputter coater

Capillaries were filed in a glass petri dish and placed into the SC7620 Mini Sputter Coater (Emitech). The sputter coater was operated at pressurised atmosphere maintained by argon. The plasma sputtering time lasted 160 sec, following the manufacturer's instructions.

2.4.3 Calibrations with known, globular protein standards

All spectra were collected using a Synapt G2 HDMS instrument (Waters, Manchester, UK) by use of gold coated home-made borosilicate nano-capillaries in positive ion mode. Instrumental settings were extensively optimised by varying the backing pressure, bias, cone and capillary voltages of the standards predominantly under native conditions. Optimised instrumental settings for data acquisition were: capillary voltage of 1.70-1.90 kV, cone voltage of 30-70 V, source temperature of 60 °C, trap collision energy of 4.0 V, transfer collision energy of 10 V, trap bias 45, backing pressure of 3.0-3.1 mbar unless otherwise stated. IMS separations were performed at T-wave velocities of Trap: 311, IMS: 800 and Transfer: 200 m/s and T-wave amplitudes of 4-15 V using 3.6 mbar pressure of nitrogen gas maintained by a 90 mL/min gas flow. Native spectra were obtained by dissolving the protein in question to a 10-20 pM final concentration in aqueous solution of 50 mM AA at pH 6.8 or pH 7.0. For attaining denatured spectra, all calibrants and mass standards were prepared before injection at 10-20 pM and a-syn at 10 and 40 pM and dissolved in 50 % acetonitrile, 10 % formic acid and 40 % ultrapure water (vol/vol/vol). Calibration curve for Os was obtained based on of multiple charge states of cytochrome c from horse heart (Sigma, C7752), myoglobin from equine heart

(Sigma, M1882) and ubiquitin from bovine erythrocyes (Sigma, U6253) as described previously (Smith *et al.* 2009). ESI-IMS-MS data of ADH from yeast (Sigma, A8656), a-lactalbumin from bovine milk (Sigma, L5385), bovine albumin (Sigma, A8531), (32 microglobulin from human urine (Sigma, M4890), carbonic anhydrase from bovine erythrocytes (C7025), lysozyme from chicken egg (Sigma, L6876), porcine elastase from porcine pancreas (Sigma, E7882) was also obtained in the same manner. Mass calibration was carried out by an infusion of CsI cluster ions, and arrival time distributions were determined by using the Mass Lynx v4.1 software (Waters, Manchester, UK).

2.4.4 ESI-IMS-MS analysis of unknown proteins

2.4.4.1 Mass spectrometry of metal ions

Stock solutions of monomeric a-syn, $CuCl_2$, $FeCl_3$ and $ZnCl_2$ were prepared to a final concentration of 50 pM working strength in 40 mM AA at pH 6.8. Similarly, 50 pM solutions of the metals were also prepared without Gly or in 6-fold excess of Gly, pH 6.8 and used for the experimentation performed on the Synapt G2 HDMS (Waters, Manchester, UK) in positive ion mode. The protein to metal ratios were 1:0, 1:1 and 1:2 (v/v) using the 50 pM working strength solutions directly prepared and mixed before analysis except for Cu(II) for which an extra 1: 0.5 (v/v) ratio was set up. The following instrument parameters were used for data acquisition: capillary voltage 1.5 kV-2.0 kV, sample cone 50-60 V, backing pressure 3.0 mbar, trap collision energy 4.0 V, transfer 20 V, IMS wave velocity 800 m/s, IMS wave height 4 V, IMS gas flow 90 mL/min. The instrument was calibrated using an aqueous CsI solution beforehand. Calibration for Q measurements was performed as mentioned above.

2A.4.2 ESI-IMS-MS of oligomers

The mass spectra were acquired by using the Synapt G2 HDMS instrument (Waters, Manchester, UK) fitted with an nESI source and optimised to allow transmission of ions and tuned to preserve non-covalent complexes. Acqusition parameters are specified in Chapter 4. Calibration and data processing was performed as discussed above.

In silico collision Qs were calculated utilising a projection approximation script developed by and verified by the Ashcroft group (Smith *et al.* 2010). *In silico* models were assuming the monomeric a-syn subunits were spherical with a radius of 19.9 Å.

2.4A.3 Mass spectrometry of Tyr and DA binding studies

Equine cytochrome c, horse heart myoglobin, bovine ubiquitin, DA hydrochloride, glycine (Gly), a-Tyr and AA were purchased from Sigma-Aldrich (UK). Human, recombinant WT a-syn was expressed in *E. coli* BL21 (DE 3) and purified as described above. The concentration of pure monomeric a-syn was determined using the molar extinction constant 5960 cm'1 at A280 on a Jenway Spectrophotometer. Samples for ESI-IMS-MS experiments were prepared by dissolving a-syn to a 50 pM end concentration and by diluting DA or Tyr to a 6.25 mM final concentration in aqueous solution of 40-50 mM AA, pH 6.8. The following proteins to ligand ratios of the working strength solutions were analysed: 1:125, 1:30 and 1:8 molar ratios, all prepared and mixed immediately prior to analysis. The experiments were conducted either in the presence or absence of 6-fold excess of Gly to avoid non-specific interactions. Samples were introduced to the Synapt G2 HDMS instrument (Manchester, Waters, UK)

by using metal coated home-made borosilicate capillaries in positive mode. Typical instrumental settings for data acquisition were: capillary voltage of 1.70-1.90 kV, cone voltage of 50-60 V, source temperature of 60 ^{0}C, trap collision energy of 4.0 V, transfer collision energy of 10 V, trap bias 45, backing pressure of 3.1 mbar. IMS separations were performed at T-wave velocities T-wave velocities of Trap: 311, IMS: 800 and Transfer: 200 m/s and T-wave amplitudes of 4-15 V by using 3.6 mbar pressure of nitrogen gas maintained by a 90 mL/min gas flow. Calibration for obtaining Ω was undertaken as discussed earlier.

3 Chapter 3

Biochemical and biological characterisation of a range of *in vitro* a-syn oligomers

3.1 Introduction

3.1.1 a-syn oligomers are causative species in PD

PD is the second most common neurodegenerative disorder (de Lau *et al.* 2006) in which toxic a-syn oligomers have a causative role (Demuro *et al.* 2005; Winner *et al.* 2011; Malchiodi-Albedi *et al.* 2011; Gurry *et al.* 2013). However, it is still poorly understood what triggers the natively unstructured monomeric protein to misfold in the cellular environment to produce toxic, oligomeric forms instigating disease. In addition, little is known about the stability, dynamics and morphological features of oligomeric subpopulations and how they exert their cytotoxic functions causing neuronal demise. A plethora of *in vitro* preparation protocols of a-syn oligomers have been developed recently (Danzer *et al.* 2007; van Rooijen *et al.* 2010; Wang *et al.* 2010b; Giehm *et al.* 2011; Nasstrom *et al.* 2011; Cremades *et al.* 2012; Singh *et al.* 2013; Roostaee *et al.* 2013) with the aim of determining the potential modes of action *in vivo.* Different oligomeric procedures have shown disparate results regarding the size and biological effects of a-syn oligomers (detailed in Chapter 1), implying that different conditions alter the self-assembly pathway in their own manner. These oligomers can be both on pathway to amyloid self-assembly or represent an off pathway product (Lashuel *et al.* 2002; Ding *et al.* 2002; Cappai *et al.* 2005; Danzer *et al.* 2007; Kim *et al.* 2009; Angot *et al.* 2012; Gurry *et al.* 2013).

3.1.2 Alternative toxic modes of action of a-syn oligomers

3.1.3 a-syn oligomers are capable of disrupting membranes

Several biological modes of action have been presented as hypotheses of how these oligomers elicit toxic effects. The first unifying notion that has gained importance is that these oligomers are potent disruptors of biological membranes (Davidson *et al.* 1998; van Rooijen *et al.* 2010; Ruiperez *et al.* 2010; Stockl *et al.* 2013). When the monomeric protein converts to oligomers a structural transition takes place from natively unfolded state to a p-sheet rich conformation that is concomitant with amyloid fibril formation (Uversky *et al.* 2009). It has been demonstrated that oligomeric species bind tighter to mainly phosphatidylglycerol (PG) containing synthetic membranes than monomeric or mature fibrillar forms (Voiles *et al.* 2001). In this study, disruption of fluorescent dye loaded vesicles by oligomeric a-syn was directly visualised by AFM and fluorescence increased in a concentration dependent manner. When oligomeric forms (~5 pM) bound to vesicles a p-sheet rich conformation was seen by CD spectroscopy, indicating that p-sheet conformation of these pre-fibrillar species was retained (Voiles *et al.* 2001) in contrast to the a-syn monomer which obtains an a-helical conformation upon membrane association (Davidson *et al.* 1998). Oligomers binding to membranes may act on the ordering of the lipids within the membrane. It has been postulated that membrane disintegration may occur by decreasing the lipid order of the membrane or by formation of transient pores followed by rearrangement of the lipid bilayer or by insertion of ordered p-structure membrane spanning pores that then lead to death of neurons (Stockl *et al.* 2013; Stockl *et al.* 2012). It is plausible that the toxicity of a-syn oligomers

is not solely due to the formation of membrane spanning channel like pores but may originate from disruption of lipid packaging through insertion of specific regions into the lipid bilayer (Stockl *et al.* 2013). a-syn oligomers have a net negative charge but contain positively charged residues within their core as determined by Lys residues at aa 6, 10, 12, 96, 97 and 102 may therefore interact favourably with negatively charged lipid head groups in the bilayer facilitating binding. Hydrophobic residues located near the N-terminal region are conceived to have higher affinities for negatively charged lipid head groups which then cause “phase separation” in membranes. An initial separation disturbing membrane packaging then may allow intrusion of further hydrophobic segments of a-syn into the inside of the membrane. This embedding of hydrophobic motifs could permit access to small hydrophilic molecules such as Ca(II) (Stockl *et al.* 2013). a-syn oligomers also appear to facilitate “lipid flip-flop” as the resultant membrane rearrangements promote the movement of hydrophilic lipid head groups between two parts of the bilayer (Stockl *et al.* 2012).

3.1.3.1 a-syn oligomers can induce Ca(II) influx

Biological consequences of membrane permeabilisation could be Ca(II) influx into the cytosol, depolarisation of the mitochondrial membrane (Demuro *et al.* 2005; Danzer *et al.* 2007; Kim *et al.* 2009; Giehm *et al.* 2011; Danzer *et al.* 2012; Mattson 2012) or an increase of cytosolic dopamine in the cytoplasm (Lotharius *et al.* 2002b; Lundblad *et al.* 2012). Ca(II) dysfunction leading to influx has been reported in relation to numerous other amyloidogenic peptides such as Api-40, amylin and serum amyloid suggesting a common mechanism (Quist *et al.* 2005). Oligomers of these amyloidogenic proteins and peptides

share a common conformational epitope detected first in A(31-40 oligomers and this can be recognised by the anti-oligomeric antibody A11 (Kayed *et al.* 2007). This antibody reacts with numerous *in vivo* and *in vitro* oligomeric forms of different amyloidogenic proteins with p-sheet content. It has now been proved to be increasingly important in detecting shared generic oligomeric epitopes across protein aggregation diseases (Morten *et al.* 2007; Wang *et al.* 2009; Krishnan *et al.* 2012; Colla *et al.* 2012; Aidt *et al.* 2013).

Wang *et al.* hypothesised that elevated Ca(II) levels in turn may activate CaN. This dephosphorylates a mitochondrial proapoptotic protein, BAD, which is member of the Bcl2 family, ultimately leading to cell death of neurons (Wang *et al.* 1999). Similarly, CaN dependent cell death upon oligomeric treatment has been reported by Martin *et al.* (Martin *et al.* 2012).

3.1.4 Extracellular a-syn oligomers cause seeding of a-syn

An alternative prevailing theory proposes that a set of a-syn oligomers act as seeds of aggregation and initiate the build-up of proteinaceous inclusions resembling Lewy bodies. Soluble a-syn oligomers have been detected in the extracellular space (Chai *et al.* 2013). Secretion of a-syn and its aggregates via exocytosis has been demonstrated in neuronal cells (Lee *et al.* 2005) as well as the internalisation of a-syn intermediates by endocytosis (Lee *et al.* 2008a). *In vivo* transmission of a-syn to neighbouring neurons and neuronal precursors, especially when lysosomal function was inhibited has been demonstrated in cell culture and *in vivo* transgenic mouse brains engrafted with stem cells. The inhibition of proteosomal system had little effect, inclusions were still observed but not at significant levels in the various cells, indicating that clearance occurs

mainly in the lysosomes. The recipient cells containing abnormal protein inclusions displayed fragmented nuclei and signs of caspase-3 activation both *in vivo* and *in vitro* (Desplats *et al.* 2009). In another study, propagation of a-syn has been observed in co-culture model systems, where after endocytosis the extracellulary added a-syn associated with and seeded the aggregation of intracellular a-syn. a-syn injected into rats was internalised and its uptake abolished by supplementing endocytosis inhibitors such as dynasore and monodansylcadaverine. In addition, transmission of a-syn from host to grafted cells has been illustrated in transgenic mice overexpressing WT a-syn by confocal microscopy, flow cytometry and Western blotting (Hansen *et al.* 2011). In two isolated cases of PD patients who had received grafts of foetal mesencephalic dopaminergic neurons, Lewy bodies developed in the transplants after several years (Li *et al.* 2008).

Remarkably, prion diseases characterised by the misfolding of the cellular prion protein PrPc into infectious PrPSc particles can be readily transmitted by a self-propagating mechanism in the central nervous system (Prusiner 2012; Kraus *et al.* 2013). Therefore, a-syn and its oligomeric intermediates appear to replicate this pathology in many ways (Angot *et al.* 2010; Hilker *et al.* 2011; Angot *et al.* 2012).

3.1.5 The toxic oligomers of a-syn have heterogeneous morphologies and effects

In vitro preparation methods for a-syn oligomers lead to aggregates with a broad range of sizes and biological function. Cremades *et al.* have shown subpopulations of small size ~2-5-mers, medium size ~5-15-mers and larger

assemblies ~15-150-mers by employing single molecule Fluorescence Resonance Energy Transfer (FRET). These oligomers were prepared by labelling α-syn at residue 90 with Alexa Fluor 488 and Alexa Fluor 647 beside unlabelled α-syn at protein concentration of 6 μM (Cremades *et al.* 2012). The heterogeneous mixture of oligomers was classed as type A small, A medium, B medium and B large oligomers. Type B oligomer appreared to be resistant to proteinase K digestion as opposed to type A oligomers and the natively unfolded monomer. Treatment with type B oligomers induced a rapid increase of ROS production in the cytosol. Type A oligomers had a less significant effect on cytoplasmic ROS exposure to monomers or fibrils had no effect. Fibril disaggregation samples contained a variety of species some of which were identical to the higher β-sheet containing type B oligomers at early incubation times. The energetics and assembly kinetics differed for the type A and B oligomers but interconversion was possible. All α-syn species were shown to be internalised rapidly within 6-8 min both in rat primary neurons and astrocytes and exposure to these oligomers did not affect cell viability over 24 hr (Cremades *et al.* 2012). Of note, oxidative stress can then enhance the rate of further oligomerisation (Maries *et al.* 2003) and ROS was found to trigger apoptotic cascades (Jenner 2007) driving a vicious circle. Oligomeric species may also damage mitochondrial DNA leading onto impairment of respiratory complex-I (Jenner 2003).

Two studies performed by Danzer *et al.* recapitulated some of the above mentioned cytotoxic aspects of recombinant *in vitro* α-syn oligomers such as different morphologies as judged by AFM, Ca(II) influx and initiation of intracellular aggregation post-oligomeric treatment in SH-SY5Y cells (Danzer *et al.* 2007; Danzer *et al.* 2009). Type A preparations included freeze drying the

soluble fraction during the lag phase of fibril growth and this yielded spherical structures under Fe(III) free conditions, while addition of Fe(III) resulted in more extended protofibrillar structures. These preparations spanned 40-45 nm in diameter as shown by AFM. This oligomer preparation had pore forming Ca(II) channel-like activities that mediated Ca(II) influx from the extracellular milieu. Exposure to these latter oligomers activated caspase-3 in a-syn overexpressing cell lines. Alternative type C oligomers produced in the presence or absence of Fe(III) C1 and C2 respectively by spin concentrating the soluble fraction during the lag phase did not differ morphologically from each other and were observed to be a mixture of globular and protofibrillar species with spherical appearance. These oligomers were found to be nucleating species as they induced intracellular aggregation upon exposure in a-syn overexpressing cell lines (Danzer *et al.* 2007). With these findings in mind, it was clear that there was a gap in understanding how secondary and tertiary structure of these groups of *in vitro* oligomers correlated with their respective biological properties and cytotoxicity.

3.2 Aims and objectives

Overall aims

To examine the hypothesis (Section 1.9), oligomer preparation protocols reported by Danzer *et al.* were adapted to MS compatible conditions and assayed by a number of methods to reveal biological key biochemical and functional differences between alternate oligomeric types.

The specific goals were:

i. to produce type A and type C a-syn oligomers with the same biochemical and biological properties as published by Danzer *et. al* in the presence or absence of FeCl3.

ii. to modify exisiting protocols to produce oligomers suited to detailed structural characterisation by ESI-IMS-MS.

iii. to carry out spectroscopic measurements and epitope mapping as a novel aspect to understand more about oligomeric structure and folding entities.

iv. to evaluate and contrast the biological effects of alternate oligomeric subsets by an array of cell culture techniques in human SH-SY5Y cells.

3.3 Materials and methods

Protein expression and purification, oligomer preparation, ThT assay, dot blotting, Tyr and ANS fluorescence scans, MTT, Ca(II) influx and ROS assay and immunocytochemistry were performed as described in Chapter 2.

3.4 Results and discussion

3.4.1 Protein expression, formation of a-syn oligomers and fibrils

a-syn is a natively disordered protein that has a high tendency to aggregate (Uversky 2008; Fink 2006). Oligomers are aggregation intermediates that precede fibril formation and have been shown to be key in the pathogenesis of PD (Jellinger 2011; Lashuel *et al.* 2013). Toxic *in vitro* oligomers prepared in various laboratories using alternate protocols have given vital clues as to how *in vivo* oligomers evoke their toxic gain of function (Lashuel *et al.* 2002; Kim *et al.*

2009; Angot *et al.* 2012; Cremades *et al.* 2012 Dettmer *et al.* 2013; Gurry *et al.* 2013). Limited evidence has been shown about how a particular oligomer type's biochemical and biological functional properties correlate with its underlying structural properties (Bernstein *et al.* 2004; Rekas *et al.* 2010; Cremades *et al.* 2012). A group of *in vitro* α-syn oligomers reported by Danzer *et al.* were shown to have diverse biophysical properties and essential functional properties contributing to neuronal damage (Danzer *et al.* 2007; Danzer *et al.* 2009). However, information about the composition of these heterogeneous oligomers regarding subunit size and shape was yet to be explored. To this end, preparation protocols were adapted and modified enabling structural characterisation of these oligomers by ESI-IMS-MS as discussed in detail in the following chapter.

One technical constraint of ESI-IMS-IMS is that data acquisition of oligomeric complexes near native states can only be undertaken in volatile buffers such as AA. The preparation protocol established above requires the use of 50 mM SP which would lead to extensive adduct formation and prevent ionisation. To overcome this limitation, buffer exchange was a conceivable approach; initial experimentation methods were hampered by the genuinely low yield of amyloid oligomers during preparation and resulted in loss of material during size SEC or in a loss through non-specific binding to the filter membrane during spin concentration. Therefore, it seemed a more plausible alternative to produce α-syn oligomers directly in AA buffer and address whether such modification of the protocol alters biochemical and biological properties when compared to well-defined oligomeric populations generated in SP buffer. First, it was necessary to demonstrate that features of type A and type C oligomers produced in SP were consistent with published literature (Danzer *et al.* 2007;

Danzer *et al.* 2009). In order to produce the required recombinant protein BL21 (DE3) *Escherichia coli* competent cells were transformed with pET 23 a+ vector containing the human WT α-syn sequence. Expressed protein was first isolated by acid precipitation and purified by anion exchange and gel filtration to have a continuous supply for producing α-syn oligomers (**Appendix Figure 8.1.**). The mass of the protein was confirmed by mass spectrometry and by Western blotting using a polyclonal full length anti α-syn antibody (**Appendix Figure 8.2.**).

To confirm formation of low MW oligomers, SEC was performed that revealed that a small proportion of the monomeric protein converted to oligomeric forms consistently eluting near the void volume at ~6.5-8 mL on a Superdex 200 10/300 GL column as shown in **Appendix Figure 8.3.**.

Amyloid formation α-syn fibrillisation proceeds by a nucleation dependent fashion entailing a slow lag phase including the formation of a partially folded intermediate (Uversky *et al.* 2001a; Uversky *et al.* 2001), followed by the growth phase which then plateaus off (Lomakin *et al.* 1996; Fink 2006). Addition of preformed intermediate oligomeric species can accelerate the rate of fibril formation by shortening the lag phase and providing seeds for recruitment of monomers to assemble into large mature fibrils (Wood *et al.* 1999; Kim *et al.* 2009). As it has been shown, metals including Fe(III) and Cu(II), lower pH, higher temperature have influence on the kinetics of this self-assembly (Uversky *et al.* 2001c; Uversky *et al.* 2002). Certain conditions disfavour fibril growth and do not facilitate recruitment of further monomers as in the case of DA (Leong *et al.* 2009a; Lee *et al.* 2011) or even disassemble fibrils (Li *et al.* 2004) and may divert the aggregation pathway or halt it. In order to confirm that the

recombinant α-syn was able to form amyloid fibrils, aggregation of the 70 μM monomeric protein in both SP and AA was monitored over 7 days using ThT fluorescent dye (Naiki *et al.* 1989; Biancalana *et al.* 2010). The data showed a typical sigmoidal fibril growth profile consistent with previous observations (Uversky 2008). ThT incorporates into amyloid-like fibrils and its quantum yield significantly increases (Stsiapura *et al.* 2008) as shown for mature α-syn fibrils in **Appendix Figure 8.4.**.

To investigate the seeding effect of the oligomers (type A1, A2, C1 and C2) prepared in SP buffer, the fibril formation of 70 μM α-syn was monitored in the presence of 10 % v/v of each oligomer types over 7 days. These oligomers were added at day 0 before incubation and are referred to as A1 SP, A2 SP, C1 SP and C2 SP is illustrated in **Figure 3.1. *A***. Oligomers were prepared in the same fashion but with the modification of the buffer, using 50 mM AA instead of SP to obtain oligomers suitable for ESI-IMS-MS measurements. This latter group of oligomers are referred to as A1 AA, A2 AA, C1 AA and C2 AA. Fibril formation of 70 μM α-syn in the presence of these oligomers was monitored over 7 days by ThT fluorescence with continuous shaking at 37 °C as shown in **Figure 3.1. *B***. Fibril specific, conformation dependent antibodies have become available in recent years and here the LOC anti-amyloid fibrils antibody (Millipore) was used in parallel with ThT fluorescent measurements each day to verify the formation of amyloid material over non-specific aggregates. This antibody recognises generic epitopes common to many amyloid fibrils and fibrillar oligomers, but not monomers, prefibrillar oligomers or natively folded proteins according to Kayed *et al.* (Kayed *et al.* 2007) (**Appendix Figure 8.5.**).

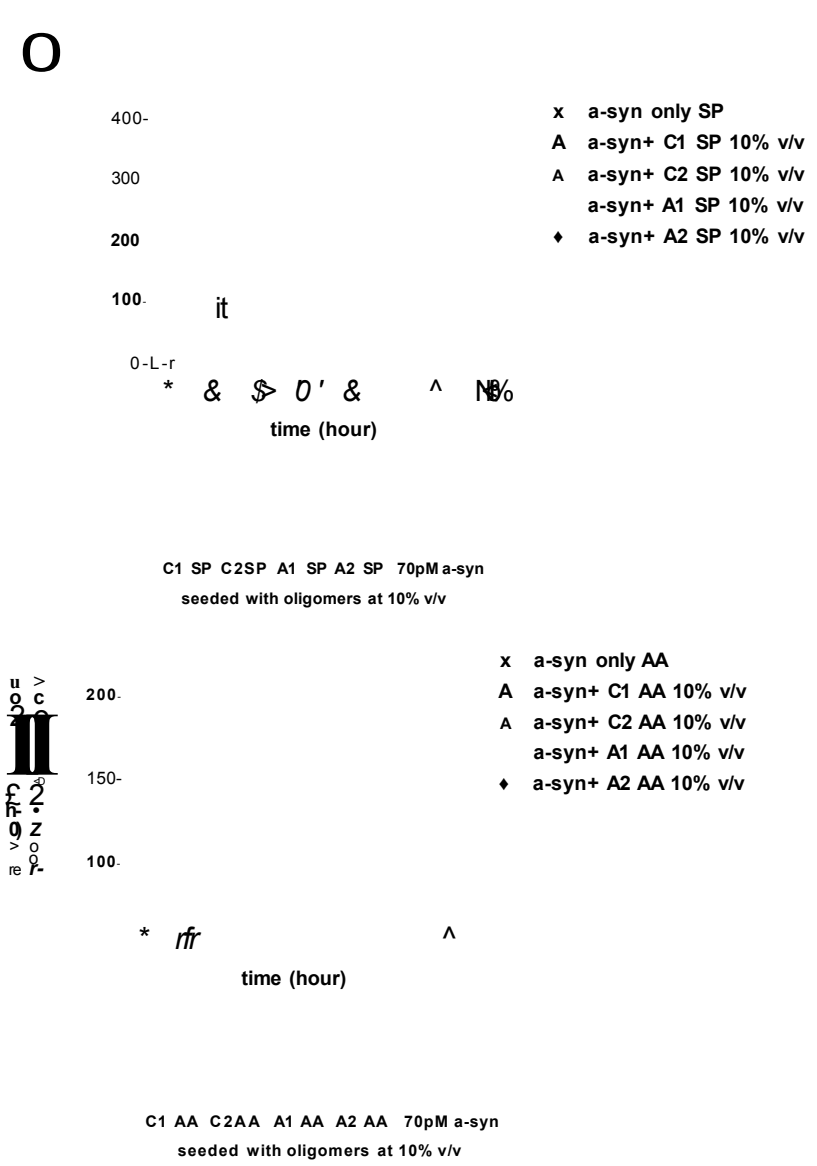

Figure 3.1. *Fibril formation monitored over 7 days in the presence or absence of additional oligomers at 10 % v/v either in SP (A). Type A oligomers prepared in SP (open and closed blue triangles) seeded the aggregation of a-syn (black cross) and abolished the lag phase of assembly, whereas type C oligomers prepared in SP increased the quantum yield of ThT. Oligomers prepared in AA (B) did not enhance the aggregation of a-syn over 7 days. Relative fluorescent intensity plotted as a function of time and all readings are normalised to ThT only in matched buffer at 482 nm. Dot blotting was carried out in parallel with the ThT assays, using the LOC antibody that recognised mature fibrils only.All oligomers prepared in SP gave rise to LOC positive fibrils; day 7 is shown.*

As seen in Figure 3.1. *A*, type A oligomers prepared in SP had seeding abilities, reducing the length of the lag phase and enabling conversion of a-syn to fibrils after 24 hr. However, type C oligomers in SP buffer also promoted the formation of fibrils, the aggregation of species with cross-p structure became evident >96 hr. All fibrils were readily detected by the conformation specific LOC (Millipore) antibody at the day 7 time point, suggesting conversion to a more toxic p-sheet containing conformation. When these experiments were repeated for the alternate oligomers prepared in AA (Figure 3.1. *B),* it was observed that these oligomers did not promote fibril formation effectively and the rate of fibril formation was slowed in AA buffer. Dot blotting procedure with the LOC primary antibody showed a positive immunoreaction only with the 70 pM a-syn sample on day 7, indicating that fibrils were not formed on this time scale.

3.4.2 Spectroscopic measurements

Further use of extrinsic fluorescent dyes or use of internal fluorescence based on naturally occurring fluorophores such as on Tyr or Trp residues are useful tools to study amyloidogenic structures at the molecular level (Vassar *et al.* 1959; Lindgren *et al.* 2005; Munishkina *et al.* 2007). ThT and ANS are non-covalent extrinsic fluorophores commonly used in the investigation of protofibrillar oligomeric species and their self-assembly into mature fibrils. ANS has been widely used to reveal differences in hydrophobicity in a number of disease states related to a-syn, prion, transthyretin, serum amyloid A, amylin, p2 microglobulin and Ap isoforms (Munishkina *et al.* 2007). ANS detects partially folded and molten states and associates with hydrophobic patches that is reflected in a blue shift towards lower wavelengths (Munishkina *et al.* 2007;

Roostaee *et al.* 2013). For this assay, ANS was dissolved in appropriately matched solvent. λ_{max} of most oligomeric types was located ~505 nm (black line), except type A1 and type A2 oligomers that displayed a blue shift with a λ_{max} ~495 nm as shown by the dashed line with an arrow pointing to the λ_{max}. Their quantum yield was also higher than any other oligomers' or the monomer's as shown in **Figure 3.2. *A***. Type A and C oligomers in AA had a similar emission spectra as the controls and type C oligomers or the monomer in SP, devoid of any apparent shifts towards lower wavelengths as indicated in ***B***. ANS fluorescence screen of the alternate oligomeric types therefore indicated that type A1 and A2 oligomers fold such way that ANS could bind to the exposed hydrophobic residues and cause a λ_{max} blue shift at 488 nm. In contrast, no λ_{max} shift was observed for oligomers type C oligomers prepared in SP and type A and C prepared in AA.

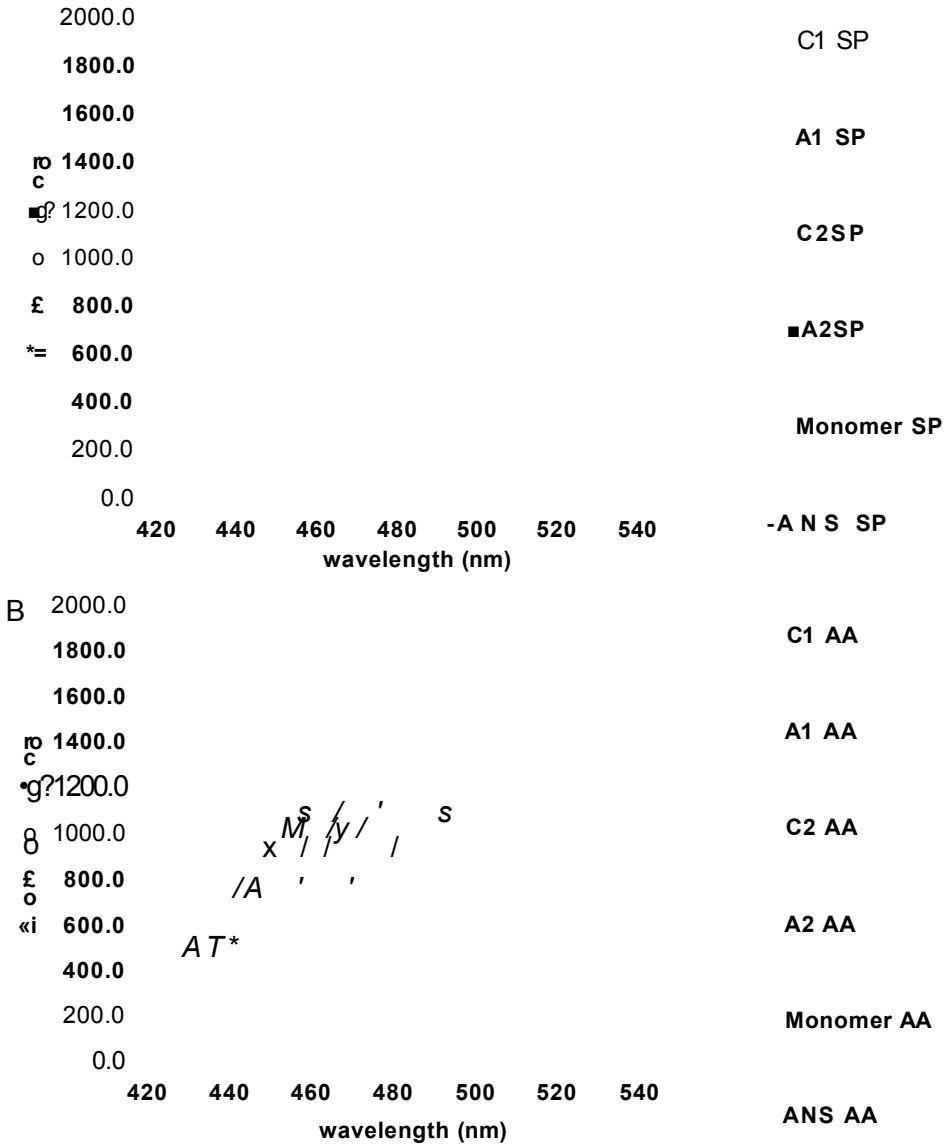

Figure 3.2. *ANS fluorescence emissions scan of alternate oligomeric forms between 420-550 nm. Emission spectra of alternate oligomers alongside with the monomeric protein prepared in SP are shown in A or those prepared in AA illustrated in B. All measurements were performed in triplicates and mean values have been plotted. The dashed line indicates a -10 nm blue shift in the case of type A1 and A2 SP oligomers (A) in their Amax as compared to the Amax of all other types of oligomers or monomeric protein or buffer control shown by vertical black lines.*

Internal Tyr fluorescence is a valuable indicator of the environment (Munishkina *et al.* 2007) of the four a-syn Tyr residues per monomer situated at aa Y39, Y125, Y133 and Y136. Upon performing a Tyr scan at 344 nm it was evident that quantum yields of type A1 and type A2 oligomers in SP was dramatically increased as opposed to all other oligomeric or monomeric form of a-syn as illustrated in Figure 3.3.. However, no shift in λ_{max} occurred in either of these oligomeric types.

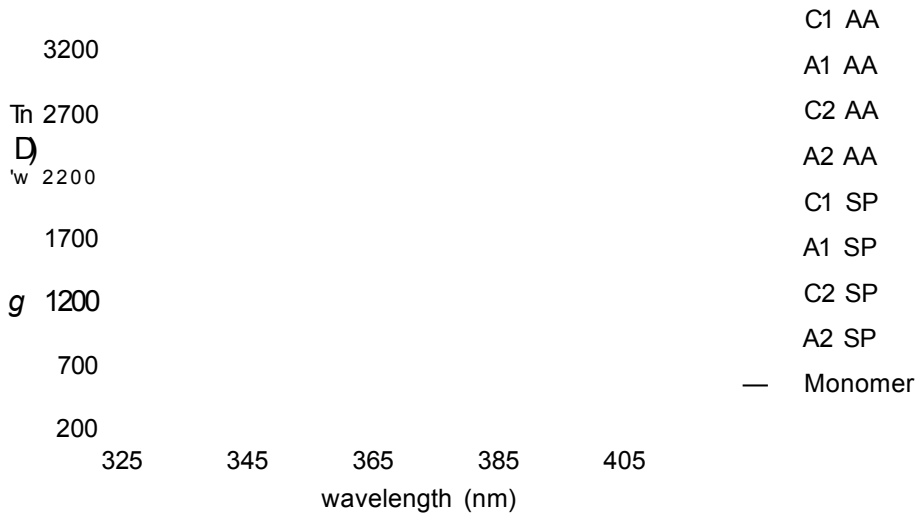

Figure 3.3. *Intrinsic Tyr fluorescence emission of alternate oligomers and monomeric a-syn. All values represent three repeated measurements, mean values and ±SEM have been plotted. The relative fluorescence intensity of type A1 and A2 SP oligomers exceeded the value of all other types of oligomers or the monomer.*

3.4.3 Epitope mapping studies of a-syn oligomers

To investigate the structural elements guiding the assembly of alternate oligomers, a range of specific monoclonal antibodies directed against different

epitopes of the three main structural domains of α-syn were utilised for immunodetection. Dot blotting procedures have become a standard method to determine availability of antigenic epitopes on the surface of amyloid oligomers (**Figure 3.4.** ***A***). In addition, an ever increasing number of conformational antibodies (Kayed et al. 2006) have identified common conformational epitopes towards oligomeric, protofibrillar or fibrillar species involved in AD, haemodialysis related amyloidosis and prion disease among others (Kayed *et al.* 2007; Morten *et al.* 2007; Yanamandra *et al.* 2011; Colla *et al.* 2012; Wall *et al.* 2012; Guilliams *et al.* 2013). Here, α-syn oligomers were subjected to dot blotting to probe their epitopes by a conformation dependent anti-oligomeric A11 antibody (Milipore) (**a**) and an in-house full length rabbit polyclonal antibody (**b**) at the 800 nm, green channel shown in **Figure 3.4.** ***B***. A range of in-house monoclonal antibodies towards alternate regions of α-syn were also assayed and were a kind gift from Prof. R. Cappai, University of Melbourne. All oligomeric forms and positive and negative controls were subjected to dot blotting procedures using 35/10-7D2 antibody (developed against oxidised methionine containing epitope at the N-terminal, with a sequence of H-M[Ox]DVFM[Ox]KGLSKAKC-OH in mice) (**a**), 4H4-14-27-12 antibody (middle region, raised against KKDQLGK motif in mice) (**b**), a commercial antibody syn 211 (aa 121-126) (**c**) and 45/08-5G7-1, (C-terminal, mice immunised with EAYEMP) (**d**) as demonstrated in **Figure 3.4.** ***C***.

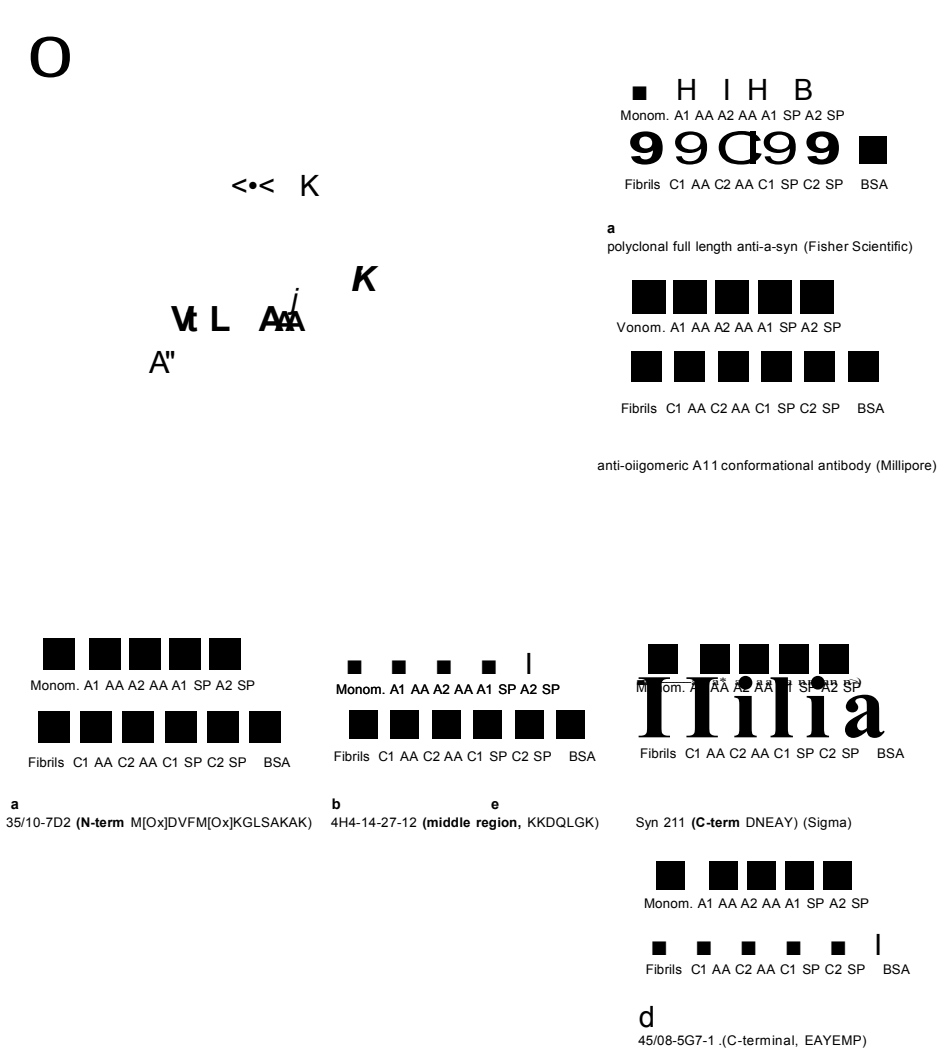

Figure 3.4. *Epitope mapping studies of different oligomeric populations performed by using a range of antibodies in the presence of bovine serum albumin control. A: a picture of oligomers with epitopes available for binding with a primary antibody detected by use of an appropriate secondary antibody; B: binding profile of oligomers and controls with polyclonal, anti-a-syn antibody (a) or A11 antibody (b); C: a-syn is illustrated as a linear structure divided into three structural segments by two dotted vertical lines; 1 being the N-termini and 140 being the C-termini. Alternate binding profile of oligomers or controls is shown on each blot that were probed with a range of mouse monoclonal antibodies developed against specific regions of the monomeric protein (a-d with given aa sequences) and placed underneath the corresponding region of the monomeric protein.*

When a positive immunoreaction is observed a dot is detected on the nitrocellulose membrane due to by binding of a specific antibody (λ) to its respective epitope that is visualised by an appropriate fluorescent secondary antibody marked with (λ*). The absence or protection of the epitope by a particular structural rearrangement or folding renders the antibody unable to bind to the specific sequence and no dot is visible on the nitrocellulose membrane. All samples bound to rabbit polyclonal full length antibody except the control showing that all contained α-syn protein except the bovine serum albumin control (**Figure 3.4. *A***). Two of these oligomers, A1 and A2 in SP gave a strong fluorescent signal when probed with the conformational antibody A11 and weaker positivity was observed for type A1 and A2 oligomers prepared in AA with the same antibody (**Figure 3.4. *B***). **Figure 3.4. *C*** illustrates the range of epitopes localised at various domains of the monomeric proteins that were detected by using mouse monoclonal antibodies. Dot blot **a** shows that 35/10-7D2 antibody (N-terminal, where mice were immunised with H-M[Ox]DVFM[Ox]KGLSKAKC-OH peptide containing oxidised Met at aa position 1 and 5 in mice) recognised A1 and A2 oligomers prepared in SP and none of the other forms. Dot blot **b** illustrates that the middle region in these two types of oligomers is buried such that it was no longer available for binding of the 4H4-14-27-12 antibody (middle region, raised against KKDQLGK motif in mice) as opposed to other forms of monomeric, oligomeric or fibrillar α-syn. Dot blot **c** indicates that the epitope comprised of the 121-126 residues was exposed and detectable by the commercial syn 211 antibody. Dot blots **d** illustrate that C1 and C2 SP oligomers gave a strong signal with the 45/08-5G7-1 antibody, (C-terminal, mice immunised with EAYEMP) and all other types appeared to be recognised to a lesser extent by this monoclonal antibody. The sequence of

45/08-5G7-1 overlaps the sequence of syn 211 and incorporates the last Tyr residue out of the four as marked by navy blue stars.

Importantly, dot blotting is unable to separate out subpopulations within the oligomeric mixture thus it gives a picture of gross immunoreactivity between a specific antibody and its respective epitope bound to it. Data of different α-syn oligomers indicated, that type A1 and A2 oligomers may have an exposed C terminal region, a buried middle region and probably have moieties that are partially exposed in the proximity of the C terminal. They also indicated that the N-terminal region has become oxidised. Of significance, these oligomers bound strongly to the A11 antibody indicative of the presence of a generic toxic conformational epitope shared between other amyloid disease states (Morten *et al.* 2007; Wang *et al.* 2009; Krishnan *et al.* 2012; Aidt *et al.* 2013). All other oligomers were unable to bind to the antibody raised against an oxidised N terminal epitope at aa 1-12, and displayed an exposed region at aa 96-102 and an accessibly exposed C-terminal epitope at aa 121-126. Another finding was that type C1 and C2 SP oligomers bound well to the antibody recognising the epitope encompassing aa 124-129, although none of the other oligomeric types were able to bind or bound less readily to this 45/08 5G7-1. These results gave a characteristic pattern for each type of oligomer produced in SP buffers and allowed to compare the oligomers produced in AA to those. Oligomers prepared in AA resembled to type C oligomers in SP associated with intracellular seeding properties.

3.4.4 Migration of a-syn oligomers on native gels

To estimate the size of the oligomers, native gel electrophoresis followed by Silver staining were performed (Figure 3.5.). A variety of gel systems have been used here, however inconclusive indications were obtained about the sizes of alternate oligomers. Using a 12 % Tris-Glycine gel (Novex) native sample buffers and native Tris-Glycine running buffer, a smeared background was observed produced by oligomeric species as reported by others under different electrophoretic conditions (Cappai *et al.* 2005, Rekas *et al.* 2010; Nasstrom *et al.* 2011). A streaked background was visible for all of the alternate oligomers except A1 and A2 SP, however distinct bands of alternate subpopulations could not be resolved. A1 and A2 SP oligomers appeared to be >1048 kDa without a smeared background using the Tris-Glycine gel system. The monomeric protein migrated with an apparent molecular weight (MW) of 146 kDa as noted by others in this native gel system (Fauvet *et al.* 2012), suggesting that determination of sizes would be inaccurate *(A).* NuPAGE®Tris-Acetate mini gels are recommended for the separation of large MW species by the manufacturer, however they have yielded limited information about the size and range of oligomers under native conditions as displayed below (*B*).

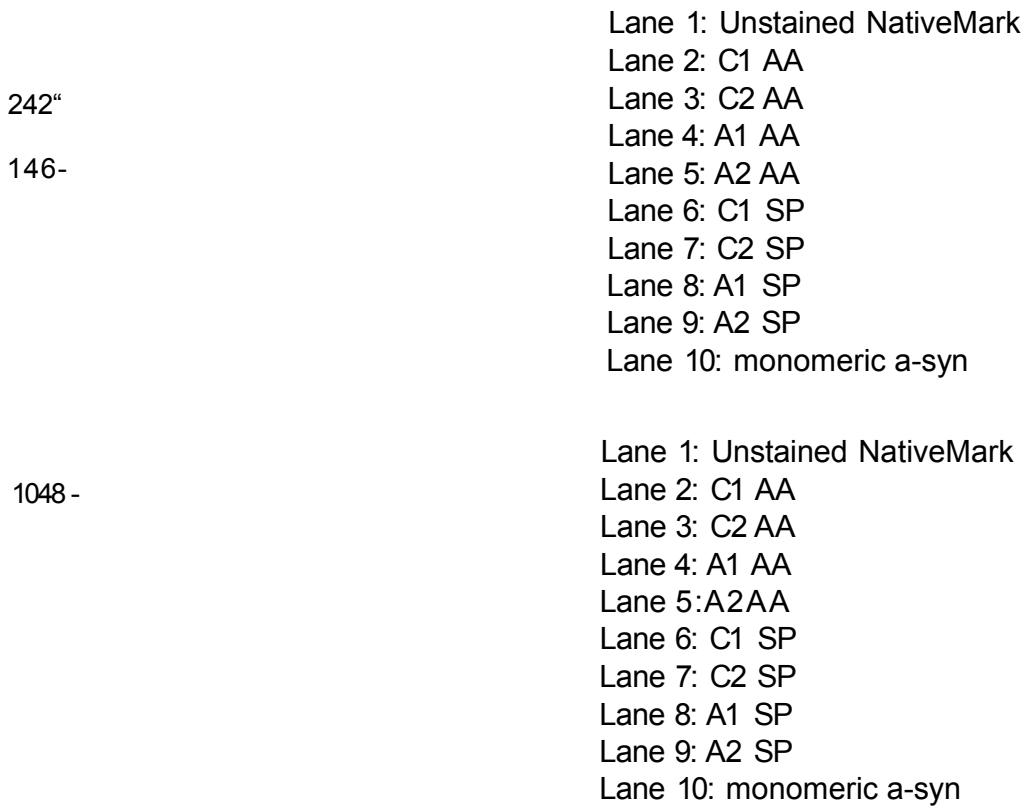

Figure 3.5. *Silver stained 12 % Tris-Glycine gel with alternate oligomeric forms and monomeric a-syn (A). Silver stained NuPAGE® Tris-Acetate mini native gel is shown with different oligomers and a-syn (B).*

Employing reducing conditions such as inclusion of SDS resulted in fragmentation or precipitation of a-syn oligomers, raising concerns once again about accurate sizing of the alternate groups (Appendix Figure 8.6.). More intense streaking in the background suggested formation of higher order oligomers, however they could not be individually resolved. The monomeric protein migrated as a -146 kDa species pointed out by the arrow in A. Type A1 and A2 SP oligomers appeared to be larger than any other species and had no background. NuPAGE® Tris-Acetate mini gels were not able to resolve the

different types of oligomers and samples did not fully enter the stacking gel as indicated by the presence of dark lines in the loading wells, suggesting poor solubility of oligomers in this system. Interestingly, A1 and A2 SP had clearer backgrounds and two populations, one with -720 kDa and another with >720 kDa. The monomer did not display a distinct band perhaps due to a limitation of the gel's resolving range (-30 kDa-400 kDa) as seen in *B.* These discrepancies demonstrated the technical limitations of using native gel systems and alternate buffer systems in which a-syn and its oligomers are still poorly characterised (Bartels *et al.* 2011; Fauvet *et al.* 2012).

3.4.5 MTT cell viability assay demonstrates that type A oligomers are toxic upon 48 hr incubation

Having undertaken spectroscopic studies and epitope mapping it remained to be seen whether the alternate oligomeric forms had relevant toxic gain of function in a cell culture model. To examine the functional features of a-syn oligomers, SH-SY5Y cell were cultured and treated with alternate oligomeric forms after which a number of selected bioassays were performed. This neuroblastoma cell line has been widely used to study PD due to its dopaminergic nature, its endogenous expression of a-syn and its suitability for mammalian overexpression of mutant a-syn (Forloni *et al.* 2000; Danzer *et al.* 2007; Wright *etal.* 2009; Danzer *et al.* 2009; Camilleri *etal.* 2013)

Firstly, to address the influence of oligomeric forms on cell viability, MTT assays were performed at different time points of 4 hr *(A),* 24 hr (*B)* and 48 hr (C) post exposure to 10 % v/v oligomeric treatment or matched vehicle controls as shown in Figure 3.6.. This technique is based on measuring the ability of

mitochondrial dehydrogenase (mtDH) to convert the yellow MTT to purple formazan crystals following oligomeric treatment for different periods of time. This assay is unable to differentiate between apoptosis or cell cycle arrest, therefore it cannot reflect cell proliferation accurately; its use is restricted to giving a snapshot of the metabolic state of treated cells based on the activity of mtDH.

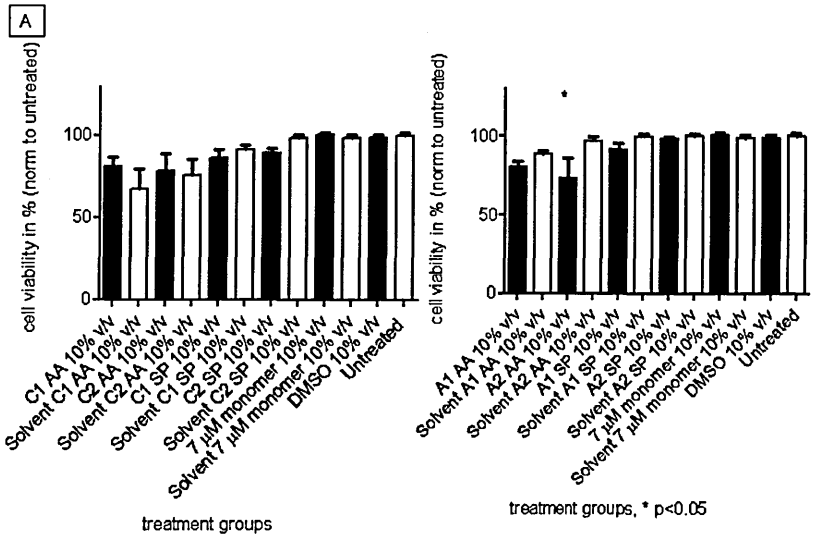
A
cell viability in % (norm to untreated)
100
50
0
C1 AA 10% v/v
Solvent C1 AA 10% v/v
C2 AA 10% v/v
Solvent C2 AA 10% v/v
C1 SP 10% v/v
Solvent C1 SP 10% v/v
C2 SP 10% v/v
Solvent C2 SP 10% v/v
7 µM monomer 10% v/v
Solvent 7 µM monomer 10% v/v
DMSO 10% v/v
Untreated
treatment groups
*
A1 AA 10% v/v
Solvent A1 AA 10% v/v
A2 AA 10% v/v
Solvent A2 AA 10% v/v
A1 SP 10% v/v
Solvent A1 SP 10% v/v
A2 SP 10% v/v
Solvent A2 SP 10% v/v
7 µM monomer 10% v/v
Solvent 7 µM monomer 10% v/v
DMSO 10% v/v
Untreated
treatment groups, * p<0.05

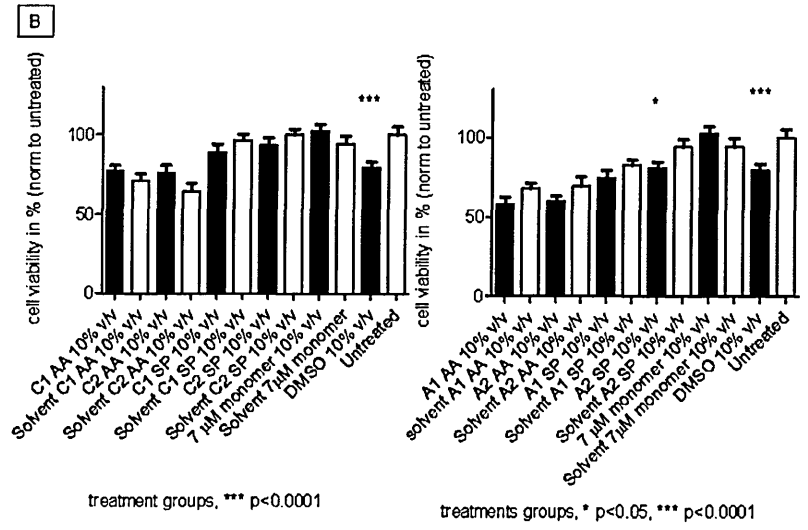
B
cell viability in % (norm to untreated)
100
50
0
***
C1 AA 10% v/v
Solvent C1 AA 10% v/v
C2 AA 10% v/v
Solvent C2 AA 10% v/v
C1 SP 10% v/v
Solvent C1 SP 10% v/v
C2 SP 10% v/v
Solvent C2 SP 10% v/v
7 µM monomer 10% v/v
Solvent 7µM monomer
DMSO 10% v/v
Untreated
treatment groups, *** p<0.0001
*
***
A1 AA 10% v/v
solvent A1 AA 10% v/v
A2 AA 10% v/v
Solvent A2 AA 10% v/v
A1 SP 10% v/v
Solvent A1 SP 10% v/v
A2 SP 10% v/v
Solvent A2 SP 10% v/v
7 µM monomer 10% v/v
Solvent 7µM monomer 10% v/v
DMSO 10% v/v
Untreated
treatments groups, * p<0.05, *** p<0.0001

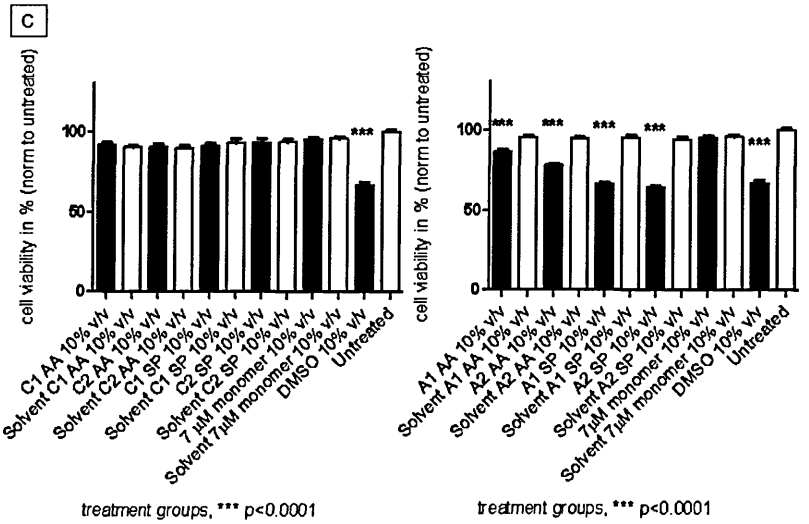
C
cell viability in % (norm to untreated)
100
50
0
***
C1 AA 10% v/v
Solvent C1 AA 10% v/v
C2 AA 10% v/v
Solvent C2 AA 10% v/v
C1 SP 10% v/v
Solvent C1 SP 10% v/v
C2 SP 10% v/v
Solvent C2 SP 10% v/v
7 µM monomer 10% v/v
Solvent 7µM monomer 10% v/v
DMSO 10% v/v
Untreated
treatment groups, *** p<0.0001
***
***
***
***
***
A1 AA 10% v/v
Solvent A1 AA 10% v/v
A2 AA 10% v/v
Solvent A2 AA 10% v/v
A1 SP 10% v/v
Solvent A1 SP 10% v/v
A2 SP 10% v/v
Solvent A2 SP 10% v/v
7µM monomer 10% v/v
Solvent 7µM monomer 10% v/v
DMSO 10% v/v
Untreated
treatment groups, *** p<0.0001

Figure 3.6. *MTT cell viability assay of SH-SY5Y human neuroblastoma cells performed at $1.0x10^5$ cells/well seeding density.* ***A*** *shows data obtained following a 4 hr treatment with 10 % v/v oligomers, their matched solvent controls and other controls.* ***B*** *represents values obtained post exposure of 24 hr incubation with alternate oligomeric treatments in addition to controls at 10 % v/v.* ***C*** *indicates MTT values in % obtained after 48 hr incubation with alternate oligomeric forms and respective controls at 10 % v/v. All treatments were set up in triplicates and read at 570 nm and 690 nm. DMSO caused significant cell death over 24 hr treatment ($p<0.0001$). All readings were averaged, appropriate solvent controls were included and subsequently values have been normalised to untreated cells (100 %). Means are plotted with ±SEM, levels of significance and p values are indicated under each group.*

Following 4 hr treatment, only type A2 AA oligomer appeared to have a significant effect on cell viability and none of the other treatments reduced the viability of neuroblastoma cells at this time point. Essentially, type A oligomers seemed to be more toxic than any other type C oligomers following the 48 hr incubation period at statistically significant levels. These findings regarding type A1 and A2 SP oligomers are in agreement with Danzer *et al.,* who showed that type A oligomers are more toxic in neuronal culture and act through activating caspase-3 leading to apoptotic pathways (Danzer *et al.* 2007). Experiments were repeated in the same way at 20 % v/v oligomeric treatment and controls and it was found that type A oligomers, in particular type A1 and A2 SP oligomers were capable of inducing cell death even at earlier type points to a statistically significant level (Appendix Figure 8.7.). These data demonstrated that type A oligomers in both AA and SP buffer had a propensity to reduce cell viability, whereas type C oligomers in both AA and SP buffer were not toxic to SH-SY5Y neuroblastoma cells.

3.4.6 Type A oligomers prepared in SP evoke a Ca(II) influx in SH-SY5Y neuroblastoma cells

The dot blotting performed in section 3.4.3. would indicate that the type A oligomers would have Ca(II) channel like behaviour due to their ability to bind A11. To confirm that the type A oligomers had Ca(II) channel-like properties, unlike type C oligomers (Danzer *et al.* 2007; Danzer *et al.* 2009), an assay was performed utilising a new generation, high specificity fluorophore, FLIPR Fluo6 Assay Kit (Molecular Devices) developed for measurement of Ca(II) influx. SH-SY5Y cells were seeded in monolayer, allowed to adhere and next day loaded with 50 pL, 2X FLIPR Fluo6 fluorophore diluted in modified Krebs buffer

followed by incubation for 60 min at 37 °C, 5 % CO_2. Following the loading of cells with the FLIPR Fluo6 fluorophore, equal volumes of treatments were injected directly onto the fluorescent dye loaded cells. Fluorescence intensities were monitored immediately at multiple time points in triplicates. Only type A1 and A2 oligomers had a propensity to increase intracellular Ca(II) to statistically significant levels (Figure 3.7.), in good agreement with previously published results (Danzer *et al.* 2007; Danzer *et al.* 2009).

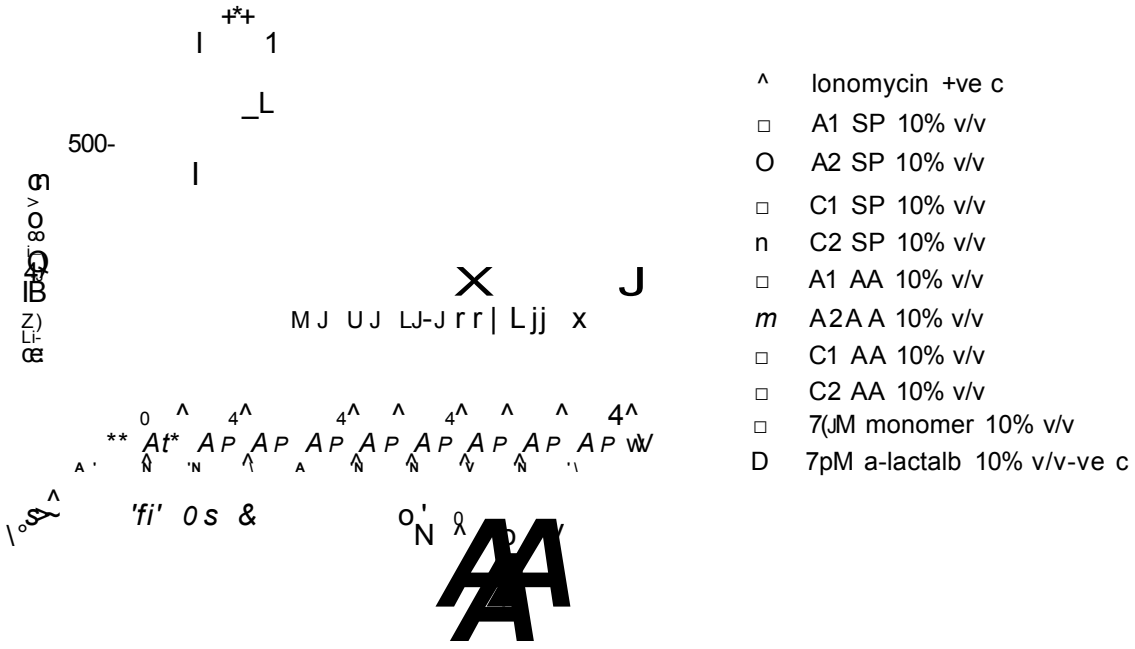

Figure 3.7. *Ca(II) influx of SH-SY5Y human neuroblastoma cells performed at 1.0x105 cells/well seeding density. A1 and A2 SP evoked a significant increase (p<0.0001) in Ca(II) levels as well as the positive control, ionomycin (p<0.001). Appropriate solvents were subtracted and means have been plotted with ±SEM, n-3, at the 60 min time point.*

As reported previously, treatment with A1 and A2 SP oligomers caused a rise in intracellular Ca(II) levels comparable to ionomycin that is powerful bacterial

ionophore (Abramov *et al.* 2003) produced by *Streptomyces conglobatus.* No other oligomer types or controls had the same effect on intracellular Ca(II) levels. α-lactalbumin was included as a negative control with similar mass to monomeric α-syn. It is important to emphasise that none of the oligomers affected cell viability significantly <4 hr so the increase in Ca(II) levels was not a secondary effect of cell death as shown by MTT assay.

Results obtained by using an older generation fluorophore, FLIPR Calcium 4 Assay Kit (Molecular Devices) (data not shown) were in agreement with findings discussed here. In previous reports, it has been demonstrated through use of defined inhibitors of Ca(II) homeostasis that this increase was attributed to influx of Ca(II) from extracellular sources and not from mobilisation of intracellular stores e.g. endoplasmatic reticulum (ER) or co-activation of other cation selective ion channels. Conducting experiments in the presence of specific inhibitors i.e. thapsigarin that block ATPase Ca(II) pumps of ER or cobalt (non-specific inhibitor) (Demuro *et al.* 2005, Danzer *et al.* 2007) can further elucidate the mechanism of action and the involvement or exclusion of particular Ca(II) channels evoking Ca(II) imbalances (Zakharov *et al.* 2007; Martin *et al.* 2012; Reznichenko *et al.* 2012) and was not of primary interest here. The gold standard would be to carry out live cell imaging or electrophysiology measurements that are capable of monitoring conductivity changes at cellular levels, however this was not completed during the time of this thesis.

These data of the Ca(II) influx assay in combination with the epitope mapping studies futher indicated that an A11 reactivity correlates with a Ca(II) channel like activity as seen for type A1 and A2 SP α-syn oligomers. None of the other

oligomers bound to the A11 antibody or bound to this conformational antibody weakly and were not capable of inducing Ca(II) imbalances.

3.4.7 Reactive oxidative stress by CMF-DA

In addition to dysregulation of Ca(II) homeostasis, a-syn oligomers have been shown to be involved in formation of reactive free radicals (Cremades *et al.* 2012) that can lead to lipid peroxidation and oxidation of vital proteins in neuronal networks (Jenner 2003). In contrast, there are theories that suggest a primary causative role for ROS and free radical formation rather than being a mere consequence, implying that they are key triggers of a complex sequence of events that initiate mitochondrial dysfunction, protein misfolding and neurotoxicity (Nasstrom *et al.* 2011; Ruiperez *et al.* 2010; Mattson 2011). To assess the formation of free radicals of protein oxidation resulting from cellular exposure to oligomers, a fluorescent cell tracker CMF-DA was utilised (Watabe *et al.* 2007; Idkowiak-Baldys *et al.* 2010). This marker diffuses freely across the membrane and once it is inside the cell intracellular esterases can cleave it and convert it to a fluorescent impermeable form that is able to react with thiols of proteins or peptides. To examine whether oligomers can cause detectable oxidative stress, neuroblastoma cell were exposed to oligomeric treatments for alternate lengths of time, where matched solvent controls and H_2O_2 were included as controls. Figure 3.8. *A* shows data collected after 4 hr incubation of SH-SY5Y cells with each alternate oligomers matched and vehicle controls. *B* represents fluorescent intensity measurements of SH-SY5Y cell overexpressing A53T mutant that were treated in the same manner. The neuronal phenotype of these cell lines was confirmed by staining for neurofilament as shown in Appendix Figure 8.11.. A stable overexpression of the A53T mutant was kindly

established by Mafalda Ramos, Erasmus Programme. Expression levels were confirmed by immunocytochemistry as illustrated in **Appendix Figure 8.8.**. These cells were maintained in DMEM with 250 µg/mL G418 selective antibiotics and used here to detect free radicals post-oligomeric treatment.

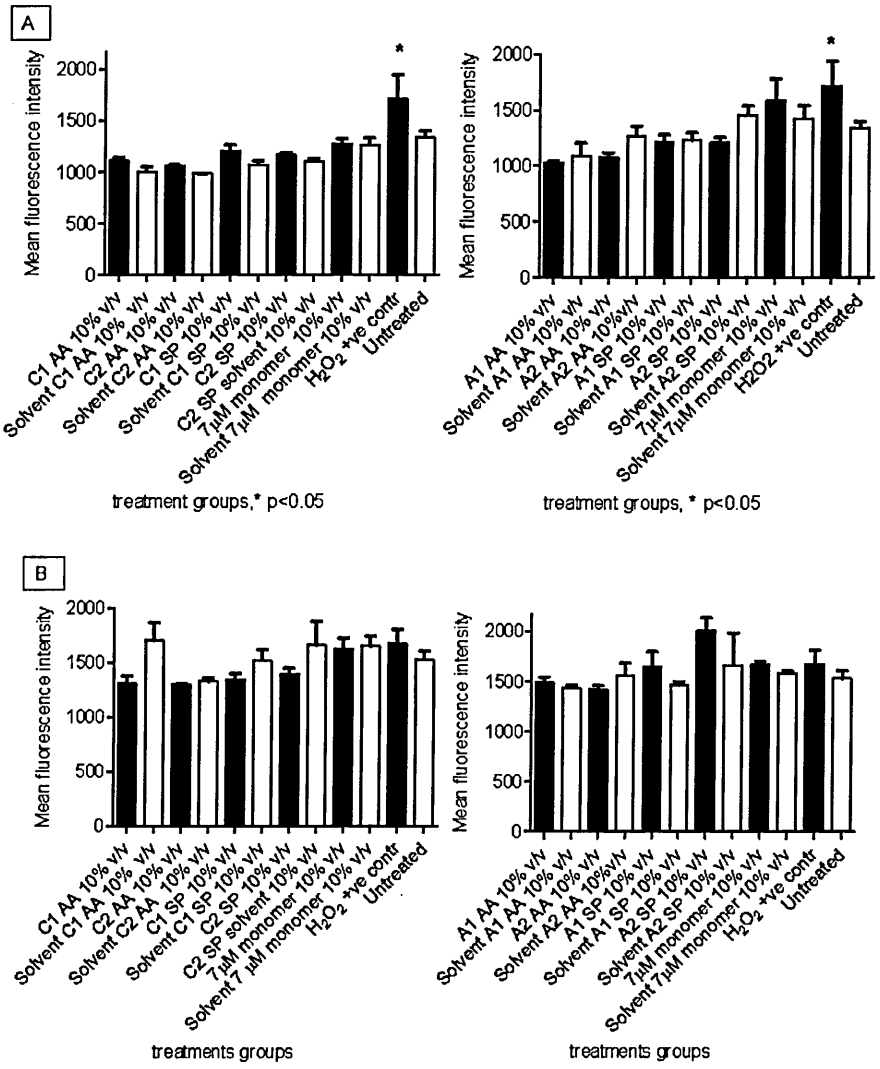

Figure 3.8. *ROS induction and protein oxidation after alternate treatments. SH-SY5Y cells (1x10^5 cells/ well) were treated with 10 % v/v oligomers, vehicle controls or other controls for 4 hr and measurements were taken in triplicates at 485 nm and 530 nm (**A**). SH-SY5Y cells overexpressing A53T α-syn were exposed to the same treatments for 4 hr and readings were recorded and plotted as mean values ±SEM of three biological replicates (**B**).*

All other data collected after 8 hr treatment or overnight with alternate oligomers and the appropriate controls is shown in Appendix Figure 8.9.. None of the oligomeric treatments evoked statistically significant production of reactive oxidative species detectable by CMF-DA at 10 % v/v following 4 hr treatment in these cell lines, indicating that the oligomers do not exert their biological effect through the production of ROS. Another explanation may be that the assay was not sensitive enough to detect subtle changes in the production of ROS upon a-syn oligomeric treatment of neuroblastoma cells.

3.4.8 Functional assays in cell culture- Intracellular aggregation induced by extracellularly added oligomers

It has been documented that certain forms of a-syn from the extracellular environment are internalised and induce a seeding mechanism (Danzer *et al.* 2007; Danzer *et al.* 2009; Luk *et al.* 2009; Angot *et al.* 2012) resulting in intracellular a-syn being triggered to self-aggregate. The notion of intracellular propagation of a-syn is in its infancy (Angot *et al.* 2010; Prusiner 2012; Kraus *et al.* 2013) and much research has been performed to dissect this intracellular cell-to-cell transfer mechanisms (Danzer *et al.* 2012) and follow the fate of a-syn species through from intake, processing (Lee *et al.* 2005) to elimination of toxic aggregates (Emmanouilidou *et al.* 2010a; Emmanouilidou *et al.* 2010b; Esteves *et al.* 2011). Treatment with type C1 and C2 SP oligomers has been shown to cause a marked reduction in otherwise homogeneous cytoplasmic staining of a-syn and cause a striking increase of punctate, aggregate formation in the cytosol and near the nucleus in neuronal cultures (Danzer *et al.* 2009). To test the propensity of the previously described oligomers and other oligomers compatible with mass spectrometry to induce intracellular aggregation of a-syn,

SH-SY5Y cells overexpressing the α-syn A53T mutant were exposed to treatments. Effects of exposure of SH-SH5Y cells overexpressing A53T α-syn, to monomeric and solvent controls for 8 hr were also assessed. In brief, after exposure to and removal of excess extracellular α-syn treatments for 8 hr, fixation and washing steps were done followed by using monoclonal mouse, syn 211 (Sigma) primary antibody that was detected by a fluorescent secondary Alexa Fluor 594 conjugated goat anti-mouse antibody for immunofluorescent microscopy imaging as described in more detail earlier. In a control experiment, primary antibody was omitted and confirmed that background fluorescence with the secondary antibody was not considerably high.

The findings shown here demonstrated that indeed type C1 and C2 SP oligomers prepared had a propensity to induce intracellular aggregation (Danzer *et al.* 2007; Danzer *et al.* 2009) (**Figure 3.9.**). In contrast, type A1 and A2 SP oligomer did not show an altered cytoplasmic staining in neuroblastoma cells overexpressing A53T α-syn mutation, indicating that these oligomers lacked the ability to induce intracellular aggregation (**Figure 3.10.**). Together, all types of oligomers produced in AA had an enhanced ability to induce intracellular aggregation. In line with this activity, their dot blotting profile matched type C1 and C2 SP oligomers' that have earlier been demonstrated to exclusively seed transmembrane aggregation of A53T α-syn overexpressed in neuronal cell types (Danzer *et al.* 2007; Danzer *et al.* 2009).

Experiments were repeated three times and results were uniform throughout, indicating that type C1 SP, C2 SP, C1 AA, C2 AA, A1 AA, A2 AA had a pronounced effect on seeding aggregation of intracellular α-syn when applied extracellularly. The same results were obtained in non-transfected SH-SY5Y

cells (**Appendix Figure 8.10.**). Punctate formation of these α-syn oligomers was evident in contrast to their respective vehicle controls or in contrast to type A1 and A2 SP. These data of the intracellular aggregation assay showed that all mass spectrometry compatible oligomer types and type C oligomers prepared in SP induced intracellular seeding when added extracellularly in human neuroblastoma cells.

magnification. The arrows indicate intracellular aggregates of a-syn in the cytoplasm following treatment with type C oligomers.

luawjeajj. }U0A|OS

3.5 Conclusions

a-syn oligomers are believed to be toxic in PD and other neurodegenerative diseases (El-Agnaf *et al.* 2006; Jellinger 2011; Eller *et al.* 2011), however a comprehensive understanding of the role of these amyloid precursors is still lacking. Many oligomeric preparation protocols of a-syn have been developed *in vitro* in recent years with the aim to reveal the dynamics governing aggregation of the natively unfolded protein into these toxic forms and to elucidate how they exert their toxicity whilst interacting with biological membranes and cellular organelles such as mitochondria and lysosomes (Lashuel *et al.* 2002, Demuro *et al.* 2005; Kim *et al.* 2009; Danzer *et al.* 2007; Danzer *et al.* 2009; Giehm *et al.* 2011; Winner *et al.* 2011; Cremades *et al.* 2012; Gurry *et al.* 2013). The presence of specific modulatory ligands during the oligomerisation process and their correlating biophysical and biochemical characteristics have also been addressed (Li *et al.* 2005; Wright *et al.* 2009; Leong *et al.* 2009b; Singh *et al.* 2013). It has been previously shown that alternate preprative methods lead to distinct classes of *in vitro* oligomeric forms of a-syn with alternate toxic gain of function. Type A oligomers were associated with Ca(II) channel-like properties and were more toxic in neuronal cells (Danzer *et al.* 2007), whereas type C oligomers had a propensity to induce transmembrane seeding in a dose and time dependent fashion in both primary cortical neurons and neuronal cell lines (Danzer *et al.* 2009). AFM experiments suggested that type A oligomers had an annular morphology ~2-4 nm in height and type C oligomers were protofibrillar and globular structures with -4-10 nm in height (Danzer *et al.* 2007). No further information about the structural details of these oligomers has been uncovered to date. To reveal additional insights into the secondary and tertiary structures

of these oligomers by mass spectrometry and to establish links between their structure and toxic gain of function, oligomer preparation protocols were adapted (Danzer *et al.* 2007) to aid further characterisation. The described biological properties of type A and type C oligomers both Fe(III)-free (type A1 and type C1 SP) and Fe(III)-supplemented (type A2 and C2) prepared in SP were consistently reproducible in SH-SY5Y cells.

The main aim of this work was to determine the mass and geometry of prefibrillar aggregates by means of ESI-IMS-MS in a similar manner to other amyloidogenic proteins (Bernstein *et al.* 2009; Smith *et al.* 2010; Bleiholder *et al.* 2011; Grabenauer *et al.* 2010a; Woods *et al.* 2012). To achieve this, the previously established preparation protocols with using a relatively low concentration of the monomeric protein (7 μM α-syn) had to be altered by substituting SP buffer with AA buffer.

It was crucial to investigate whether these second set of oligomers had any similarity with those reported in the literature and are referred to as type A1 and A2 AA and type C1 and C2 AA. Since α-syn's native conformation and assembly is largely influenced by its immediate environment is was necessary to perform comparisons of the mass spectrometry compatible oligomers with established variants produced in SP. Membrane binding properties and the aggregation kinetics of α-syn are also thought to be affected by alternative use of solvent. α-syn preferentially binds to small (20-25 nm) vesicles rather than larger vesicles with a composition of phosphatidic acid (PA), phosphatidylserine (PS) and phosphatidylglycerol (PG) and not to vesicles with a net neutral charge like phosphatidylcholine (PC) (Davidson *et al.* 1998; Munishkina *et al.* 2007). It has been shown that an increase in NaCl concentration (0-500 mM)

resulted in a decrease of α-helix content and an increase in the random coil content, correlating with a decreased ability of α-syn to bind to synthetic vesicles as shown by biophysical structural tools (Davidson *et al.* 1998). Secondary structure analysis of α-syn using FTIR demonstrated that different types and percentages of alcohols as well as changes in pH cause alterations in the relative populations of partially folded state, β-structure and α-helix (Munishkina *et al.* 2003).

Regarding fibril formation, addition of SP oligomers could seed fibrillisation to amyloid fibrils or at least the quantum yield of fluorescence was increased in SP when monitored by ThT assay. Type A oligomers produced in SP promoted the formation of mature fibrils with cross β-sheet as indicated by both the ThT assay and the use of fibril specific anti-amyloid fibril LOC antibody, whereas type C led to an increased ThT signal. By contrast, fibrillisation of α-syn by agitation was slightly slowed in AA and the seeding effect of oligomers prepared in AA was negligible as measured by ThT assay. Oligomers with seeding ability diminish or shorten the otherwise slow lag phase of α-syn are considered as on pathway to fibril formation (Kim *et al.* 2009). This would infer that the cellular seeding oligomers are off pathway or that the concentration of oligomers produced in AA is below that required for an observable *in vitro* seeding effect.

The next step in addressing any differences between these alternate oligomers was to perform spectroscopic methods reliant on internal fluorescence of Tyr residues or externally added fluorescent ANS dye. Tyr fluorescence measurements showed that type A1 and A2 SP oligomers had enhanced quantum yields as compared to all other oligomeric types and again only these two oligomers displayed a blue shift upon addition of ANS that favours binding

to hydrophobic patches. All other oligomer types had a lower fluorescence signal upon Tyr emission scanning and did not show λ_{max} shift during ANS fluorescence emission scanning. These measurements indicated that the Ca(II) channel-like oligomers are more hydrophobic and perhaps the mainly the C-terminally located Tyr residues reside on the surface and relatively unquenched in their assembly.

Epitope mapping studies by dot blotting have provided further support for this concept and indicated that A1 and A2 SP oligomer types bound strongly with the conformational antibody, A11 that has been indicated in pathogenic conformations (Morten *et al.* 2007; Wang *et al.* 2009; Krishnan *et al.* 2012; Aidt *et al.* 2013). Type A1 and A2 AA oligomers bound weakly to A11 antibody and no binding was detected for type C oligomers in AA or SP. Kremer *et al.* reported that aggregated Aβ had a propensity to reduce membrane fluidity and an enhanced aggregation rate and surface hydrophobicity correlated with lower membrane fluidity (Kremer *et al.* 2000). In accordance with this, prefibrillar aggregates of a variant of Aβ 1-42 peptide showed a pronounced binding to ANS and alterations in its ANS binding ability correlated with changes in toxicity in SH-SY5Y cells (Bolognesi *et al.* 2010). An increment in ANS binding was reflected in an increased effect on cell death in case of of WT Aβ1-42, I59T mutant of human lysozyme and an SH3 motif of PI3 kinase, indicating that the exposure of hydrophobic motifs are central to cytotoxicity. The intensity of ThT binding did not correspond to ANS binding or cytotoxicity when monitoring these peptides or proteins in a time dependent manner (Bolognesi *et al.* 2010). Furthermore, another recent finding showed that a region of yeast prion Sup35 (NM) could be arrested in its assembly pathway to produce either A11 positive aggregates by use of a number of small molecules or cross-linking. The

oligomers generated were either A11 reactive, more hydrophobic and toxic in neuroblastoma cells or produced OC positive, larger oligomeric states exhibiting less toxicity and hydrophobicity (Krishnan *et al.* 2012). These observations regarding an increased hydrophobicity and A11 reactivity hold true for type A1 and A2 SP oligomers.

Probing the different oligomers with monoclonal in-house antibodies raised against distinct epitopes of α-syn dispersed on its 3 structural domains revealed further deviations in their epitope mapping profiles. Using the 4H4-14-27-12 antibody raised against aa 96-102 did not bind to A1 and A2 SP oligomers. This could mean that these residues are folded in the core of A1 and A2 SP oligomers in a shielded position, prohibiting binding to this antibody. These observations may well be reflective of the toxic gain of function to disorder lipids and give an entry to extracellular Ca(II) (Kremer *et al.* 2000; Stockl *et al.* 2012). It may be possible that such kind of folding affects packing of the lipid bilayer, where an initial membrane binding could be facilitated by the N-terminal domain that cause membrane perturbations that then permit penetration of further hydrophobic residues into the interior and access for small molecules i.e. Ca(II). As shown by syn 211 antibody, the epitope located at aa 121-125 was exposed on each oligomers and binding was observed. This observation was similar to recent findings that suggested that the C-terminal region is not likely to be significantly involved in the formation of β-sheet structure of fibrils and it remains solvent accessible (Miake *et al.* 2002), enabling binding of nanobodies to C-terminal epitopes (Guilliams *et al.* 2013). Furthermore, the C terminal of α-syn contains numerous acidic residues and prolines described as structure breaking motifs (Zakharov *et al.* 2007) and tends not to acquire a structured fold.

It was intriguing to examine whether the oligomers prepared in AA had biologically relevant characteristics that were comparable to those of SP ones. MTT cell viability assay demonstrated that type A oligomers, both AA and SP became significantly toxic after longer incubation times at 10 % v/v post exposure and toxicity was more pronounced at 20 % v/v. This gives support to the fact that weakly (A1 and A2 AA) or strongly positive (A1 and A2 SP) A11 oligomers appear to be more toxic in neuronal cells. Type C oligomers did not cause statistically significant cell death when compared to matched solvents after the duration of 4 hr, 24 hr or 48 hr treatment.

Neither of these oligomers evoked significant protein oxidation when measuring cellular thiol content using CMF-DA probe following 4, 8 and 24 hr treatment with alternate oligomeric types. However, literature suggest that combined use of dihydroethydium measuring superoxyde anion levels (Yang *et al.* 2010; Cremades *et al.* 2012; You *et al.* 2013), C11-BODYPY581/591 (Chen *et al.* 2007) measuring lipid peroxidation and MitoSOX measuring mitochondrial species (Cremades *et al.* 2012) could have given more comprehensive information about ROS.

Ca(II) measurements confirmed that type A1 and A2 SP oligomers evoked an increase in intracellular Ca(II) levels consistently with Danzer *et al.* and none of the other subsets showed Ca(II) channel-like properties (Danzer *et al.* 2007). It is interesting to note Campioni *et al.* inferred that high hydrophobicity of HypF-N oligomers correlated with an increased propensity to penetrate the cell membrane and caused intracellular influx of Ca(II) (Campioni *et al.* 2010).

As the next step in functional characterisation, the transmembrane seeding of oligomers was assessed it was found that all oligomers prepared in AA induced

intracellular aggregation after treatment for 8 hr akin to C1 and C2 SP oligomers (Danzer *et al.* 2007; Danzer *et al.* 2009). Considering all spectroscopic data and the epitope mapping data alongside the intracellular (IC) seeding assay, it seems likely that type A1 AA, A2 AA, C1 AA, C2 AA, C1 SP and C2 SP oligomers have very similar biochemical and biological properties. The only features that set type A1 and A2 AA apart from type C oligomers in either SP or AA is that they reduced cell viability to a higher extent and they bound weakly to A11 antibody (**Figure 3.11.**). The assembly of oligomers is a very dynamic process and the aggregation conditions such as concentration and buffer conditions will determine what types of oligomers are formed. It has been shown that type A pore forming oligomers could convert to type C oligomers inducing intracellular seeding poperties in neuroblastoma cells when the preformed type A oligomers underwent an additional "ultrafiltration step". It is possible that type A1 and A2 AA had a subset of oligomers types that produced an A11 positive structure but these oligomers were not capable of introducing Ca(II) influx at the conditions used here. Perhaps type A1 and A2 AA oligomers had subpopulations of type C like states and a minor subpopulation of oligomers resembling A1 and A2 SP oligomers that could be detected by the A11 antibody. This would employ a roll in buffer competition in tipping the aggregation between the two oligomer assembly pathways and will be investigated further in Chapter 4.

Figure 3.11. *The key findings of alternate a-syn oligomers formed from the monomer are shown regarding their biochemical and cytotoxic properties. Intriguingly, distinct oligomers of a-syn possess different degree of hydrophobicity and immunoreactivity with A11 antibody and elicit different responses in SH-SY5Y cells regarding cytotoxicity, transmembrane seeding or Ca(II) imbalances. The oligomeric forms developed under mass spectrometry compatible conditions are highlighted by a blue line. The dotted line indicates that the pore forming type A oligomers can convert to the type C oligomers with seeding properties following ultrafiltration of preformed type A oligomers as reported earlier by Danzer et al.* (Danzer *et al.* 2009).

Finding clues as to why intracellular, transmembrane seeding was observed for all oligomers prepared in AA when seeding properties were moderate as judged by ThT will remain to be an endeavour.

Additional biochemical evidence mainly via spectrometric measurements and epitope mapping studies has been provided that in part helped to better explain some of the toxic functions of a set of *in vitro* oligomers. By revealing details about epitopes located at various regions and by shedding light on basic biochemical entities supporting biological behaviour of these oligomers it is conceivable that these new insights may inform the design of therapeutic agents targeting prefibrillar intermediates. It would be of particular interest to isolate oligomeric species from the CSF and sera of PD patients and examine whether there are any biophysical and biochemical similarities between *in vivo* and *in vitro* oligomeric populations of α-syn. In addition, a new group of altered oligomers with tangible biochemical and biological functions have been prepared reproducing previously described cytotoxic aspects of oligomers reported by Danzer *et al.* (Danzer *et al.* 2007). These oligomers have allowed the ascertainment of much needed structural information about subunit size and geometry and will be discussed in the next chapter.

4 Chapter 4

Structural insights into oligomerisation of a-syn

4.1 Introduction

4.1.1 Applications of ESI-IMS-MS

The early pioneering work of Jarrold, Kemper, Bowers and their co-workers has laid down the foundations of investigating gas phase ion structures of atomic carbon clusters (Shvartsburg *et al.* 1998) cluster ion isomers (von Helden *et al.* 1991; von Helden *et al.* 1993) and metal ions in the gas phase and built a framework for calculating and modelling mobilities of these molecules by projection approximation (PA) (Wyytenbach *et al.* 1997) or by exact hard sphere scattering (EHSS) (Shvartsburg *et al.* 2008; Shvartsburg *et al.* 1996; Shvartsburg *et al.* 2007). ESI-IMS-MS has subsequently become a favourable tool in analysing a broad array of inorganic and organic, biological systems (Heck *et al.* 2004; Koeniger *et al.* 2006). Due to its sensitivity, speed of analysis and ability to determine structural transitions, ESI-IMS-MS has been harnessed in investigating the structure and complex assembly of proteins (Ruotolo *et al.* 2005; Frimpong *et al.* 2010), peptides (Michaelevski *et al.* 2010b; Harvey *et al.* 2011), carbohydrates (El-Hawiet *et al.* 2012b) and nucleic acids (Rosu *et al.* 2008). ESI-IMS-MS has also found applications in analysing the structure and identity of small molecules, monitoring ligand binding interactions (Grabenauer *et al.* 2008; El-Hawiet *et al.* 2012a; Kitova *et al.* 2012; Deng *et al.* 2012; Soper *et al.* 2013), dissecting multisubunit amyloidogenic complexes (Bernstein *et al.* 2009; Smith *et al.* 2010; Kloniecki *et al.* 2011), bacterial pili complexes (Leney

et al. 2011), bacteriophage (Shepherd *et al.* 2011) and complex multi-symmetric viral (Uetrecht *et al.* 2011) assemblies. This technique lends support when answering research questions regarding topology and dynamics of co-populated complexes (Smith *et al.* 2010; Grabenauer *et al.* 2010a), dissociation of complexes or conformers (Ruotolo *et al.* 2007; Giganti *et al.* 2011; Kukrer *et al.* 2012) and characteristics of small molecules that are pertinent in therapeutic applications (Woods *et al.* 2012; Marcoux *et al.* 2013b; Niu *et al.* 2013).

4.1.2 Instrumentational characteristics of ESI-IMS-MS

During an ion mobility experiment, the time taken for an ion to travel through a neutral gas under the influence of an electric field is measured. This time is dependent on the charge, mass and conformation of the ion; for a given ion of the same mass and charge an ion with a large Q would take longer to traverse through the buffer gas, while an ion of smaller Q would travel faster (Mason *et al.* 1988). The Q of an ion is therefore closely linked to its structural properties (von Helden *et al.* 1991; Wyytenbach *et al.* 1997; Jarrold 2000; Shvartsburg *et al.* 2008).

The introduction of biological molecules into the gas phase while preserving conformation and non-covalent interactions requires the use of so-called soft ionisation techniques. Electrospray ionisation is one such method that is strongly associated with the legacy of Fenn who was awarded a Nobel prize in Chemistry for his invention enabling “molecular elephants to fly” into the gas phase *(“in vacuo")* (Fenn *et al.* 1989). During this soft ionisation technique, samples are introduced in conductive gold coated borosilicate capillaries or by an automated sampling source (nanoMate) in the presence of a weak electric

field and these parameters are critical in obtaining a stable electrospray for a good quality mass spectrum (Michaelevski *et al.* 2010b). The analyte of interest is subsequently extracted by the sample cone of the instrument. An electrospray source generates a "Taylor cone" from which a fine mist of molecules is produced. The use of volatile solvents result in highly charged droplets. Evaporation occurs when the Coulombic repulsion of the charges on the surface of the droplet overcomes the surface tension of the molecule resulting in fission. The point at which the fission occurs is termed as the Rayleigh limit (Rayleigh 1882, Konermann 2009). The progeny droplets undergo further evaporation and fission until only gas phase ions are present as illustrated in **Figure 4.1.** (University of Bristol, School of Chemistry). The number of charges on the ion is then dependent on the accessible surface area and the presence of ionisable groups. The size of the initial droplet also influences the ionisation process and such nanoESI (nESI) has been developed to facilitate a more efficient ionisation, using a fine tapered capillary with a filling volume of ~5-10 µL.

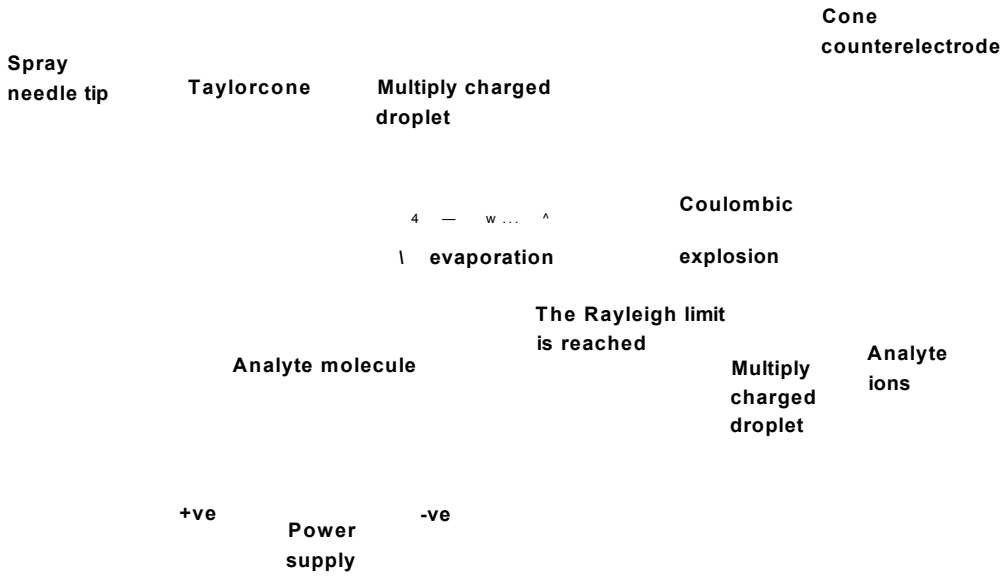

Figure 4.1. *Diagram of the mechanism of electrospray ionisation, releasing dehydrated multiply charged analyte ions. Image taken from Univeristy of Bristol's website (htpp://www.chm.bris.ac.uk/ms/images/esi-mechanism.gif)* (University of Bristol, School of Chemistry).

There are two models to describe the ionisation: i, the ion evaporation model that is associated with smaller ions (Thomson *et al.* 1979; Tang *et al.* 1993) and ii, the charge residue model that is associated with larger molecules e.g. proteins (Fernandez de la Mora, J. 2000; Kaltashov *et al.* 2005). According to the latter mechanism, the droplets evaporate completely and ions become desolvated. The protein is charged by the residual charges that located on the surface and provided that charge is conserved, during the ESI process the surface charges are transferred to the basic sites of proteins. The number of the basic residues on the surface will determine how many charges that protein obtains (de la Mora, J., F. 2000). The number of charges that the complex will obtain can be estimated based on the mass of the protein when sprayed from aqueous AA at neutral pH. The calculated charge can be estimated by the

Rayleigh limit, with the size equivalent to the protein in question as follows (Heck *et al.* 2004):

$$z_R = 8\pi\sqrt{\gamma\varepsilon_0 R^3}$$

Equation 2. *Predicted charge calculation, where γ is the surface tension of the water droplet, ε0 is empirical permittivity of vacuum, e is the elementary charge and R is the radius of the droplet.*

Making an assumption that the radius of the protein correlates to the mass of the protein and its density is similar to water a simplified equation can be created as shown below:

$$z_R = 0.078\sqrt{M}$$

Equation 3. *Calculated charge of a protein (z), in which M is the Mass in Da.*

Hence, an 18.4 kDa folded globular protein for example would be expected to have 8 charges and a 36.9 kDa globular dimer would accommodate 12 charges and a 72.7 kDa heptamer would possess 18 charges (Heck *et al.* 2004).

During acquisition multiple charge states can be observed due to the inherent feature of basic amino acid side chains of proteins to pick up several charges when protonated. The range of these charges is referred to as the charge states distribution (CSD) or envelope. The highest observed charge state is dictated by the number of basic residues (Covey *et al.* 1988; Loo *et al.* 1988) and the electrostatic repulsions (Schnier *et al.* 1995) between protonated basic residues. Folded proteins are known to display a narrower CSD, with 2 to 4 being observed due to the limited number of basic residues located on the surface of the protein. Unfolded proteins display a wide CSD distribution due to

all ionisation sites being available and the highest observed charge state is therefore shifted to the lower *m/z* ratios. This correlation between the surface area of proteins and the maximum CSD has been well researched and documented (Fernandez de la Mora, J. 2000; Heck *et al.* 2004; Kaltashov *et al.* 2005).

Solvent accessibility adds another layer of complexity where folded protein conformations are likely to have residues that are inaccessible, buried and unable to carry as many charges as their unfolded counterparts. Another alternative theory hypothesizes that intramolecular interactions have a role to play and neutralisation of opposite charges may occur (Grandori 2003; Samalikova *et al.* 2003).

In experimental work, solvent compositions such as pH can practically alter basicity and CSD (Smith *et al.* 2007), high acid, base or alcohol can effectively unfold a closed conformation and shift CSDs to high charge states (Loo *et al.* 1991; Samalikova *et al.* 2004; Grabenauer *et al.* 2008; Natalello *et al.* 2011; Santambrogio *et al.* 2011). Mutations with amino acid substitutions and the presence of binding partners i.e. metals, polycations may modulate the CSD (Loo *et al.* 1991; Grabenauer *et al.* 2008; Natalello *et al.* 2011; Grabenauer *et al.* 2010b; Hilton *et al.* 2010). Instrumental settings such as desolvating voltages, temperature (Loo *et al.* 1988; Benesch *et al.* 2003; Ruotolo *et al.* 2005; Grabenauer *et al.* 2010b; Dupuis *et al.* 2009), sprayer tips and gas pressures (Michaelevski *et al.* 2010b; Sterling *et al.* 2012) are crucial to be controlled as they can cause artefacts and substantially alter CSDs. The use of supercharging additives e.g. m-nitrobenzyl alcohol, sulfolane and metals that change CSDs with potential technical benefits has been demonstrated as a new

approach in ESI-IMS-MS analysis (Lomeli *et al.* 2009; Sterling *et al.* 2011; Sterling *et al.* 2012; Flick *et al.* 2012). Here a commercially available ESI-IMS-MS instrument, the Synapt G2 HDMS (illustrated in Figure 4.2.) has been utilised in the study of a-syn monomer and complex formation.

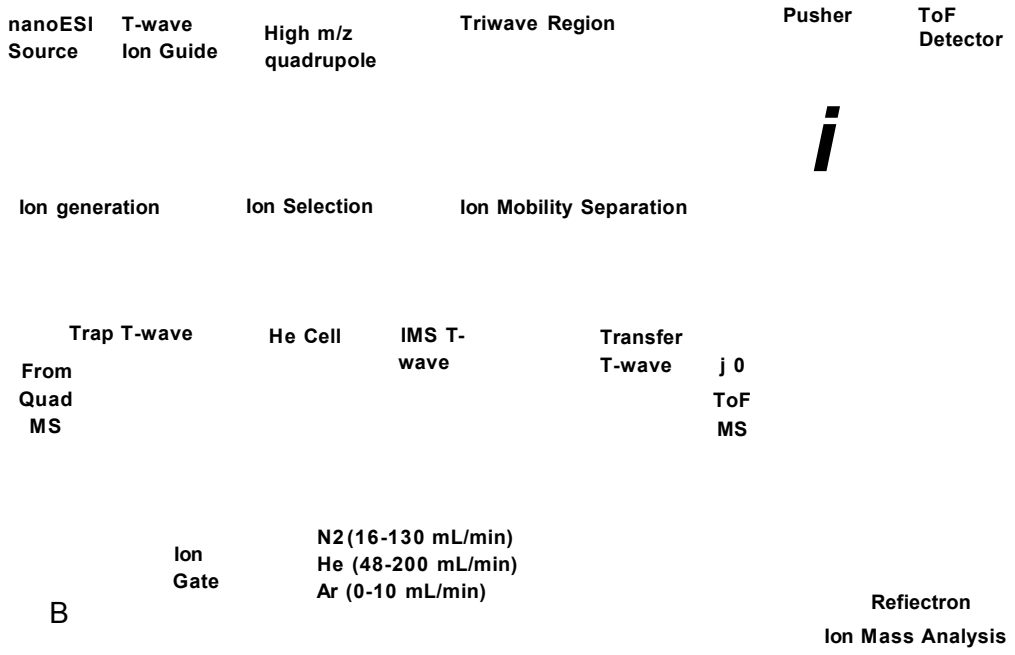

Figure 4.2. *A diagram of the Synapt G2 instrument. Reproduced by permission of The Royal Society of Chemistry,* (Zhong *et al.* 2011). *The main compartments are: ionisation (nESI), ion selection (modified quadrulope mass analyser), ion mobility separation containing the triwave region and ion mass analysis (time-of-flight mass analyser). B is a detailed picture of the triwave region. Three major travelling waves operate to enable ion mobility separation. The light blue region is the trap region pressurised by Ar where pockets of ions are collected, the green He pressurised gate region pulses the ions across into the middle darker blue regions where the ion mobility separation takes place in N2. The pink region is the transfer region filled with Ar allows furthering ions for mass detection.*

The ion mobility separation region consists of 168 x0.5 mm wide plates 1 mm apart in which the RF field operates to align ions axially, whilst travelling waves perform ion mobility separation by superimposing transient direct current (DC) to the electrodes in the stacked ion rings. Ions then enter the transfer region in which slower moving triwaves help to limit the diffusion of post- ion mobility ions in Ar gas. Subsequently, ions are separated and detected by their *m/z* values in the mass analyser (Giles *et al.* 2004; Harvey *et al.* 2011). Each region has a controlled gas flow that is critical in maintaining non-covalent interactions similarly to other parameters during the electrospray process such as desolvation voltages (cone and capillary).

The wave heights and wave velocities in the ion mobility separation region should also be tuned to enable adequate separation of ions and accurate experimental Ω and informative of the molecular species under those particular conditions (Jurneczko *et al.* 2011; Zhong *et al.* 2011). Following a gated release of a pocket of ions 200 mass spectra are acquired and this process is repeated during which the next 200 spectra are added to the corresponding spectra until the next summation period commences. The cumulative mass spectrum is then produced by combining the total mobility data over a given acquisition time. Fragmentation of ions can be performed both pre- ion mobility enabling separation of product ions by ion mobility and post- ion mobility separations.

Protein confirmations are usually studied both in their denatured states dissolved in 50 % methanol 50 % water with 0.1% formic acid or in 10 % formic acid 50 % acetonitrile and 40 % deionised water and in their native states using AA as a solvent (Jurneczko *et al.* 2011). Ion mobility acquisitions presented in a mass spectrum that reports *m/z* values of ions (x axis) and on the y axis relative

abundance of ions is seen. In addition, it provides mobilograms in the form of mobility plots, where drift time (in msec) is plotted as a function of *m/z*.

Due to the sensitivity of this technique isobaric species can be resolved as well as stereoisomers and conformational isomers. Isomers of Leu and Ileu (131 Da) have been distinguished with Ωs of 68.95 $Å^2$ and 70.51 $Å^2$, respectively (Knapman *et al.* 2010).

Ions resulting from proteins or complexes of the same conformation series cluster on a mobility plot due to the fact that ions with higher charge states traverse the drift cell more rapidly than larger molecular ions with greater *m/z* values and lower charge states. Conformational families can be distinguished from each other by comparison of these distributions (Kanu *et al.* 2008). As such, higher charge states of proteins and peptides tend to fall towards the bottom of mobility plots and decrease by 1 $[H]^+$ between adjacent charge states in a diagonal fashion as it can be seen in case of cytochrome c on **Figure 4.3.**. Similarly to heat maps, the colour intensity of the Driftscope is reflective of the intensity of a respective molecular ion's relative abundance and the peak maxima of its extracted drift time as illustrated for the commonly used globular protein standard cytochrome c. For example, the most abundant charge state ion of cytochrome c under native conditions is the +6 charge state ion being the darkest peak on the mobility plot (**Figure 4.3. *A***) and the +15 charge state is the most dominant ion under denaturing conditions (**Figure 4.3. *B***).

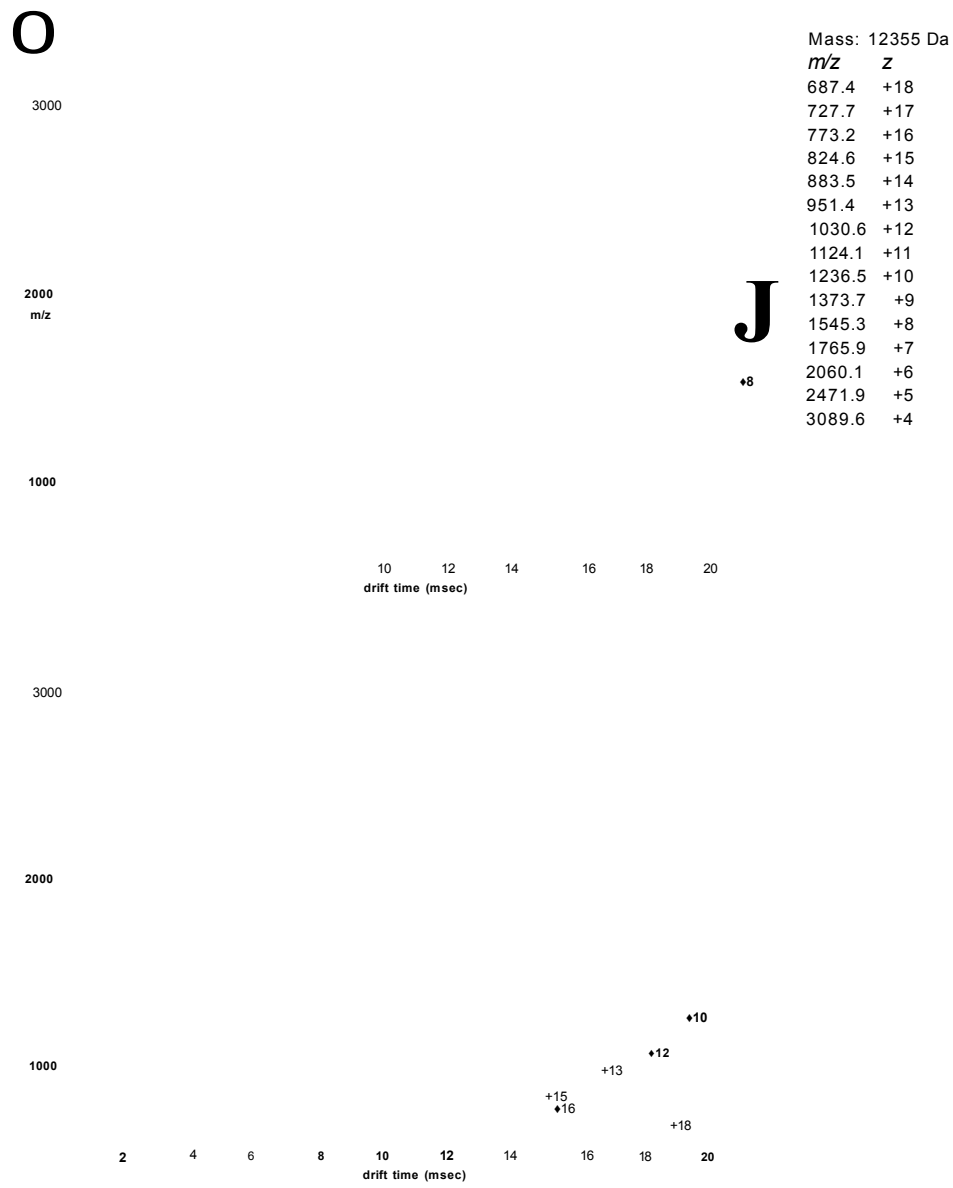

Figure 4.3. *Mobility plots of cytochrome c and corresponding mass spectra overlaid on the right. Under native-like conditions in 40 mM AA (pH 6.8) the protein maintained its globular structure and adopted fewer charges (A), showing a narrow CSD (+5 to +8). Under denaturing conditions (50 % acetonitrile, 10 % formic acid, 40 % ultrapure water) cytochrome c was fully unfolded and became easily protonated hence its CSD was much broader (+5 to +18) (B). The nominal mass, calculated m/z values and corresponding charge states are indicated on the right for equine cytochrome c.*

By acquiring drift time measurements Os can be obtained for which protocols and workflow has been described in detail by and number of groups (Clemmer *et al.* 1997; Ruotolo *et al.* 2007; Ruotolo *et al.* 2008; Smith *et al.* 2009). In brief, in conventional ion mobility measurements the mobility of a gas phase ion (K) is determined by its drift velocity *(VD)* and by the electric field (E), where the drift velocity *(VD)* is related to the drift time (*t*D) of an ion and the length (*l*) of the drift cell (Revercomb *et al.* 1975) as shown here:

$$K = \frac{VD}{E} = \frac{L}{tDE}$$

Equation 4. *The mobility (K) of an ion can be calculated from drift velocity (VD) and the electric field that relates to the length of the drift tube (L) and and the drift time (tD) of the ion of interest.*

The buffer gas density in which the ions are separated such as He or N_2 influence the mobility of ion and such reduced mobility (*K*0) is reported, where E is the electric field, *L* is the length of the drift cell, *P* is the buffer gas pressure and *T* is the temperature of the buffer gas and for simplicity the reduced mobility is normalised to the standard buffer gas pressure of 760 torr and temperature of 273.2 K (Clemmer *et al.* 1997):

$$K0 = K \times \frac{273.2}{T} \times \frac{P}{760} = \frac{L}{tDE} \times \frac{273.2}{T} \times \frac{P}{760}$$

Equation 5. *Calculation of reduced mobility (K0)*

Then mobility of an ion *(K)* can be calculated from its drift time and then Q can be determined as indicated by the equation below. The number of charges on the ion is z, e is the charge on an electron (1.6022×10^{-19} C), *kb* is the Boltmann constant, *T* is the temperature and *N* is the number density of the buffer gas

(Lerme ***et al.*** 1999; Mosier ***et al.*** 2002). The reciprocal of the reduced mass between the ion's and the buffer gas's molecular mass is

i

Equation 6. *Calculation of the mobility of an ion by conventional linear ion mobility*

Expressing *K0* (Equation 5) by use of *K* (Equation 6) and rearranging to express Q, the following Equation 7 can be obtained. It describes the relationship between Q (A2) and drift time (*t*D) of an ion of interest with mass of rrij and charge of z, in which P is the buffer gas pressure (torr), *T* is the temperature (K) and *L* is the length of the drift cell (Revercomb *et al.* 1975; Valentine *et al.* 1999).

i

Equation 7. *Calculation of* O *based on measurements of drift times of ions in the presence of a buffer gas*

For triwave ion mobility separation, correction factors have been incorporated into conventional ion mobility equations developed for linear drift tubes (Revercomb *et al.* 1975; Mosier *et al.* 2002). This is required due to non-linear effects resulting from uneven electric fields, temperature and pressure in newer generation instruments.

Determination of the relationship between the drift time of an ion and its Q is more complex in triwave instrument than in a linear mobility cell. Hence,

methods for experimental calibration of triwave instruments have been described and constants arising from the total effects of triwave parameters can be determined empirically once the acquisition parameters have been optimised. Compensation parameter *A* and *B* can be introduced into Equation 7 to give Equation 8. *A* is the correction factor for the electric field parameters (E and *L* in conventional ion mobility equations) and *B* is a compensatory factor for the non-linear effect of the triwave instrumentation.

In Equation 8, *kb* is the Boltzmann constant, z is the charge of the ion, *e* is the charge of an electron (1.6022x1 O19 C), P is the pressure of the gas (in Torr), *T* is the gas temperature (in K), *N* is the gas number density (in rrf3), *mN* is the gas mass (mN (N2)=28 Da), mi is the ion mass and tD is the drift time of the ion (in msec).

i i

Equation 8. Q *calculation for triwave instruments. A is a correction factor for electric field parameters and B is a correction factor for the non-linear effect of triwaves.*

The Q can be defined as a charge and mass independent measure, termed as reduced Q (O') by dividing Equation 8 by the absolute charge (ze) and reduced mass as shown in Equation 9.

$$O' = \frac{(18\pi)^{\frac{1}{2}}}{16} \cdot \frac{1}{(k_b T)^{\frac{1}{2}}} \cdot \frac{760}{P} \cdot \frac{T}{273.2} \cdot \frac{1}{N} \cdot \frac{1}{A} \cdot \frac{1}{z^2} \cdot \frac{p}{w}$$

Equation 9. *Calculation of reduced O' (Cl) incorporating A and B calibration coefficients*

These parameters can then be incorporated into one constant, *A'* as shown in Equation 10. *A'* is a correction factor for the temperature, pressure and the electric field and *B* is a correction factor for the non-linear effects of triwave device.

$$n' = A' \, tDB$$

Equation 10. *Calculation of* O' *(in A2C'1Da'1) incorporating A' and B correction factors*

Based on Equations 8, 9 and 10 the O can be combined as shown in Equation **11**.

$$n = ze\left(\frac{l}{\backslash m i}; + \frac{1}{mNJ}\right)^{i} A' \, tD^{B} = ze\left(\frac{l}{\backslash m i}7 + \frac{1}{mNJ}\right)^{i} \backslash 2 \, 7l'$$

Equation 11. Q *calculations incorporating constant A' that factors for temperature, electric field, pressure and other parameters.*

It is also necessary to compensate for the mass dependent transit time of an ion outside of the mobility of region of the instrument and this is achieved by use of Equation 12 (Ruotolo *et al.* 2008).

$$\mathbf{t\hat{}o = tD — (C\,yjm/z) / 1000}$$

Equation 12. *Calculation of correct calibrant drift times (at a single wave-height value) for mass dependent flight time, where t'o is the corrected drift time (msec), tDmeasured drift time (msec), C is a constant.*

C is found in the control software of IMS instrument as the enhanced duty cycle delay coefficient. C differs slightly from instrument to instrument and it is ~ 1.4-1.6. This correction factor results in a difference of -0.2 msec and does not modify the data overall.

Given a known charge, mass and Ω, Ω' of an ion can be determined empirically. *A'* and *B* can be determined experimentally from drift times (t_D) obtained from a range of multicharged ions of known protein standards with known Ωs. Such standards are readily avalible from the work of Clemmer (Clemmer, D. E., Indiana University, Cross Section Database) and others (Bush, M.F., University of Washington, Cross Section Database). For example, the +15 charge state ion of cytochrome c (*mi*: 12355 Da) had a measured drift time 6.95 msec acquired in N_2 (*mN* (N_2): 28 Da) and its reported Ω from conventional IMS-MS experiments of 2579 $Å^2$. The Ω' can be calculated (**Equation 13**) by substituting these values into Equation 10.

$$\Omega' = \frac{2579\ Å^2}{15\text{x}\ 1.6022\text{x}\ 10^{-19}\text{C}} x \frac{1}{0.1892}\ \text{Da} = 5.6726\ \text{x}10^{-21}\ Å^2\ \text{C}^{-1}\ \text{Da}^{-1}$$

Equation 13. *An example of calculating Ω' of +15 charge state ion of cytochrome c*

Ω's can be plotted against the measured drift times for which an example is shown below (Figure 4.4.). The calibration curve can be obtained by fitting these data directly to the equation $y = Ax^B$, giving values of *A'* and *B* (Smith *et al.* 2009).

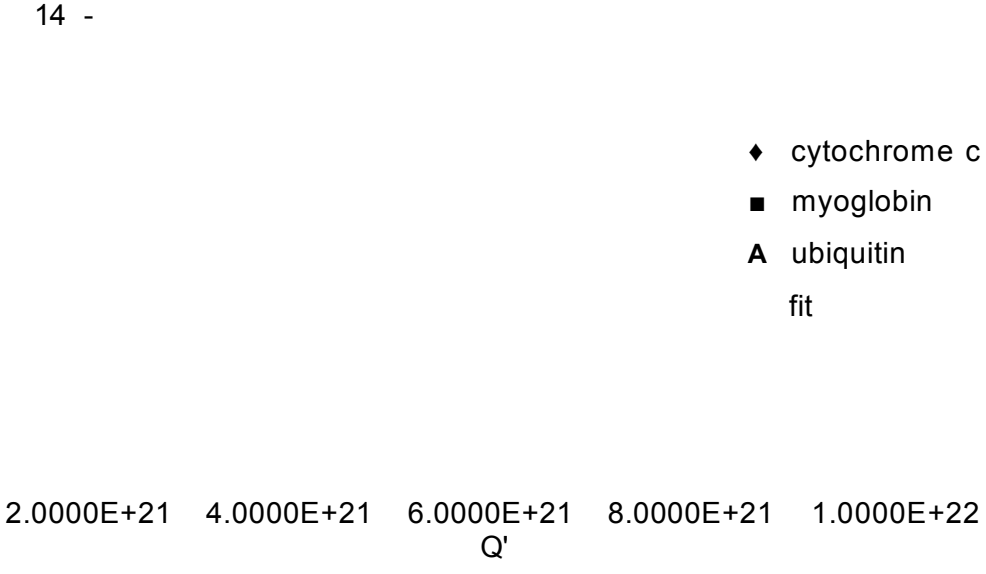

Figure 4.4. O' *(in A2 C 1 Da'1) calculated from Equation 10 versus measured drift times (msec) for the multiply charged ions arising from cytochrome c (blue diamonds), myoglobin (red squares) and ubiquitin (green triangles) under denaturing solution conditions. The line of best fit is shown by a continuous black line.*

Thereafter, experimentally determined A' and *B* values can be used to calculate the Q's of unknown proteins then their respective Os. For example, the +7 charge state ion of myoglobin (17562 Da) under native solvent conditions had an observed drift time of 11.356 msec, which from the O' vs drift time calibration graph indicated a O' of 7.24x 10^{21} A^2 C^{-1} Da^{-1}. Substituting this value for O' in Equation 11, along with the charge state (+7), the charge on an electron (1.6022x 10^{-19} C) and the mass of the protein *(mi:* 17562 Da retaining its haem group) and the buffer gas *(mN* (N_2): 28 Da), a O value of 1536 A^2 was calculated. As proteins display multiple charge states, Os were calculated

individually for each charge states and the mean Ωs were determined for each protein.

Once Ωs have been obtained the gross morphology of a protein or protein complex can be determined by comparison with model structures. Comparing experimental Ωs with coordinates of modelling allows the ascertainment of geometries and arrangements in 3 D. A freely available, often used modelling programme is MOBCAL (Jurneczko *et al.* 2011) that is based on the previously mentioned PA method (Wyytenbach *et al.* 1997), trajectory method (TM) (Shvartsburg *et al.* 1998) and EHSS (Shvartsburg *et al.* 1996; Shvartsburg *et al.* 2007). Theoretical Ωs can alternatively be calculated from Protein Data Bank (PDB) format structures using an algorithm scripted in Leeds (Leeds Method) translated from MATLAB that allows modelling of a hard sphere interaction between the buffer gas and a protein (Smith *et al.* 2009; Knapman *et al.* 2010). Measured Ωs have been shown to be comparable to calculated Ωs using PDB coordinates from X-ray crystallography measurements and NMR coordinates, providing detailed structural data of biomolecular systems (Jurneczko *et al.* 2011).

To date, a wealth of information has been unravelled about numerous amyloidogenic systems and this presents opportunities to define assembly pathways, to monitor the presence or absence of particular species in a rapid analysis. These aspects of assembly and dynamics could not be elucidated by using other high resolution biophysical techniques such as CD or NMR. This is partly due to the low abundance of subspecies and because these structural tools represent data of the total populations or bulk solutions (Ashcroft 2010). However, it is important to bear in mind that information obtained from ESI-IMS-

MS measurements are limited to the gas phase and molecules may well display altered shapes due to dehydration and charge repulsion when in solution. Therefore such data require careful interpretation and the use of combinatory methods e.g. molecular modelling to better correlate those with native solution conditions (Grabenauer *et al.* 201 Oa; Wyttenbach *et al.* 2011).

4.1.3 ESI-IMS-MS studies of a-syn and its oligomers

Despite the tremendous advances that have been made in characterising oligomeric states of Ap peptides (Murray *et al.* 2009a; Bernstein *et al.* 2009; Murray *et al.* 2009b), variants of prion proteins (Eghiaian *et al.* 2007; Grabenauer *et al.* 2010a; Grabenauer *et al.* 2010b; Hilton *et al.* 2010), human IAPP (Dupuis *et al.* 2009; Salamekh *et al.* 2011), p2 microglobulin (Smith *et al.* 2010; Santambrogio *et al.* 2011; Woods *et al.* 2012;) and transthyretin (Zhou *et al.* 2012), the structural determination of a-syn oligomers and protofibrils by ESI-IMS-MS has been missing.

ESI-MS analysis of the monomeric protein has been undertaken by Frimpong *et al.* (Frimpong *et al.* 2010) and ESI-IMS-MS measurements of a-syn have been been carried out Natatello *et al.* (Natalello *et al.* 2011) and Grabenauer *et al.* (Grabenauer *et al.* 2008). Prior to these investigations, Electrospray Ionisation-Electron Capture Dissociation- Fourier Transform Ion Cyclotron Resonance (ESI-ECD-FT-ICR) (Xie *et al.* 2006) measurements have uncovered effects of metals and alcohols or pH and the effect of spermine on the structure of a-syn, respectively.

The only ion mobility experimentation of type A oligomers established by Danzer *et al.* (Danzer *et al.* 2007) has been demonstrated by the work of Vlad

et al. (Vlad *et al.* 2012). Type A oligomers produced in SP were subjected to desalting on a column with a gradient after which monomeric, dimeric as well as a proteolytic, truncated peptide species of aa 40-140, aa 14-133 and aa 40-140 of a-syn were observed. N-terminal Edman sequencing was also carried out alongside with gel electrophoresis to ascertain the identity of peptides, the intact protein and its dimeric oligomers. A follow up report by the same group has highlighted the emergence of key autoproteolytic fragments of a-syn in aggregation (Vlad *et al.* 2011). In this study, type A oligomers were incubated for varied lengths of time from 4 to ~21 day, deviating slightly from the preparation protocol to examine degradation of a-syn over time. The oligomers were subjected to gel electrophoresis, tryptic digest, MALDI-MS and high performance liquid chromatography- electrospray ionisation- mass spectrometry (HPLC-ESI-MS) and ESI-MS/MS analysis. MALDI-MS identified aa 40-140 and aa 72-140 truncated proteins and IMS-MS revealed intrinsic autoproteolytic fragments, aa 7-140 after a short incubation and aa 40-140 and aa 72-140 truncated a-syn forms beside intact and dimeric forms at later time points. No higher order oligomers have been reported here.

4.1.4 Objectives

Overall aims

The oligomer preparation protocols reported by Danzer *et al.* (Danzer *et al.* 2007) were adapted and further characterised in Chapter 3 to produce both type A and type C oligomers suitable for ESI-IMS-MS experiments.

Type A oligomers in SP deemed to be the most hydrophobic, cytotoxic and capable of binding to A11 antibody. The question remained as to how these oligomers differed in their structure from type C oligomers and how their molecular organisation might have dictated or influenced their effects observed in SH-SY5Y cells.

The specific aims were:

i. to tune instrumental parameters and resolve conformational families of monomeric a-syn by ESI-IMS-MS.

ii. to establish parameters enabling detailed structural characterisation of alternate oligomeric forms in the gas phase.

iii. to investigate the compactness of oligomeric subpopulations by measurements of Os and to compare those to Os of known proteins or other known oligomers.

iv. to understand how additional factors i.e. ionic strength, ethanol and metal ions might cause structural transitions and induce oligomerisation leading to aggregation.

4.2 Methods and Materials

For detailed protocols of expression and purification of the monomeric a-syn, formation of oligomers, pulling and sputter coating of capillaries, conducting calibration with known protein standards and ESI-IMS-MS analysis see Chapter 2.

4.3 Results and discussion

4.3.1 Establishment of appropriate tuning parameters for calibration and calculation of Q of unknown protein

Selection of optimal settings is important in maintaining native like conditions. It is known that experimental parameters largely affect calculated Os (Ruotolo *et al.* 2008; Zhong *et al.* 2011; Bush *et al.* 2010). Wave heights, wave velocities can influence O meaurements (Grabenauer *et al.* 2008; Michaelevski *et al.* 2010a) and adequate desolvating voltages have shown to be critical during ion mobility acquisition (Bernstein *et al.* 2004; Grabenauer *et al.* 2008). Thus, using a range of proteins of known structure experimental conditions were extensively optimised both in their denatured states and native-like states in AA to avoid fragmentations and obtain Os consistent with published values. The main considerations were given to backing pressure, bias and desolvating voltages. Having established acquisition settings, ESI-IMS-MS data for the monomeric protein was collected and mean O values were all incorporated into an accumulative data set serving validation of instrumental settings and shown in Table 4.1..

		Experimental values			Theoretical values		
Protein	Mass (Da)	Mean Ω ($Å^2$)	Standard deviation	Published values ($Å^2$)	Leeds algorithm ($Å^2$)	PA ($Å^2$)	EHSS ($Å^2$)
Bovine ubiqutitin native	8565	1199	65	1079	1059	1100	1313
Equine cytochrome c native	12355	1622	94	1444	1293	1130	1422
Bovine α-lactalbumin native	14178	1459	93	1360	1493	1207	1513
Hen egg lysozyme native	14305	1469	60	1496	1386	1568	1909
Horse heart myoglobin native	17562	1971	267	1639	1488	1628	1995
α-syn extended	14460	2482	159	2530	-	-	-
α-syn compact	14460	1851	276	1500	-	-	-
α-syn denatured	14460	2620	220	-	-	-	-

Table 4.1. *Compiled Ωs of a range of model proteins under native conditions expressed. The reported values are the mean Ω over all charge states of the proteins and standard deviations represent the spread in the recorded Ω across all charge states. Theoretical values were calculated by the Leeds algorithm based on their PDB coordinates from NMR and X-ray crystallography measurements. The MOBCAL calculations are also shown for the projection approximation (PA) and the exact hard sphere scattering (EHSS) model. Experimental published values were obtained from references* (Smith *et al.* 2009) *and* (Bernstein *et al.* 2004).

Ω values obtained and shown in **Table 4.1.** were consistent with values published in the literature (Smith *et al.* 2009; Bernstein *et al.* 2004), demonstrating that instrument settings did not cause significant artifacts. Comparison of obtained Ωs for globular proteins with α-syn revealed that indeed α-syn appeared to be more expanded than other globular protein standards with a similar mass. The fully denatured state of α-syn in 50 % acetonitrile, 10 % formic acid and 40 % water however yielded a larger Ω than that of the

extended conformation (**Figure 4.5.**), implying that the extended state has retained some structural arrangement. The Ωs of the denatured and extended state exceeded the average Ω of the compact conformation by ~34-41 %.

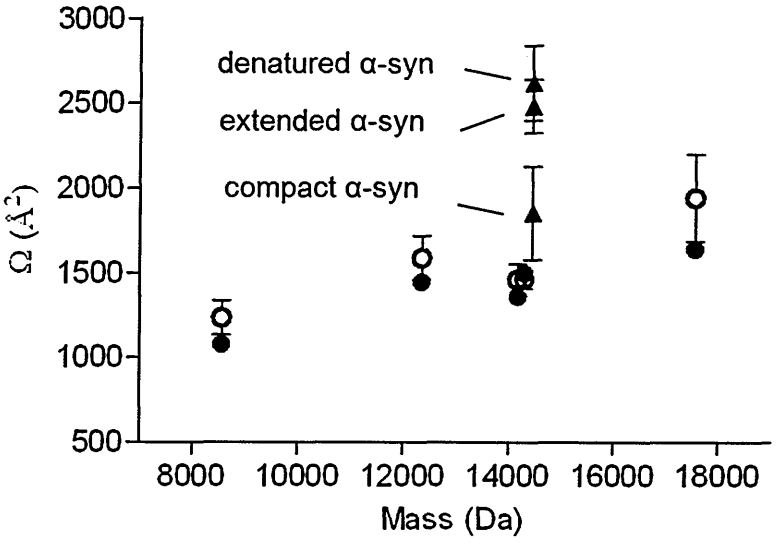

Figure 4.5. *Experimental Ωs for bovine ubiquitin, equine cytochrome c, α-lactalbumin, hen egg lysozyme and horse heart myoglobin, native α-syn and denatured α-syn. Ωs are plotted as mean values across all charge states, error bars represent the spread in the recorded Ω. White circles represent the experimental values acquired here, black circles represent previously published Ω values* (Smith *et al.* 2009)*, black triangles represent the native extended and the compact conformational states of α-syn alongside with the fully denatured protein. All spectra were acquired using a Synapt G2 HDMS instrument (Waters, Manchester, UK) by use of gold coated home-made borosilicate nano-capillaries in positive mode.*

4.3.2 ESI-IMS-MS of a-syn monomer

It is widely accepted that compact states in solution when subjected to ESI acquire fewer charges and have a narrow charge state distribution, whereas unfolded states acquire a large number of charges and have a wide charge state distribution (Fenn *et al.* 1989; Kaltashov *et al.* 2005). The mass spectrum of a-syn clearly showed multiple charge state distributions centered at the +13 and +7 charge state ions Figure 4.6. *A.* Both the +7 and $^{+8}$ charge state ions were more intense than would be expected for a completely unfolded protein. This charge state distribution is consistent with data for known globular proteins and given the mass of the protein (14.6 kDa), a narrow distribution can be expected based on Equation 3, centering around the +7 charge state ion (Heck *et al.* 2004) as observed here.

In order to further confirm that the compact conformation reflected populations present in solution and did not arise due to transfer to the gas phase, the mass spectrum of a-syn was acquired under fully denaturing conditions (50 % acetonitrile, 10 % formic acid and 40 % ultrapure water) as showed earlier in Chapter 4 (Figure 4.6. *B).* If the lower charge state ions of the protein underwent collapse during acquisition then one would expect this to be observed regardless of the solution conditions from which the protein was acquired. By contrast, charge state ions between +18 and $^{+8}$ were observed for fully denatured a-syn with no evidence of compact conformations at the lower charge state ions. The intensity of the charge state ions +9 to $^{+8}$ were markedly lower than that observed under native conditions indicating a single extended conformation. Hence, data of the control experiment supports the fact the

compact conformational forms of a-syn are co-populated under native conditions where residual structure of the protein is retained.

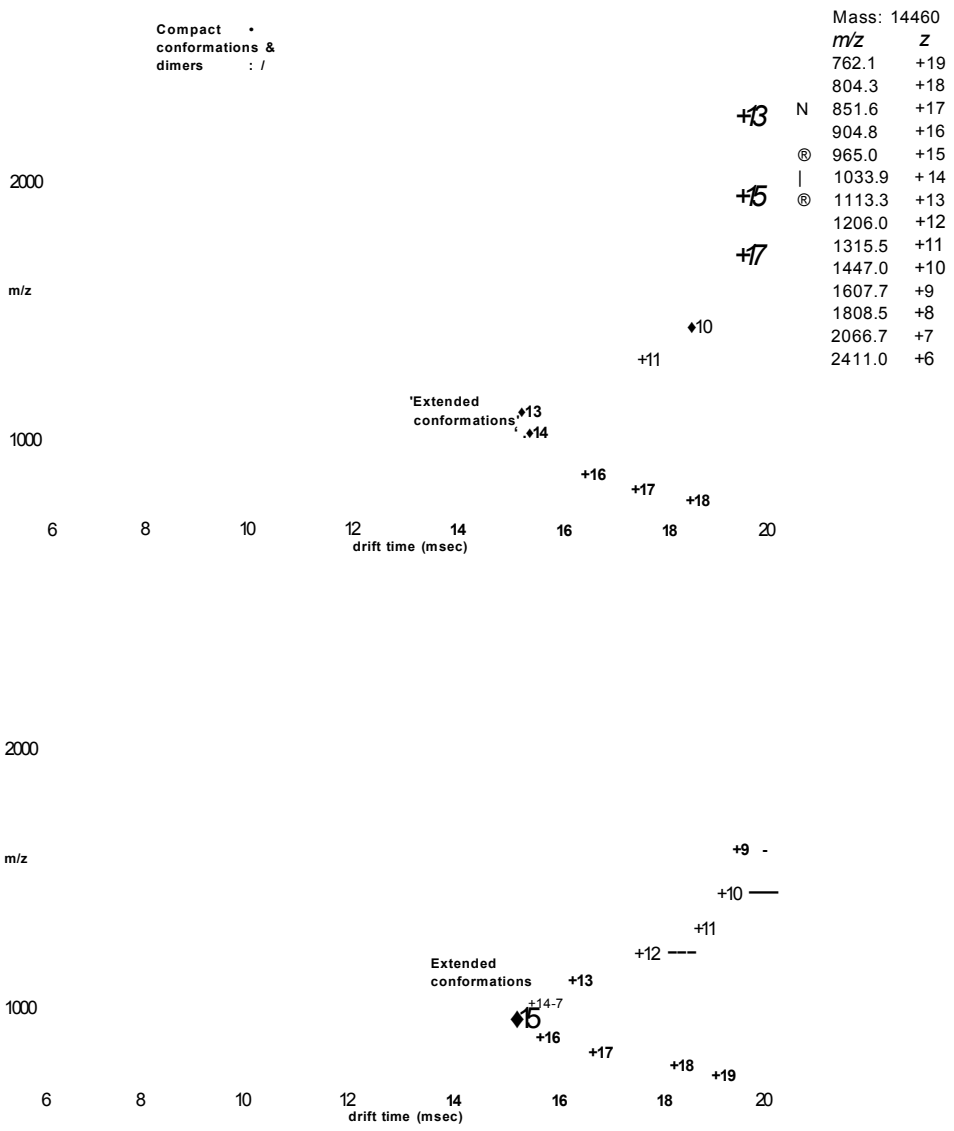

Figure 4.6. *Mobility plots of a-syn and corresponding mass spectra overlaid on the right hand side. Under native-like conditions in 40 mM AA (pH 6.8) the protein consisted of extended, compact populations and dimeric species. Natively occurring conformational families were observed with a CSD of +6 to +18, where the most dominant charge state ion was [M+13H]13+ (A). Under denaturing conditions, a-syn was fully unfolded with CSD of +8 to +19 with the most dominant charge state of [M+15H]15+ (B). The nominal mass, calculated m/z values and corresponding charge states are indicated on the right for a-syn.*

In comparison with other published data, Frimpong *et al.* ascertained 4 states of the protein in the pH range of 4-8: an expanded form (U) at high charge states (+21 to +13 charge state ions), h representing helix-rich intermediates (+16 to +10 charge state ions), I_2 entailing (3-rich intermediate state (+13 to +7 charge state ions) and a highly compact forms spanning low charge states (+9 to +6 charge state ions) (Frimpong *et al.* 2010). In negative ion mode study, two main conformational families for WT, A53T and A30P a-syn have been reported by the Bowers group, one dominating the lower charge states (-6 to -16 charge state ions) centered at -11 with multiple features and one prevalent in high charge states (-6 to -8 charge state ions) (Grabenauer *et al.* 2008). These conformational forms were in close agreement with data shown here, demonstrating multiple extended and compact features.

4.3.3 Conformational families of a-syn

Q was calculated for each charge state ion of a-syn and data was plotted against its respective charge state (Figure 4.7.) that enabled determination of the compactness of alternate molecular ions and resolution of alternatate conformational families. From the analysis of Os according to charge states, it was evident that at near native conditions a-syn had two main conformational families, an extended conformation with charge states +6 to +18 and a more compact conformational family with charge states +6 to +8, having multiple series in both families in addition to less prevalent dimers.

Published theoretical values were superimposed on the collected experimental Os to help comparison of molecular arrangements.

The compact state of a-syn has been modelled by a globular structure -1500 A2 previously, whereas the extended state has been reported to have a O of 2530 A2 (Bernstein *et al.* 2004) with a spread between -1800 A2 and 3000 A2 over all charge states (Grabenauer *et al.* 2008). Moreover, the extended state was shown to be more compact than a fully random coil conformation as predicted by small angle X-ray scattering and NMR (Uversky *et al.* 2001a). These models and reported O values have been taken from a previous publication (Bernstein *et al.* 2004) and plotted onto Figure 4.7. to aid comparison. Os of each of the charge states and conformational families observed here were in agreement with these previously reported values (Bernstein *et al.* 2004; Grabenauer *et al.* 2008).

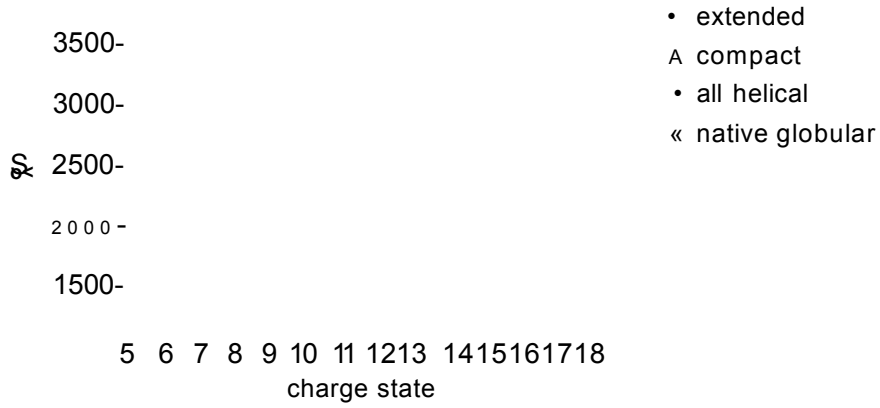

Figure 4.7. *Conformational series of a-syn. Filled, black circles: experimental* Os *of extended conformational features, black triangles: experimental* Os *of compact conformational forms. The dotted line represents theoretical Qs calculated for structures having all helical conformation and the cross haired line represents calculated values for native globular structures as reported by Bernstein et al.* (Bernstein *et al.* 2004). *Experimentally measured values represent means of three independent measurements with ±SD, taken on alternate days using independent protein preparations.*

Despite the fact that α-syn is considered as a natively unfolded protein, it displays considerable conformational heterogeneity (Beveridge *et al.* 2013). It contains ordered regions as judged by the wide CSD and as shown previously by other biophysical methods including NMR and CD. The Bowers group has reported extended and more compact structures of α-syn observed by nESI analysis at various pH. It was demonstrated that WT, A30P and A53T mutants of α-syn populate compact and partially folded conformations whose Ωs have been determined in negative ESI-IMS-MS (Grabenauer *et al.* 2008). Moderate dimer formation was observed in each of the ion mobility experiments. The presence of the compact state was reported in this study which is thought to play a role in the misfolding of α-syn into toxic aggregates (Uversky *et al.* 2001a; Uversky *et al.* 2009).

Here, Ω analysis of WT α-syn revealed a primarily extended population (charge state ions +8 to +18) and a subpopulation of a more compact conformational series (charge state ions +6 to +8) with multiple overlapping features in both series and less observable dimeric species under native conditions (**Figure 4.8.**). Within the extended series three charge state ions +11, +12 and +13 showed at least two major resolvable conformations. Since these charge states represented the most intense peaks within the mass spectrum it may be likely that the other charge state ions have also had multiple features but it was not possible to resolve them due their very low intensity. Alternatively, the larger Ω of these three charge states could have been an artifact induced by coulombic repulsion due to the high charge on the molecule. Another alternative explanation is that there were indeed two major distinguishable conformational families present within the extended conformations, the first encompassing

charge states ions $^{+8}$ to +13 and the second encompassing charge states ions $^{+11}$ to +18, these two major states would therefore have the $^{+11}$ to +13 charge state ions in common. This theory is consistent with the charge state distribution analysis of Frimpong *et al.* (Frimpong *et al.* 2010) mentioned earlier.

4.3.4 Addressing the effects of metal ions by ESI-IMS-MS

Since metal ions such as Fe(III) have been added during the preparation of type A2 and C2 oligomers and Cu(II) has been shown to alter the the aggregation kinetics (Uversky *et al.* 2001c) of a-syn, the interaction of these cations with a-syn and their effect on the conformations of the monomeric protein was examined.

Natatello *et al.* carried out a systematic study to determine structural transitions induced by a range of alcohols and Cu(II) on a QTOF instrument (QStar Elite) equipped with an ESI source and demonstrated how these alternate conformational forms respond to co-factors and cause a shift in the CSDs of a-syn (Natalello *et al.* 2011). It was concluded that one high affinity Cu(II) binding site could be detected by this experimental setup. CD, calorimetric titrations, NMR and EPR spectroscopy (Binolfi *et al.* 2008, Drew *et al.* 2008; Binolfi *et al.* ^{2010}) demonstrated the presence of a collapsed species in the presence of Cu(II).

While most metals predominantly interact with a-syn non-specifically or bind with low-affinities, Cu(II) has high binding affinity and is highly effective in inducing fibrillation of a-syn via the increased population of this partially folded conformation. The high affinity binding sites for Cu(II) are located in at ^{1}MDVFMKGLS^{9} and ^{48}VAHGV^{52} and their respective binding affinity has been

estimated as K_d ~0.1 μM. Notably, increased concentrations of Cu(II), aluminium (Hirsch *et al.* 1991), zinc (Dexter *et al.* 1989) and sequestered iron deposits (Riederer *et al.* 1989; Castellani *et al.* 2000) have been found in the *substantia nigra* of the brain and elevated levels of copper in the CSF of PD patients have been reported (Pall *et al.* 1987).

It is clear that bi- and trivalent metal ions are involved in neuronal dysfunction and they have the propensity to shift the conformational equilibrium and trigger structural rearrangements of α-syn. Adding conformational information through Ω calculations, it was therefore worthwhile to address binding of Cu(II), Fe(III) and a range of other bivalent and trivalent ions (Co(II), Mn(II), Zn(II), Fe(II), Al(III)) to monomeric α-syn.

Representative charge state ions have been selected here for both the extended state and the co-populated compact conformational state to discuss metal binding events. The +13 charge state ion with a Ω of 2635 $Å^2$ in its apo-form is a member of the extended conformational population with only a minor population of the more extended conformer. The second representative ion is the +7 charge state ion that belongs to the compact conformational family as shown in **Figure 4.7.**, co-populating two compact states in its apo-form with Ωs of 1845±65 $Å^2$ and 1628±80 $Å^2$ and having a very minor population assigned to the extended state with Ω of 2080±82 $Å^2$.

Three different protein:metal ratios (1:0, 1:1 and 1:2 relative to a set concentration of α-syn at 50 μM working strength) were analysed for each of the metals. As displayed in **Figure 4.8.**, it is noticeable that a maximum two Cu(II) copper ions could bind to all conformational ions of monomeric α-syn, causing a mass shift of 1x or 2x 61.5 Da given that each Cu(II) repels two

protons from the protein to conserve charge. To investigate the specificity of binding, Gly was included in repeated reactions as a commonly used inhibitor of non-specific metal binding (Hong *et al.* 2009). Both in the absence and presence of Gly α-syn could facilitate the binding of 2 Cu(II) ions. These results indicate that initial metal binding is determined at the primary structural level as the extended, disordered state is capable of binding two metal ions rather than a conformational change being required prior to metal binding. It is evident that molecular ions indicative of the more compact conformations become more dominant in the mass spectra post co-ordination of one or two molecules of Cu(II) and the binding of the metal stabilised the compact conformations. This can be observed by the increased intensity of the lower charge state ions.

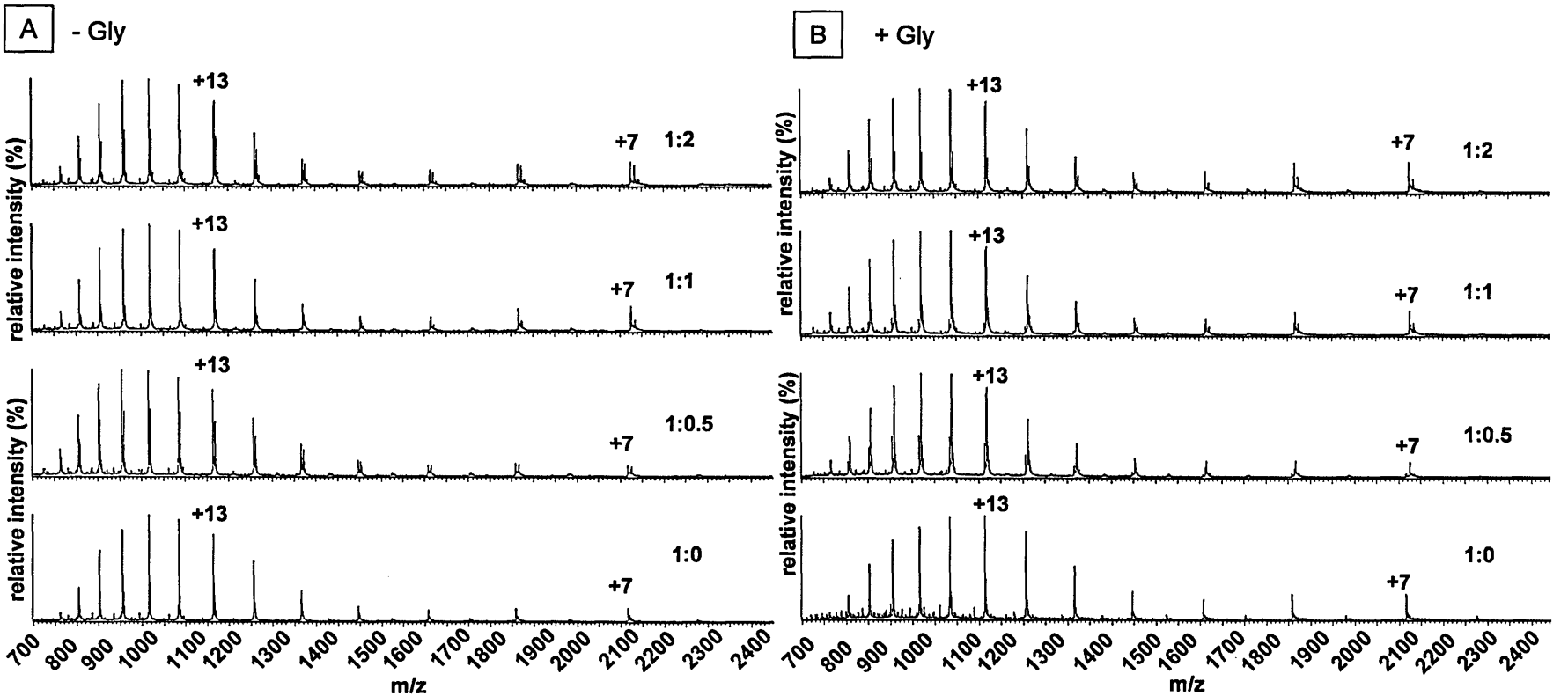

Figure 4.8. *The unbound forms of α-syn are marked with 1:0 ratio, the mass spectrum of one Cu(II)-bound α-syn is seen at the 1:0.5 ratio and two Cu(II)-bound forms are represented by the 1:1 and 1:2 ratios. The x axis represents m/z and the y axis shows relative abundance in %. In **A**, spectra are shown without any Gly added and in **B** peaks are shown upon addition of Gly.*

With a closer focus on the chosen representative charge states +13 and +7, it was apparent that Cu(II) could bind to both conformations with or without Gly as shown in Figure 4.9., containing peaks magnified in the region of interests.

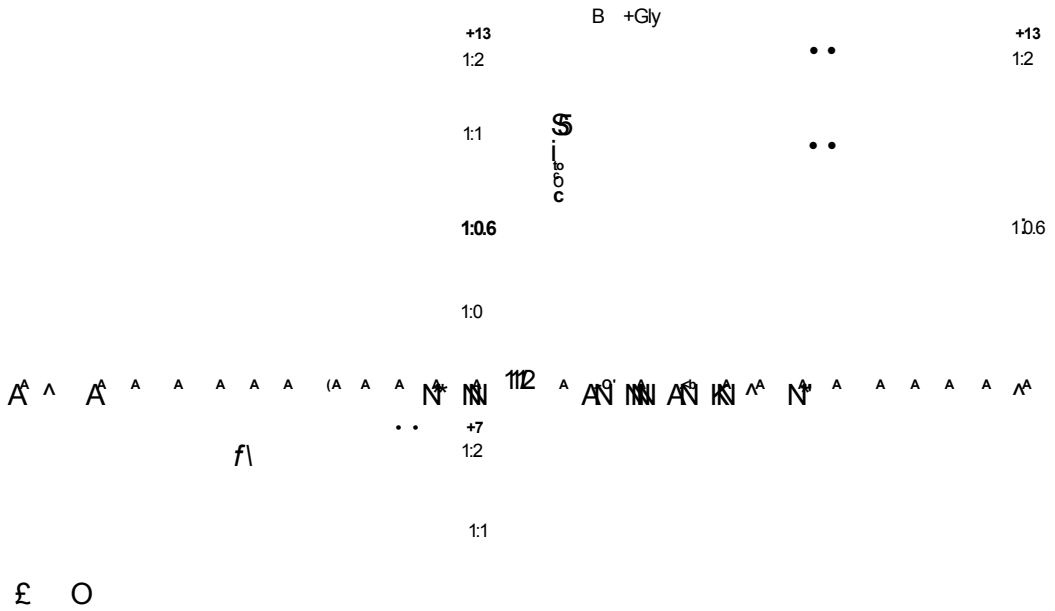

Figure 4.9. *The unbound forms of a-syn are marked with open blue circles, 1 Cu(II)-bound forms of the protein are marked with single, filled, blue circles, the 2 Cu(II)-bound forms of a-syn are denoted with two blue filled circles. The x axis represents m/z and the y axis is relative abundance in %. Respective ratios are indicated on the right of each spectrum. On the left hand side, spectra are shown without Gly (A) and on the right peaks are shown with Gly (B). Cu(II) binding was observed to both representative charge states denoted as +13 and +7.*

Upon calculations of Os of the Cu(ll) adducts, it was found that at the lower +7 charge state ion a structural rearrangement occurred that shifted the more extended populations toward the most compact conformation (Figure 4.10.)-

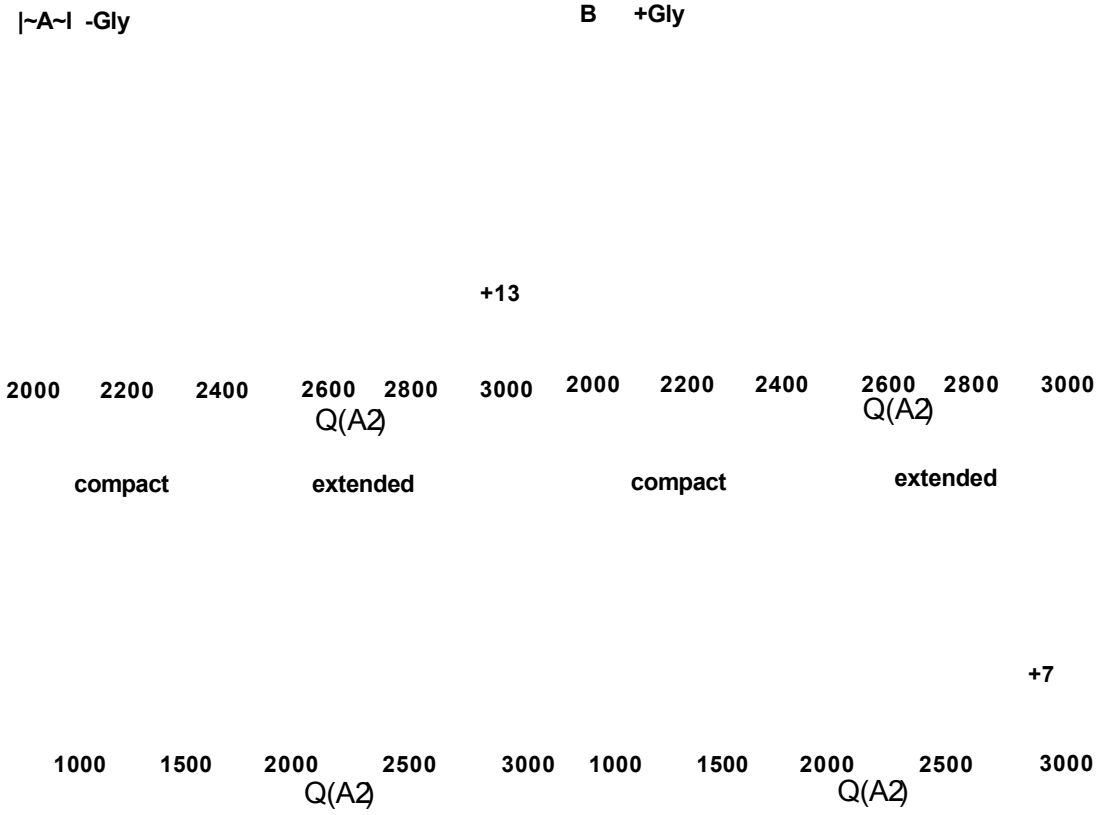

Figure 4.10. *Experimental* Qs *(A2) of +13 and +7 charge states of wild type a-syn either in apo- or holo- forms without (A) or with Gly (B) displayed on an intensity scale. Blue traces represent the apo-form of a-syn, purple traces the one Cu(ll)-bound form and grey traces the two Cu(ll)-bound form of the protein at the 1:1 ratio. Changes occurred most apparently at the +7 charge states, where the compact forms became more dominant at the expense of more extended conformational structures after binding of Cu(ll), yielding a conformer with a common Ω of 1547.6 A2as marked by the asterisks.*

Changes in the Ωs were not discernible between the apo- or holo- forms of the protein at the extended +13 charge state. In contrast, at the +7 charge state ion there was a shift upon Cu(II) binding towards the most compact conformation when comparing to the unbound form of the protein. This transition was pronounced both in the absence and in the presence of Gly, resulting in a predominantly compact conformation with a Ω of 1547.6 $Å^2$. The Ω of 2075.5 *m/z* peak corresponded to the addition of one Cu(II) molecule both without and with Gly. The Ω of the 2084.3 peak *m/z* that is associated with the binding of two Cu(II) ions populated only one dominant conformational population with the same experimental Ω as the apo-protein's second more collapsed state (**Figure 4.11.**).

The respective mobility plots also reflected the formation of α-syn-1 Cu(II) adducts and α-syn-2 Cu(II) complexes at both ratios 1:1 and 1:2 both without or with Gly. The mobility plot representation of the data at the 1:1 protein to ligand ratio is shown in **Appendix Figure 8.12.**. The affinity of α-syn for Cu(II) was so substantial that almost all of the protein was in its holo-form either incorporating one or two Cu(II) ions.

Neither significant adduct formation, nor changes in the Ωs could be observed after addition of other metals such as Zn(II), Co(II), Fe(II) and Al(III) to α-syn at the time scale and conditions of these experiments (<5 min) (data not shown).

The binding of Fe(III) was of particular interest as the previously mentioned oligomeric preparation protocols include the use of 10 μM $FeCl_3$ to produce type C2 and type A2 oligomers. Upon repeated attempts of ESI-IMS-MS analysis, no binding was observed in the case of Fe(III), or Fe(II). Peng *et al.* have reported observable adduct formation of Fe(II) using $Fe(NH_4)_2(SO_4)_2$ and recombinant α-

syn in methanol water solvent (1:1 v/v) under which conditions the monomeric protein was fully unfolded (Peng *et al.* 2010). Complex formation between Fe(III) as well as Fe(II) and a-syn was shown by further cyclic voltammetry and fluorescence spectroscopy measurements. It is possible that alternate anion combinations could either promote or attenuate the binding of the cation to a-syn. For example FeCh did not result in an apparent binding to the protein, whereas literature reported complex formation of Fe(II) with a-syn where Fe(II) was present in $Fe(NH_4)_2(SO_4)_2$ solution. Another concern is that oxidation of Fe(II) to Fe(III) could have also occurred in solution prior to mixing a-syn with the metal ion (Peng *et al.* 2010).

4.3.5 Investigation of the effects of ethanol prior to oligomerisation and other buffer conditions

Due to the inclusion of ethanol in the oligomeric preparation protocols it was necessary to address its effect on changing the conformational populations of a-syn. Previous evidence has indicated that alternate concentrations (%) and types of alcohols, both fluorinated hexafluoropropanol, trifluoroethanol and methanol modulated the conformational forms of a-syn and could selectively enrich specific intermediates (Munishkina *et al.* 2003; Natalello *et al.* 2011). It is important to note that the formation of partially folded conformer is a key event in conversion to toxic conformations (Uversky *et al.* 2001a; Uversky *et al.* 2009). To investigate the contribution of ethanol used in the particular oligomerisation protocol of a-syn adapted here, a set of experiments were performed at alternate alcohol percentages of 0, 10, 20 or 30 % added to 7 pM a-syn in 50 mM aequeous AA, pH 7.0. Previous evidence have suggested that ethanol and other types of alcohols help promoting the formation of a partially folded

intermediate of a-syn and subsequent formation of (3-sheet rich oligomeric forms as revealed by CD, FTIR and dynamic light scattering and ESI-IMS measurements (Munishkina *et al.* 2003; Natalello *et al.* 2011). In ESI-IMS-MS experiments performed here, no direct evidence was found for inducing structural conformations during the rapid time frame of the analysis (Figure 4.11.).

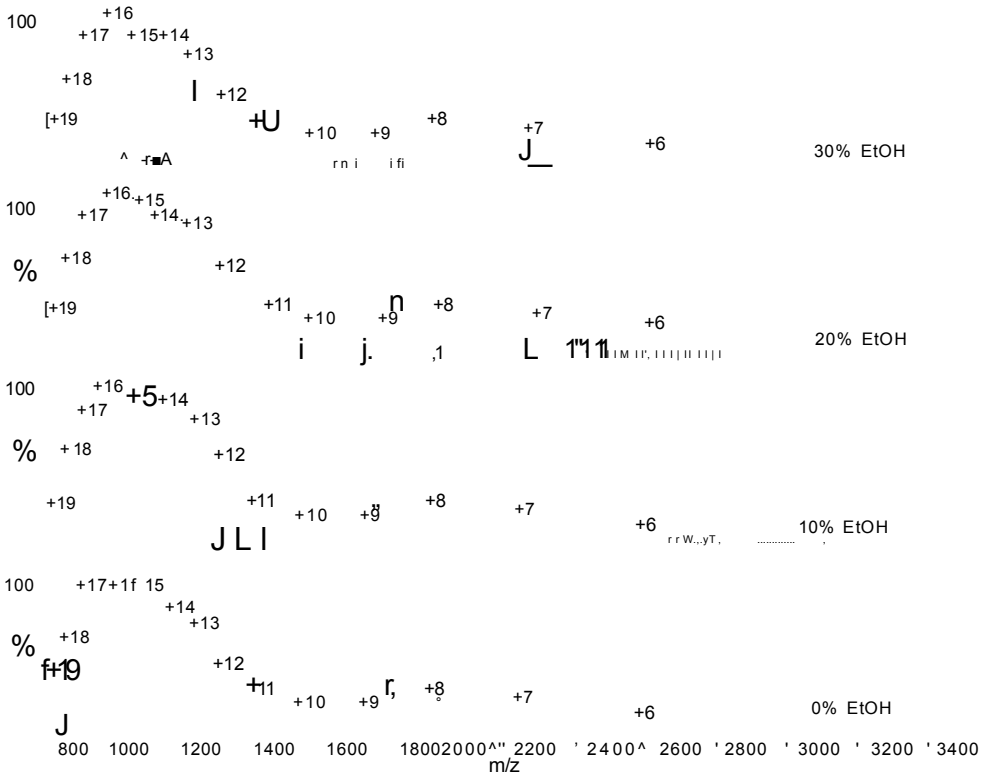

Figure 4.11. *Comparison of mass spectra after incremental ethanol concentrations added to 7 pM monomeric a-syn and analysed immediately by ESI-IMS-MS. The x axis represents m/z values, the y axis is relative abundance in (%). No apparent changes could be detected in the distributions of extended or compact series. Instrument settings were: capillary 1.9 kV, cone 50 V, trap 4 V, transfer 10V, helium gas flow 180.0 mUmin, IMS gas flow 90 mUmin, bias 45, source wave velocity 200 m/s, trap wave velocity 311 m/s, IMS wave velocity 800 m/s, transfer wave velocity 200 m/s, backing 3.0 mbar.*

One environmental determinant of amyloid formation is ionic strength that influences the kinetics and thermodynamics of aggregation. Ions may concentrate non-specifically in the proximity of oppositely charged moieties. Grouping of ions therefore cause the dielectric charges of water to be elevated and cause the energy of electrostatic protein-protein interactions to fall off more readily with distance (Debye- Hückel screening). Repulsive interactions may become weakened giving way to intramolecular associations. Specific interactions with ions may affect the isoelectric point that is 4.7 for α-syn with possible changes in its solubility. In addition, specific types of salts dictate alternate effects (Klement *et al.* 2007).

To test the effect of the ionic strength of AA on the production rate of α-syn oligomers, incremental concentrations of AA were used during preparation protocols and each stage of the protocol was monitored. Oligomers were set up in increasing concentrations of AA at 50 mM, 100 mM, 250 mM and 450 mM and samples taken after a 4 hr incubation step are shown. It was clearly observable that the intensities of +6 to +8 ions belonging to the compact conformational forms (**Figure 4.6.** and **Figure 4.7**) were more dominant at higher AA concentrations than those at the lowest, 50 mM AA concentration (**Figure 4.12.**). Hence increased AA concentrations resulted in a higher population of the compact state.

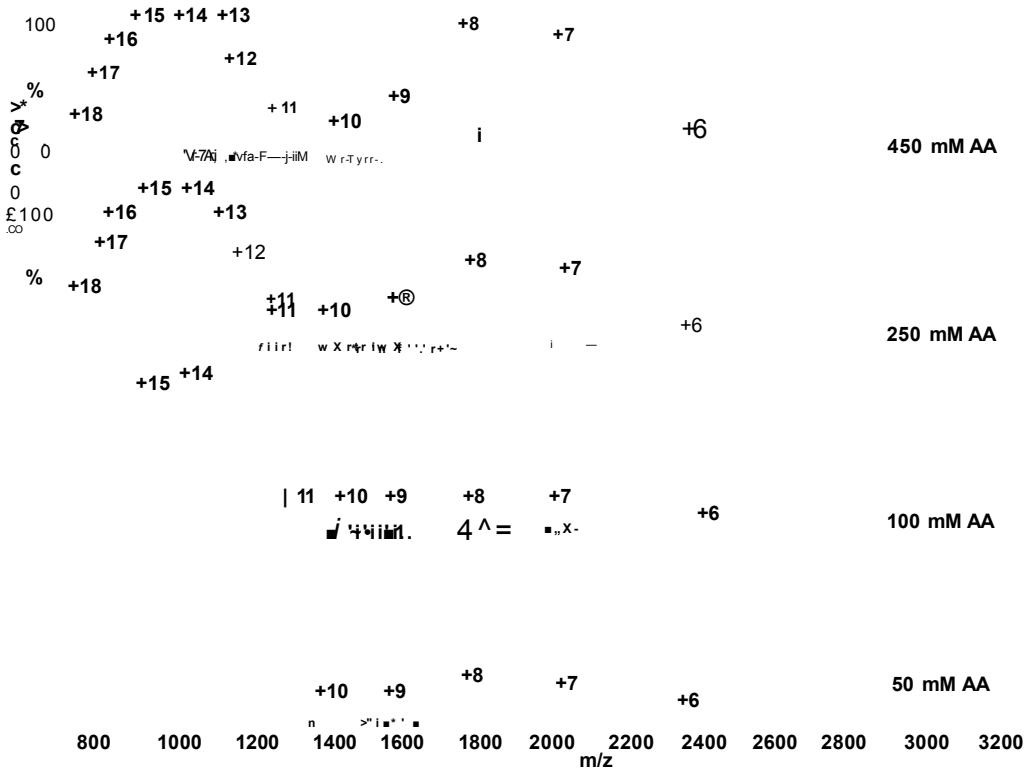

Figure 4.12. *Comparison of the mass spectra of type A2 AA oligomers dissolved in alternate AA concentrations during preparation from 7 pM a-syn at pH 7.0 that were analysed after the 4 hr shaking step by ESI-IMS-MS. The x axis represents m/z values, the y axis is relative abundance in (%). Apparent changes could be detected in the populations of the compact ion series (+6 to +9). Instrument settings were: capillary 1.7 kV, cone 50 V, trap 4 V, transfer 10 V, helium gas flow 180.0 mUmin, IMS gas flow 90 mUmin, bias 45, source wave velocity 200 m/s, trap wave velocity 311 m/s, IMS wave velocity 800 m/s, transfer wave velocity 200 m/s, backing 3.0 mbar.*

Beside an increase in the relative abundance of the compact conformers of monomeric a-syn, the formation of oligomers were detectable early on at a 4 hr incubation time point ranging from dimers to trimers as seen in the corresponding mobility plots (Figure 4.13.). At 250 mM and 450 mM AA concentration, a broader range of trimers were observed with charge states

from +12 to +20 (T^{+12}-T^{+20}) and a set of tetramers (Q^{+17}- Q^{+19}) were present in the sample prepared in 250 mM AA (**Figure 4.13.**). These data suggest that increasing the AA concentrations led to a higher population of low order oligomers in the mass spectra. These oligomers and all other oligomers discussed later on in this chapter were assigned by creating a table of theoretical *m/z* values and charges (*z*) as shown in **Appendix Table 8.1.**. In addition to this, an in-house algorithm lent support to ascertaining the alternate subunit sizes by matching theoretical *m/z* values against measured *m/z* values and determining the associated series with the appropriate charge state distributions.

f l 7

U . / / &
i - ?ffl
i *

o
LO
<
CM
<

CT
LO

Sc
« 2

1 ?

<
<

o o
<
CM
<

A2 AA 50 nM AA

<
<

o
LO
<
CM
<

A2 AA 250 nM AA

Figure 4.13. *Mobility plots of A2 AA oligomers after 4 hr shaking at 21 °C prepared in increasing concentrations of AA, pH 7. It was evident that with increasing ionic strength the relative abundance of more compact (+6 to +8) populations increased as highlighted by black brackets on each mass spectrum located on the right of each mobility plot on a log scale display. Corresponding charge states of each series is denoted on the mobility plots. M is an abbreviation for monomer, D for dimer, T for trimer, Q for tetramer. Capillary and cone voltages, backing pressure was kept to the minimum to avoid artefacts and fragmentation. Settings were: capillary 1.70 kV, cone 50 V, trap 4 V, transfer 10 V, helium gas flow 180.0 mL/min, IMS gas flow 90 mL/min, bias 45, source wave velocity 200 m/s, trap wave velocity 311 m/s, IMS wave velocity 800 m/s, transfer wave velocity 200 m/s, backing 3.0 mbar.*

4.3.6 Structural analysis of a group of *in vitro* a-syn oligomers- A1 and A2 AA oligomers

The oligomer prepation for A1 AA oligomer involved a number of successive steps over 7 days, including steps of freeze-drying and resuspension in buffer and incubation with or without agitation whilst the starting concentration of 7 pM monomer was retained throughout the process, serving as a pool for oligomerisation. To further probe structural properties of alternate oligomers resulted from the aggregation protocols adapted here, ESI-IMS-MS data was collected for each type of oligomers nearer to the final stages. The mass spectrum and mobility plot of type A1 AA oligomers revealed a range of oligomers from dimers to hexamers with a dominant population of both extended and compact populations of monomeric protein (Figure 4.14.). Calculation of corresponding Os was performed as outlined in section 4.3.8.

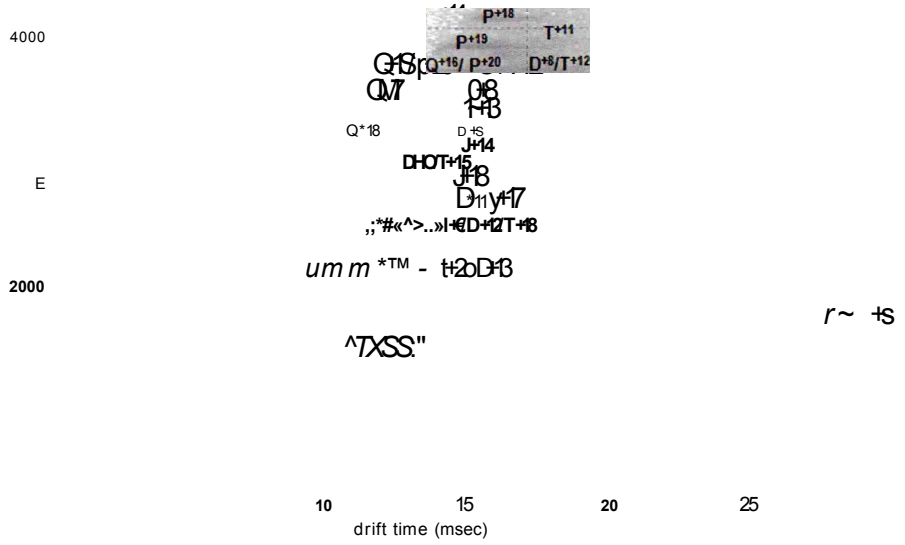

Figure 4.14. *Type A1 AA oligomer prepared in 50 mM AA, pH 7.0. The mobility plot is a log scale display with the corresponding mass spectrum on the right. The region >2900 m/z was enlarged by x82 to visualise the lower abundance, higher order oligomeric series. Oligomers fell into the populations of dimers (D), trimers (T), tetramers (Q), pentamers (P) and hexamers (H). Their respective charge states are indicated as superscripts. Charge states of the monomeric protein denoted on the mass spectrum on the right. Instrument settings were: capillary 1.30 kV, source temperature 60 °C, cone 30 V, trap collision energy 4 V, transfer collision energy 10 V, IMS gas flow 90 mL/min, helium gas flow 180 mUmin, bias 45, source wave velocity 200 m/s, trap wave velocity 311 m/s, IMS wave velocity 800 m/s, transfer wave velocity 200 m/s, backing 3.20 mbar.*

In this oligomeric preparation, dimers with a CSD of +8 to +29 were observed, trimers spanned a CSD of +11 to +20, whereas the tetramers displayed a CSD of +16 to +18. The higher order pentamers had a CSD of +17 to +20 charge

state ions and the largest hexameric oligomers comprised of +18 to +21 charge state ions.

Observation of each oligomeric series from dimer to hexamer suggests that oligomer growth progressed by in an isotropic manner, recruiting one monomer at a time in order to increase oligomer size. As seen in **Figure 4.14.** and as it appears in **Appendix Table 8.1.**, some *m/z* values are shared between the alternate oligomeric series and have arisen from multiple populations with the same *m/z* value. Clustering and drift times of CSDs give clues to resolving these overlapping species, however in certain instances for example in case of the *m/z* 2066.7 and 2411.0 peaks populations could not categorically be assigned to only a monomeric, dimeric or trimeric series. During extraction of drift times of these particular peaks the individual peak maxima was taken and used to determine the associated Ω.

Akin to type A1 AA oligomers, the mobility plot and mass spectrum of type A2 AA oligomers consisted of the same range of oligomeric subpopulations (**Figure 4. 15**).

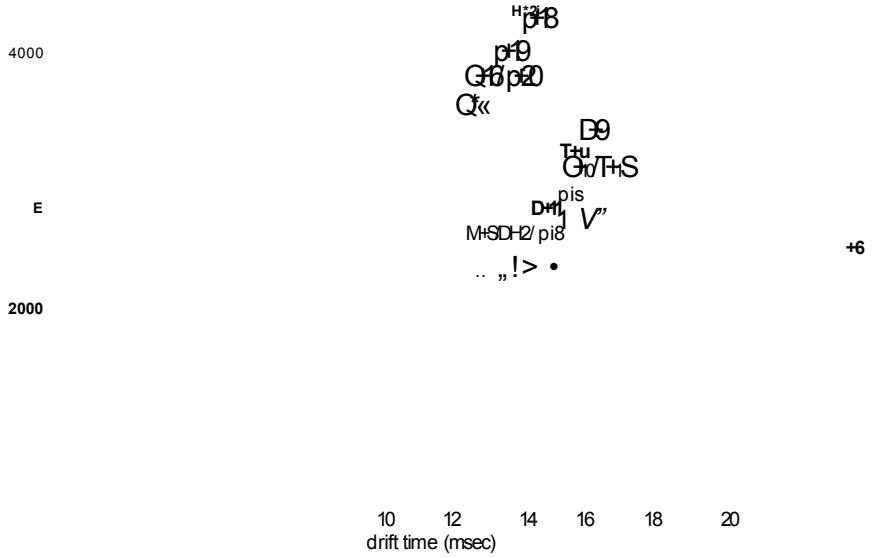

Figure 4.15. *Type A2 AA oligomer prepared in 50 mM AA, pH 7.0. The mobility plot is a log scale display with the corresponding mass spectrum on the right. The region >2900 m/z was enlarged by x82 to visualise the lower abundance, higher order oligomeric series. Oligomers encompassed populations of dimers (D), trimers (T), tetramers (Q), pentamers (P) and hexamers (H). Instrument settings were: capillary 1.60 kV, source temperature 60 °C, cone 30 V, trap collision energy 2 V, transfer collision energy 2 V, IMS gas flow 90 mUmin, helium gas flow 180 mUmin, bias 45, source wave velocity 200 m/s, trap wave velocity 311 m/s, IMS wave velocity 800 m/s, transfer wave velocity 200 m/s, backing 3.10 mbar.*

Inclusion of Fe(III) for the preparation of type A2 AA oligomer had a moderate effect on the aggregation of a-syn, however it is possible that larger aggregates were formed but the conditions employed and the time of sampling did not allow detection of those. Obtaining a stable spray from oligomeric solutions containing Fe(III) proved to be somewhat challenging that may supports the notion the

larger aggregates could have been present and remained inaccessible by ESI-IMS-MS analysis.

4.3.7 Structural analysis of a group of *in vitro* a-syn oligomers- C1 and C2 AA oligomers

Type C oligomers were prepared involving an overnight incubation step at continuous agitation followed by the use of 30, 000 Da MWCO VivaSpin500 (Sartorius, Life Technologies) spin concentrators that retained the prefibrillar aggregates over this cut-off limit. The mass spectrum and ion mobility data indicated the presence of minimal monomeric peaks, peaks resultant of fragmentation and dimeric to hexameric oligomers that were interspersed with peaks that could not be assigned (Figure 4. 16.). The fragmentation observed in C1 AA oligomer type may have stemmed from the procedure itself e.g. from an interaction with the spin concentrator's membrane or arose inherently for unknown reason.

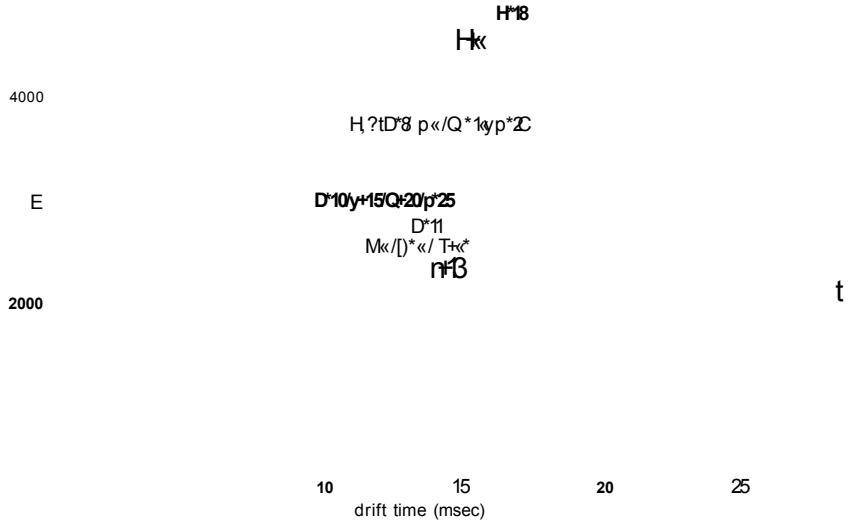

Figure 4.16. *Mobility plot (log scale display) and mass spectrum of C1 AA oligomer type prepared in 50 mM AA, pH 7.0. Instrument settings were: capillary 1.30 kV, source temperature 60 °C, cone 40 V, trap collision energy 4 V, transfer collision energy 10 V, IMS gas flow 90 mL/min, helium gas flow 180 mUmin, bias 45, source wave velocity 200 m/s, trap wave velocity 311 m/s, IMS wave velocity 800 m/s, transfer wave velocity 200 m/s, backing 3.20 mbar. Oligomeric populations of dimers (D), trimers (T), tetramers (Q), pentamers (P) and hexamers (H) were observed and CSDs indicated in superscripts. The monomeric protein's CSDs are shown on the mass spectrum on the right.*

An increase in the relative population of tetramers, pentamers and most dominant hexamers with charge state ions of +18 to +25 populating the mass spectrum of C1 AA oligomers was the main difference as compared to type A1 or A2 AA oligomers. The dominance of higher order oligomers suggested that preparation protocols tipped the balance towards enrichment of higher order species.

Addition of FeCh during the shorter preparation procedure resulted in lower order oligomers up to trimers, however this may be reflective of a technical impediment to attain an ideally stable spray for type C2 AA shown in Figure 4.17.. Others have commented on amyloid proteins disfavouring ESI ionisation and clogging up tips in the time course of ion mobility separation (Bernstein *et al.* 2009; Murray *et al.* 2009a).

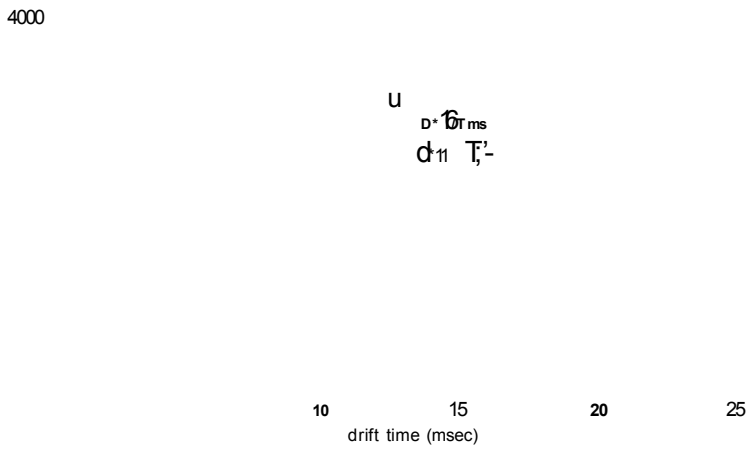

Figure 4.17. *Mobility plot (log scale display) and mass spectrum of type C2 AA oligomer prepared in 50 mM AA, pH 7.0. Settings were: capillary 1.40 kV, source temp 60 °C, cone 30 V, trap collision energy 4 V, transfer collision energy 10 V, IMS gas flow 90 mUmin, helium gas flow 180 mUmin, bias 45, source wave velocity 200 m/s, trap wave velocity 311 m/s, IMS wave velocity 800 m/s, transfer wave velocity 200 m/s, backing 3.20 mbar. Monomeric populations, a set of dimers (D), and trimers (T) were detected.*

The lower order species observed could have represented residual oligomers left over after aggregation into larger protofibrils. It was an interesting

observation that presumably more unfolded trimers with higher charge state ions of +14 to +21 were present in type C2 AA oligomers and no +12 and +13 charge state ions were detected as opposed to type C1 AA oligomers. Furthermore, tetramers, pentamers and hexamers were not detected it the mass spectrum of type C2 AA oligomers, yet these oligomers were capable of inducing intracellular aggregation and appeared to be non-toxic to neuroblastoma cells. Obtaining a mass spectrum for type C2 AA oligomer was challenging from solution and it is possible that the aggregation of a-syn was accelerated in the presence of Fe(III) such that species larger than trimers could not be detected at the final stage of the preparation protocol due to their assembly into higher MW protofibrils inaccessible to MS experimentation. Therefore, occurrence of this technical barrier does not allow conclusions to be drawn about the detected populations and observed functional properties.

4.3.8 Comparing CSDs and Qs of MS compatible oligomers with demonstrated biological functions to each other

For a detailed analysis of the ion mobility data of alternate oligomeric types, drift times were converted into Os as discussed in section 4.1.2. Oligomeric Os incrementally increased with subunit size but not in a linear fashion that pointed to structural rearrangements with a p-sheet formation during assembly into larger oligomers. Os values suggested a higher degree of compactness indicative of folding with increasing subunit size as shown by plotting O data as a function of oligomer order (Figure 4.18. *A).*

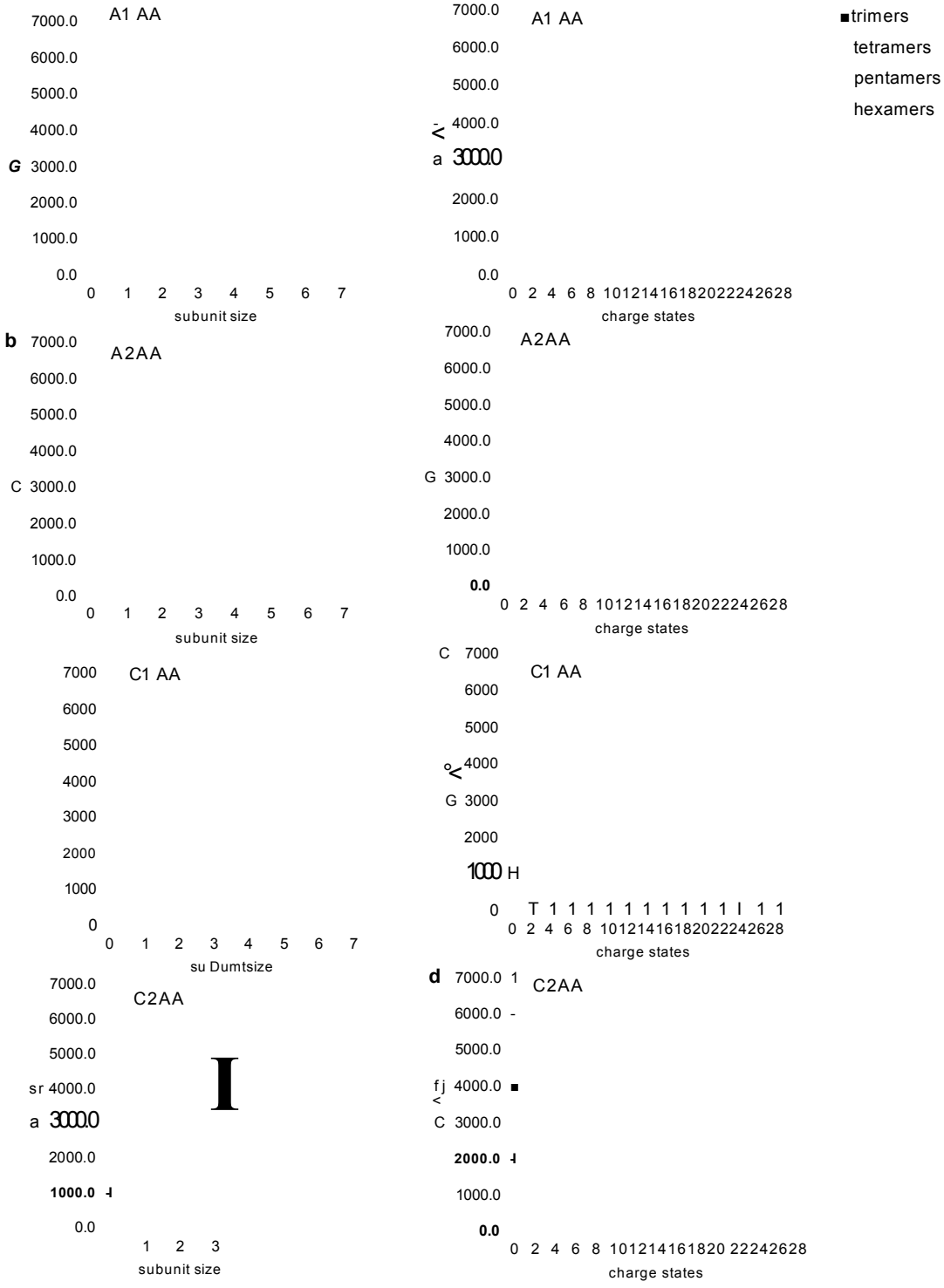
♦ dimers
■ trimers
tetramers
pentamers
hexamers
A1 AA
subunit size
charge states
A2AA
C1 AA
su Dumtsize
C2AA
I
T 1 1 1 1 1 1 1 1 1 1 1 I 1 1
0 2 4 6 8 10121416182022242628
0 1 2 3 4 5 6 7
1 2 3
0 2 4 6 8 10121416182022242628
0 2 4 6 8 10121414161820 22242628

Figure 4.18. *Ωs of oligomeric series according to oligomer size are shown for each mass spectrometry compatible oligomer types in panel **A**. The x axis shows subunit size and the y axis shows obtained Ωs in Å^2. Oligomeric conformational series are denoted in the legends, where blue diamonds represent dimers, red squares represent trimers, green triangles mark tetramers, purple cross hairs highlight pentamers and blue cross hairs indicate hexamers. Dimers are broad ranging in their Ωs in type A1 (**a**) and A2 AA oligomers (**b**). Higher order oligomers (>dimers) the spread in Ω became narrower reflective of compactness. Experimental Ωs and oligomer size of Type C1 and C2 oligomers are shown in **c** and **d**, respectively. For type C1 AA oligomer, due to the low intensity of dimeric and trimeric peaks drift times could not be accurately extracted and calculation of Ω was not carried out. The most prevalent oligomers were hexamers for for type C1 AA oligomer. In C2 AA oligomer, dimeric and trimeric families were present. In panel **B**, Ωs (in Å^2) are plotted as a function of charge states for A1 AA oligomer (**a**), A2 AA oligomer (**b**), C1 AA oligomer (**c**) and C2 AA oligomer (**d**). Oligomeric series are listed in the legend.*

Experimental Os of dimers were ~ 2153 to 5584 Å^2 and trimers spanned Os of 3365 to 4454 Å^2, whereas the O of tetramers was calculated to be 4279 to 4695 Å^2, 4657 to 5015 Å^2 for pentamers and 5604 to 5671 Å^2 for hexamers in case of type A1 AA oligomers. These values were very similar in range for type A2 AA oligomers. In addition, dimers and trimers appeared to be less tightly packed, extended structures as compared to higher order oligomers, encompassing wide CSD ~+8 to +26 and ~+14 to ~+20 charge states in case of type A1 and A2 AA oligomers. The higher order oligomers were more compact and retained fewer charge states; for example tetramers had a CSD of ~+15 to +18, pentamers displayed charges of +17 to +18 and hexamers obtained +18 to +20 charges.

Type C1 AA oligomers encompassed tetramers with Qs of 3913 to 4158 Å^2, pentamers with 4490 to 4697 Å^2 and hexamers with 5138 to 5473 Å^2. Type C1 AA oligomers had dimers and trimers whose Q's could not be calculated due to the low intensity of the signal, however the presence of tetramers, pentamers and more intense hexamers allowed to determination of experimental Qs. The calculated Qs for type C2 AA oligomers were between 2195-3118 Å^2 for dimeric series and 3558-4381 Å^2 for trimeric populations and no apparent higher order oligomers could be observed.

4.3.9 Comparing experimental Qs to standards and to model structures

Qs of a number of proteins with known Qs were acquired under native solution conditions. Appendix Table 8.2. shows all mean Q values with ±SD obtained over repeated measurements (n>3).

Comparison of Os of the oligomers with Os of known protein structures in the mass range of 5734 to 159216 Da confirmed that higher order oligomers became more compact as their subunit size increased (Figure 4.19.)-

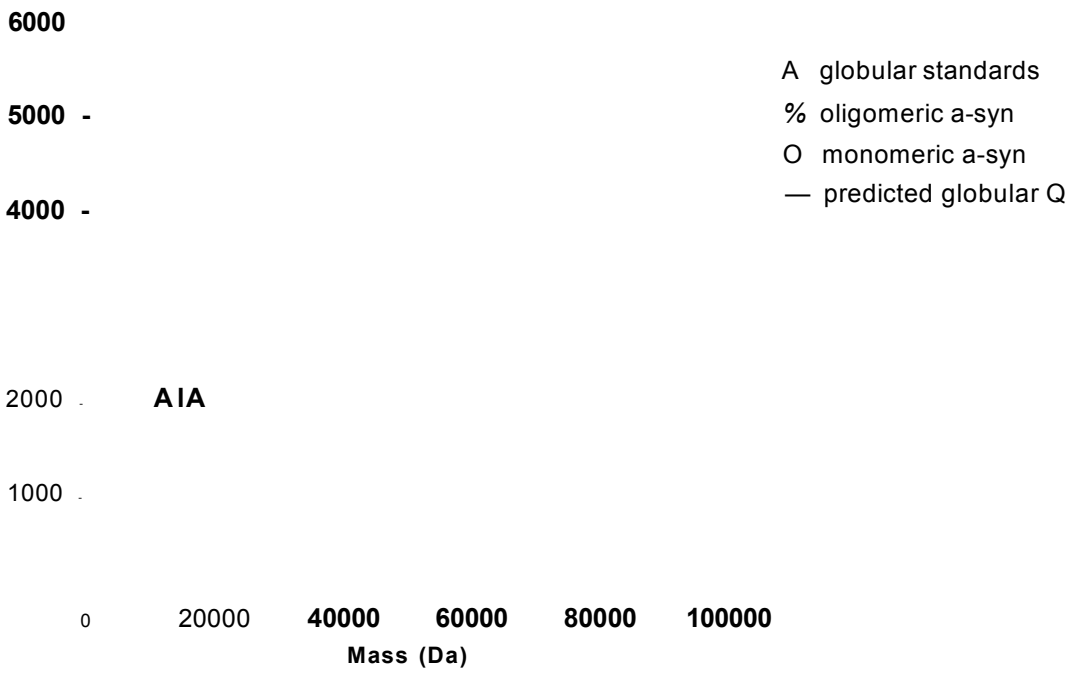

Figure 4.19. *Comparison of* Qs *of a-syn oligomers with that of known globular protein standards under native conditions. All measurements were carried out in triplicates, except two measurements, all represent mean values if it was possible to calculate; error bars show spread in Q. Oligomeric series (filled, red circles) are means of both Fe(III)-free and Fe(III)-supplemented preparations. D: dimeric* Q, *T: trimeric Q, Q: tetrameric Q, P: pentameric* Q, *Fl: hexameric Q, open triangles: different Qs of alternate protein standards under native conditions are shown as a function of mass in Da. Fully denatured, compact and extended populations of a-syn is shown by filled, grey circles. The continuous black line represents expected Qs of globular structures as decribed in detail earlier* (Smith *et al.* 2010). *For full details of experimental Q of all proteins see Appendix Table 8.2..*

The Ω of α-syn dimer was greater than that of folded porcine elastase and folded carbonic anhydrase (Mass: 29090 Da). The Ω of α-syn trimer was larger than that of the folded ADH monomer (Mass: 39804 Da) and the pentamer's Ω (Mass: 72300 Da) was slightly greater than the Ω of folded albumin monomer (Mass: 66463 Da).

Computational approaches complement ESI-IMS-MS data and provide additional value in determination of potential geometries of structural features of multisubunit systems (Ruotolo *et al.* 2008; Politis *et al.* 2010). Through calculation of theoretical Ωs it is possible to estimate whether a protein of unknown structure is likely to adopt a globular conformation by comparing its respective measured Ωs with predicted values. Thus a set of expected Ωs for globular proteins was adapted alongside with 3 D assemblies of compact subunits from Smith *el al.* (Smith *et al.* 2010) to gauge experimentally obtained Ω areas. The theoretical Ωs were calculated from spherical structures with an average density of 0.44 Da/Å^3 calculated from a range of proteins of known structure (Smith *et al.* 2009). The measured Ωs of α-syn oligomers were greater than that of the predicted globular proteins suggesting that they were not as compact as fully spherical structures. Measured Ωs of globular protein standards did however show a good agreement with the theoretically derived values. This correlation between simulated and experimental Ωs of globular proteins demonstrated that the experimentally obtained values being consistent with values documented by others (Smith *et al.* 2009) and that the acquisition did not dramatically alter the Ω of protein in question **(Figure 4.19.)**.

To further ascertain the topology of type A1 AA oligomers, Ω values were compared to theoretically derived Ωs. Here, an in house algorithm was used to

define theoretical Ωs and guide *in silico* modelling. It was assumed in this modelling approach that the monomer is a fully folded sphere with a 19.9 Å radius.This value was determined by assuming a mass of 14.6 kDa, with a density of 0.44 Da/Å^3 consistent with the most compact conformational form of the protein. A 4 Å overlap between different subunits was allowed, giving a centre to centre distance of 36 Å (Smith *et al.* 2009). This model is similar to that reported for the oligomers involved in Alzheimer's disease Bleiholder *et al.* (Bleiholder *et al.* 2011), permitting some surface interaction between subunits. Both linear structures and partially packed trimers, more compact tetramers and ring-like pentameric and hexameric forms have been constructed to guide experimentally acquired Ωs and plotted in addition to experimentally determided Ωs of type A1 AA oligomers or the monomeric protein as shown in **Figure 4.20.**.

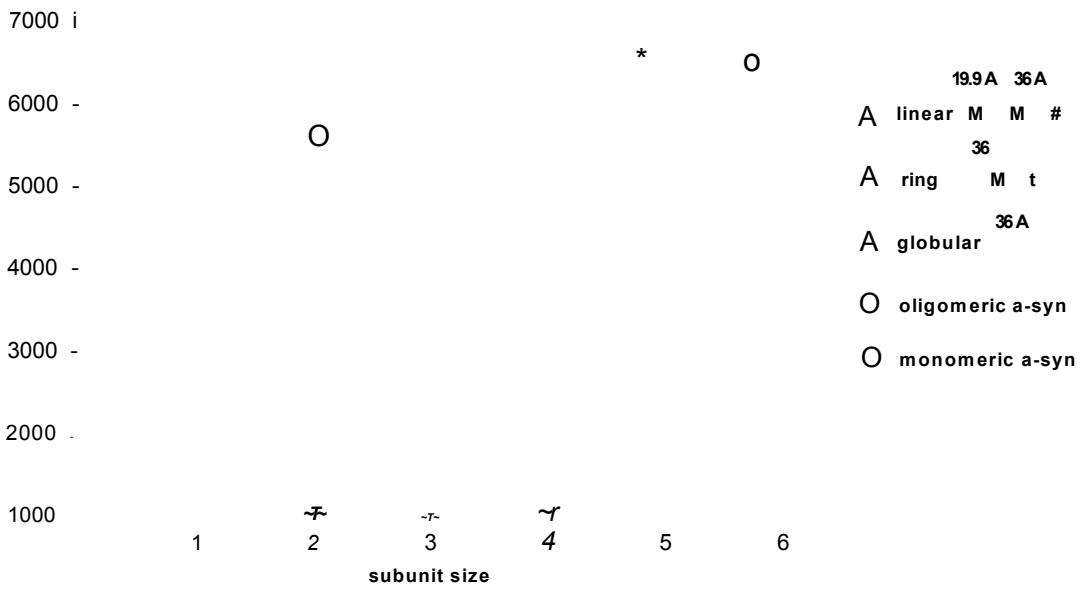

Figure 4.20. Os *of monomeric a-syn, oligomeric series of type A1 AA are shown in addition to theoretical* Qs *of linear, ring and globular structures as a function of subunit size. The filled, grey dots represent mean values of a-syn as shown in Appendix Table 8.2., lighter grey circles at subunit size 1 represent average* Os *of extended monomeric charge states of a-syn* as *shown in Figure Figure 4.7. and* Os *of oligomeric series (2 to 6 subunit size) of type A1 AA denoted with open circles. Yellow, filled triangles: theoretical* Os *of linear structures, orange, filled triangles: theoretical* Os *of ring-like structures and red, filled triangles are theoretical* Os *of fully globular structures obtained by an algorithm described before* (Smith *et al.* 2009). *The blue coloured 3 D shapes above the graph depict possible molecular organisations based on the agreement or disagreement of theoretical and experimental* Os.

Experimental and modelling data indicated that although the monomeric protein is predominantly unfolded when it forms oligomers, in particular type A1 AA oligomers, a structural collapse takes place, resulting in a variety of multimers in

size and compactness. Trimers appeared to be largely unstructured, open assemblies, the tetramers are not significantly packed, however they had fewer charges and they were less dispersed in Qs that indicated some degree of folding. Oligomers of the pentameric and hexameric series however deemed to be near ring-like or ring-like structures respectively as judged by molecular modelling and experimental data, having very narrow CSD and little spread in their Os. Similarly, Os of pentamers fitted to a near ring-like structure and hexamers of C1 AA oligomer fitted best to ring-like structures modelled *in silico* (data not shown).

4.3.10 Addressing the addition of Cu(II) in oligomerisation

Owing to the high affinity binding of Cu(II) to a-syn seen at the monomeric protein level, a-syn oligomers were also prepared with the addition of 10 pM Cu(II), rather than FeCl3. The interactions between Cu(II) and a-syn were markedly preserved both after an overnight or over a 7 day incubation period. High intensity adduct peaks of one Cu(II) a-syn were detected beside the lower intensity second Cu(II)-bound peaks of the monomeric region of the mass spectrum. A full mass shift in the presence of Cu(II) by 61.5 Da could still be observed after these extended incubation times and a variety of oligomers were detected in the monomeric Cu(II)-bound and oligomeric ensemble. Oligomeric series were assigned as if they arose from the fully one Cu(II)-bound, mass shifted protein (14521.5 Da). In the presence of Cu(II) oligomers were rapidly formed. After a brief incubation and freeze-drying step at further 24 hr shaking monomer-adducts, dimers to tetramers were identified Appendix Figure 8.13.. Pentamers were not observed and hexamers could not be assigned unambiguously either. At the final stage of preparation protocol, type A oligomer

prepared with $CuCl_2$ in 50 mM AA (pH 7.0) was comprised of monomeric adducts with predominantly one Cu(II) bound to α-syn and dimeric, trimeric and tetrameric oligomers. The maximum subunit size observed here was tetrameric, with no evidence for pentameric and hexameric forms as opposed to previously discussed oligomer types (**Figure 4.21.**)

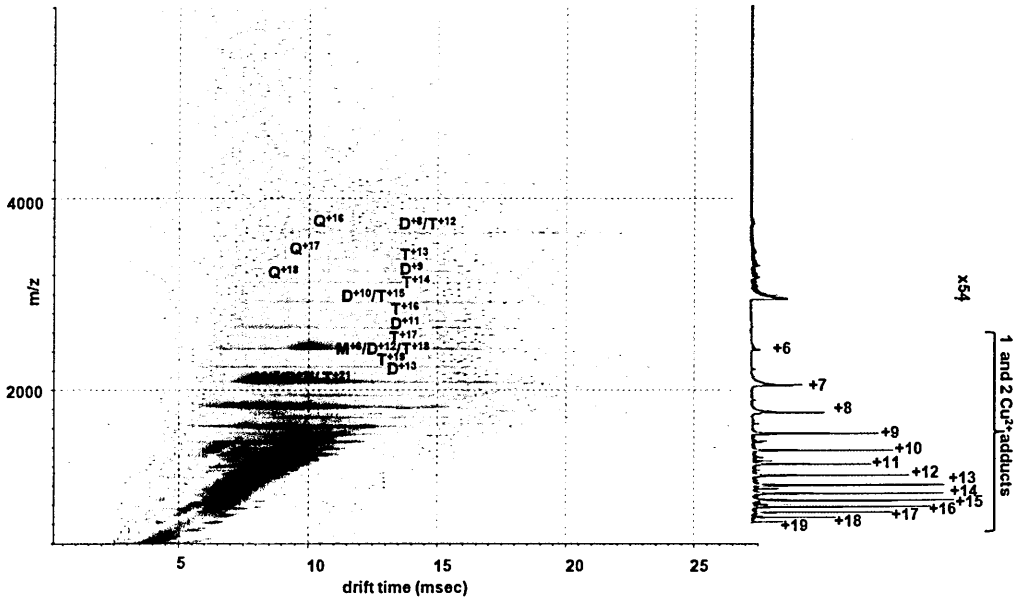

Figure 4.21. *Mobility plot (log scale display) and corresponding mass spectrum of type A oligomer prepared with $CuCl_2$ in 50 mM AA, pH 7.0. Instrument settings were: capillary 1.30 kV, source temp 60 ^{0}C, cone 30V, trap collision energy 4 V, transfer collision energy 10 V, IMS gas flow 90 mL/min, helium gas flow 180 mL/min, bias 45, source wave velocity 200 m/s, trap wave velocity 311 m/s, IMS wave velocity 800 m/s, transfer wave velocity 200 m/s, backing 3.10 mbar. Monomeric populations, a set of dimers (D), and trimers (T) and a broad range of tetramers (Q) were detected. Charge states of the oligomers denoted as superscripts in each series on the mobility plot. Monomeric adduct series with one Cu(II) or two Cu(II) are shown in brackets alongside their charge states. The region >2900 m/z was enlarged x54 to visualise the low abundance oligomeric components.*

The dominance of tetramers was obvious upon analysis of type C oligomer in AA that contained $CuCl_2$ as an enhancer of aggregation instead of $FeCl_3$ (**Figure 4.22.**).

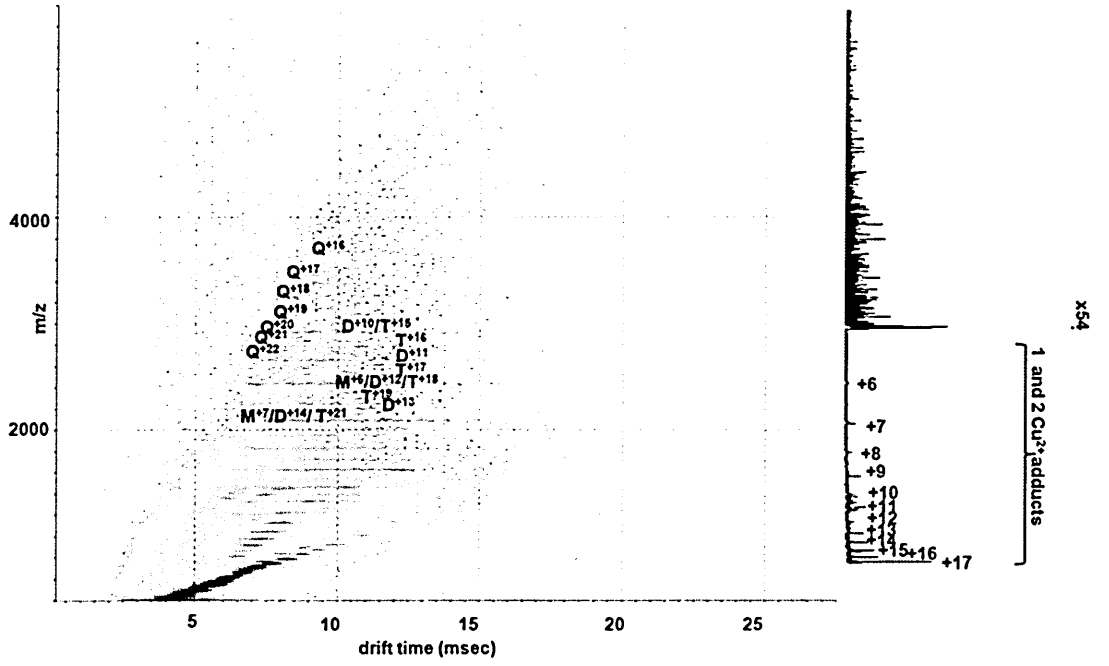

Figure 4.22. *Mobility plot and mass spectrum of type C oligomer prepared with 10 μM $CuCl_2$ instead of $FeCl_3$ in 50 mM AA, pH 7.0. Instrument settings were: capillary 1.30 kV, source temp 60 ^{0}C, cone 30V, trap collision energy 4 V, transfer collision energy 10 V, IMS gas flow 90 mL/min, helium gas flow 180 mL/min, bias 45, source wave velocity 200 m/s, trap wave velocity 311 m/s, IMS wave velocity 800 m/s, transfer wave velocity 200 m/s, backing 3.10 mbar. Monomeric Cu(II)-bound populations, a set of dimers (D), and trimers (T) and a broad range of tetramers (Q) were detected. Charge states of the oligomers appear as superscripts in each series on the mobility plot. Monomeric adduct series with one Cu(II)-bound or another, second Cu(II)-bound are shown in the mass spectrum with appropriate charge states. The region >2900 m/z was enlarged x54 to display the low abundance oligomeric components more visibly.*

The maximum subunit size was tetameric in case of these $CuCl_2$ induced oligomers. Q areas of Cu(II) induced type A oligomers appeared to be only ~1 % greater than respective Qs of all other previously discussed oligomer types, making them directly comparable across all conditions tested as shown in Figure 4. 23..

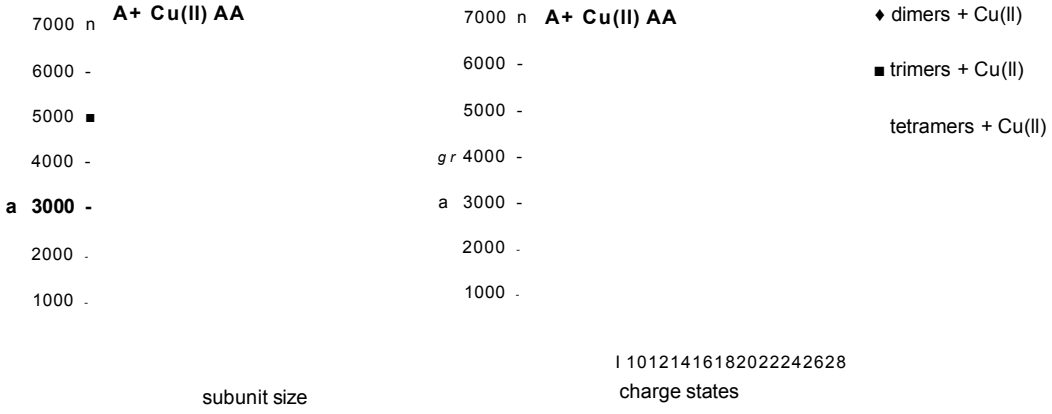

Figure 4.23. Qs *of oligomeric series observed for type A oligomer prepared in the presence of 10 pM Cu(II) are shown according to subunit size. The x axis indicates subunit size and the y axis shows obtained* Qs *in A2. Oligomeric conformational series are denoted in the legends, where the blue diamonds represent dimers, red squares represent trimers and the green triangles mark tetramers (A). Measured* Qs *plotted as a function of charge states for modified type A2 AA oligomer prepared with CuCI2 in 50 mM AA, pH 7.0. X axis shows subunit size and y axis shows obtained* Qs *in A2 (B). The blue diamonds represent dimers, red squares represent trimers and the green triangles denote tetramers.*

It would be very interesting to investigate the behaviour and biochemical propensities of these oligomers prepared in the presence of Cu(II) as it was carried out for type A1, A2, C1 and C2 oligomers both in AA and SP (Chapter

3). The presence of low order oligomers up to tetramers might be relevant in understanding the behaviour of low order species observed in type A 1 and A2 AA oligomers including an increased toxicity.

4.4 Conclusions

In order to obtain a better understanding of structure and function relationships of a group of *in vitro* a-syn oligomers, it was necessary to characterise their structure and topology by ESI-IMS-MS in detail. NMR and CD and other complementary structural biology methods are vital in precisely elucidating amyloid assemblies, although limitations originating from large molecular weights, low concentrations and transient formation of oligomers may pose technical obstacles. Since ESI-IMS-MS has been shown to have unique advantages in probing multi-subunit complexes and determining in-depth structural characteristics (Ashcroft 2010; Woods *et al.* 2012; Marcoux *et al.* 2013a), this technique was the method of choice to uncover structural information about *in vitro* a-syn oligomers.

The conformational heterogeneity of a-syn has now become widely documented (Uversky *et al.* 2009; Ullman *et al.* 2011; Beveridge *et al.* 2013) and data presented here confirmed that under equilibrium monomeric a-syn consists of more extended and several more compact conformational forms that are co-populated at near native conditions, at neutral pH (Frimpong *et al.* 2010). The Os measured here are in agreement with previously published values (Bernstein *et al.* 2004; Grabenauer *et al.* 2008; Smith *et al.* 2009). Ion mobility instrumentation allows observing ligand binding at low concentrations and

monitoring resultant complex formation by detection of mass shifts (Kaltashov *et al.* 2006).

Upon investigation of co-ordination of bi- and trivalent ions to α-syn over different protein to metal ratios, Cu(II) bound most strongly to the monomeric protein detectable on the rapid time scale of ESI-IMS-MS analysis, which was retained over increased lengths of time. One and two Cu(II)-bound metal-protein adducts were observed at each conformational states of the protein, however evidence for a structural transition towards a more collapsed conformation was observed only for the compact conformational form of the protein. This may be important in understanding why this metal drives amyloid fibril formation *in vitro* (Uversky *et al.* 2001c; Uversky *et al.* 2009) and why in the ageing brain increased level of metals including copper could trigger undesirable effects on the structure of α-syn (Pall *et al.* 1987; Hirsch *et al.* 1991).

A number of reports have highlighted the influence of various salts altering the aggregation specifics of amyloid proteins. For example, the effect of ionic strength on the amyloid formation of amylin (Marek *et al.* 2012) or human or rat variant of Aβ(1-42) (Kriz *et al.* 2013), the particulars of different salt ions affecting the propensity and aggregation of Aβ(1-40) (Klement *et al.* 2007). Using ESI-IMS-MS, it was apparent that increased ionic strength was capable of altering the conformational states of the α-syn analysed at 4 hr into oligomerisation. Higher AA concentrations enriched the compact conformations of the monomeric α-syn. Data suggested an increased aggregation rate in the presence of higher AA concentrations with an increase in oligomeric distribution of trimers.

Structural characterisation of type A oligomers prepared in AA have shown that dimers to hexamers were co-populated in addition monomeric conformations. Type C1 AA oligomer consisted of mainly tetrameric, pentameric assemblies and were enriched in hexameric oligomer series. Although addition of $FeCl_3$ is thought to increase yield of oligomeric species, it may have altered or diverted the aggregation pathway of these oligomers, however conclusive evidence could not be obtained either for immediate binding of this metal or for its influence on the oligomerisation of α-syn. Type A2 AA oligomers prepared with Fe(III) were similar to type A1 AA oligomers in the series of oligomeric species observed. Nevertheless, type C2 AA oligomers seemed to be lower order oligomers ranging from dimers to trimers that could have reflected the assembly at the point of sampling but could have been an artefact arising from an uneven electrospray due to clogging of capillaries.

To determine structural organisation of alternate oligomers, Ωs were calculated that revealed that in proportion to subunit increase, the compactness of oligomers increased. Charge state distribution of oligomers became narrower as the subunit size grew which indicated folding into more ordered self-assemblies. The experimental Ωs were greater for larger oligomers, yet they did not increase in a linear fashion supporting the notion of a structural collapse upon oligomerisation. The β-sheet content of oligomers presumably increased as a result of a structural collapse. A similar collapse was described from trimers to tetramers in case of β_2 microglobulin, however the Ωs of these series was larger than would be expected for globular proteins of a similar mass and corresponded to elongated assemblies (Smith *et al.* 2010).

Molecular modelling (Smith *et al.* 2009) and experimental data suggested that dimers and trimers were primarily extended structures; however increasing oligomer size resulted in more compact features, whereby pentamers resembled a near ring-like structure and hexamers were reminiscent of a closed ring-like structure with considerable compactness. The assembly of oligomers proceeded up to the hexameric stage. This hexameric ring-like structure would have needed to reopen to recruit a further monomer that may have presented an energy barrier halting the aggregation process.

The low yield of oligomeric species and broad peak areas could not rule in or rule out the presence of oxidised Met residues.

It is important to consider that these A1, A2, C1 and C2 AA oligomers have been demonstrated to have biological propensities promoting aggregation of intracellular α-syn.

Structural properties of type A2 and type C1 oligomers incorporating Cu(II) were shown here with a maximum tetrameric order. Obtaining data from functional assays could aid further characterisation of the Cu(II) induced assemblies performed in a similar fashion as for Fe(III)-free or Fe(III) containing oligomers.

One shared observation among these alternate oligomers was that oligomeric assembly proceeded through by addition of one monomer at a time with even and odd number oligomers co-populated in each of these (Jang *et al.* 2010) assemblies. In case of Aβ42 oligomers dimers, tetramers, hexamers and dodecamers were observed, whereas in case of WT Aβ isoform only dimers and tetramers were observed and no odd number oligomers (Bernstein *et al.* 2009; Clemmer *et al.* 2009). β_2 microglobulin self-aggregation was shown to

proceed by monomeric addition (Smith *et al.* 2006) at pH 2.5. However, the β_2 microglobulin oligomers in that system gave rise to monomers to tetramers, and these oligomers were more expanded than assumed with Ωs consistent with elongated structures (Smith *et al.* 2010).

Taken together, the ESI-IMS-MS experiments described here showed parameters of mass, size and shape of *in vitro* α-syn oligomers with functional propensities for the first time. Molecular modelling of type A1 AA oligomers implied that theoretical Ωs of dimers and trimers and tetramers resembled most closely to unstructured features. In contrast, theoretical Ω of a nearly closed ring-like structure showed an excellent agreement with observed Ωs of pentamers and a theoretical Ω of a fully closed ring organisation agreed with the measured Ω of hexamers. ESI-IMS-MS data in conjunction with functional characterisation suggest that hexamers and pentamers show a correlation with intracellular seeding and that the lower order oligomers may be responsible for cytotoxicity in SH-SY5Y neuroblastoma cells.

Evidence has also been shown that alternate preparation protocols can tip the balance between the formation and enrichment of certain subpopulations and oligomeric series, demonstrating the dynamics and complexity of α-syn self-assembly. In-depth details of kinetics and stability would be of additional value in future investigations for these α-syn oligomers.

5 Chapter 5

Binding of dopamine to a-syn assessed by ESI-IMS-MS

5.1 Introduction

Oxidative stress has been shown to be one of the key mechanisms involved in neurotoxicity giving a possible explanation as to why dopaminergic neurons are highly vulnerable to cell death. In the cytoplasm, dopamine (DA) can undergo oxidation due to its labile quinone ring in the presence of molecular oxygen producing ROS such as hydrogen peroxide, superoxide and dopamine-quinones e.g. dopamine-o-quinone (Graham 1978). ROS can then account for the damage in the cellular components, for example in the mitochondria association of a-syn with oxidised lipids alters viable membrane properties (Ruiperez *et al.* 2010). Alternatively, DA can also be a target of enzymatic degradation by monoamine oxidase (MAO), yielding free radicals and potentially reactive DA-metabolites such as 3,4-dihydroxyphenylacetaldehyde (DOPAL) (Jinsmaa *et al.* 2011). However, following its synthesis DA is taken up into synaptic vesicles by the vesicular monoamine transporter 2 (MAT2) where the low pH prevents its degradation and the subsequent re-uptake of DA to the pre-synapses is undertaken by the dopamine-transporter (DAT) (Lotharius *et al.* 2002 b).

a-syn is thought to play an essential role in the modulation of synaptic vesicle recycling, DA storage and release at the nerve terminals (Chadchankar *et al.* 2011). Mutations in the protein in the familiar form of the disease or changes in its expression or aberrant folding in the sporadic forms can consequently result

in impairment of neurotransmitter storage or release contributing to PD. In case of a breakdown in vesicle handling, an increased level of cytoplasmic DA may trigger the production of free radicals and the formation of toxic intermediates with α-syn (Lotharius *et al.* 2002a; Lundblad *et al.* 2012). Importantly, administration of levodopa and its derivatives alleviate the symptoms of PD in many cases (Muller 2012).

Recent research has focused on revealing the biochemical and molecular interactions of α-syn and DA with implications on the rate of secretion of DA-α-syn oligomers to the extracellular space, mitochondrial respiration and autophagy (Lee *et al.* 2011; Outeiro *et al.* 2009; Munoz *et al.* 2012). *In vitro*, DA-α-syn oligomers are devoid of a defined secondary structure, exhibit various non-ordered aggregate morphologies with alternate size and shape under electron microscopy (EM) and are SDS resistant (Cappai *et al.* 2005). However, it is still debated whether the DA-α-syn oligomers are primarily covalent or non-covalent by nature, therefore the type of interaction between α-syn and DA remains elusive. Some early evidence has indicated that oxidated ligation of DA stabilised α-syn, yielding accumulation of DA-α-syn protofibrils (Conway *et al.* 2001). Since this report, inhibitory effects of DA and several other analogues on fibrillation of α-syn have also been demonstrated and the cytotoxicity of predominantly large oligomeric intermediates of cross-linked DA-α-syn to neuronal cells was underpinned (Li *et al.* 2005). The covalently cross-linked α-syn DA oligomeric intermediate forms have demonstrated an altered ability for self-assembly and propensity to disrupt biomembranes in a yeast model and may also be critical in sustaining neurodegeneration in PD (Rochet *et al.* 2004).

Met oxidation seems to be relevant in the formation of a-syn-DA polymers in addition to hydrophobic and long-range interactions (Zhou *et al.* 2010b; Zhu *et al.* 2013). Leong *et al.* defined Met oxidation as a primary mechanism for generating soluble, SDS-resistant a-syn-DA oligomers (Leong *et al.* 2009b) rather than the necessity of the C-terminal sequence $_{125}$YEMPS$_{129}$ partaking in a non-specific hydrophobic interaction leading to DA-a-syn complexes which inhibit fibrillisation as concluded by others (Herrera *et al.* 2008; Norris *et al.* 2005). Small angle X-ray scattering (SAXS) and CD data indicated that Met oxidised monomers are extended worm-like features akin to a-syn monomers, while DA-a-syn dimers and trimers had some degree of secondary structure (Rekas *et al.* 2010). By contrast, an ESI-MS study in conjunction with other biophysical methods demonstrated that one intact, unoxidised a-syn was capable of binding three DA molecules that in turn led to oligomerisation to a range of higher order protofibril species (Shimotakahara *et al.* 2012).

5.2 Materials and Methods

The relevant methods have been described in section. 2.4.4.3.

5.3 Objectives

Here, the aim was to examine how binding of DA affects the alternate conformational populations of human, recombinant WT a-syn and their respective Os at the initial phase of assembly. In order to investigate this, the potential of ESI-IMS-MS has been harnessed to provide in-depth structural information in the gas phase.

5.4 Results and Discussion

5.4.1 Addressing binding of Tyr and DA to a-syn by ESI-IMS-MS

Numerous *in vitro* studies have shown that DA and some of its metabolites act as modulators of a-syn oligomerisation and inhibit its fibrillisation (Conway *et al.* 2001; Cappai *et al.* 2005; Norris *et al.* 2005; Jinsmaa *et al.* 2011). ESI-MS in conjunction with other biophysical methods has demonstrated that one intact, unoxidised a-syn is capable of binding three DA molecules that in turn led to oligomerisation to a range of higher order protofibril species (Shimotakahara *et al.* 2012).

Here, the effect of DA binding on the population of conformational states of a-syn (Figure 5.1. *A)* was examined in conjunction with changes in the corresponding Os. a-syn-DA complexes observed by ESI-IMS-MS are shown in Figure 5.1. C DA ligands are highlighted with black dots on the mass spectrum in Figure 5.1. C and are only observed on the +17 to +10 charge states. If the expanded state was the sole conformation present or DA binding was non-specific, then it might be expected that DA adducts would be present on all charge state ions (+17 to $+_6$) in the gas phase. However, binding of three DA can only be observed to the +17 to $+_{10}$ charge state ions in the same envelope that contains the most expanded forms of the protein. The +10 charge state ion bound only a single DA ligand. The lower charge state ions +9 to $+_6$ did not show any DA binding and these ions in the absence of DA still retained the structural features of the most compact conformation Figure 5.1. C. It is possible that ligand binding stabilises the extended state preventing structural collapse, however the conformational states that the ligand binds to appeared to

be present in the absence of the ligand. This data can therefore be interpreted as DA binding to only the most extended conformations in solution.

Tyr serves as an early precursor in the synthesis of DA (Felger *et al.* 2012) and differs only by a carboxyl group in its chemical composition. The assess the co-ordination of DA and Tyr experiments were performed upon the addition of these ligands compared to α-syn only and α-syn-DA complex with excess of Gly as shown in **Figure 5.1.**.

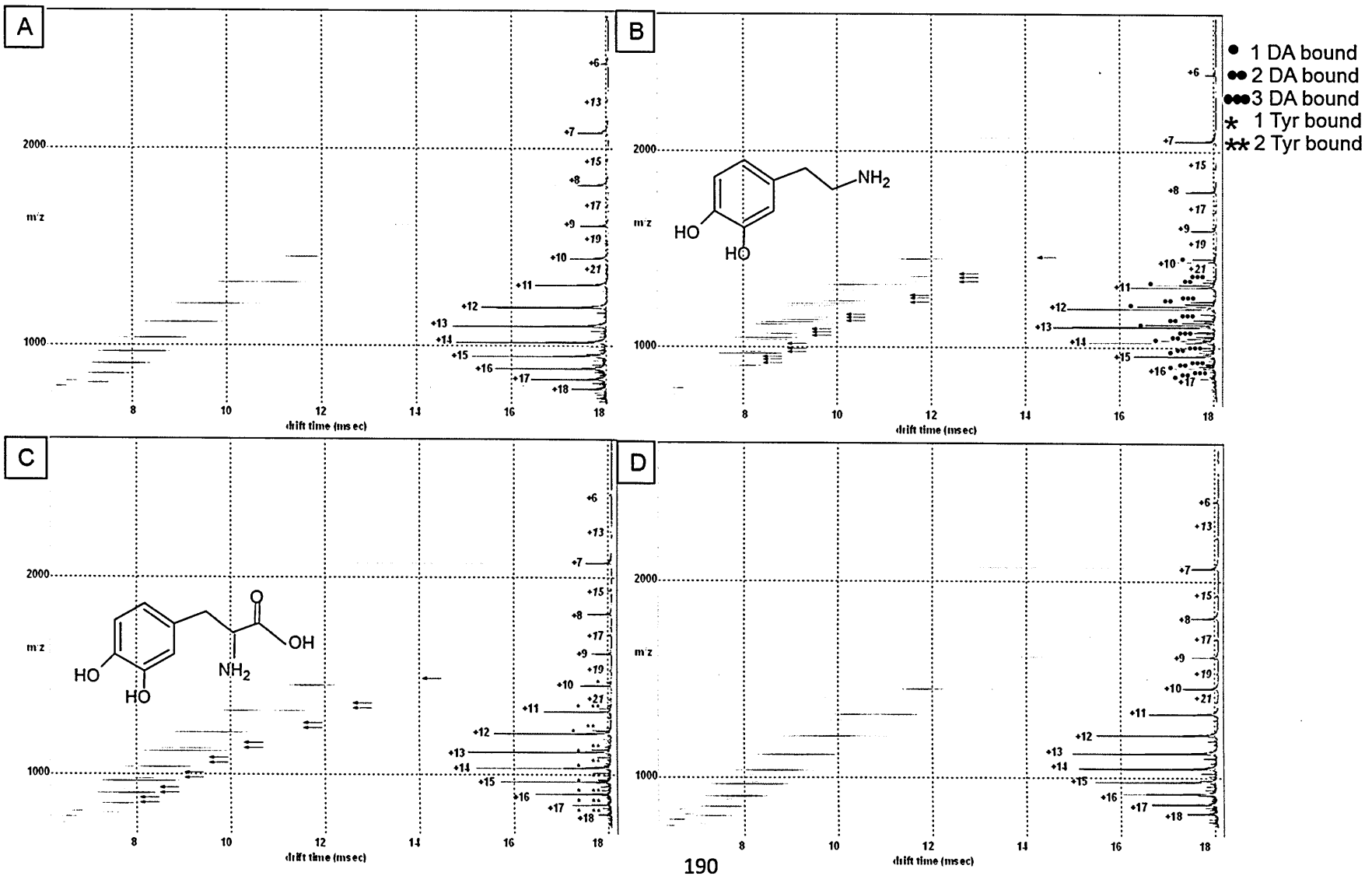
A
B
C
D
● 1 DA bound
●● 2 DA bound
●●● 3 DA bound
* 1 Tyr bound
** 2 Tyr bound
m/z
drift time (msec)
NH2
HO
OH
O

Figure 5.1. *Mobility plots obtained from 50 mM aqueous AA solution of 50 μM α-syn, at pH 6.8 with or without further addition of either DA or Tyr at 6.25 mM. The x axis represents drift time (msec), on the y axis m/z is shown; square root display. Corresponding spectra for each acquisition is overlaid on the right of each mobility plot indicating charge states and the presence or absence of the appropriate ligands* ***A****: WT α-syn,* ***B****: α-syn in the presence of Tyr,* ***C****: α-syn in the presence of DA,* ***D****: α-syn in the presence of DA and Gly.*

Figure 5.1. ***B*** details the resultant α-syn-Tyr spectra obtained from a 1:125 ratio of α-syn:Tyr. A maximum of two molecules of Tyr were involved in complex formation with α-syn indicated by one or two stars above the respective peaks, these ions however had a markedly lower intensity as compared to apo- and DA bound forms of α-syn. Again, ligand binding was only observed to the +17 to +10 charge state ions for DA, and no binding was observed to the more compact conformational populations of α-syn. Inclusion of Gly is useful when preventing non-specific or low affinity binding and here it completely negated the ability of DA to bind to α-syn as shown on **Figure 5.1.** ***D***, suggesting the interactions were low affinity and electrostatic in nature. Together these results demonstrated that the extended conformations populating the +17 to +10 charge state ions of α-syn bound up to one to three DA molecules and that this binding could be overcome by the presence of Gly. In addition to the mobility plots, the ESI-IMS-MS spectra of apo α-syn (***A***), α-syn-DA (***B***), α–syn-Tyr (***C***) and α-syn-DA-Gly (***D***) are included (**Figure 5.2.**).

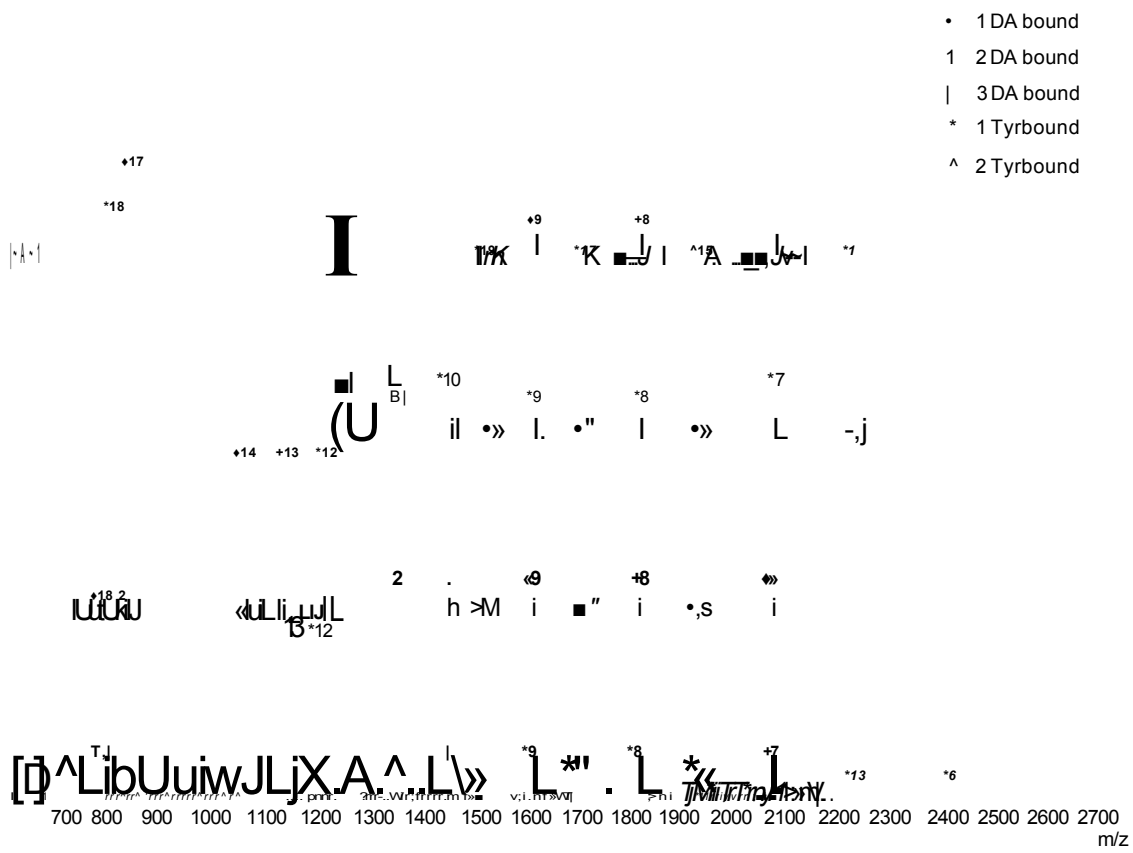

Figure 5.2. *a-syn only and a-syn and DA or Tyr complexes observed by ESI-IMS-MS are shown. ESI-MS spectra extracted from the mobility plots of Figure 5.1. were obtained from 50 mM AA solution of 50 pM a-syn, at pH 6.8 with or without further addition of either DA or Tyr at 6.25 mM. Charge states and the presence or absence of the appropriate ligands are indicated on the plots. A: WT a-syn, B: a-syn in the presence of Tyr, C: a-syn in the presence of DA and D: a-syn in the presence of DA and Gly.*

DA ligands are highlighted with black dots on the mass spectrum in B and were only observed on the +17 to +10. A maximum of two molecules of Tyr were involved in complex formation with a-syn indicated by one or two stars above the respective peaks, these ions however had a markedly lower intensity as compared to apo- and DA-bound forms of a-syn.

As revealed by the mobility plots, the main observations were that a maximum of three DA molecules were co-ordinated to the extended charge state ions of a-syn and up to two Tyr molecules could bind to the extended conformational series of monomeric a-syn. Adduct formation was not observed at charge state ions of the compact conformational form of the protein.

5.4.2 Elucidating conformational transitions upon ligand binding

To further elucidate the conformational transitions taking place upon DA co-ordination, selected populations of the extended and compact conformational families of a-syn have been chosen (Figure 5.3.).

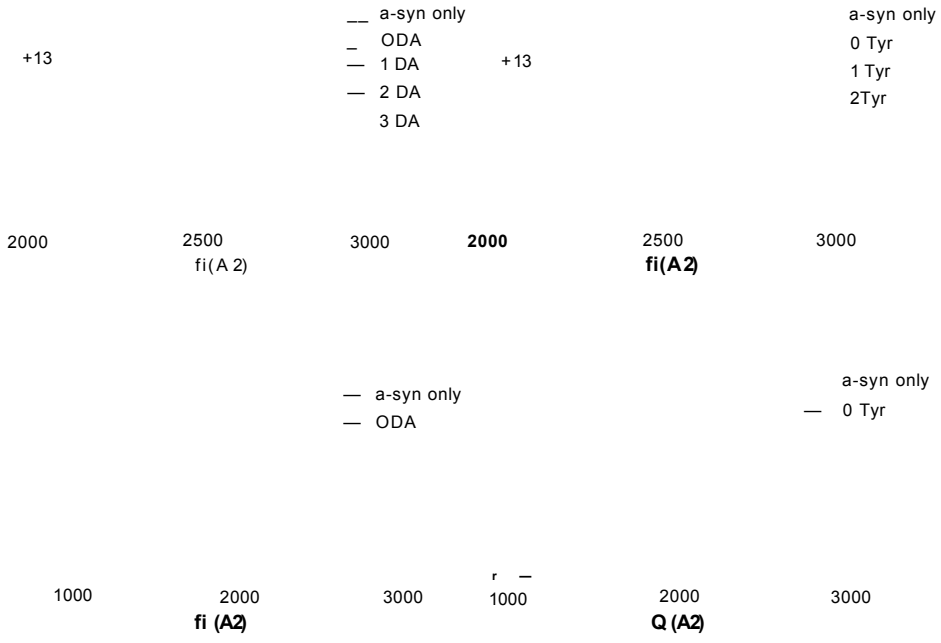

Figure 5.3. Qs *determined from alternate DA and Tyr adducts at 1:125 protein to metal ratio or from the apo-form of a-syn without any ligand binding at the +13 charge state ion (a member of the extended conformation) and at the +7 charge state ion (a member of the compact conformation). The alternate colours highlighted in the legends denote the number of ligand bound or a-syn only.*

The +13 charge state ion was assigned as being representative of the extended conformational family. The arrival time distribution for the +13 charge state ion acquired in the absence of any DA is shown in **Figure 5.3. *A***: black line and indicates two clearly resolvable peaks at ~2590 $Å^2$ and ~2720 $Å^2$ along with another feature at ~2500 $Å^2$. In the presence of DA the most extended forms of the protein bound to the ligand with a shift toward the more extended states. The stepwise binding of one, two or three DA ligands initiated a shift in the conformation towards the more expanded conformations (**Figure 5.3. *A***) as evidenced by an increasing drift time and increase in the Ωs. Upon binding of three DA ligands, the ~2500 $Å^2$ and ~2590 $Å^2$ states were absent and the highly extended state, ~2720 $Å^2$ was uniquely observed. The remaining apo-form of the protein acquired in the presence of DA predominantly showed the populations of the ~2500 $Å^2$ conformations and significant depletion of the ~2590 $Å^2$ and ~2720 $Å^2$ conformations. The +7 charge state ion was taken as being representative of the compact states of α-syn and co-populated compact conformations along with a minor population of the extended state. DA binding was not observed to +7 charge state ion, nor a shift in its Ω was observed.

One or two Tyr ligands were also observed to bind to the extended states of α-syn charge state ions of +10 to +17. Analogously to DA, the binding was to the most extended forms of the protein. However, as **Figure 5.3. *B*** demonstrates this binding yielded lower intensity adducts as compared to DA at the same protein to ligand ratios. Therefore Tyr was able to bind to α-syn in a similar manner to DA but a maximum of two Tyr molecules were co-ordinated to the protein, and structural changes caused by this binding were minimal as

compared to DA. These results demonstrated that DA binds to a-syn in a conformational dependent manner, binding exclusively to the most extended states of the protein.

To assess that adduct formation and subsequent conformational rearrangement following DA ligation occured across repeated measurements and at alternate protein to ligand dilutions, replicate experiments have been conducted at 1:125, 1:30 and 1:8 ratios (a-syn:DA). Up to three DA molecules were co-ordinated in each case, however the intensity of the adduct peaks were lower as the ligand concentration decreased (Figure 5.4.).

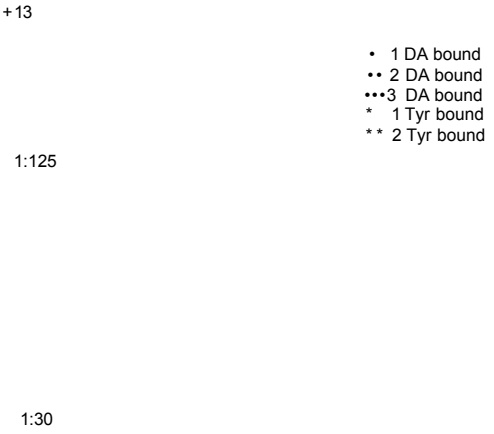

Figure 5.4. *Binding of DA or Tyr to a-syn at alternate protein to metal ratios as shown on the left hand side. DA adducts denoted with black circles, Tyr-bound forms of the protein indicated by asterisks and finally apo-form of the protein remained unmarked at the +13 charge state ion.*

The corresponding theoretical and measured *m/z* ratios are given in **Table 5.1.** both at the +13 and at the +7 charge state ions depending on the number of DA or Tyr molecules bound to α-syn.

		DA		Tyr	
Charge state ion	Number of ligand bound	Theoretical *m/z*	Measured *m/z*	Theoretical *m/z*	Measured *m/z*
+13	0 ligand bound	1113.3	1113.0	1113.3	1113.0
	1 ligand bound	1125.1	1125.0	1127.2	1127.0
	2 ligand bound	1136.9	1136.8	1141.2	1141.0
	3 ligand bound	1148.7	1148.6	n/a	n/a
+7	0 ligand bound	2066.7	2066.4	2066.7	2066.4

Table 5.1. *The theoretical and measured m/z ratios are shown both in case of DA and Tyr at the +13 and +7 charge state ions according to the number of ligands bound to α-syn.*

The measured *m/z* values were in close agreement with the expected *m/z* values, indicating 1 Da of mass error. Calculated Ωs of the one DA bound forms of α-syn were consistent at 1:8 and 1:30 and 1:125 protein to ligand ratios, similarly to those of the two DA bound forms. Ωs of the three DA bound adducts were the same at the 1:30 and 1:125 protein to ligand ratios. One Tyr adducts also gave the same Ωs at all three protein to ligand ratios and the two Tyr bound adducts had the same Ωs both at the 1:30 and 1:125 protein to ligand ratio. Binding was observed to the extended form of the protein only such as the +7 charge state ion remained ligand-free whose Ωs are shown below in **Figure 5.5.**.

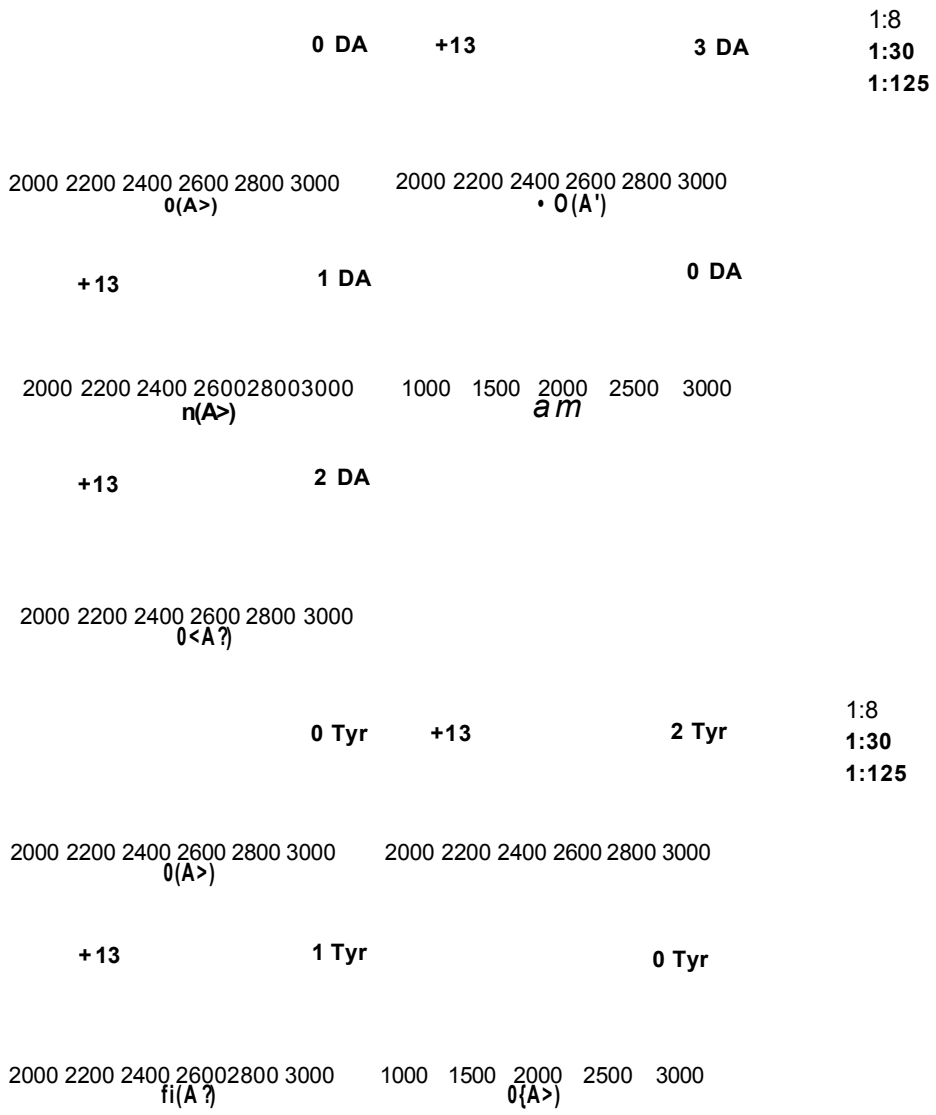

Figure 5.5. Qs *determined upon repeated measurements of alternate DA and Tyr adducts at 1:8, 1: 30 and 1:125 protein to ligand ratio or of the apo-from of the protein without the binding of any ligand at the +13 charge state ion (a member of the extended conformation) and at the +7 charge state ion (a member of the compact conformation). The x axis is the* Q *(A2), the y axis is intensity (%).*

As indicated by Figure 5.5., the alternate a-syn:DA ratios did not dramatically affect the absolute Qs recorded for the extended state conformations, with two

and three DA bound at low ratios inducing the same Q as two and three DA bound at high ratios. These results indicate that it is the specific binding of the ligand that causes the conformational change rather than a change in the solution environment.

5.4.3 Met oxidised residues

a-syn contains four Met residues; two Met residues are located at aa positions 1 and 5 on the N terminal and further two Met residues reside at aa positions of 116 and 127 on the C terminal. Met oxidation has been shown to affect both electrostatic and hydrophobic interactions of a-syn. Furthermore, oxidation of Met is thought to play a role in inhibiting fibrillisation of the protein *in vitro,* yielding non toxic oligomers of a-syn (Zhou *et al.* 2010a). Previous evidence have suggested that Met oxidation of a-syn occurs upon interaction with DA (Leong *et al.* 2009b). Consistently with this, Rekas *et al.* also reported Met oxidised monomeric and lower order oligomeric species of a-syn. This study speculated that Met oxidation in the presence of DA stabilises oligomers and is a key event in inhibiting the end-to-end association of a-syn molecules, preventing the formation of large fibrils with a cross-(3 structure (Rekas *et al.* 2010).

Utilising short time frames during these experiments performed here, no direct evidence was found for pronounced Met oxidation upon addition of DA as judged by ESI-IMS-MS analysis (Figure 5.6.).

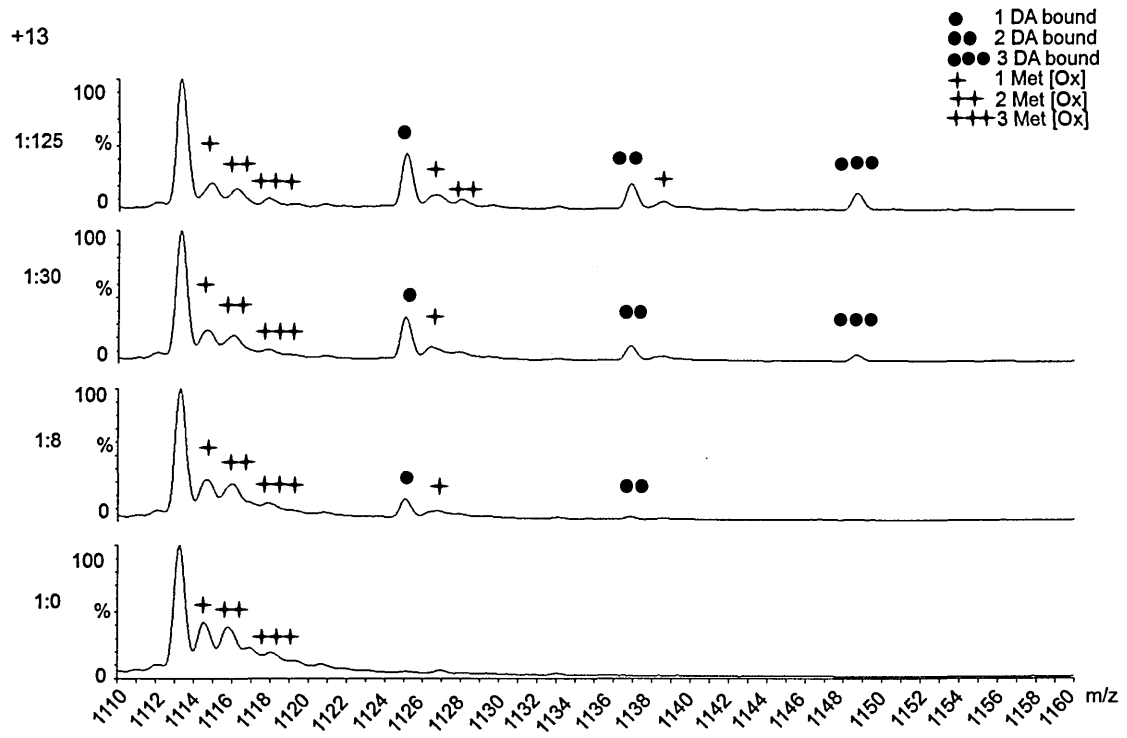

Figure 5.6. *Met oxidised peaks are shown at alternate α-syn to DA ratios (1:125, 1: 30 and 1:8) or at the apo-form of the protein as indicated by black crosses on each mass spectrum. The x axis represents m/z values and the y axis indicates relative intensities in %. The relative intensity of Met oxidised peaks was negligible as compared to the intensity of DA bound adduct peaks (black circles) and apo-forms of α-syn.*

As it is seen in **Figure 5.6.**, low intensity peaks indicative of Met oxidation of the monomeric protein were observed prior to the addition of DA and remained negligible even after binding of DA. Similarly, the intensity of Met oxidised adduct peaks of α-syn-DA were very low as compared to that of un-oxidised DA bound peaks. Hence Met oxidation is not required for DA binding.

5.5 Conclusions

Crucial insights have been gained into how DA might be involved in aggregation and the fibrillisation of a-syn from *in vitro* studies (Conway *et al.* 2001; Cappai *et al.* 2005; Li *et al.* 2005; Jinsmaa *et al.* 2011) and evidence now emerges that polymers of a-syn-DA or other reactive intermediates are linked to neuronal cell death in PD (Outeiro *et al.* 2009). Although the co-ordination of DA to a-syn has been observed before (Shimotakahara *et al.* 2012), here it has been shown that co-ordination of three DA molecules to WT a-syn induced a highly extended conformation specifically binding to the extended states and caused an increase in O. No binding of DA was observed under the employed conditions to the compact states. This concept of expansion is not dissimilar from that which Rekas *et al.* have reported, however, the experimental conditions, buffer conditions and protein concentration used by Rekas *et al.* (Rekas *et al.* 2010) were different. In that study, a-syn was incubated for 5 to 7 days in the presence of DA after which the protein was observed to be oxidised. The resulting Met oxidised a-syn monomer and a-syn-DA trimer had elongated shapes versus untreated monomers based on SAXS and CD results which could be brought about by the association of the DA bound extended states observed here prior to incubation. Met oxidation has been observed to be required for DA induced oligomerisation (Leong *et al.* 2009a; Leong *et al.* 2009b). Utilising short time frames, only low intensity Met oxidised DA bound peaks of a-syn have been observed which were seen beside the more pronounced, un-oxidised higher intensity DA-bound peaks and ligand-free peaks. Minor Met oxidation was present without any prior addition of ligand and hence it did not result from DA

exposure. By contrast, longer incubations of α–syn in the presence of DA (12 hr) have been previously shown to result in a pronounced oxidation of the monomeric protein (**Appendix Figure 8.14.**) similarly to other studies (Chan *et al.* 2012). Regardless of this observation, during the time frame of the experiments discussed here the un-oxidised α-syn-DA complex was considerably more dominant, demonstrating oxidation is not required for initial binding and further oxidation is a result of longer term exposure to DA.

Alternate ligands have been reported to bind to α-syn, each affecting the conformational state of the monomer in its own way. Electrospray Ionisation-Electron Capture Dissociation- Mass Spectrometry/ Mass Spectrometry (ESI-ECD-MS/MS) has been used in probing non-covalent protein-ligand binding interactions in relation to α-syn. Spermine is a polyamine compound widely found in many tissues and has a role in increasing the aggregation rate of α-syn (Antony *et al.* 2003). The spermine binding site has been localised to the C-terminal 106-138 residues of the WT α-syn, as demonstrated by Xie *et al.* (Xie *et al.* 2006) using ESI-ECD-MS/MS consistent with previous NMR data (Fernandez *et al.* 2004). Changes in the charge state distribution were however not observed in this study. The DA binding site of α-syn is also located on the highly negatively charged C-terminal region of the protein, at ^{125}YEMPS^{129} that has been implicated in DA interactions and in modulation of DA induced aggregation (Norris *et al.* 2005). This region however has been reported to be necessary only for oxidation but not complete binding (Leong *et al.* 2009b). Interestingly and similarly to the DA binding results here, data presented in the Supplementary Information of the paper by Xie *et al.* showed the 1:2 protein-ligand complex binding only to the high charge state ions (+18 to +11 charge

state ions) (Xie *et al.* 2006). ESI-IMS-MS has also been used to gain conformational information for the familial point mutation of α-syn A53T upon spermine binding. Evidence from NMR data suggested that although spermine binds specifically to the C-terminal of the α-syn, it induces changes in the N-terminal in the proximity of Gly and Tyr residues in the region of amino acids 22-93 and it leads to the adoption of a β-sheet conformation typical of fibrillar α-syn (Fernandez *et al.* 2004). Spectra acquired in negative ion mode by Grabenauer *et al.* reported a significantly greater percentage of the population of the spermine:protein complex in the compact form as compared to the unbound protein. Either the presence of the A30P point mutation may be involved in the binding on spermine through long range interactions and or its inclusion facilitates aggregation through preferential population of the compact state.

Here, the shift in the population towards a more extended state on DA binding may well be the point at which the aggregation pathway is switched from the amyloid forming pathway linked to the collapsed state (Uversky *et al.* 2001; Uversky *et al.* 2001b; Natalello *et al.* 2011) to the pathway resulting in soluble DA induced oligomers. DA first binds to extended conformations of the protein, followed by oxidation of Met residues (Leong *et al.* 2009a, Leong *et al.* 2009b) resulting in oligomer formation. Previous SAXS data has demonstrated that DA induced α-syn oligomers on extended incubation have highly expanded conformations (Rekas *et al.* 2010) and these structures may well result from the stabilisation of a highly extended monomeric state. DA is therefore a potent modulator of α-syn assembly and exerts its effect at the very early stages of aggregation by influencing the conformational dynamics of the monomeric protein.

6 Chapter 6

Main conclusions

6.1 Background to the investigations

a-syn instigates both sporadic and idiopathic PD by various modes of action (Lashuel *et al.* 2013). It is the major component of intracellular LBs and Lewy neurites in the brain (Forno 1996) that are characteristic features of PD. Both *in vivo* and *in vitro* a-syn forms soluble toxic oligomers and larger fibrils with typical amyloid properties (Conway *et al.* 2000; Kim *et al.* 2009).

Growing evidence suggests that soluble oligomeric forms of a-syn are causative triggers of neurodegeneration with dopaminergic cell loss (Kalia *et al.* 2013). A number of recent reports have described the appearance and detection of the monomeric and soluble oligomeric forms of a-syn in the CSF and sera of PD patients (El-Agnaf *et al.* 2006; Tokuda *et al.* 2010; Foulds *et al.* 2012; Toledo *et al.* 2013). Data obtained from numerous *in vitro* a-syn oligomer studies have implicated relevant toxic gain of function in the disease state *via* two main pathways: i, causing Ca(II) imbalances and ii, inducing transmembrane seeding (Lashuel *et al.* 2013). a-syn pathology has been shown to spread from cell to cell in both cell culture models and *in vivo* models of PD (Prusiner 2012). As such, concentrated efforts have been made to elucidate the seeding properties of exogenously applied a-syn and its alternate forms in primary and secondary cell culture models (Luk *et al.* 2009; Angot *et al.* 2012; Cremades *et al.* 2012; Danzer *et al.* 2012). The morphology and associated toxicity displayed by these

alternate types of *in vitro* oligomers are largely dependent on the environmental conditions under which they have been prepared from the natively unstructured monomeric protein (Danzer *et al.* 2007; Giehm *et al.* 2011; Wang *et al.* 2010b; Nasstrom *et al.* 2011; van Rooijen *et al.* 2010; Cremades *et al.* 2012; Singh *et al.* 2013; Roostaee *et al.* 2013). Structural characterisation of these assemblies by the use of high resolution biophysical methods i.e. NMR spectroscopy and CD remains however challenging due to their low concentrations and transient nature in solution.

ESI-IMS-MS addresses these issues by providing information about the mass, the shape of oligomeric assemblies in a rapid time frame using submolar concentrations (Ashcroft 2010). Ion mobility meaurements accompanied by molecular modelling permit assignment of possible geometries for unknown protein complexes giving insights into the topology of self-assemblies (Ruotolo *et al.* 2008; Politis *et al.* 2010).

In this thesis, a previously reported group of *in vitro*, toxic, transient, oligomeric forms of α-syn have been adapted and their different biochemical characteristics have been further examined (Danzer *et al.* 2007; Danzer *et al.* 2009). The main aim of this project was to determine the structure and subunit size of this selected group of α-syn oligomers, and correlate those with their toxic gain of function, in order to obtain a fuller understanding of structure and function relationships.

6.2 Advancements in understanding oligomeric structure and function

6.2.1 a-syn shows two main conformational familes under equilibrium

In preparation of elucidating the subunit size and topology of oligomers, it was of critical importance to establish optimised acquisition settings for both detection and sensitivity by ESI-IMS-MS. Qs consistent with values published in the literature (Smith *et al.* 2009) were obtained through a wide mass range using common protein standards both under denaturing and native conditions. Conformational families of a-syn from pure and non-degraded recombinant protein were resolved consistent with other studies (Bernstein *et al.* 2004; Grabenauer *et al.* 2008) upon successive ESI-IMS-MS measurements, a-syn co-populated both a family of extended structures and a family of compact structures under equilibrium at neutral pH, showing a good agreement with previous negative mode ESI-MS or ESI-IMS-MS measurements (Bernstein *et al.* 2004; Grabenauer *et al.* 2008; Frimpong *etal.* 2010).

6.2.2 DA selectively binds to the extended populations of monomeric a-syn and causes a conformational shift towards an expanded conformational state

In the presence of DA a-syn yields a diverse range of SDS resistant, non-amyloid oligomers (Conway *et al.* 2001; Cappai *et al.* 2005; Li *et al.* 2005; Lee *et al.* 2011), however the precursor state conformation has not been established. Previously, three DA molecules have been observed to bind per a-syn monomer using ESI-MS (Shimotakahara *et al.* 2012). In accord with this, a

alternate types of *in vitro* oligomers are largely dependent on the environmental conditions under which they have been prepared from the natively unstructured monomeric protein (Danzer *et al.* 2007; Giehm *et al.* 2011; Wang *et al.* 2010b; Nasstrom *et al.* 2011; van Rooijen *et al.* 2010; Cremades *et al.* 2012; Singh *et al.* 2013; Roostaee *et al.* 2013). Structural characterisation of these assemblies by the use of high resolution biophysical methods i.e. NMR spectroscopy and CD remains however challenging due to their low concentrations and transient nature in solution.

ESI-IMS-MS addresses these issues by providing information about the mass, the shape of oligomeric assemblies in a rapid time frame using submolar concentrations (Ashcroft 2010). Ion mobility meaurements accompanied by molecular modelling permit assignment of possible geometries for unknown protein complexes giving insights into the topology of self-assemblies (Ruotolo *et al.* 2008; Politis *et al.* 2010).

In this thesis, a previously reported group of *in vitro*, toxic, transient, oligomeric forms of α-syn have been adapted and their different biochemical characteristics have been further examined (Danzer *et al.* 2007; Danzer *et al.* 2009). The main aim of this project was to determine the structure and subunit size of this selected group of α-syn oligomers, and correlate those with their toxic gain of function, in order to obtain a fuller understanding of structure and function relationships.

6.2 Advancements in understanding oligomeric structure and function

6.2.1 a-syn shows two main conformational familes under equilibrium

In preparation of elucidating the subunit size and topology of oligomers, it was of critical importance to establish optimised acquisition settings for both detection and sensitivity by ESI-IMS-MS. Os consistent with values published in the literature (Smith *et al.* 2009) were obtained through a wide mass range using common protein standards both under denaturing and native conditions. Conformational families of a-syn from pure and non-degraded recombinant protein were resolved consistent with other studies (Bernstein *et al.* 2004; Grabenauer *et al.* 2008) upon successive ESI-IMS-MS measurements, a-syn co-populated both a family of extended structures and a family of compact structures under equilibrium at neutral pH, showing a good agreement with previous negative mode ESI-MS or ESI-IMS-MS measurements (Bernstein *et al.* 2004; Grabenauer *et al.* 2008; Frimpong *et al.* 2010).

6.2.2 DA selectively binds to the extended populations of monomeric a-syn and causes a conformational shift towards an expanded conformational state

In the presence of DA a-syn yields a diverse range of SDS resistant, non-amyloid oligomers (Conway *et al.* 2001; Cappai *et al.* 2005; Li *et al.* 2005; Lee *et al.* 2011), however the precursor state conformation has not been established. Previously, three DA molecules have been observed to bind per a-syn monomer using ESI-MS (Shimotakahara *et al.* 2012). In accord with this, a

maximum of three DA molecules formed adducts with α-syn but the additional dimension of ion mobility separation has allowed demonstration of DA molecules bound exclusively to the extended conformation of α-syn only. Binding was not observed to the compact state of the protein such as the +7 charge state ion. Measurements of Ω areas showed that the incremental uptake of the DA pushed the protein towards a highly extended population, becoming fully populated upon the binding of three DA ligands that was illustrated at the +13 charge state here. The primary binding site for DA has been assigned to residues ^{125}YEMPS^{129} (Norris *et al.* 2005) on the C-terminal of the protein. It would be intriguing to ascertain exactly to which motif of α-syn each of the three DA molecules can bind to through repeating similar experiments with truncation mutants of the protein.

Tyr as a closely related structural analogue differing only by a carboxyl group in its chemical structure exhibited limited binding to the protein as compared to DA, with a maximum of two ligands being observed to co-ordinate to α-syn. An expansion upon DA or Tyr binding to α-syn has shown another example of how α-syn is capable of undergoing different types of structural transitions under alternate conditions. The conformational rearrangement conferred by DA or Tyr occurred in the opposite way to that described as a structural collapse during ligation of Cu(II) to α-syn discussed in the next section. Calculation of Ωs suggested that DA was able to modulate α-syn self-assembly by inducing the population of a highly extended state, consistently across various protein to ligand ratios.

6.2.3 Cu(II) binds to monomeric a-syn and causes a conformational collapse towards a more compact state

The conformational equilibrium of a-syn between the compact and extended states can be modulated by altering the protein environment, for example by the addition of bi- and trivalent metal cations. To determine the effects of metals on the conformations of a-syn, especially Fe(III) due to its inclusion in the oligomerisation protocol, ESI-IMS-MS experiments were carried out at three alternate protein to metal molar ratios in AA at neutral pH. Experiments were also conducted in the presence or absence of Cu(II), Zn(II), Mn(II), Co(II), Fe(II), and Al(III). No immediate binding was observed for any of these metal ions, except Cu(II). Despite of the fact that no direct binding was detectable with these metals apart from Cu(II), they are thought to have a role in altering the fibrillisation of a-syn *in vitro* and their binding sites have been mapped out (Bisaglia *et al.* 2009). Binding of one or two Cu(II) was observed to a-syn at all charge states of the monomeric protein. These adducts remained preserved even upon addition of Gly that acts as a metal chelator preventing non-specific binding. This high affinity binding correlated with a conformational transition towards a more compact conformational form and may indicate an increased aggregation in the presence of Cu(II). These data may help to understand how a-syn reacts with Cu(II) in the aging brain and is promoted to misfold into a more compact conformational form that can assemble into soluble oligomers and fibrillar forms. Evidence into the toxic aspects of Cu(II) derived a-syn has been emerging from a number of *in vitro* studies (Brown 2007; Paik *et al.* 1999; Gaggelli *et al.* 2006; Drew *et al.* 2008; Dudzik *et al.* 2011; Lucas *et al.* 2011).

Elucidation of the the dynamics of Cu(II) co-ordination to a-syn will continue to be invaluable in understanding how an increase of metal load (Pall *et al.* 1987) upon environmental exposure or age related changes may lead to predisposing this protein in an altered milieu to self-assemble into toxic species (Paik *et al.* 1999). In addition, oxidative stress is an important element of redox-metal induced neurotoxicity associated with amyloidogenic proteins and peptides. As such, Ap and a-syn can directly bind metal ions such as Cu(II) and the resultant complexes have been shown to give rise to H20 2by reacting with ascorbic acid and 0 2in a cellular environment. H20 2is a powerful ROS and is a precursor of other free radicals. Uncomplexed, free redox metal ions can also produce hydroxyl radicals (OH*) by reacting with H20 2wathe Harber-Weiss and Fenton reactions. Thus, a-syn-Cu(II) complexes are thought to be responsible for oxidative damage, contributing to the loss of dopaminergic cells in PD (Wang *et al.* 2010a).

6.2.4 *In vitro* a-syn oligomers suitable for ion mobility mass spectrometry analysis have functional properties

To produce a-syn oligomers suitable for ESI-IMS-MS analysis, previously described oligomer preparation protocols have been adapted such that SP was substituted by AA buffer. Evidence has shown that alterations both in buffer conditions and ionic strength affect the way in which natively unstructured proteins such as a-syn fold (Kriz *et al.* 2013; Buell *et al.* 2013). In order to examine the changes caused by altering the buffer conditions from 50 mM SP to 50 mM AA, a range of *in vitro* functional assays have been performed such

as fibril formation experiments, spectroscopic measurements, dot blotting, MTT, Ca(II) influx, ROS assay and transmembrane seeding. Findings from these assays were compared to the original subset of oligomers as discussed in detail in Chapter 3 and summerised in 6.2.7-10.

6.2.5 Di- and trivalent metal ions influence the assembly of a-syn oligomers

Insights into the assembly of a-syn have been gained from alteration of conditions during the preparation protocols such as inclusion of $FeCl_3$. Addition of Fe(III) may have accelerated the self-assembly and at the time of sampling the mass range of oligomers was not accessible by the Synapt G2 HDMS and only a subpopulation of monomers, dimers, trimers could be seen in type C2 AA oligomers. By contast, ion mobility data collected from type A2 AA oligomers prepared in the presence of Fe(III) did not deviate from that of Fe(III)-free type A1 AA oligomers. These discrepancies could be resolved by monitoring of assembly over frequent time intervals during the overnight incubation to better discern the role of Fe(III) in oligomerisation.

When Fe(III) was replaced by Cu(II), monomers to tetramers were detected that could have assembled from Cu(II)-bound a-syn, which unambiguously retained its Cu(II) adducts throughout the entire incubation protocols (either overnight or >7 days). It would be interesting to uncover how these oligomers stalled at a tetrameric subunit size could compare in their functional properties to those discussed in section 6.2.7-9.

6.2.6 Alteration in buffer conditions affect the kinetics of oligomerisation

When the ionic strength of AA was incresead, to examine the effect on oligomerisation, it was observed that the more compact conformational ion series of the monomeric protein became more predominant early on at 4 hr into oligomerisation. In addition, a broader range of trimers and tetramers were early present at 250 mM and 450 mM AA concentrations as opposed to 50 mM AA concentration. These data suggest that higher ionic strength promotes the formation of lower order oligomeric species and increases the relative population of the compact conformational forms of the monomeric protein. The importance of salt ions and ionic strength with regards to other amyloidogenic systems has gained attention (Klement *et al.* 2007; Marek *et al.* 2012; Kriz *et al.* 2013; Buell *et al.* 2013). For example, molecular dynamics simulations of rat and human p-amyloids in three alternate salt environments have been carried out and implied that ionic strength affected the stability of internal hydrogen bonds. Increment in ionic strength raised atomic fluctuations in the hydrophobic core of the human variant and decreased it in the non-fibrillar rat variant. Changes in flexibilities subsequently may promote formation of helices or p-sheet elements (Kriz *et al.* 2013).

6.2.7 Mass spectrometry compatible oligomers have distinguishable epitope mapping profiles and transmembrane seeding properties

Mass spectrometry compatible *in vitro* a-syn oligomers appeared to have unique, distinguishable properties as demonstrated by epitope mapping and recapitulated toxic aspects of previously reported transmembrane seeding in

human neuroblastoma cells (Danzer *et al.* 2007; Danzer *et al.* 2009). Ca(II) imbalances induced by the mass spectrometry compatible type A1, A2, C1, C2 AA oligomers were not detectable in contrast to the results seen with type A1 and A2 SP oligomers.

6.2.8 Mass spectrometry compatible type A oligomers are toxic; lower order oligomers may be associated with cytotoxicity in SH-SY5Y neuroblastoma cells

Ion mobility mass spectrometry experiments indicated a range of oligomeric species, consisting of dimers to hexamers for type A1 and A2 AA oligomers with increasing compactness proportional to subunit size. These data in conjunction with findings of the MTT assay suggested that neuronal toxicity correlated with the presence of smaller order oligomers within the ensemble. In agreement with this, dimers of a-syn produced in a different manner have been shown to be toxic and critical in the early phase of aggregation and could be worthwhile targets of therapeutic agents (Roostaee *et al.* 2013).

In an alternate oligomeric system, Cremades *et al.* described a population of cross-linked, lower molecular weight yeast Sup35 (NM) oligomers ranging from dimers to trimers that displayed a blue shift upon addition of Nile Red dye, reacted with A11 and were very toxic in neuroblastoma cells (Cremades *et al.* 2012). In addition, Ono *et al.* reported that dimers were -3 times more toxic than the monomeric A(3 protein and tetramers -13 times more toxic than the monomer itself. It is proposed in this study that it would be logical to design

therapeutic interventions targeting dimers or develop agents that could stabilise the monomeric disordered state to prevent its assembly (Ono *et al.* 2009).

6.2.9 Non-toxic type C oligomers are predominantly pentameric and hexameric and cause intracellular aggregation in SH-SY5Y neuroblastoma cells

Type C1 AA oligomers displayed pentamers and hexamers and less tightly packed tetramers with Os comparable to type A1 and A2 AA oligomers. These oligomers were however not toxic to human neuroblastoma cells. The lack of toxicity was perphaps due to the scarcity of monomeric, dimeric and trimeric series as compared to type A1 and A2 AA oligomers in which the lower order oligomers were more intense. The observed differences in enrichment of particular subsets were most likely due to alternate preparation protocols tipping the balance between lower order and higher order species. Type C2 AA oligomers displayed only lower order oligomers up to largely unstructured trimers, however this data may not reflect solution conditions as data acquisition was limited by an exacerbated aggregation in the sample perturbing the electrospray process. All mass spectrometry compatible oligomers induced intracellular aggregation in SH-SY5Y cells post-exposure to oligomeric treatment. The ability to induce intracellular aggregation may be attributable to the higher order e.g. tetrameric, pentameric and hexameric populations.

6.2.10 Assembly of *in vitro* a-syn oligomers progresses in an isotropic fashion up to a ring-like hexameric structure

Oligomers assigned here followed an isotropic growth where each series differed by one subunit size from the next up to hexameric stage being the most compact molecular organisation. Experimentally determined Os alongside with molecular modelling (Smith *et al.* 2009) suggested that the smaller oligomeric species (dimer, trimer and tetramer) were unordered structures that became gradually more akin to fully compact, globular shapes as they increased in subunit size. Pentameric assemblies are consistent with an open ring-like topology and the most compact hexamers represent the end point of assembly with a closed ring-like morphology. The energetics and complexity governing of aggregation at the early stages of oligomerisation have been illustrated by recent molecular modelling experiments, showing that each aggregated form of dimers, trimers and tetramers could have a number of different morphologies (Gurry *et al.* 2013) akin to the dispersed Os observed here. These closed ring conformations are similar to those observed by the Bowers group for the Ap peptide and may represent a common oligomeric architecture (Bernstein *et al.* 2009). It would be highly desirable to obtain more comprehensive information about a-syn oligomers that have been successfully detected in the CSF and sera of PD patients (El-Agnaf *et al.* 2006; Foulds *et al.* 2011; Foulds *et al.* 2012). The challenge will remain to isolate oligomers from clinical specimens of PD patients or other living systems under near native conditions (Bartels *et al.* 2011; Fauvet *et al.* 2012) and elucidate how the oligomers produced *in vitro* would compare to those. Further structural and functional characterisation of *in*

vitro α-syn oligomers however may inform finding points of interaction against self-assembly into toxic α-syn oligomers that occur in the disease state.

7 References

ABRAMOV, A.Y. and DUCHEN, M.R., 2003. Actions of ionomycin, 4-BrA23187 and a novel electrogenic Ca2+ ionophore on mitochondria in intact cells. *Cell Calcium*, 33, 101-112

AHN, B.H., RHIM, H., KIM, S.Y., SUNG, Y.M., LEE, M.Y., CHOI, J.Y., WOLOZIN, B., CHANG, J.S., LEE, Y.H., KWON, T.K., CHUNG, K.C., YOON, S.H., HAHN, S.J., KIM, M.S., JO, Y.H. and MIN, D.S., 2002. Alpha-synuclein interacts with phospholipase D isozymes and inhibits pervanadate-induced phospholipase D activation in human embryonic kidney-293 cells. *The Journal of Biological Chemistry*, 277, 12334-12342

AIDT, F.H., HASHOLT, L.F., CHRISTIANSEN, M. and LAURSEN, H., 2013. Localization of A11-reactive oligomeric species in prion diseases. *Histopathology*, 62, 994-1001

ALLSOP, D., 2000. Introduction to Alzheimer's disease. *Methods in Molecular Medicine*, 32, 1-21

ANDREU, J.M. and TIMASHEFF, S.N., 1986. The measurement of cooperative protein self-assembly by turbidity and other techniques. *Methods in Enzymology*, 130, 47-59

ANGOT, E., STEINER, J.A., HANSEN, C., LI, J.Y. and BRUNDIN, P., 2010. Are synucleinopathies prion-like disorders?. *Lancet Neurology*, 9, 1128-1138

ANGOT, E., STEINER, J.A., LEMA TOME, C.M., EKSTROM, P., MATTSSON, B., BJORKLUND, A. and BRUNDIN, P., 2012. Alpha-synuclein cell-to-cell transfer and seeding in grafted dopaminergic neurons in vivo. *PloS One*, 7, e39465

ANTONY, T., HOYER, W., CHERNY, D., HEIM, G., JOVIN, T.M. and SUBRAMANIAM, V., 2003. Cellular polyamines promote the aggregation of alpha-synuclein. *The Journal of Biological Chemistry*, 278, 3235-3240

APPEL-CRESSWELL, S., VILARINO-GUELL, C., ENCARNACION, M., SHERMAN, H., YU, I., SHAH, B., WEIR, B., THOMPSON, C., SZU-TU, C., TRINH, J, AASLY, J.O., RAJPUT, A., RAJPUT, A. H., STOESSL, A. J. and FARRER, M. J., 2013. *Movement Disorders*, 28, 811-813

ASHCROFT, A.E., 2010. Mass spectrometry and the amyloid problem-how far can we go in the gas phase?. *Journal of the American Society for Mass Spectrometry*, 21, 1087-1096

BARTELS, T., CHOI, J.G. and SELKOE, D.J., 2011. Alpha-synuclein occurs physiologically as a helically folded tetramer that resists aggregation. *Nature*, 477, 107-110

BATE, C., GENTLEMAN, S. and WILLIAMS, A., 2010. Alpha-Synuclein Induced Synapse Damage is Enhanced by Amyloid-Beta1-42. *Molecular Neurodegeneration*, 5, 55

BEARDSLEY, R.L., JONES, C.M., GALHENA, A.S. and WYSOCKI, V.H., 2009. Noncovalent protein tetramers and pentamers with "n" charges yield monomers with n/4 and n/5 charges. *Analytical Chemistry*, 81, 1347-1356

BENESCH, J.L., SOBOTT, F. and ROBINSON, C.V., 2003. Thermal dissociation of multimeric protein complexes by using nanoelectrospray mass spectrometry. *Analytical Chemistry*, 75, 2208-2214

BERNSTEIN, S.L., DUPUIS, N.F., LAZO, N.D., WYTTENBACH, T., CONDRON, M.M., BITAN, G., TEPLOW, D.B., SHEA, J.E., RUOTOLO, B.T., ROBINSON, C.V. and BOWERS, M.T., 2009. Amyloid-beta protein oligomerization and the importance of tetramers and dodecamers in the aetiology of Alzheimer's disease. *Nature Chemistry*, 1, 326-331

BERNSTEIN, S.L., LIU, D., WYTTENBACH, T., BOWERS, M.T., LEE, J.C., GRAY, H.B. and WINKLER, J.R., 2004. Alpha-synuclein: stable compact and extended monomeric structures and pH dependence of dimer formation. *Journal of the American Society for Mass Spectrometry*, 15, 1435-1443

BEVERIDGE, R., CHAPPUIS, Q., MACPHEE, C. and BARRAN, P., 2013. Mass spectrometry methods for intrinsically disordered proteins. *The Analyst*, 138, 32-42

BEYER, K. and ARIZA, A., 2013. Alpha-synuclein posttranslational modification and alternative splicing as a trigger for neurodegeneration. *Molecular Neurobiology*, 47, 509-524

BIANCALANA, M. and KOIDE, S., 2010. Molecular mechanism of Thioflavin-T binding to amyloid fibrils. *Biochimica Et Biophysica Acta*, 1804, 1405-1412

BINOLFI, A., LAMBERTO, G.R., DURAN, R., QUINTANAR, L., BERTONCINI, C.W., SOUZA, J.M., CERVENANSKY, C., ZWECKSTETTER, M., GRIESINGER, C. and FERNANDEZ, C.O., 2008. Site-specific interactions of Cu(II) with alpha and beta-synuclein: bridging the molecular gap between metal binding and aggregation. *Journal of the American Chemical Society*, 130, 11801-11812

BINOLFI, A., RASIA, R.M., BERTONCINI, C.W., CEOLIN, M., ZWECKSTETTER, M., GRIESINGER, C., JOVIN, T.M. and FERNANDEZ, C.O., 2006. Interaction of alpha-synuclein with divalent metal ions reveals key

differences: a link between structure, binding specificity and fibrillation enhancement. *Journal of the American Chemical Society,* 128, 9893-9901

BINOLFI, A., RODRIGUEZ, E.E., VALENSIN, D., D'AMELIO, N., IPPOLITI, E., OBAL, G., DURAN, R„ MAGISTRATO, A., PRITSCH, O., ZWECKSTETTER, M., VALENSIN, G., CARLONI, P., QUINTANAR, L., GRIESINGER, C. and FERNANDEZ, C.O., 2010. Bioinorganic chemistry of Parkinson's disease: structural determinants for the copper-mediated amyloid formation of alpha-synuclein. *Inorganic Chemistry,* 49, 10668-10679

BISAGLIA, M., TESSARI, I., MAMMI, S. and BUBACCO, L., 2009. Interaction between alpha-synuclein and metal ions, still looking for a role in the pathogenesis of Parkinson's disease. *Neuromolecular Medicine,* 11, 239-251

BITO, H., DEISSEROTH, K. and TSIEN, R.W., 1996. CREB phosphorylation and dephosphorylation: a Ca(2+)- and stimulus duration-dependent switch for hippocampal gene expression. *Cell,* 87, 1203-1214

BLEIHOLDER, C., DUPUIS, N.F., WYTTENBACH, T. and BOWERS, M.T., 2011. Ion mobility-mass spectrometry reveals a conformational conversion from random assembly to beta-sheet in amyloid fibril formation. *Nature Chemistry,* 3, 172-177

BOLOGNESI, B„ KUMITA,J.R., BARROS, T.P., ESBJORNER, E.K., LUHESHI, L.M., CROWTHER, D.C., WILSON, M.R., DOBSON, C.M., FAVRIN, G. and YERBURY, J.J., 2010. ANS binding reveals common features of cytotoxic amyloid species. *ACS Chemical Biology,* 5, 735-740

BRAAK, H., DEL TREDICI, K., RUB, U., DE VOS, R.A., JANSEN STEUR, E.N. and BRAAK, E., 2003. Staging of brain pathology related to sporadic Parkinson's disease. *Neurobiology of Aging,* 24, 197-211

BROWN, D.R., 2007. Interactions between metals and alpha-synuclein-function or artefact?. *The FEBS Journal,* 274, 3766-3774

BUELL, A.K., HUNG, P., SALVATELLA, X., WELLAND, M.E., DOBSON, C.M. and KNOWLES, T.P., 2013. Electrostatic effects infilamentous protein aggregation. *Biophysical Journal,* 104, 1116-1126

BURRE, J., SHARMA, M., TSETSENIS, T., BUCHMAN, V., ETHERTON, M.R. and SUDHOF, T.C., 2010. Alpha-synuclein promotes SNARE-complex assembly in vivo and in vitro. *Science,* 329, 1663-1667

Bush, M.F., University ofWashington, Cross Section Database, http://depts.washington.edu/bushlab/ccsdatabase/.

BUSH, M.F., HALL, Z., GILES, K., HOYES, J., ROBINSON, C.V. and RUOTOLO, B.T., 2010. Collision cross sections of proteins and their

complexes: a calibration framework and database for gas-phase structural biology. *Analytical Chemistry*, 82, 9557-9565

CAMILLERI, A., ZARB, C., CARUANA, M., OSTERMEIER, U., GHIO, S., HOGEN, T., SCHMIDT, F., GIESE, A. and VASSALLO, N., 2013. Mitochondrial membrane permeabilisation by amyloid aggregates and protection by polyphenols. *Biochimica Et Biophysica Acta*, 1828, 2532-2543

CAMPIONI, S., MANNINI, B., ZAMPAGNI, M., PENSALFINI, A., PARRINI, C., EVANGELISTI, E., RELINI, A., STEFANI, M., DOBSON, C.M., CECCHI, C. and CHITI, F., 2010. A causative link between the structure of aberrant protein oligomers and their toxicity. *Nature Chemical Biology*, 6, 140-147

CAPPAI, R., LECK, S.L., TEW, D.J., WILLIAMSON, N.A., SMITH, D.P., GALATIS, D., SHARPLES, R.A., CURTAIN, C.C., ALI, F.E., CHERNY, R.A., CULVENOR, J.G., BOTTOMLEY, S.P., MASTERS, C.L., BARNHAM, K.J. and HILL, A.F., 2005. Dopamine promotes alpha-synuclein aggregation into SDS-resistant soluble oligomers via a distinct folding pathway. *FASEB Journal : Official Publication of the Federation of American Societies for Experimental Biology*, 19, 1377-1379

CASTELLANI, R.J., SIEDLAK, S.L., PERRY, G. and SMITH, M.A., 2000. Sequestration of iron by Lewy bodies in Parkinson's disease. *Acta Neuropathologica*, 100, 111-114

CHADCHANKAR, H., IHALAINEN, J., TANILA, H. and YAVICH, L., 2011. Decreased reuptake of dopamine in the dorsal striatum in the absence of alpha-synuclein. *Brain Research*, 1382, 37-44

CHAI, Y.J., KIM, D., PARK, J., ZHAO, H., LEE, S.J. and CHANG, S., 2013. The secreted oligomeric form of alpha-synuclein affects multiple steps of membrane trafficking. *FEBS Letters*, 587, 452-459

CHAN, T., CHOW A., M., CHENG, X., R., Tang, D., W., F., BROWN I., R. and KERMAN, K., 2012. Oxidative Stress Effect of Dopamine on Alpha-synuclein: Electroanalysis of Solvent Interactions. *ACS Chem. Neurosci.*, 3, 569-574.

CHANDRA, S., GALLARDO, G., FERNANDEZ-CHACON, R., SCHLUTER, O.M. and SUDHOF, T.C., 2005. Alpha-synuclein cooperates with CSPalpha in preventing neurodegeneration. *Cell*, 123, 383-396

CHARTIER-HARLIN, M.C., KACHERGUS, J., ROUMIER, C., MOUROUX, V., DOUAY, X., LINCOLN, S., LEVECQUE, C., LARVOR, L., ANDRIEUX, J., HULIHAN, M., WAUCQUIER, N., DEFEBVRE, L., AMOUYEL, P., FARRER, M. and DESTEE, A., 2004. Alpha-synuclein locus duplication as a cause of familial Parkinson's disease. *Lancet*, 364, 1167-1169

CHEN, C.H., LIU, T.Z., CHEN, C.H., WONG, C.H., CHEN, C.H., LU, F.J. and CHEN, S.C., 2007. The efficacy of protective effects of tannic acid, gallic acid,

ellagic acid, and propyl gallate against hydrogen peroxide-induced oxidative stress and DNA damages in IMR-90 cells. *Molecular Nutrition & Food Research,* 51, 962-968

CHITI, F. and DOBSON, C.M., 2006. P. *Annual Review of Biochemistry,* 75, 333-366

Clemmer, D. E., Indiana University, Cross Section Database http://www.indiana.edu/~clemmer/Research/Cross_____ Section Database/cs database.php.

CLEMMER, D.E. and JARROLD, M.F., 1997. Ion mobility measurements and their applications to clusters and biomolecules. *J Mass Spectrom,* 32, 577-592.

CLEMMER, D.E. and VALENTINE, S.J., 2009. Bioanalytical chemistry: Protein oligomers frozen in time. *Nature Chemistry,* 1, 257-258

COHLBERG, J.A., LI, J., UVERSKY, V.N. and FINK, A.L., 2002. Heparin and other glycosaminoglycans stimulate the formation of amyloid fibrils from alpha-synuclein in vitro. *Biochemistry,* 41, 1502-1511

COLLA, E., JENSEN, P.H., PLETNIKOVA, O., TRONCOSO, J.C., GLABE, C. and LEE, M.K., 2012. Accumulation of toxic alpha-synuclein oligomer within endoplasmic reticulum occurs in alpha-synucleinopathy in vivo. *The Journal of Neuroscience: The Official Journal of the Society for Neuroscience,* 32, 3301-3305

CONWAY, K.A., HARPER, J.D. and LANSBURY, P.T., 1998. Accelerated in vitro fibril formation by a mutant alpha-synuclein linked to early-onset Parkinson disease. *Nature Medicine, 4,* 1318-1320

CONWAY, K.A., LEE, S.J., ROCHET, J.C., DING, T.T., WILLIAMSON, R.E. and LANSBURY, P.T.,Jr, 2000. Acceleration of oligomerization, not fibrillization, is a shared property of both alpha-synuclein mutations linked to early-onset Parkinson's disease: implications for pathogenesis and therapy. *Proceedings of the National Academy of Sciences of the United States of America,* 97, 571-576

CONWAY, K.A., ROCHET, J.C., BIEGANSKI, R.M. and LANSBURY, P.T.,Jr, 2001. Kinetic stabilization of the alpha-synuclein protofibril by a dopamine-alpha-synuclein adduct. *Science,* 294, 1346-1349

COON, S., STARK, A., PETERSON, E., GLOI, A., KORTSHA, G., POUNDS, J., CHETTLE, D. and GORELL, J., 2006. Whole-body lifetime occupational lead exposure and risk of Parkinson's disease. *Environmental Health Perspectives,* 114, 1872-1876

COVEY, T.R., BONNER, R.F., SHUSHAN, B.I. and HENION, J., 1988. The determination of protein, oligonucleotide and peptide molecular weights by ion-

spray mass spectrometry. *Rapid Communications in Mass Spectrometry: RCM*, 2, 249-256

CREMADES, N., COHEN, S.I., DEAS, E., ABRAMOV, A.Y., CHEN, A.Y., ORTE, A., SANDAL, M., CLARKE, R.W., DUNNE, P., APRILE, F.A., BERTONCINI, C.W., WOOD, N.W., KNOWLES, T.P., DOBSON, C.M. and KLENERMAN, D., 2012. Direct observation of the interconversion of normal and toxic forms of alpha-synuclein. *Cell*, 149, 1048-1059

DANZER, K.M., HAASEN, D., KAROW, A.R., MOUSSAUD, S., HABECK, M., GIESE, A., KRETZSCHMAR, H., HENGERER, B. and KOSTKA, M., 2007. Different species of alpha-synuclein oligomers induce calcium influx and seeding. *The Journal of Neuroscience : The Official Journal of the Society for Neuroscience*, 27, 9220-9232

DANZER, K.M., KRANICH, L.R., RUF, W.P., CAGSAL-GETKIN, O., WINSLOW, A.R., ZHU, L., VANDERBURG, C.R. and MCLEAN, P.J., 2012. Exosomal cell-to-cell transmission of alpha synuclein oligomers. *Molecular Neurodegeneration*, 7, 42

DANZER, K.M., KREBS, S.K., WOLFF, M., BIRK, G. and HENGERER, B., 2009. Seeding induced by alpha-synuclein oligomers provides evidence for spreading of alpha-synuclein pathology. *Journal of Neurochemistry*, 20090804, 111, 192-203

DAVIDSON, W.S., JONAS, A., CLAYTON, D.F. and GEORGE, J.M., 1998. Stabilization of alpha-synuclein secondary structure upon binding to synthetic membranes. *The Journal of Biological Chemistry*, 273, 9443-9449

de la Mora, J., F., 2000. Electrospray ionization of large multiply charged species proceeds via Dole's charged residue mechanism. *Anal. Chim. Acta*, 406, 93-104.

DE LAU, L.M. and BRETELER, M.M., 2006. Epidemiology of Parkinson's disease. *Lancet Neurology*, 5, 525-535

DEMURO, A., MINA, E., KAYED, R., MILTON, S.C., PARKER, I. and GLABE, C.G., 2005. Calcium dysregulation and membrane disruption as a ubiquitous neurotoxic mechanism of soluble amyloid oligomers. *The Journal of Biological Chemistry*, 280, 17294-17300

DENG, L., BROOM, A., KITOVA, E.N., RICHARDS, M.R., ZHENG, R.B., SHOEMAKER, G.K., MEIERING, E.M. and KLASSEN, J.S., 2012. Kinetic Stability of the Streptavidin-Biotin Interaction Enhanced in the Gas Phase. *Journal of the American Chemical Society*, 134, 16586-16596

DESPLATS, P., LEE, H.J., BAE, E.J., PATRICK, C., ROCKENSTEIN, E., CREWS, L., SPENCER, B., MASLIAH, E. and LEE, S.J., 2009. Inclusion formation and neuronal cell death through neuron-to-neuron transmission of

alpha-synuclein. *Proceedings of the National Academy of Sciences of the United States of America*, 106, 13010-13015

DETTMER, U., NEWMAN, A.J., LUTH, E.S., BARTELS, T. and SELKOE, D., 2013. In Vivo Cross-linking Reveals Principally Oligomeric Forms of alpha-Synuclein and beta-Synuclein in Neurons and Non-neural Cells. *The Journal of Biological Chemistry*, 288, 6371-6385

DEVINE, M.J., GWINN, K., SINGLETON, A. and HARDY, J., 2011. Parkinson's disease and alpha-synuclein expression. *Movement Disorders : Official Journal of the Movement Disorder Society*, 26, 2160-2168

DEXTER, D.T., WELLS, F.R., LEES, A.J., AGID, F., AGID, Y., JENNER, P. and MARSDEN, C.D., 1989. Increased nigral iron content and alterations in other metal ions occurring in brain in Parkinson's disease. *Journal of Neurochemistry*, 52, 1830-1836

DING, T.T., LEE, S.J., ROCHET, J.C. and LANSBURY, P.T.,Jr, 2002. Annular alpha-synuclein protofibrils are produced when spherical protofibrils are incubated in solution or bound to brain-derived membranes. *Biochemistry*, 13, 41, 10209-10217

DOBO, A. and KALTASHOV, I.A., 2001. Detection of multiple protein conformational ensembles in solution via deconvolution of charge-state distributions in ESI MS. *Analytical Chemistry*, 73, 4763-4773

DREW, S.C., LEONG, S.L., PHAM, C.L., TEW, D.J., MASTERS, C.L., MILES, L.A., CAPPAI, R. and BARNHAM, K.J., 2008. Cu2+ binding modes of recombinant alpha-synuclein-insights from EPR spectroscopy. *Journal of the American Chemical Society*, 130, 7766-7773

DUDZIK, C.G., WALTER, E.D. and MILLHAUSER, G.L., 2011. Coordination features and affinity of the Cu(2)+ site in the alpha-synuclein protein of Parkinson's disease. *Biochemistry*, 50, 1771-1777

DUPUIS, N.F., WU, C., SHEA, J.E. and BOWERS, M.T., 2009. Human islet amyloid polypeptide monomers form ordered beta-hairpins: a possible direct amyloidogenic precursor. *Journal of the American Chemical Society*, 131, 18283-18292

EGHIAIAN, F., DAUBENFELD, T., QUENET, Y., VAN AUDENHAEGE, M., BOUIN, A.P., VAN DER REST, G., GROSCLAUDE, J. and REZAEI, H., 2007. Diversity in prion protein oligomerization pathways results from domain expansion as revealed by hydrogen/deuterium exchange and disulfide linkage. *Proceedings of the National Academy of Sciences of the United States of America*, 104, 7414-7419

EL-AGNAF, O.M., JAKES, R., CURRAN, M.D., MIDDLETON, D., INGENITO, R., BIANCHI, E., PESSI, A., NEILL, D. and WALLACE, A., 1998. Aggregates

from mutant and wild-type alpha-synuclein proteins and NAC peptide induce apoptotic cell death in human neuroblastoma cells by formation of beta-sheet and amyloid-like filaments. *FEBS Letters*, 440, 71-75

EL-AGNAF, O.M., SALEM, S.A., PALEOLOGOU, K.E., CURRAN, M.D., GIBSON, M.J., COURT, J.A., SCHLOSSMACHER, M.G. and ALLSOP, D., 2006. Detection of oligomeric forms of alpha-synuclein protein in human plasma as a potential biomarker for Parkinson's disease. *FASEB Journal: Official Publication of the Federation of American Societies for Experimental Biology*, Mar, 20, 419-425

EL-HAWIET, A., KITOVA, E.N., ARUTYUNOV, D., SIMPSON, D.J., SZYMANSKI, C.M. and KLASSEN, J.S., 2012a. Quantifying ligand binding to large protein complexes using electrospray ionization mass spectrometry. *Analytical Chemistry*, 84, 3867-3870

EL-HAWIET, A., KITOVA, E.N. and KLASSEN, J.S., 2012b. Quantifying carbohydrate-protein interactions by electrospray ionization mass spectrometry analysis. *Biochemistry*, 51, 4244-4253

ELLER, M. and WILLIAMS, D.R., 2011. alpha-Synuclein in Parkinson disease and other neurodegenerative disorders. *Clinical Chemistry and Laboratory Medicine: CCLM / FESCC*, 49, 403-408

ELLER, M. and WILLIAMS, D.R., 2009. Biological fluid biomarkers in neurodegenerative parkinsonism. *Nature Reviews.Neurology*, 5, 561-570

EMMANOUILIDOU, E., MELACHROINOU, K., ROUMELIOTIS, T., GARBIS, S.D., NTZOUNI, M., MARGARITIS, L.H., STEFANIS, L. and VEKRELLIS, K., 2010a. Cell-produced alpha-synuclein is secreted in a calcium-dependent manner by exosomes and impacts neuronal survival. *The Journal of Neuroscience: The Official Journal of the Society for Neuroscience*, 30, 6838-6851

EMMANOUILIDOU, E., STEFANIS, L. and VEKRELLIS, K., 2010b. Cell-produced alpha-synuclein oligomers are targeted to, and impair, the 26S proteasome. *Neurobiology of Aging*, 20080820, 31, 953-968

ESTEVES, A.R., ARDUINO, D.M., SILVA, D.F., OLIVEIRA, C.R. and CARDOSO, S.M., 2011. Mitochondrial Dysfunction: The Road to Alpha-Synuclein Oligomerization in PD. *Parkinson's Disease*, 2011, 693761

FAUVET, B., MBEFO, M.K., FARES, M.B., DESOBRY, C., MICHAEL, S., ARDAH, M.T., TSIKA, E., COUNE, P., PRUDENT, M., LION, N., ELIEZER, D., MOORE, D.J., SCHNEIDER, B., AEBISCHER, P., EL-AGNAF, O.M., MASLIAH, E. and LASHUEL, H.A., 2012. alpha-Synuclein in central nervous system and from erythrocytes, mammalian cells, and Escherichia coli exists predominantly as disordered monomer. *The Journal of Biological Chemistry*, 287, 15345-15364

FELGER, J.C., LI, L., MARVAR, P.J., WOOLWINE, B.J., HARRISON, D.G., RAISON, C.L. and MILLER, A.H., 2012. Tyrosine metabolism during interferon-alpha administration: Association with fatigue and CSF dopamine concentrations. *Brain, Behavior, and Immunity*, 31, 153-160

FENN, J.B., MANN, M., MENG, C.K., WONG, S.F. and WHITEHOUSE, C.M., 1989. Electrospray ionization for mass spectrometry of large biomolecules. *Science,* 246, 64-71

Fernandez de la Mora, J., 2000. Electrospray ionization of large multiply charged species proceeds via Dole's charge residue mechanism. *Anal. Chim. Acta*, 406, 93-104.

FERNANDEZ, C.O., HOYER, W., ZWECKSTETTER, M., JARES-ERIJMAN, E.A., SUBRAMANIAM, V., GRIESINGER, C. and JOVIN, T.M., 2004. NMR of alpha-synuclein-polyamine complexes elucidates the mechanism and kinetics of induced aggregation. *The EMBO Journal*, 23, 2039-2046

FINK, A.L., 2006. The aggregation and fibrillation of alpha-synuclein. *Accounts of Chemical Research*, 39, 628-634

FLICK, T.G. and WILLIAMS, E.R., 2012. Supercharging with trivalent metal ions in native mass spectrometry. *Journal of the American Society for Mass Spectrometry*, 23, 1885-1895

FORLONI, G., BERTANI, I., CALELLA, A.M., THALER, F. and INVERNIZZI, R., 2000. Alpha-synuclein and Parkinson's disease: selective neurodegenerative effect of alpha-synuclein fragment on dopaminergic neurons in vitro and in vivo. *Annals of Neurology*, 47, 632-640

FORMAN-KAY, J.D. and MITTAG, T., 2013. From sequence and forces to structure, function, and evolution of intrinsically disordered proteins. *Structure* 21, 1492-1499

FORNO, L.S., 1996. Neuropathology of Parkinson's disease. *Journal of Neuropathology and Experimental Neurology*, 55, 259-272

FOULDS, P., MANN, D.M. and ALLSOP, D., 2012. Phosphorylated alpha-synuclein as a potential biomarker for Parkinson's disease and related disorders. *Expert Review of Molecular Diagnostics*, 12, 115-117

FOULDS, P.G., MITCHELL, J.D., PARKER, A., TURNER, R., GREEN, G., DIGGLE, P., HASEGAWA, M., TAYLOR, M., MANN, D. and ALLSOP, D., 2011. Phosphorylated alpha-synuclein can be detected in blood plasma and is potentially a useful biomarker for Parkinson's disease. *FASEB Journal : Official Publication of the Federation of American Societies for Experimental Biology*, 25, 4127-4137

FOULDS, P.G., YOKOTA, O., THURSTON, A., DAVIDSON, Y., AHMED, Z., HOLTON, J., THOMPSON, J.C., AKIYAMA, H., ARAI, T., HASEGAWA, M., GERHARD, A., ALLSOP, D. and MANN, D.M., 2012. Post mortem cerebrospinal fluid alpha-synuclein levels are raised in multiple system atrophy and distinguish this from the other alpha-synucleinopathies, Parkinson's disease and Dementia with Lewy bodies. *Neurobiology of Disease*, 20110810, 45, 188-195

FUJIOKA, S., OGAKI, K., TACIK, P. M., UITTI, R. J., ROSS, O.A. and WSZOLEK, Z. K., 2014. Update on novel familial forms of Parkinson's disease and multiple system atrophy. *Parkinsonism and Related Disorders*, 20S1, S29-S34

FREDENBURG, R.A., ROSPIGLIOSI, C., MERAY, R.K., KESSLER, J.C., LASHUEL, H.A., ELIEZER, D. and LANSBURY, P.T.,Jr, 2007. The impact of the E46K mutation on the properties of alpha-synuclein in its monomeric and oligomeric states. *Biochemistry*, 46, 7107-7118

FRIEDHOFF, P., VON BERGEN, M., MANDELKOW, E.M., DAVIES, P. and MANDELKOW, E., 1998. A nucleated assembly mechanism of Alzheimer paired helical filaments. *Proceedings of the National Academy of Sciences of the United States of America*, 95, 15712-15717

FRIMPONG, A.K., ABZALIMOV, R.R., UVERSKY, V.N. and KALTASHOV, I.A., 2010. Characterization of intrinsically disordered proteins with electrospray ionization mass spectrometry: conformational heterogeneity of alpha-synuclein. *Proteins*, 78, 714-722

GAGGELLI, E., KOZLOWSKI, H., VALENSIN, D. and VALENSIN, G., 2006. Copper homeostasis and neurodegenerative disorders (Alzheimer's, prion, and Parkinson's diseases and amyotrophic lateral sclerosis). *Chemical Reviews*, 106, 1995-2044

GAO, H.M., ZHANG, F., ZHOU, H., KAM, W., WILSON, B. and HONG, J.S., 2011. Neuroinflammation and α-Synuclein Dysfunction Potentiate Each Other, Driving Chronic Progression of Neurodegeneration in a Mouse Model of Parkinson's Disease. *Environmental Health Perspectives*, 119, 807-814

GESSEL, M.M., BERNSTEIN, S., KEMPER, M., TEPLOW, D.B. and BOWERS, M.T., 2012. Familial Alzheimer's disease mutations differentially alter amyloid beta-protein oligomerization. *ACS Chemical Neuroscience*, 3, 909-918

GIASSON, B.I., DUDA, J.E., MURRAY, I.V., CHEN, Q., SOUZA, J.M., HURTIG, H.I., ISCHIROPOULOS, H., TROJANOWSKI, J.Q. and LEE, V.M., 2000. Oxidative damage linked to neurodegeneration by selective alpha-synuclein nitration in synucleinopathy lesions. *Science,* 290, 985-989

GIEHM, L., SVERGUN, D.I., OTZEN, D.E. and VESTERGAARD, B., 2011a. Low-resolution structure of a vesicle disrupting α-synuclein oligomer that

accumulates during fibrillation. *Proceedings of the National Academy of Sciences of the United States of America*, 108, 3246-3251

GIGANTI, V.G., KUNDOOR, S., BEST, W.A. and ANGEL, L.A., 2011. Ion mobility-mass spectrometry study of folded ubiquitin conformers induced by treatment with cis-[Pd(en)(H2O2]2+. *Journal of the American Society for Mass Spectrometry*, 22, 300-309

GILAD, G.M. and GILAD, V.H., 1991. Polyamines can protect against ischemia-induced nerve cell death in gerbil forebrain. *Experimental Neurology*, 111, 349-355

GILES, K., PRINGLE, S.D., WORTHINGTON, K.R., LITTLE, D., WILDGOOSE, J.L. and BATEMAN, R.H., 2004. Applications of a travelling wave-based radio-frequency-only stacked ring ion guide. *Rapid Communications in Mass Spectrometry: RCM*, 18, 2401-2414

GLASER, C.B., YAMIN, G., UVERSKY, V.N. and FINK, A.L., 2005. Methionine oxidation, alpha-synuclein and Parkinson's disease. *Biochimica Et Biophysica Acta*, 1703, 157-169

GOERS, J., UVERSKY, V.N. and FINK, A.L., 2003. Polycation-induced oligomerization and accelerated fibrillation of human α-synuclein in vitro. *Protein Science: A Publication of the Protein Society*, 12, 702-707

GORELL, J.M., JOHNSON, C.C., RYBICKI, B.A., PETERSON, E.L., KORTSHA, G.X., BROWN, G.G. and RICHARDSON, R.J., 1999. Occupational exposure to manganese, copper, lead, iron, mercury and zinc and the risk of Parkinson's disease. *Neurotoxicology*, 20, 239-247

GORELL, J.M., PETERSON, E.L., RYBICKI, B.A. and JOHNSON, C.C., 2004. Multiple risk factors for Parkinson's disease. *Journal of the Neurological Sciences*, 217, 169-174

GOREVIC, P.D., MUNOZ, P.C., CASEY, T.T., DIRAIMONDO, C.R., STONE, W.J., PRELLI, F.C., RODRIGUES, M.M., POULIK, M.D. and FRANGIONE, B., 1986. Polymerization of intact beta 2-microglobulin in tissue causes amyloidosis in patients on chronic hemodialysis. *Proceedings of the National Academy of Sciences of the United States of America*, 83, 7908-7912

GRABENAUER, M., BERNSTEIN, S.L., LEE, J.C., WYTTENBACH, T., DUPUIS, N.F., GRAY, H.B., WINKLER, J.R. and BOWERS, M.T., 2008. Spermine binding to Parkinson's protein alpha-synuclein and its disease-related A30P and A53T mutants. *The Journal of Physical Chemistry.B*, 112, 11147-11154

GRABENAUER, M., WU, C., SOTO, P., SHEA, J.E. and BOWERS, M.T., 2010a. Oligomers of the prion protein fragment 106-126 are likely assembled from beta-hairpins in solution, and methionine oxidation inhibits assembly

without altering the peptide's monomeric conformation. *Journal of the American Chemical Society*, 132, 532-539

GRABENAUER, M., WYTTENBACH, T., SANGHERA, N., SLADE, S.E., PINHEIRO, T.J., SCRIVENS, J.H. and BOWERS, M.T., 2010b. Conformational stability of Syrian hamster prion protein PrP(90-231). *Journal of the American Chemical Society*, 132, 8816-8818

GRAHAM, D.G., 1978. Oxidative pathways for catecholamines in the genesis of neuromelanin and cytotoxic quinones. *Molecular Pharmacology*, 14, 633-643.

GRANDORI, R., 2003. Origin of the conformation dependence of protein charge-state distributions in electrospray ionization mass spectrometry. *Journal of Mass Spectrometry: JMS*, 38, 11-15

GREENBAUM, E.A., GRAVES, C.L., MISHIZEN-EBERZ, A.J., LUPOLI, M.A., LYNCH, D.R., ENGLANDER, S.W., AXELSEN, P.H. and GIASSON, B.I., 2005. The E46K mutation in alpha-synuclein increases amyloid fibril formation. *The Journal of Biological Chemistry*, 280, 7800-7807

GUILLIAMS, T., EL-TURK, F., BUELL, A.K., O'DAY, E.M., APRILE, F.A., ESBJORNER, E.K., VENDRUSCOLO, M., CREMADES, N., PARDON, E., WYNS, L., WELLAND, M.E., STEYAERT, J., CHRISTODOULOU, J., DOBSON, C.M. and DE GENST, E., 2013. Nanobodies Raised against Monomeric alpha-Synuclein Distinguish between Fibrils at Different Maturation Stages. *Journal of Molecular Biology*, 425, 2397-2411

GURRY, T., ULLMAN, O., FISHER, C.K., PEROVIC, I., POCHAPSKY, T. and STULTZ, C.M., 2013. The dynamic structure of alpha-synuclein multimers. *Journal of the American Chemical Society*, 135, 3865-3872

HANSEN, C., ANGOT, E., BERGSTROM, A.L., STEINER, J.A., PIERI, L., PAUL, G., OUTEIRO, T.F., MELKI, R., KALLUNKI, P., FOG, K., LI, J.Y. and BRUNDIN, P., 2011. alpha-Synuclein propagates from mouse brain to grafted dopaminergic neurons and seeds aggregation in cultured human cells. *The Journal of Clinical Investigation*, 121, 715-725

HARDY, J. and ALLSOP, D., 1991. Amyloid deposition as the central event in the aetiology of Alzheimer's disease. *Trends in Pharmacological Sciences*, 12, 383-388

HARPER, J.D. and LANSBURY, P.T.,Jr, 1997. Models of amyloid seeding in Alzheimer's disease and scrapie: mechanistic truths and physiological consequences of the time-dependent solubility of amyloid proteins. *Annual Review of Biochemistry*, 66, 385-407

HARVEY, S.R., MACPHEE, C.E. and BARRAN, P.E., 2011. Ion mobility mass spectrometry for peptide analysis. *Methods* , 54, 454-461

HAYASHITA-KINOH, H., YAMADA, M., YOKOTA, T., MIZUNO, Y. and MOCHIZUKI, H., 2006. Down-regulation of alpha-synuclein expression can rescue dopaminergic cells from cell death in the substantia nigra of Parkinson's disease rat model. *Biochemical and Biophysical Research Communications*, 341, 1088-1095

HECK, A.J., 2008. Native mass spectrometry: a bridge between interactomics and structural biology. *Nature Methods*, 5, 927-933

HECK, A.J. and VAN DEN HEUVEL, R.H., 2004. Investigation of intact protein complexes by mass spectrometry. *Mass Spectrometry Reviews*, 23, 368-389

HEEGAARD, N.H., 2009. Beta(2)-Microglobulin: from Physiology to Amyloidosis. *Amyloid : The International Journal of Experimental and Clinical Investigation : The Official Journal of the International Society of Amyloidosis*, 16, 151-173

HERRERA, F.E., CHESI, A., PALEOLOGOU, K.E., SCHMID, A., MUNOZ, A., VENDRUSCOLO, M., GUSTINCICH, S., LASHUEL, H.A. and CARLONI, P., 2008. Inhibition of alpha-synuclein fibrillization by dopamine is mediated by interactions with five C-terminal residues and with E83 in the NAC region. *PloS One*, 3, e3394

HILKER, R., BROTCHIE, J.M. and CHAPMAN, J., 2011. Pros and cons of a prion-like pathogenesis in Parkinson's disease. *BMC Neurology*, 11, 74

HILTON, G.R., THALASSINOS, K., GRABENAUER, M., SANGHERA, N., SLADE, S.E., WYTTENBACH, T., ROBINSON, P.J., PINHEIRO, T.J., BOWERS, M.T. and SCRIVENS, J.H., 2010. Structural analysis of prion proteins by means of drift cell and traveling wave ion mobility mass spectrometry. *Journal of the American Society for Mass Spectrometry*, 21, 845-854

HIRSCH, E.C., BRANDEL, J.P., GALLE, P., JAVOY-AGID, F. and AGID, Y., 1991. Iron and aluminum increase in the substantia nigra of patients with Parkinson's disease: an X-ray microanalysis. *Journal of Neurochemistry*, 56, 446-451

HOEPKEN, H.H., GISPERT, S., AZIZOV, M., KLINKENBERG, M., RICCIARDI, F., KURZ, A., MORALES-GORDO, B., BONIN, M., RIESS, O., GASSER, T., KOGEL, D., STEINMETZ, H. and AUBURGER, G., 2008. Parkinson patient fibroblasts show increased alpha-synuclein expression. *Experimental Neurology*, 212, 307-313

HOFFMAN-ZACHARSKA, D., KOZIOROWSKI, D., ROSS, O.A., MILEWSKI, M., POZNANSKI, J., JUREK, M., WSZOLEK, Z.K., SOTO-ORTOLAZA, A., SLAWEK, J., JANIK, P., JAMROZIK, Z., POTULSKA-CHROMIK, A., JANISKA-MYGA, B., OPALA, G., KRYGOWSKA-WAJS, A., CZYZEWSKI, K., DICKSON, D. W., BAL, J. and FRIEDMAN, A., 2013. Novel A18T and pA29S substitutions

in alpha-synuclein may be associated with sporadic Parkinson's disease. *Parkinsonism and Related Disorders*, 19, 1057-1060

HOLDORFF, B., 2002. Friedrich Heinrich Lewy (1885-1950) and his work. *Journal of the History of the Neurosciences*, 11, 19-28

HONG, L. and SIMON, J.D., 2009. Binding of Cu(II) to human alpha-synucleins: comparison of wild type and the point mutations associated with the familial Parkinson's disease. *The Journal of Physical Chemistry.B*, 113, 9551-9561

HORNYKIEWICZ, O., 2010. A brief history of levodopa. *Journal of Neurology*, 257, 249-252

HOULDEN, H. and SINGLETON, A.B., 2012. The genetics and neuropathology of Parkinson's disease. *Acta Neuropathologica*, 124, 325-338

HYUNG, S.J., DETOMA, A.S., BRENDER, J.R., LEE, S., VIVEKANANDAN, S., KOCHI, A., CHOI, J.S., RAMAMOORTHY, A., RUOTOLO, B.T. and LIM, M.H., 2013. Insights into antiamyloidogenic properties of the green tea extract (-)-epigallocatechin-3-gallate toward metal-associated amyloid-beta species. *Proceedings of the National Academy of Sciences of the United States of America*, 110, 3743-3748

IDKOWIAK-BALDYS, J., APRAIZ, A., LI, L., RAHMANIYAN, M., CLARKE, C.J., KRAVEKA, J.M., ASUMENDI, A. and HANNUN, Y.A., 2010. Dihydroceramide desaturase activity is modulated by oxidative stress. *The Biochemical Journal*, 427, 265-274

INGLIS, K.J., CHEREAU, D., BRIGHAM, E.F., CHIOU, S.S., SCHOBEL, S., FRIGON, N.L., YU, M., CACCAVELLO, R.J., NELSON, S., MOTTER, R., WRIGHT, S., CHIAN, D., SANTIAGO, P., SORIANO, F., RAMOS, C., POWELL, K., GOLDSTEIN, J.M., BABCOCK, M., YEDNOCK, T., BARD, F., BASI, G.S., SHAM, H., CHILCOTE, T.J., MCCONLOGUE, L., GRISWOLD-PRENNER, I. and ANDERSON, J.P., 2009. Polo-like kinase 2 (PLK2) phosphorylates alpha-synuclein at serine 129 in central nervous system. *The Journal of Biological Chemistry*, 284, 2598-2602

International Parkinson Disease Genomics Consortium, NALLS, M.A., PLAGNOL, V., HERNANDEZ, D.G., SHARMA, M., SHEERIN, U.M., SAAD, M., SIMON-SANCHEZ, J., SCHULTE, C., LESAGE, S., SVEINBJORNSDOTTIR, S., STEFANSSON, K., MARTINEZ, M., HARDY, J., HEUTINK, P., BRICE, A., GASSER, T., SINGLETON, A.B. and WOOD, N.W., 2011. Imputation of sequence variants for identification of genetic risks for Parkinson's disease: a meta-analysis of genome-wide association studies. *Lancet*, 377, 641-649

IRWIN, D.J., LEE, V.M. and TROJANOWSKI, J.Q., 2013. Parkinson's disease dementia: convergence of alpha-synuclein, tau and amyloid-beta pathologies. *Nature Reviews.Neuroscience*, 14, 626-636

IWATA, A., MARUYAMA, M., KANAZAWA, I. and NUKINA, N., 2001. alpha-Synuclein affects the MAPK pathway and accelerates cell death. *The Journal of Biological Chemistry*, 276, 45320-45329

JAHN, T.R., MAKIN, O.S., MORRIS, K.L., MARSHALL, K.E., TIAN, P., SIKORSKI, P. and SERPELL, L.C., 2010. The common architecture of cross-beta amyloid. *Journal of Molecular Biology*, 395, 717-727

JAN, A., GOKCE, O., LUTHI-CARTER, R. and LASHUEL, H.A., 2008. The ratio of monomeric to aggregated forms of Abeta40 and Abeta42 is an important determinant of amyloid-beta aggregation, fibrillogenesis, and toxicity. *The Journal of Biological Chemistry*, 283, 28176-28189

JANG, H., ARCE, F.T., RAMACHANDRAN, S., CAPONE, R., AZIMOVA, R., KAGAN, B.L., NUSSINOV, R. and LAL, R., 2010. Parkinson's disease dementia: convergence of alpha-synuclein, tau and amyloid-beta pathologies. *Proceedings of the National Academy of Sciences of the United States of America*, 107, 6538-6543

JANKOVIC, J., 2008. Parkinson's disease: clinical features and diagnosis. *Journal of Neurology, Neurosurgery, and Psychiatry*, 79, 368-376

JARRETT, J.T., BERGER, E.P. and LANSBURY, P.T.,Jr, 1993. The carboxy terminus of the beta amyloid protein is critical for the seeding of amyloid formation: implications for the pathogenesis of Alzheimer's disease. *Biochemistry*, 32, 4693-4697

JARROLD, M.F., 2000. Peptides and proteins in the vapor phase. *Annual Review of Physical Chemistry*, 51, 179-207

JELLINGER, K.A., 2012. Interaction between pathogenic proteins in neurodegenerative disorders. *Journal of Cellular and Molecular Medicine*, 16, 1166-1183

JELLINGER, K.A., 2011. Interaction between alpha-synuclein and other proteins in neurodegenerative disorders. *TheScientificWorldJournal*, 11, 1893-1907

JENNER, P., 2007. Oxidative stress and Parkinson's disease. *Handbook of Clinical Neurology*, 83, 507-520

JENNER, P., 2003. Oxidative stress in Parkinson's disease. *Annals of Neurology*, 53, S26-S38

JINSMAA, Y., FLORANG, V.R., REES, J.N., MEXAS, L.M., ECKERT, L.L., ALLEN, E.M., ANDERSON, D.G. and DOORN, J.A., 2011. Dopamine-derived biological reactive intermediates and protein modifications: Implications for Parkinson's disease. *Chemico-Biological Interactions*, 192, 118-121

JURNECZKO, E. and BARRAN, P.E., 2011. How useful is ion mobility mass spectrometry for structural biology? The relationship between protein crystal structures and their collision cross sections in the gas phase. *The Analyst*, 136, 20-28

KALIA, L.V., KALIA, S.K., MCLEAN, P.J., LOZANO, A.M. and LANG, A.E., 2013. alpha-Synuclein oligomers and clinical implications for Parkinson disease. *Annals of Neurology*, 73, 155-169

KALTASHOV, I.A. and MOHIMEN, A., 2005. Estimates of protein surface areas in solution by electrospray ionization mass spectrometry. *Analytical Chemistry*, 77, 5370-5379

KALTASHOV, I.A., ZHANG, M., EYLES, S.J. and ABZALIMOV, R.R., 2006. Investigation of structure, dynamics and function of metalloproteins with electrospray ionization mass spectrometry. *Analytical and Bioanalytical Chemistry*, 386, 472-481

KANU, A.B., DWIVEDI, P., TAM, M., MATZ, L. and HILL, H.H.,Jr, 2008. Ion mobility-mass spectrometry. *Journal of Mass Spectrometry: JMS*, 43, 1-22

KAYED, R. and GLABE, C.G., 2006. Conformation-dependent anti-amyloid oligomer antibodies. *Methods in Enzymology*, 413, 326-344

KAYED, R., HEAD, E., SARSOZA, F., SAING, T., COTMAN, C.W., NECULA, M., MARGOL, L., WU, J., BREYDO, L., THOMPSON, J.L., RASOOL, S., GURLO, T., BUTLER, P. and GLABE, C.G., 2007. Fibril specific, conformation dependent antibodies recognize a generic epitope common to amyloid fibrils and fibrillar oligomers that is absent in prefibrillar oligomers. *Molecular Neurodegeneration*, 2, 18

KHURANA, R., IONESCU-ZANETTI, C., POPE, M., LI, J., NIELSON, L., RAMIREZ-ALVARADO, M., REGAN, L., FINK, A.L. and CARTER, S.A., 2003. A general model for amyloid fibril assembly based on morphological studies using atomic force microscopy. *Biophysical Journal*, 85, 1135-1144

KIELY, A. P., ASI, Y.T., KARA, E., LIMOUSIN, P., LEWIS, P., PROUKAKIS, C., QIUNN, N., LEES, A.J., HARDY, J., REVESZ, T., HOULDEN, H. and HOLTON, J. L., 2013. Alpha-synucleinopathy associated with G51D SNCA mutation: a link between Parkinson's disease and multiple system atrophy? *Acta Neuropathologica, 125, 753-769*

KIM, H.Y., CHO, M.K., KUMAR, A., MAIER, E., SIEBENHAAR, C., BECKER, S., FERNANDEZ, C.O., LASHUEL, H.A., BENZ, R., LANGE, A. and ZWECKSTETTER, M., 2009. Structural properties of pore-forming oligomers of alpha-synuclein. *Journal of the American Chemical Society*, 131, 17482-17489

KITOVA, E.N., EL-HAWIET, A., SCHNIER, P.D. and KLASSEN, J.S., 2012. Reliable determinations of protein-ligand interactions by direct ESI-MS

measurements. Are we there yet?. *Journal of the American Society for Mass Spectrometry*, 23, 431-441

KLEMENT, K., WIELIGMANN, K., MEINHARDT, J., HORTSCHANSKY, P., RICHTER, W. and FANDRICH, M., 2007. Effect of different salt ions on the propensity of aggregation and on the structure of Alzheimer's abeta(1-40) amyloid fibrils. *Journal of Molecular Biology*, 373, 1321-1333

KLONIECKI, M., JABLONOWSKA, A., POZNANSKI, J., LANGRIDGE, J., HUGHES, C., CAMPUZANO, I., GILES, K. and DADLEZ, M., 2011. Ion mobility separation coupled with MS detects two structural states of Alzheimer's disease Abeta1-40 peptide oligomers. *Journal of Molecular Biology*, 407, 110-124

KNAPMAN, T.W., BERRYMAN, J.T., CAMPUZANO, I., HARRIS, S.A. and ASHCROFT, A.E., 2010. Considerations in Experimental and Theoretical Collision Cross-section Measurements of Small Molecules Using Travelling Wave Ion Mobility Spectrometry-Mass Spectrometry . *International Journal of Mass Spectrometry*, 298, 17-23.

KOENIGER, S.L., MERENBLOOM, S.I., VALENTINE, S.J., JARROLD, M.F., UDSETH, H.R., SMITH, R.D. and CLEMMER, D.E., 2006. An IMS-IMS analogue of MS-MS. *Analytical Chemistry*, 78, 4161-4174

KONERMANN, L., 2009. A simple model for the disintegration of highly charged solvent droplets during electrospray ionization. *Journal of the American Society for Mass Spectrometry*, 20, 496-506

KRAUS, A., GROVEMAN, B.R. and CAUGHEY, B., 2013. Prions and the Potential Transmissibility of Protein Misfolding Diseases. *Annual Review of Microbiology*, 67, 543-564

KREMER, J.J., PALLITTO, M.M., SKLANSKY, D.J. and MURPHY, R.M., 2000. Correlation of beta-amyloid aggregate size and hydrophobicity with decreased bilayer fluidity of model membranes. *Biochemistry*, 39, 10309-10318

KRISHNAN, R., GOODMAN, J.L., MUKHOPADHYAY, S., PACHECO, C.D., LEMKE, E.A., DENIZ, A.A. and LINDQUIST, S., 2012. Conserved features of intermediates in amyloid assembly determine their benign or toxic states. *Proceedings of the National Academy of Sciences of the United States of America*, 109, 11172-11177

KRIZ, Z., KLUSAK, J., KRISTOFIKOVA, Z. and KOCA, J., 2013. How ionic strength affects the conformational behavior of human and rat beta amyloids--a computational study. *PloS One*, 8, e62914

KRUGER, R., KUHN, W., MULLER, T., WOITALLA, D., GRAEBER, M., KOSEL, S., PRZUNTEK, H., EPPLEN, J.T., SCHOLS, L. and RIESS, O., 1998. Ala30Pro mutation in the gene encoding alpha-synuclein in Parkinson's disease. *Nature Genetics*, 18, 106-108

KUKRER, B., BARBU, I.M., COPPS, J., HOGAN, P., TAYLOR, S.S., VAN DUIJN, E. and HECK, A.J., 2012. Conformational isomers of calcineurin follow distinct dissociation pathways. *Journal of the American Society for Mass Spectrometry*, 23, 1534-1543

LASHUEL, H.A., HARTLEY, D., PETRE, B.M., WALZ, T. and LANSBURY, P.T.,Jr, 2002. Neurodegenerative disease: amyloid pores from pathogenic mutations. *Nature*, 418, 291

LASHUEL, H.A., OVERK, C.R., OUESLATI, A. and MASLIAH, E., 2013. The many faces of alpha-synuclein: from structure and toxicity to therapeutic target. *Nature Reviews.Neuroscience*, 14, 38-48

LASHUEL, H.A., PETRE, B.M., WALL, J., SIMON, M., NOWAK, R.J., WALZ, T. and LANSBURY, P.T.,Jr, 2002. Alpha-synuclein, especially the Parkinson's disease-associated mutants, forms pore-like annular and tubular protofibrils. *Journal of Molecular Biology*, 322, 1089-1102

LEE, H.J., BAEK, S.M., HO, D.H., SUK, J.E., CHO, E.D. and LEE, S.J., 2011. Dopamine promotes formation and secretion of non-fibrillar alpha-synuclein oligomers. *Experimental & Molecular Medicine*, 43, 216-222

LEE, H.J., PATEL, S. and LEE, S.J., 2005. Intravesicular localization and exocytosis of alpha-synuclein and its aggregates. *The Journal of Neuroscience : The Official Journal of the Society for Neuroscience*, 25, 6016-6024

LEE, H.J., SUK, J.E., BAE, E.J., LEE, J.H., PAIK, S.R. and LEE, S.J., 2008a. Assembly-dependent endocytosis and clearance of extracellular alpha-synuclein. *The International Journal of Biochemistry & Cell Biology*, 40, 1835-1849

LEE, J.C., GRAY, H.B. and WINKLER, J.R., 2008b. Copper(II) binding to alpha-synuclein, the Parkinson's protein. *Journal of the American Chemical Society*, 130, 6898-6899

LENEY, A.C., PHAN, G., ALLEN, W., VERGER, D., WAKSMAN, G., RADFORD, S.E. and ASHCROFT, A.E., 2011. Second order rate constants of donor-strand exchange reveal individual amino acid residues important in determining the subunit specificity of pilus biogenesis. *Journal of the American Society for Mass Spectrometry*, 22, 1214-1223

LEONG, S.L., CAPPAI, R., BARNHAM, K.J. and PHAM, C.L., 2009a. Modulation of alpha-synuclein aggregation by dopamine: a review. *Neurochemical Research*, 34, 1838-1846

LEONG, S.L., PHAM, C.L., GALATIS, D., FODERO-TAVOLETTI, M.T., PEREZ, K., HILL, A.F., MASTERS, C.L., ALI, F.E., BARNHAM, K.J. and CAPPAI, R., 2009b. Formation of dopamine-mediated alpha-synuclein-soluble oligomers requires methionine oxidation. *Free Radical Biology & Medicine*, 46, 1328-1337

LERME, L., DUGOURD, P., HUDGINS, R., R. and JARROLD, M.F., 1999. High resolution ion mobility measurement of indium clusters: electron spill-out in metal cluster anions and cations. *Chem. Phys. Lett.*, 304, 19-22.

LESAGE, S., ANHEIM, M., LETOURNEL, F., BOUSSET, L., HONORE, A., ROZAS, N., PIERI, L., MADIONA, K., DURR, A., MELKI, R., VERNY, C. and BRICE, A., 2013. G51D alpha-synuclein mutation causes a novel parkinsonian-pyramidal syndrome. *Annals of Neurology*, ahead of print, doi: 10.1002/ana.23894

LESNE, S., KOH, M.T., KOTILINEK, L., KAYED, R., GLABE, C.G., YANG, A., GALLAGHER, M. and ASHE, K.H., 2006. A specific amyloid-beta protein assembly in the brain impairs memory. *Nature*, 440, 352-357

LESNE, S.E., 2013. Breaking the Code of Amyloid- Oligomers. *International Journal of Cell Biology*, 2013, 950783

LI, H.T., LIN, D.H., LUO, X.Y., ZHANG, F., JI, L.N., DU, H.N., SONG, G.Q., HU, J., ZHOU, J.W. and HU, H.Y., 2005. Inhibition of alpha-synuclein fibrillization by dopamine analogs via reaction with the amino groups of alpha-synuclein. Implication for dopaminergic neurodegeneration. *The FEBS Journal*, 272, 3661-3672

LI, J., ZHU, M., RAJAMANI, S., UVERSKY, V.N. and FINK, A.L., 2004. Rifampicin inhibits alpha-synuclein fibrillation and disaggregates fibrils. *Chemistry & Biology*, 11, 1513-1521

LI, J.Y., ENGLUND, E., HOLTON, J.L., SOULET, D., HAGELL, P., LEES, A.J., LASHLEY, T., QUINN, N.P., REHNCRONA, S., BJORKLUND, A., WIDNER, H., REVESZ, T., LINDVALL, O. and BRUNDIN, P., 2008. Lewy bodies in grafted neurons in subjects with Parkinson's disease suggest host-to-graft disease propagation. *Nature Medicine*, 14, 501-503

LI, W., WEST, N., COLLA, E., PLETNIKOVA, O., TRONCOSO, J.C., MARSH, L., DAWSON, T.M., JAKALA, P., HARTMANN, T., PRICE, D.L. and LEE, M.K., 2005. Aggregation promoting C-terminal truncation of alpha-synuclein is a normal cellular process and is enhanced by the familial Parkinson's disease-linked mutations. *Proceedings of the National Academy of Sciences of the United States of America*, 102, 2162-2167

LINDGREN, M., SORGJERD, K. and HAMMARSTROM, P., 2005. Detection and characterization of aggregates, prefibrillar amyloidogenic oligomers, and protofibrils using fluorescence spectroscopy. *Biophysical Journal*, 88, 4200-4212

LIU, L.L. and FRANZ, K.J., 2007. Phosphorylation-dependent metal binding by alpha-synuclein peptide fragments. *Journal of Biological Inorganic Chemistry : JBIC : A Publication of the Society of Biological Inorganic Chemistry*, 12, 234-247

LO BIANCO, C., RIDET, J.L., SCHNEIDER, B.L., DEGLON, N. and AEBISCHER, P., 2002. Alpha -synucleinopathy and selective dopaminergic neuron loss in a rat lentiviral-based model of Parkinson's disease. *Proceedings of the National Academy of Sciences of the United States of America*, 99, no. 16, 10813-10818

LOMAKIN, A., CHUNG, D.S., BENEDEK, G.B., KIRSCHNER, D.A. and TEPLOW, D.B., 1996. On the nucleation and growth of amyloid beta-protein fibrils: detection of nuclei and quantitation of rate constants. *Proceedings of the National Academy of Sciences of the United States of America*, 93, 1125-1129

LOMELI, S.H., YIN, S., OGORZALEK LOO, R.R. and LOO, J.A., 2009. Increasing charge while preserving noncovalent protein complexes for ESI-MS. *Journal of the American Society for Mass Spectrometry*, 20, 593-596

LOO, J.A., UDSETH, H.R., SMITH, R., D. and FUTRELL, J.H., 1988. Collisional effects on the charge distribution of ions from large molecules, formed by electrospray- ionization mass spectrometry. *Rapid Commun.Mass Spectrom.*, 2, 207-210.

LOO, J.A., LOO, R.R., UDSETH, H.R., EDMONDS, C.G. and SMITH, R.D., 1991. Solvent-induced conformational changes of polypeptides probed by electrospray-ionization mass spectrometry. *Rapid Communications in Mass Spectrometry: RCM*, 5, 101-105

LOTHARIUS, J. and BRUNDIN, P., 2002a. Impaired dopamine storage resulting from alpha-synuclein mutations may contribute to the pathogenesis of Parkinson's disease. *Human Molecular Genetics*, 11, 2395-2407

LOTHARIUS, J. and BRUNDIN, P., 2002b. Pathogenesis of Parkinson's disease: dopamine, vesicles and alpha-synuclein. *Nature Reviews.Neuroscience*, 3, 932-942

LOWE, R., POUNTNEY, D.L., JENSEN, P.H., GAI, W.P. and VOELCKER, N.H., 2004. Calcium(II) selectively induces alpha-synuclein annular oligomers via interaction with the C-terminal domain. *Protein Science : A Publication of the Protein Society*, 13, 3245-3252

LUCAS, H.R. and LEE, J.C., 2011. Copper(II) enhances membrane-bound alpha-synuclein helix formation. *Metallomics : Integrated Biometal Science*, 3, 280-283

LUK, K.C., SONG, C., O'BRIEN, P., STIEBER, A., BRANCH, J.R., BRUNDEN, K.R., TROJANOWSKI, J.Q. and LEE, V.M., 2009. Exogenous alpha-synuclein fibrils seed the formation of Lewy body-like intracellular inclusions in cultured cells. *Proceedings of the National Academy of Sciences of the United States of America*, 106, 20051-20056

LUNDBLAD, M., DECRESSAC, M., MATTSSON, B. and BJORKLUND, A., 2012. Impaired neurotransmission caused by overexpression of alpha-synuclein in nigral dopamine neurons. *Proceedings of the National Academy of Sciences of the United States of America*, 109, 3213-3219

MALCHIODI-ALBEDI, F., PARADISI, S., MATTEUCCI, A., FRANK, C. and DIOCIAIUTI, M., 2011. Amyloid oligomer neurotoxicity, calcium dysregulation, and lipid rafts. *International Journal of Alzheimer's Disease*, 2011, 906964

MANNING-BOG, A.B., MCCORMACK, A.L., LI, J., UVERSKY, V.N., FINK, A.L. and DI MONTE, D.A., 2002. The herbicide paraquat causes up-regulation and aggregation of alpha-synuclein in mice: paraquat and alpha-synuclein. *The Journal of Biological Chemistry*, 277, 1641-1644

MANSUY, I.M., MAYFORD, M., JACOB, B., KANDEL, E.R. and BACH, M.E., 1998. Restricted and regulated overexpression reveals calcineurin as a key component in the transition from short-term to long-term memory. *Cell*, 92, 39-49

MARCOUX, J. and ROBINSON, C.V., 2013a. Twenty years of gas phase structural biology. *Structure,* 21, 1541-1550

MARCOUX, J., WANG, S.C., POLITIS, A., READING, E., MA, J., BIGGIN, P.C., ZHOU, M., TAO, H., ZHANG, Q., CHANG, G., MORGNER, N. and ROBINSON, C.V., 2013b. Mass spectrometry reveals synergistic effects of nucleotides, lipids, and drugs binding to a multidrug resistance efflux pump. *Proceedings of the National Academy of Sciences of the United States of America*, 110, 9704-9709

MARDER, K., TANG, M.X., MEJIA, H., ALFARO, B., COTE, L., LOUIS, E., GROVES, J. and MAYEUX, R., 1996. Risk of Parkinson's disease among first-degree relatives: A community-based study. *Neurology*, 47, 155-160

MAREK, P.J., PATSALO, V., GREEN, D.F. and RALEIGH, D.P., 2012. Ionic strength effects on amyloid formation by amylin are a complicated interplay among Debye screening, ion selectivity, and Hofmeister effects. *Biochemistry*, 51, 8478-8490

MARIES, E., DASS, B., COLLIER, T.J., KORDOWER, J.H. and STEECE-COLLIER, K., 2003. The role of alpha-synuclein in Parkinson's disease: insights from animal models. *Nature Reviews.Neuroscience*, 4, 727-738

MAROTEAUX, L., CAMPANELLI, J.T. and SCHELLER, R.H., 1988. Synuclein: a neuron-specific protein localized to the nucleus and presynaptic nerve terminal. *The Journal of Neuroscience : The Official Journal of the Society for Neuroscience*, 8, 2804-2815

MARTIN, L.J., PAN, Y., PRICE, A.C., STERLING, W., COPELAND, N.G., JENKINS, N.A., PRICE, D.L. and LEE, M.K., 2006. Parkinson's disease alpha-

synuclein transgenic mice develop neuronal mitochondrial degeneration and cell death. *The Journal of Neuroscience : The Official Journal of the Society for Neuroscience*, 26, 41-50

MARTIN, Z.S., NEUGEBAUER, V., DINELEY, K.T., KAYED, R., ZHANG, W., REESE, L.C. and TAGLIALATELA, G., 2012. alpha-Synuclein oligomers oppose long-term potentiation and impair memory through a calcineurin-dependent mechanism: relevance to human synucleopathic diseases. *Journal of Neurochemistry*, 120, 440-452

MASLIAH, E., ROCKENSTEIN, E., VEINBERGS, I., MALLORY, M., HASHIMOTO, M., TAKEDA, A., SAGARA, Y., SISK, A. and MUCKE, L., 2000. Dopaminergic loss and inclusion body formation in alpha-synuclein mice: implications for neurodegenerative disorders. *Science,* 287, 1265-1269

MASON, E., A. and MCDANIEL, E.W., 1988. Transport Properties of Ions in Gases. *John Wiley& Sons: New York.*

MATTSON, M.P., 2012. Parkinson's disease: don't mess with calcium. *The Journal of Clinical Investigation*, 122, 1195-1198

MATTSON, M.P., 2011. Commentary: proteooxidotoxic process of aggregation. *Neuromolecular Medicine*, 13, 91-92

MCPARLAND, V.J., KAD, N.M., KALVERDA, A.P., BROWN, A., KIRWIN-JONES, P., HUNTER, M.G., SUNDE, M. and RADFORD, S.E., 2000. Partially unfolded states of beta(2)-microglobulin and amyloid formation in vitro. *Biochemistry*, 39, 8735-8746

MEUVIS, J., GERARD, M., DESENDER, L., BAEKELANDT, V. and ENGELBORGHS, Y., 2010. The conformation and the aggregation kinetics of alpha-synuclein depend on the proline residues in its C-terminal region. *Biochemistry*, 49, 9345-9352

MIAKE, H., MIZUSAWA, H., IWATSUBO, T. and HASEGAWA, M., 2002. Biochemical characterization of the core structure of alpha-synuclein filaments. *The Journal of Biological Chemistry*, 277, 19213-19219

MICHAELEVSKI, I., EISENSTEIN, M. and SHARON, M., 2010a. Gas-phase compaction and unfolding of protein structures. *Analytical Chemistry*, 82, 9484-9491

MICHAELEVSKI, I., KIRSHENBAUM, N. and SHARON, M., 2010b. T-wave ion mobility-mass spectrometry: basic experimental procedures for protein complex analysis. *Journal of Visualized Experiments: JoVE*, 41, 10.3791/1985

MONDRAGON-RODRIGUEZ, S., BASURTO-ISLAS, G., LEE, H.G., PERRY, G., ZHU, X., CASTELLANI, R.J. and SMITH, M.A., 2010. Causes versus

effects: the increasing complexities of Alzheimer's disease pathogenesis. *Expert Review of Neurotherapeutics*, 10, 683-691

MORTEN, I.J., GOSAL, W.S., RADFORD, S.E. and HEWITT, E.W., 2007. Investigation into the role of macrophages in the formation and degradation of beta2-microglobulin amyloid fibrils. *The Journal of Biological Chemistry*, 282, 29691-29700

MOSIER, P.D., COUNTERMAN, A.E., JURS, P.C. and CLEMMER, D.E., 2002. Prediction of peptide ion collision cross sections from topological molecular structure and amino acid parameters. *Analytical Chemistry*, 74, 1360-1370

MUKAETOVA-LADINSKA, E.B. and MCKEITH, I.G., 2006. Pathophysiology of synuclein aggregation in Lewy body disease. *Mechanisms of Ageing and Development*, 127, 188-202

MULLER, T., 2012. Drug therapy in patients with Parkinson's disease. *Translational Neurodegeneration*, 1, 10

MULLIN, S. and SCHAPIRA, A., 2013. alpha-Synuclein and Mitochondrial Dysfunction in Parkinson's Disease. *Molecular Neurobiology*, 47, 587-597

MUNISHKINA, L.A. and FINK, A.L., 2007. Fluorescence as a method to reveal structures and membrane-interactions of amyloidogenic proteins. *Biochimica Et Biophysica Acta*, 1768, 1862-1885

MUNISHKINA, L.A., FINK, A.L. and UVERSKY, V.N., 2009. Accelerated fibrillation of alpha-synuclein induced by the combined action of macromolecular crowding and factors inducing partial folding. *Current Alzheimer Research*, 6, 252-260

MUNISHKINA, L.A., PHELAN, C., UVERSKY, V.N. and FINK, A.L., 2003. Conformational behavior and aggregation of alpha-synuclein in organic solvents: modeling the effects of membranes. *Biochemistry*, 42, 2720-2730

MUNOZ, P., HUENCHUGUALA, S., PARIS, I. and SEGURA-AGUILAR, J., 2012. Dopamine oxidation and autophagy. *Parkinson's Disease*, 2012, 920953

MURPHY, D.D., RUETER, S.M., TROJANOWSKI, J.Q. and LEE, V.M., 2000. Synucleins are developmentally expressed, and alpha-synuclein regulates the size of the presynaptic vesicular pool in primary hippocampal neurons. *The Journal of Neuroscience: The Official Journal of the Society for Neuroscience*, 20, 3214-3220

MURRAY, M.M., BERNSTEIN, S.L., NYUGEN, V., CONDRON, M.M., TEPLOW, D.B. and BOWERS, M.T., 2009a. Amyloid beta protein: Abeta40 inhibits Abeta42 oligomerization. *Journal of the American Chemical Society*, 131, 6316-6317

MURRAY, M.M., KRONE, M.G., BERNSTEIN, S.L., BAUMKETNER, A., CONDRON, M.M., LAZO, N.D., TEPLOW, D.B., WYTTENBACH, T., SHEA, J.E. and BOWERS, M.T., 2009b. Amyloid beta-protein: experiment and theory on the 21-30 fragment. *The Journal of Physical Chemistry.B*, 113, 6041-6046

NAIKI, H., HIGUCHI, K., HOSOKAWA, M. and TAKEDA, T., 1989. Fluorometric determination of amyloid fibrils in vitro using the fluorescent dye, thioflavin T1. *Analytical Biochemistry*, 177, 244-249

NASSTROM, T., FAGERQVIST, T., BARBU, M., KARLSSON, M., NIKOLAJEFF, F., KASRAYAN, A., EKBERG, M., LANNFELT, L., INGELSSON, M. and BERGSTROM, J., 2011. The lipid peroxidation products 4-oxo-2-nonenal and 4-hydroxy-2-nonenal promote the formation of alpha-synuclein oligomers with distinct biochemical, morphological, and functional properties. *Free Radical Biology & Medicine*, 50, 428-437

NATALELLO, A., BENETTI, F., DOGLIA, S.M., LEGNAME, G. and GRANDORI, R., 2011. Compact conformations of alpha-synuclein induced by alcohols and copper. *Proteins*, 79, 611-621

NIU, S., RABUCK, J.N. and RUOTOLO, B.T., 2013. Ion mobility-mass spectrometry of intact protein-ligand complexes for pharmaceutical drug discovery and development. *Current Opinion in Chemical Biology*, S1367-5931(13)00119-1

NORRIS, E.H., GIASSON, B.I., HODARA, R., XU, S., TROJANOWSKI, J.Q., ISCHIROPOULOS, H. and LEE, V.M., 2005. Reversible inhibition of alpha-synuclein fibrillization by dopaminochrome-mediated conformational alterations. *The Journal of Biological Chemistry*, 280, 21212-21219

ONO, K., CONDRON, M.M. and TEPLOW, D.B., 2009. Structure-neurotoxicity relationships of amyloid beta-protein oligomers. *Proceedings of the National Academy of Sciences of the United States of America*, 106, 14745-14750

ONO, K. and YAMADA, M., 2006. Antioxidant compounds have potent anti-fibrillogenic and fibril-destabilizing effects for alpha-synuclein fibrils in vitro. *Journal of Neurochemistry*, 97, 105-115

OUESLATI, A., FOURNIER, M. and LASHUEL, H.A., 2010. Role of post-translational modifications in modulating the structure, function and toxicity of alpha-synuclein: implications for Parkinson's disease pathogenesis and therapies. *Progress in Brain Research*, 183, 115-145

OUESLATI, A., SCHNEIDER, B.L., AEBISCHER, P. and LASHUEL, H.A., 2013. Polo-like kinase 2 regulates selective autophagic alpha-synuclein clearance and suppresses its toxicity in vivo. *Proceedings of the National Academy of Sciences of the United States of America*, 110, E3945-E3954

OUTEIRO, T.F., KLUCKEN, J., BERCURY, K., TETZLAFF, J., PUTCHA, P., OLIVEIRA, L.M., QUINTAS, A., MCLEAN, P.J. and HYMAN, B.T., 2009. Dopamine-induced conformational changes in alpha-synuclein. *PloS One*, 4, e6906

PAIK, S.R., SHIN, H.J., LEE, J.H., CHANG, C.S. and KIM, J., 1999. Copper(II)-induced self-oligomerization of alpha-synuclein. *The Biochemical Journal*, 340 (Pt 3), 821-828.

PALL, H.S., WILLIAMS, A.C., BLAKE, D.R., LUNEC, J., GUTTERIDGE, J.M., HALL, M. and TAYLOR, A., 1987. Raised cerebrospinal-fluid copper concentration in Parkinson's disease. *Lancet*, 2, 238-241

PANDEY, N., STRIDER, J., NOLAN, W.C., YAN, S.X. and GALVIN, J.E., 2008. Curcumin inhibits aggregation of alpha-synuclein. *Acta Neuropathologica*, 115, 479-489

PENG, Y., WANG, C., XU, H.H., LIU, Y.N. and ZHOU, F., 2010. Binding of alpha-synuclein with Fe(III) and with Fe(II) and biological implications of the resultant complexes. *Journal of Inorganic Biochemistry*, 104, 365-37

POLITIS, A., PARK, A.Y., HALL, Z., RUOTOLO, B.T. and ROBINSON, C.V., 2013. Integrative Modelling Coupled with Ion Mobility Mass Spectrometry Reveals Structural Features of the Clamp Loader in Complex with Single-Stranded DNA Binding Protein. *Journal of Molecular Biology*, S0022-2836(13)00235-0

POLITIS, A., PARK, A.Y., HYUNG, S.J., BARSKY, D., RUOTOLO, B.T. and ROBINSON, C.V., 2010. Integrating ion mobility mass spectrometry with molecular modelling to determine the architecture of multiprotein complexes. *PloS One*, 5, e12080

POLYMEROPOULOS, M.H., LAVEDAN, C., LEROY, E., IDE, S.E., DEHEJIA, A., DUTRA, A., PIKE, B., ROOT, H., RUBENSTEIN, J., BOYER, R., STENROOS, E.S., CHANDRASEKHARAPPA, S., ATHANASSIADOU, A., PAPAPETROPOULOS, T., JOHNSON, W.G., LAZZARINI, A.M., DUVOISIN, R.C., DI IORIO, G., GOLBE, L.I. and NUSSBAUM, R.L., 1997. Mutation in the alpha-synuclein gene identified in families with Parkinson's disease. *Science* 276, 2045-2047

PROUKAKIS, C., DUDZIK, C.G., BRIER, T., MACKAY, D.S., COOPER, J.M., MILLHAUSER, G. L., HOULDEN, H. and SCHAPIRA, A. H., 2013. A novel alpha-synuclein missense mutation in Parkinson's disease, *Neurology*, 80, 1062-1064

PRUSINER, S.B., 2012. Cell biology. A unifying role for prions in neurodegenerative diseases. *Science,* 336, 1511-1513

QUIST, A., DOUDEVSKI, I., LIN, H., AZIMOVA, R., NG, D., FRANGIONE, B., KAGAN, B., GHISO, J. and LAL, R., 2005. Amyloid ion channels: a common structural link for protein-misfolding disease. *Proceedings of the National Academy of Sciences of the United States of America*, 102, 10427-10432

RASIA, R.M., BERTONCINI, C.W., MARSH, D., HOYER, W., CHERNY, D., ZWECKSTETTER, M., GRIESINGER, C., JOVIN, T.M. and FERNANDEZ, C.O., 2005. Structural characterization of copper(II) binding to alpha-synuclein: Insights into the bioinorganic chemistry of Parkinson's disease. *Proceedings of the National Academy of Sciences of the United States of America*, 102, 4294-4299

RAYLEIGH, L., 1882. On the equilibrium of liquid conducting masses charged with electricity. *Philos Mag*, 5, 184-186

REKAS, A., KNOTT, R.B., SOKOLOVA, A., BARNHAM, K.J., PEREZ, K.A., MASTERS, C.L., DREW, S.C., CAPPAI, R., CURTAIN, C.C. and PHAM, C.L., 2010. The structure of dopamine induced alpha-synuclein oligomers. *European Biophysics Journal : EBJ*, 39, 1407-1419

REVERCOMB, H.E. and MASON, E.A., 1975. Theory of plasma chromatography/ gaseous electrophoresis-a review. *Analytical Chemistry*, 47, 970-983.

REZNICHENKO, L., CHENG, Q., NIZAR, K., GRATIY, S.L., SAISAN, P.A., ROCKENSTEIN, E.M., GONZALEZ, T., PATRICK, C., SPENCER, B., DESPLATS, P., DALE, A.M., DEVOR, A. and MASLIAH, E., 2012. In vivo alterations in calcium buffering capacity in transgenic mouse model of synucleinopathy. *The Journal of Neuroscience : The Official Journal of the Society for Neuroscience*, 32, 9992-9998

RIEDERER, P., SOFIC, E., RAUSCH, W.D., SCHMIDT, B., REYNOLDS, G.P., JELLINGER, K. and YOUDIM, M.B., 1989. Transition metals, ferritin, glutathione, and ascorbic acid in parkinsonian brains. *Journal of Neurochemistry*, 52, 515-520

ROCHET, J.C., OUTEIRO, T.F., CONWAY, K.A., DING, T.T., VOLLES, M.J., LASHUEL, H.A., BIEGANSKI, R.M., LINDQUIST, S.L. and LANSBURY, P.T., 2004. Interactions among alpha-synuclein, dopamine, and biomembranes: some clues for understanding neurodegeneration in Parkinson's disease. *Journal of Molecular Neuroscience: MN*, 23, 23-34

ROOSTAEE, A., BEAUDOIN, S., STASKEVICIUS, A. and ROUCOU, X., 2013. Aggregation and neurotoxicity of recombinant alpha-synuclein aggregates initiated by dimerization. *Molecular Neurodegeneration*, 8, 5-1326-8-5

ROSU, F., DE PAUW, E. and GABELICA, V., 2008. Electrospray mass spectrometry to study drug-nucleic acids interactions. *Biochimie*, 90, 1074-1087

RUIPEREZ, V., DARIOS, F. and DAVLETOV, B., 2010. Alpha-synuclein, lipids and Parkinson's disease. *Progress in Lipid Research*, 49, 420-428

RUOTOLO, B.T., BENESCH, J.L., SANDERCOCK, A.M., HYUNG, S.J. and ROBINSON, C.V., 2008. Ion mobility-mass spectrometry analysis of large protein complexes. *Nature Protocols*, 3, 1139-1152

RUOTOLO, B.T., GILES, K., CAMPUZANO, I., SANDERCOCK, A.M., BATEMAN, R.H. and ROBINSON, C.V., 2005. Evidence for macromolecular protein rings in the absence of bulk water. *Science,* 310, 1658-1661

RUOTOLO, B.T., HYUNG, S.J., ROBINSON, P.M., GILES, K., BATEMAN, R.H. and ROBINSON, C.V., 2007. Ion mobility-mass spectrometry reveals long-lived, unfolded intermediates in the dissociation of protein complexes. *Angewandte Chemie,* 46, 8001-8004

SALAMEKH, S., BRENDER, J.R., HYUNG, S.J., NANGA, R.P., VIVEKANANDAN, S., RUOTOLO, B.T. and RAMAMOORTHY, A., 2011. A two-site mechanism for the inhibition of IAPP amyloidogenesis by zinc. *Journal of Molecular Biology*, 410, 294-306

SAMALIKOVA, M. and GRANDORI, R., 2003. Role of opposite charges in protein electrospray ionization mass spectrometry. *Journal of Mass Spectrometry: JMS*, Sep, 38, 941-947

SAMALIKOVA, M., MATECKO, I., MULLER, N. and GRANDORI, R., 2004. Interpreting conformational effects in protein nano-ESI-MS spectra. *Analytical and Bioanalytical Chemistry*, 378, 1112-1123

SANTAMBROGIO, C., RICAGNO, S., SOBOTT, F., COLOMBO, M., BOLOGNESI, M. and GRANDORI, R., 2011. Characterization of beta2-microglobulin conformational intermediates associated to different fibrillation conditions. *Journal of Mass Spectrometry: JMS*, 46, 734-741

SANTNER, A. and UVERSKY, V.N., 2010. Metalloproteomics and metal toxicology of alpha-synuclein. *Metallomics: Integrated Biometal Science*, 2, 378-392

SAPER, M.A., BJORKMAN, P.J. and WILEY, D.C., 1991. Refined structure of the human histocompatibility antigen HLA-A2 at 2.6 A resolution. *Journal of Molecular Biology*, 219, 277-319

SCARFF, C.A., THALASSINOS, K., HILTON, G.R. and SCRIVENS, J.H., 2008. Travelling wave ion mobility mass spectrometry studies of protein structure: biological significance and comparison with X-ray crystallography and nuclear magnetic resonance spectroscopy measurements. *Rapid Communications in Mass Spectrometry: RCM*, 22, 3297-3304

SCHNIER, P., GROSS, D. and WILLIAMS, E., 1995. On the maximum charge state and proton transfer reactivity of peptide and protein ions formed by electrospray ionisation. *Journal of the American Society for Mass Spectrometry*, 6, 1086-1097.

SELKOE, D.J., 2011. Alzheimer's disease. *Cold Spring Harbor Perspectives in Biology*, 3, 10.1101/cshperspect.a004457

SEO, J.H., RAH, J.C., CHOI, S.H., SHIN, J.K., MIN, K., KIM, H.S., PARK, C.H., KIM, S., KIM, E.M., LEE, S.H., LEE, S., SUH, S.W. and SUH, Y.H., 2002. Alpha-synuclein regulates neuronal survival via Bcl-2 family expression and PI3/Akt kinase pathway. *FASEB Journal : Official Publication of the Federation of American Societies for Experimental Biology*, 16, 1826-1828

SERPELL, L.C., BERRIMAN, J., JAKES, R., GOEDERT, M. and CROWTHER, R.A., 2000. Fiber diffraction of synthetic alpha-synuclein filaments shows amyloid-like cross-beta conformation. *Proceedings of the National Academy of Sciences of the United States of America*, 97, 4897-4902

SHEPHERD, D.A., VEESLER, D., LICHIERE, J., ASHCROFT, A.E. and CAMBILLAU, C., 2011. Unraveling lactococcal phage baseplate assembly by mass spectrometry. *Molecular & Cellular Proteomics: MCP*, 10, M111.009787

SHIMOTAKAHARA, S., SHIROYAMA, Y., FUJIMOTO, T., AKAI, M., ONOUE, T., SEKI, H., KADO, S., MACHINAMI, T., SHIBUSAWA, Y., UÉDA, K. and TASHIRO, M., 2012. Demonstration of three dopamine molecules bound to α-Synuclein: Implication of oligomerization at the initial stage. *Journal of Biophysical Chemistry*, 3, 149-155.

SHULTS, C.W., 2006. Lewy bodies. *Proceedings of the National Academy of Sciences of the United States of America*, 103, 1661-1668

SHVARTSBURG, A.A., SCHALTZ, A.A. and JARROLD, M.F., 1998. Mobilities of carbon cluster ions: Critical importance of the molecular attractive potential. *J Chem Phys*, 108, 2416-2424.

SHVARTSBURG, A., A. and JARROLD, M., F., 1996. An exact hard-spheres scattering model for the mobilities of polyatomic ions. *Chem. Phys. Lett.*, 261, 89-91.

SHVARTSBURG, A.A., CREESE, A.J., SMITH, R.D. and COOPER, H.J., 2010. Separation of peptide isomers with variant modified sites by high-resolution differential ion mobility spectrometry. *Analytical Chemistry*, 82, 8327-8334

SHVARTSBURG, A.A., MASHKEVICH, S.V., BAKER, E.S. and SMITH, R.D., 2007. Optimization of algorithms for ion mobility calculations. *The Journal of Physical Chemistry.A*, 111, 2002-2010

SHVARTSBURG, A.A. and SMITH, R.D., 2008. Fundamentals of traveling wave ion mobility spectrometry. *Analytical Chemistry*, 80, 9689-9699

SILVA, B.A., BREYDO, L., FINK, A.L. and UVERSKY, V.N., 2013. Agrochemicals, alpha-synuclein, and Parkinson's disease. *Molecular Neurobiology*, 47, 598-612

SINGH, P.K., KOTIA, V., GHOSH, D., MOHITE, G.M., KUMAR, A. and MAJI, S.K., 2013. Curcumin modulates alpha-synuclein aggregation and toxicity. *ACS Chemical Neuroscience*, 4, 393-407

SINGLETON, A.B., FARRER, M., JOHNSON, J., SINGLETON, A., HAGUE, S., KACHERGUS, J., HULIHAN, M., PEURALINNA, T., DUTRA, A., NUSSBAUM, R., LINCOLN, S., CRAWLEY, A., HANSON, M., MARAGANORE, D., ADLER, C., COOKSON, M.R., MUENTER, M., BAPTISTA, M., MILLER, D., BLANCATO, J., HARDY, J. and GWINN-HARDY, K., 2003. alpha-Synuclein locus triplication causes Parkinson's disease. *Science,* 302, 841

SINHA, S. and LIEBERBURG, I., 1999. Cellular mechanisms of beta-amyloid production and secretion. *Proceedings of the National Academy of Sciences of the United States of America*, 96, 11049-11053

SMITH, A.M., JAHN, T.R., ASHCROFT, A.E. and RADFORD, S.E., 2006. Direct observation of oligomeric species formed in the early stages of amyloid fibril formation using electrospray ionisation mass spectrometry. *Journal of Molecular Biology*, 364, 9-19

SMITH, D.P., GILES, K., BATEMAN, R.H., RADFORD, S.E. and ASHCROFT, A.E., 2007. Monitoring copopulated conformational states during protein folding events using electrospray ionization-ion mobility spectrometry-mass spectrometry. *Journal of the American Society for Mass Spectrometry*, 18, 2180-2190

SMITH, D.P., KNAPMAN, T.W., CAMPUZANO, I., MALHAM, R.W., BERRYMAN, J.T., RADFORD, S.E. and ASHCROFT, A.E., 2009. Deciphering drift time measurements from travelling wave ion mobility spectrometry-mass spectrometry studies. *European Journal of Mass Spectrometry,* 15, 113-130 I

SMITH, D.P., RADFORD, S.E. and ASHCROFT, A.E., 2010. Elongated oligomers in beta2-microglobulin amyloid assembly revealed by ion mobility spectrometry-mass spectrometry. *Proceedings of the National Academy of Sciences of the United States of America*, 107, 6794-6798

SMITH, D.P., TEW, D.J., HILL, A.F., BOTTOMLEY, S.P., MASTERS, C.L., BARNHAM, K.J. and CAPPAI, R., 2008. Formation of a high affinity lipid-binding intermediate during the early aggregation phase of alpha-synuclein. *Biochemistry*, 47, 1425-1434

SOPER, M.T., DETOMA, A.S., HYUNG, S.J., LIM, M.H. and RUOTOLO, B.T., 2013. Amyloid-beta-neuropeptide interactions assessed by ion mobility-mass spectrometry. *Physical Chemistry Chemical Physics: PCCP*, 15, 8952-8961

SPILLANTINI, M.G., 1999. Parkinson's disease, dementia with Lewy bodies and multiple system atrophy are alpha-synucleinopathies. *Parkinsonism & Related Disorders*, 5, 157-162

SPILLANTINI, M.G., SCHMIDT, M.L., LEE, V.M., TROJANOWSKI, J.Q., JAKES, R. and GOEDERT, M., 1997. Alpha-synuclein in Lewy bodies. *Nature*, 388, 839-840

STERLING, H.J., CASSOU, C.A., SUSA, A.C. and WILLIAMS, E.R., 2012. Electrothermal supercharging of proteins in native electrospray ionization. *Analytical Chemistry*, 84, 3795-3801

STERLING, H.J., CASSOU, C.A., TRNKA, M.J., BURLINGAME, A.L., KRANTZ, B.A. and WILLIAMS, E.R., 2011. The role of conformational flexibility on protein supercharging in native electrospray ionization. *Physical Chemistry Chemical Physics: PCCP*, 13, 18288-18296

STOCKL, M., CLAESSENS, M.M. and SUBRAMANIAM, V., 2012. Kinetic measurements give new insights into lipid membrane permeabilization by alpha-synuclein oligomers. *Molecular bioSystems*, 8, 338-345

STOCKL, M.T., ZIJLSTRA, N. and SUBRAMANIAM, V., 2013. Alpha-synuclein oligomers: an amyloid pore? Insights into mechanisms of alpha-synuclein oligomer-lipid interactions. *Molecular Neurobiology*, 47, 613-621

STSIAPURA, V.I., MASKEVICH, A.A., KUZMITSKY, V.A., UVERSKY, V.N., KUZNETSOVA, I.M. and TUROVEROV, K.K., 2008. Thioflavin T as a molecular rotor: fluorescent properties of thioflavin T in solvents with different viscosity. *The Journal of Physical Chemistry.B*, 112, 15893-15902

TAKAHASHI, T. and MIHARA, H., 2008. Peptide and protein mimetics inhibiting amyloid beta-peptide aggregation. *Accounts of Chemical Research*, 41, 1309-1318

TANG, L. and KEBARLE, P., 1993. Dependence of ion intensity in electrospray mass spectrometry on the concentration of analytes in the electrosprayed solution. *Anal.Chem.*, 65, 3654-3668.

THOMSON, B.A. and IRIBARNE, J.V., 1979. Field induced ion evaporation from liquid surfaces at atmospheric pressure. *J Chem Phys*, 71, 4451-4463.

TOKUDA, T., QURESHI, M.M., ARDAH, M.T., VARGHESE, S., SHEHAB, S.A., KASAI, T., ISHIGAMI, N., TAMAOKA, A., NAKAGAWA, M. and EL-AGNAF, O.M., 2010. Detection of elevated levels of alpha-synuclein oligomers in CSF from patients with Parkinson disease. *Neurology*, 75, 1766-1772

TOLEDO, J.B., KORFF, A., SHAW, L.M., TROJANOWSKI, J.Q. and ZHANG, J., 2013. CSF alpha-synuclein improves diagnostic and prognostic performance of CSF tau and Abeta in Alzheimer's disease. *Acta Neuropathologica,* ahead of print

TOMPKINS, M.M. and HILL, W.D., 1997. Contribution of somal Lewy bodies to neuronal death. *Brain Research,* 775, 24-29

TSIGELNY, I.F., CREWS, L., DESPLATS, P., SHAKED, G.M., SHARIKOV, Y., MIZUNO, H., SPENCER, B., ROCKENSTEIN, E., TREJO, M., PLATOSHYN, O., YUAN, J.X. and MASLIAH, E., 2008. Mechanisms of hybrid oligomer formation in the pathogenesis of combined Alzheimer's and Parkinson's diseases. *PloS One,* 3, e3135

UEDA, K., FUKUSHIMA, H., MASLIAH, E., XIA, Y., IWAI, A., YOSHIMOTO, M., OTERO, D.A., KONDO, J., IHARA, Y. and SAITOH, T., 1993. Molecular cloning of cDNA encoding an unrecognized component of amyloid in Alzheimer disease. *Proceedings of the National Academy of Sciences of the United States of America,* 90, 11282-11286.

UETRECHT, C., BARBU, I.M., SHOEMAKER, G.K., VAN DUIJN, E. and HECK, A.J., 2011. Interrogating viral capsid assembly with ion mobility-mass spectrometry. *Nature Chemistry,* 3, 126-132

UETRECHT, C., ROSE, R.J., VAN DUIJN, E., LORENZEN, K. and HECK, A.J., 2010. Ion mobility mass spectrometry of proteins and protein assemblies. *Chemical Society Reviews,* 39, 1633-1655

ULLMAN, O., FISHER, C.K. and STULTZ, C.M., 2011. Explaining the structural plasticity of alpha-synuclein. *Journal of the American Chemical Society,* 20111114, 133, 19536-19546

University of Bristol, School of Chemistry, http://www.chm.bris.ac.uk/ms/imaqes/esi-mechanism.qif.

UVERSKY, V.N., 2008. Amyloidogenesis of natively unfolded proteins. *Current Alzheimer Research,* 5, 260-287

UVERSKY, V.N. and ELIEZER, D., 2009. Biophysics of Parkinson's disease: structure and aggregation of alpha-synuclein. *Current Protein & Peptide Science,* 10, 483-499

UVERSKY, V.N., GILLESPIE, J.R. and FINK, A.L., 2000. Why are "natively unfolded" proteins unstructured under physiologic conditions?. *Proteins,* 41, 415-427

UVERSKY, V.N., LEE, H.J., LI, J., FINK, A.L. and LEE, S.J., 2001. Stabilization of partially folded conformation during alpha-synuclein oligomerization in both

purified and cytosolic preparations. *The Journal of Biological Chemistry*, 276, 43495-43498

UVERSKY, V.N., LI, J., BOWER, K. and FINK, A.L., 2002. Synergistic effects of pesticides and metals on the fibrillation of alpha-synuclein: implications for Parkinson's disease. *Neurotoxicology*, 23, 527-536

UVERSKY, V.N., LI, J. and FINK, A.L., 2001a. Evidence for a partially folded intermediate in alpha-synuclein fibril formation. *The Journal of Biological Chemistry*, 276, 10737-10744

UVERSKY, V.N., LI, J. and FINK, A.L., 2001b. Evidence for a partially folded intermediate in alpha-synuclein fibril formation. *The Journal of Biological Chemistry*, 276, 10737-10744

UVERSKY, V.N., LI, J. and FINK, A.L., 2001c. Metal-triggered structural transformations, aggregation, and fibrillation of human alpha-synuclein. A possible molecular NK between Parkinson's disease and heavy metal exposure. *The Journal of Biological Chemistry*, 276, 44284-44296

UVERSKY, V.N., LI, J. and FINK, A.L., 2001d. Trimethylamine-N-oxide-induced folding of alpha-synuclein. *FEBS Letters*, 509, 31-35

UVERSKY, V.N., LI, J., SOUILLAC, P., MILLETT, I.S., DONIACH, S., JAKES, R., GOEDERT, M. and FINK, A.L., 2002. Biophysical properties of the synucleins and their propensities to fibrillate: inhibition of alpha-synuclein assembly by beta- and gamma-synucleins. *The Journal of Biological Chemistry*, 277, 11970-11978

VALENSIN, D., CAMPONESCHI, F., LUCZKOWSKI, M., BARATTO, M.C., REMELLI, M., VALENSIN, G. and KOZLOWSKI, H., 2011. The role of His-50 of alpha-synuclein in binding Cu(II): pH dependence, speciation, thermodynamics and structure. *Metallomics : Integrated Biometal Science*, 3, 292-302

VALENTINE, S.J., COUNTERMAN, A.E. and CLEMMER, D.E., 1999. A database of 660 peptide ion cross sections: use of intrinsic size parameters for bona fide predictions of cross sections. *Journal of the American Society for Mass Spectrometry*, 10, 1188-1211

VAN ROOIJEN, B.D., CLAESSENS, M.M. and SUBRAMANIAM, V., 2010. Membrane Permeabilization by Oligomeric alpha-Synuclein: In Search of the Mechanism. *PloS One*, 5, e14292

VASSAR, P.S. and CULLING, C.F., 1959. Fluorescent stains, with special reference to amyloid and connective tissues. *Archives of Pathology*, 68, 487-498

VLAD, K., IURASCU, M.I., SLAMNOIU, S., HENGERER, B. and PRZYBYLSKI, M., 2012. Characterisation of oligomerization-aggregation products of

neurodegenerative target proteins by ion mobility mass spectrometry. *Intrinsically Disordered Protein Analysis; Methods and Experimental Tools*, 2, 399-412.

VLAD, C., LINDNER, K., KARREMAN, C., SCHILDKNECHT, S., LEIST, M., TOMCZYK, N., RONTREE, J., LANGRIDGE, J., DANZER, K., CIOSSEK, T., PETRE, A., GROSS, M.L., HENGERER, B. and PRZYBYLSKI, M., 2011. Autoproteolytic fragments are intermediates in the oligomerization/aggregation of the Parkinson's disease protein alpha-synuclein as revealed by ion mobility mass spectrometry. *Chembiochem: A European Journal of Chemical Biology*, 12, 2740-2744

VOLLES, M.J., LEE, S.J., ROCHET, J.C., SHTILERMAN, M.D., DING, T.T., KESSLER, J.C. and LANSBURY, P.T.,Jr, 2001. Vesicle permeabilization by protofibrillar alpha-synuclein: implications for the pathogenesis and treatment of Parkinson's disease. *Biochemistry*, 40, 7812-7819

VON HELDEN, G., GOTTS, N., G. and BOWERS, M., T., 1993. Experimental evidence for the formation of fullerenes by collisional heating of carbon rings in the gas phase. *Nature*, 363, 60-63.

VON HELDEN, G., HSU, M., KEMPER., P.R. and BOWERS, M.T., 1991. Strucutres of carbon cluster ions from 3 to 60 atoms: Linears to rings to fullerenes. *J Chem Phys*, 95, 3835-3838.

WAKABAYASHI, K., TANJI, K., ODAGIRI, S., MIKI, Y., MORI, F. and TAKAHASHI, H., 2013. The Lewy body in Parkinson's disease and related neurodegenerative disorders. *Molecular Neurobiology*, 7, 495-508

WALL, J.S., KENNEL, S.J., WILLIAMS, A., RICHEY, T., STUCKEY, A., HUANG, Y., MACY, S., DONNELL, R., BARBOUR, R., SEUBERT, P. and SCHENK, D., 2012. AL amyloid imaging and therapy with a monoclonal antibody to a cryptic epitope on amyloid fibrils. *PloS One*, 7, e52686 ISSN

WANG, C., LIU, L., ZHANG, L., PENG, Y. and ZHOU, F., 2010a. Redox reactions of the α-Synuclein-Cu^{2+} complex and their effects on neuronal cell viability, *Biochemisty*, 49, 8134-8142

WANG, H.G., PATHAN, N., ETHELL, I.M., KRAJEWSKI, S., YAMAGUCHI, Y., SHIBASAKI, F., MCKEON, F., BOBO, T., FRANKE, T.F. and REED, J.C., 1999. Ca^{2+}-induced apoptosis through calcineurin dephosphorylation of BAD. *Science*, 284, 339-343

WANG, M.S., BODDAPATI, S., EMADI, S. and SIERKS, M.R., 2010b. Curcumin reduces alpha-synuclein induced cytotoxicity in Parkinson's disease cell model. *BMC Neuroscience*, 11, 57

WANG, X., BOWERS, S.L., WANG, F., PU, X.A., NELSON, R.J. and MA, J., 2009. Cytoplasmic prion protein induces forebrain neurotoxicity. *Biochimica Et Biophysica Acta*, 1792, 555-563

WANG, X., MOUALLA, D., WRIGHT, J.A. and BROWN, D.R., 2010c. Copper binding regulates intracellular alpha-synuclein localisation, aggregation and toxicity. *Journal of Neurochemistry*, 113, 704-714

WATABE, M. and NAKAKI, T., 2007. Mitochondrial complex I inhibitor rotenone-elicited dopamine redistribution from vesicles to cytosol in human dopaminergic SH-SY5Y cells. *The Journal of Pharmacology and Experimental Therapeutics*, 323, 499-507

WESTERMARK, P., BENSON, M.D., BUXBAUM, J.N., COHEN, A.S., FRANGIONE, B., IKEDA, S., MASTERS, C.L., MERLINI, G., SARAIVA, M.J. and SIPE, J.D., 2007. A primer of amyloid nomenclature. *Amyloid : The International Journal of Experimental and Clinical Investigation: The Official Journal of the International Society of Amyloidosis*, 14, 179-183

WESTERMARK, P., BENSON, M.D., BUXBAUM, J.N., COHEN, A.S., FRANGIONE, B., IKEDA, S., MASTERS, C.L., MERLINI, G., SARAIVA, M.J., SIPE, J.D. and Nomenclature Committee of the International Society of Amyloidosis, 2005. Amyloid: toward terminology clarification. Report from the Nomenclature Committee of the International Society of Amyloidosis. *Amyloid : The International Journal of Experimental and Clinical Investigation: The Official Journal of the International Society of Amyloidosis*, 12, 1-4

WINNER, B., JAPPELLI, R., MAJI, S.K., DESPLATS, P.A., BOYER, L., AIGNER, S., HETZER, C., LOHER, T., VILAR, M., CAMPIONI, S., TZITZILONIS, C., SORAGNI, A., JESSBERGER, S., MIRA, H., CONSIGLIO, A., PHAM, E., MASLIAH, E., GAGE, F.H. and RIEK, R., 2011. In vivo demonstration that alpha-synuclein oligomers are toxic. *Proceedings of the National Academy of Sciences of the United States of America*, 108, 4194-4199

WOOD, S.J., WYPYCH, J., STEAVENSON, S., LOUIS, J.C., CITRON, M. and BIERE, A.L., 1999. alpha-synuclein fibrillogenesis is nucleation-dependent. Implications for the pathogenesis of Parkinson's disease. *The Journal of Biological Chemistry*, 274, 19509-19512

WOOD-KACZMAR, A., GANDHI, S. and WOOD, N.W., 2006. Understanding the molecular causes of Parkinson's disease. *Trends in Molecular Medicine*, 12, 521-528

WOODS, L.A., RADFORD, S.E. and ASHCROFT, A.E., 2012. Advances in ion mobility spectrometry-mass spectrometry reveal key insights into amyloid assembly. *Biochimica Et Biophysica Acta*, 1834, 1257-1268

WRIGHT, J.A., WANG, X. and BROWN, D.R., 2009. Unique copper-induced oligomers mediate alpha-synuclein toxicity. *FASEB Journal : Official Publication*

of the Federation of American Societies for Experimental Biology, 23, 2384-2393

WYTTENBACH, T. and BOWERS, M.T., 2011. Structural stability from solution to the gas phase: native solution structure of ubiquitin survives analysis in a solvent-free ion mobility-mass spectrometry environment. *The Journal of Physical Chemistry.B*, 115, 12266-12275

WYYTENBACH, T., VON HELDEN, G., BATKA, J.J., CARLAT, D. and BOWERS, M.T., 1997. Effect of Long-Range Potential on Ion Mobility Mearurements. *J.Am.Soc.Mass Spectrom.*, 8, 275-282.

XIE, Y., ZHANG, J., YIN, S. and LOO, J.A., 2006. Top-down ESI-ECD-FT-ICR mass spectrometry localizes noncovalent protein-ligand binding sites. *Journal of the American Chemical Society*, 128, 14432-14433

YAMIN, G., UVERSKY, V.N. and FINK, A.L., 2003. Nitration inhibits fibrillation of human alpha-synuclein in vitro by formation of soluble oligomers. *FEBS Letters*, 542, 147-152

YANAMANDRA, K., GRUDEN, M.A., CASAITE, V., MESKYS, R., FORSGREN, L. and MOROZOVA-ROCHE, L.A., 2011. alpha-synuclein reactive antibodies as diagnostic biomarkers in blood sera of Parkinson's disease patients. *PloS One*, 6, e18513

YANG, X., ASKAROVA, S., SHENG, W., CHEN, J.K., SUN, A.Y., SUN, G.Y., YAO, G. and LEE, J.C., 2010. Low energy laser light (632.8 nm) suppresses amyloid-beta peptide-induced oxidative and inflammatory responses in astrocytes. *Neuroscience*, 171, 859-868

YAVICH, L., TANILA, H., VEPSALAINEN, S. and JAKALA, P., 2004. Role of alpha-synuclein in presynaptic dopamine recruitment. *The Journal of Neuroscience : The Official Journal of the Society for Neuroscience*, 24, 11165-11170

YOU, B.R. and PARK, W.H., 2013. Zebularine inhibits the growth of A549 lung cancer cells via cell cycle arrest and apoptosis. *Molecular Carcinogenesis*, ahead of print

ZAKHAROV, S.D., HULLEMAN, J.D., DUTSEVA, E.A., ANTONENKO, Y.N., ROCHET, J.C. and CRAMER, W.A., 2007. Helical alpha-synuclein forms highly conductive ion channels. *Biochemistry*, 46, 14369-14379

ZARRANZ, J.J., ALEGRE, J., GOMEZ-ESTEBAN, J.C., LEZCANO, E., ROS, R., AMPUERO, I., VIDAL, L., HOENICKA, J., RODRIGUEZ, O., ATARES, B., LLORENS, V., GOMEZ TORTOSA, E., DEL SER, T., MUNOZ, D.G. and DE YEBENES, J.G., 2004. The new mutation, E46K, of alpha-synuclein causes Parkinson and Lewy body dementia. *Annals of Neurology*, 55, 164-173

ZHONG, Y., HYUNG, S.J. and RUOTOLO, B.T., 2011. Characterizing the resolution and accuracy of a second-generation traveling-wave ion mobility separator for biomolecular ions. *The Analyst*, 136, 3534-3541

ZHOU, M., HUANG, C. and WYSOCKI, V.H., 2012. Surface-induced dissociation of ion mobility-separated noncovalent complexes in a quadrupole/time-of-flight mass spectrometer. *Analytical Chemistry*, 84, 6016-6023

ZHOU, W., LONG, C., REANEY, S.H., DI MONTE, D.A., FINK, A.L. and UVERSKY, V.N., 2010a. Methionine oxidation stabilizes non-toxic oligomers of alpha-synuclein through strengthening the auto-inhibitory intra-molecular long-range interactions. *Biochimica Et Biophysica Acta*, 1802, 322-330

ZHOU, W., LONG, C., REANEY, S.H., DI MONTE, D.A., FINK, A.L. and UVERSKY, V.N., 2010b. Methionine oxidation stabilizes non-toxic oligomers of alpha-synuclein through strengthening the auto-inhibitory intra-molecular long-range interactions. *Biochimica Et Biophysica Acta*, 1802, 322-330

ZHU, M., HAN, S. and FINK, A.L., 2013. Oxidized quercetin inhibits alpha-synuclein fibrillization. *Biochimica Et Biophysica Acta*,1830, 2872-2881

8 APPENDIX

8.1 Protein expression in *E. coli* and purification

A

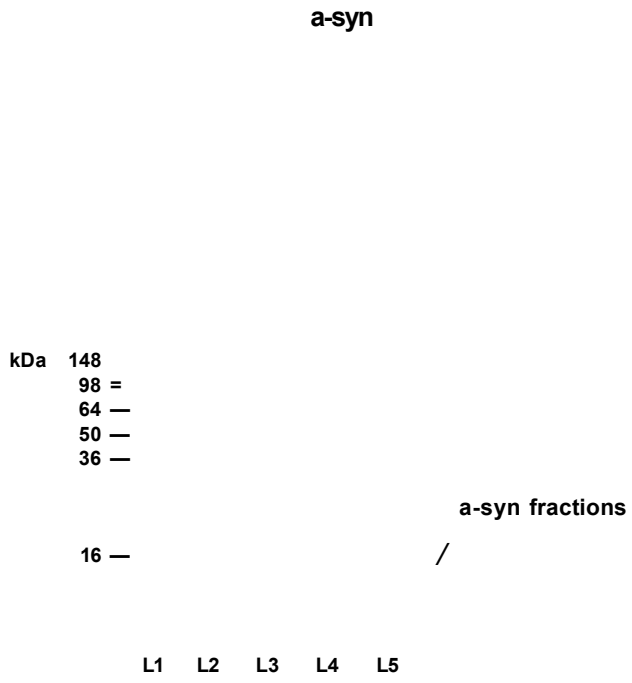

B

8-:

a-syn

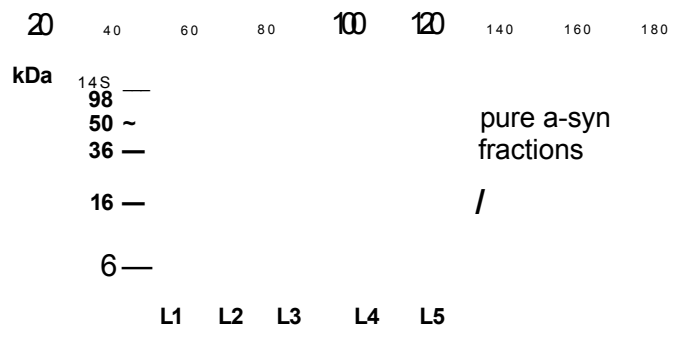

Figure 8.1. ***A*** *shows the Q- Sepharose anion exchange profile of the crude WT α-syn including a linear salt gradient marked with a green line and corresponding conductivity increase (red line) across the blue trace ($OD_{214\ nm}$) eluted on the AKTA purifier. The pooled fractions (L2-L5) were resolved on an SDS PAGE and stained with Coomassie dye and destained subsequently to reveal the monomeric protein with <16 kDa mass.* ***B*** *is a High Load 26/90 Superdex TM 75 Prep Grade gelfiltration trace and the resultant pooled fractions analysed by SDS-PAGE and Coomassie staining protocol, yielding pure monomeric α-syn. The protein then underwent dialysis and freeze drying before storage at -20 °C for ≤3 months.*

Figure 8.2. *ESI-IMS-MS spectrum of monomeric a-syn with the corresponding charge states, where charge states of less prevalent dimers is shown in italics (A). B is a Western blot of a-syn probed with rabbit polyclonal full length antibody developed in the Licor fluorescent system using a CW conjugated polyclonal anti-rabbit IgG (H+L) at 800 nm.*

8.2 Size exclusion chromatography

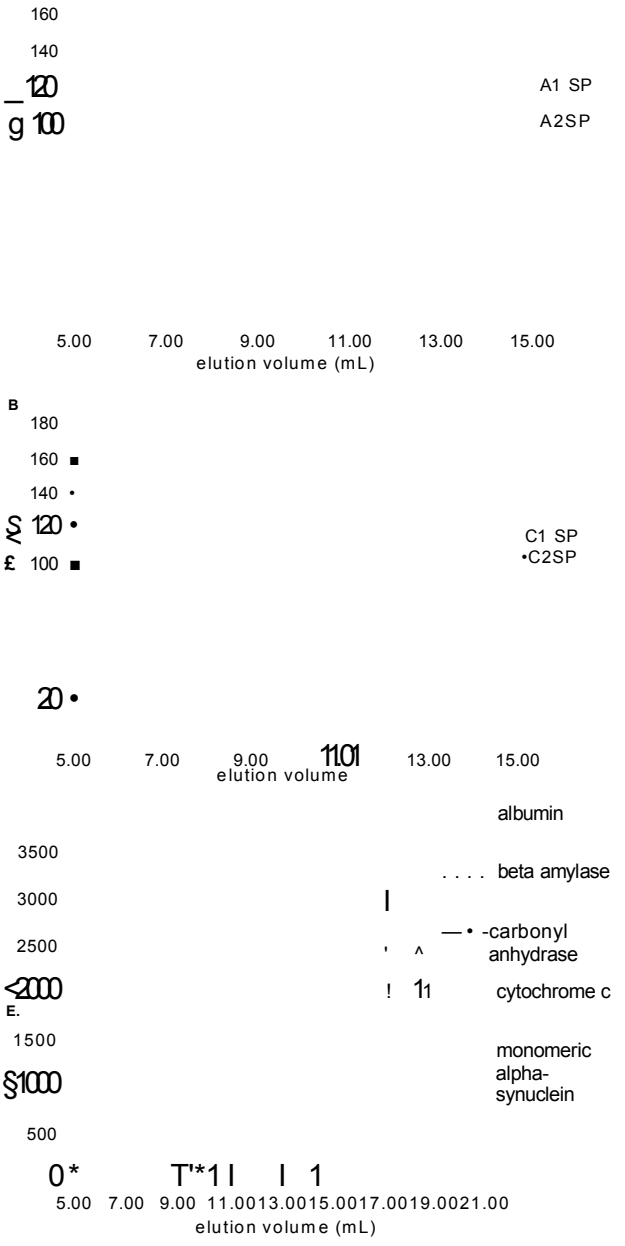

Figure 8.3. *SEC chromatography traces of A1 and A2 SP oligomers (A) and SEC traces of type C1 and C2 oligomers (B) on a Superdex 200 100/300 GL column (GE Healthcare) in 50 mM SP buffer, pH 7.2. C shows the elution profile of the monomeric protein (MW: 14.6 kDa) marked with continuous black line in relation to other globular standards in 25 mM Tris buffer with 10 mM NaCl, pH 8.0.*

Two oligomeric populations were observed in type A oligomers prepared in SP, one eluting at ~6.5 ml and another eluting ~7.5 mL in addition to a population eluting >12.5-15 mL which represented the remnants of the monomer. For type C oligomers, an oligomeric population eluted at ~8 mL and another dominant population eluted ~10 mL that could be a lower order, higher yield oligomeric population i.e. dimers and trimers and noticeably the monomeric protein peak was no longer observable, probably due to the use of 30,000 Da spin concentrator that allows retention of only higher MW species above the cut off limit.

SEC of MW standards was performed Superdex 200 100/300 GL column (GE Healthcare). Discontinuous green line represents beta amylase from sweet potato (MW: 200 kDa), dotted pink line represents albumin from bovine serum (MW: 66 kDa), purple discontinuous purple line represents carbonyl anhydrase from bovine erythrocyte (MW: 29 kDa), discontinuous brown line depicts cytochrome c from horse heart (MW: 12.5 kDa). It is evident that the natively unfolded monomeric protein elutes later than that would be expected for its MW close to the carbonyl anhydrase with a globular structure and mass of 39.5 kDa. This aberrant elution profile with apparently larger hydrodynamic radii has been widely documented and consistent with those observations by Conway *et al.* (Conway *et al.* 2000). Additionally, the monomer perhaps underwent some structural rearrangements or oxidisation during the different types of oligomer preparation protocols that may have caused a structural collapse with shorter elution volumes in case of type A, however the elution buffers were also different not allowing to draw conclusions.

8.3 ThT emission spectra and dot blotting of a-syn fibrils

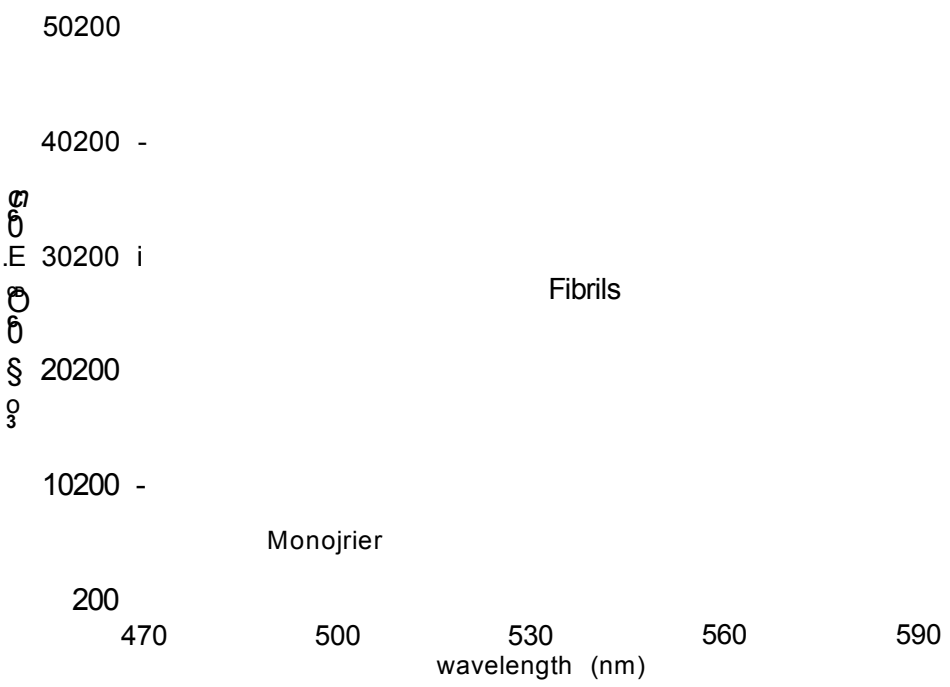

Figure 8.4. *Fluorescence emission spectra of monomeric protein and fibrils (after 7 day agitation at 37 °C) after ThT buffer subtraction at 470-600 nm in triplicates. All samples were dissolved in 20 mM Tris buffer at pH 7.2. A quantum yield increase (~250-fold) is seen in case of mature fibrils (dotted lines) when compared with 7 pM monomeric a-syn (asterisks).*

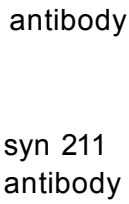

Figure 8.5. *Dot blotting of 7 pM monomeric a-syn, 70 pM quiescent fibrils in the presence of bovine serum albumin (BSA) negative control probed with anti-amyloid fibrils LOC antibody (Millipore) primary antibody and syn 211 antibody. The mature fibrils showed a positive immunoreaction, whereas the natively unfolded monomer did not react with LOC as described by Kayed et al.* (Kayed *et al.* 2007). *Both the monomeric protein and fibrils were detectable by the mouse monoclonal anti-a antibody, syn 211 (Sigma).*

8.4 a-syn oligomers on native gels under denaturing conditions

A

10% Bis-Tris gel under denaturing conditions

Lane 1: Unstained NativeMark
Lane 2: C1 AA
Lane 3: C2 AA
Lane 4: A1 AA
Lane 5: A2 AA
Lane 6: a-syn monomer

Lane 1: Unstained NativeMark
Lane 2: C1 SP
Lane 3: C2 SP
Lane4:A1 SP
Lane 5: A2 SP

B **kDa**

220“ —
H I -

55-
41“

Tris acetate gel under denaturing conditions (LDS 4x sample)

Lane 1: SeeBlue Plus2
Lane 2: C1 AA
Lane 3: C2 AA
Lane 4: A1 AA
Lane 5: A2 AA
Lane 6: C1 SP
Lane 7: C2 SP
Lane 8: A1 SP
Lane 9: A2 SP
Lane 10: monomeric a-syn

Figure 8.6. *Migration of oligomeric forms and α-syn under denaturing conditions. 10 % Bis-Tris gel showed an array of oligomeric subsets in each sample that could have resulted from the solvent conditions used. The monomeric protein also displayed multiple bands in lane 6. A1 and A2 SP deemed to be more sensitive to reducing conditions, producing an array of bands detectable by Silver staining (**A**). Tris acetate gel, 4X LDS sample buffer and Tris-Acetate running buffer system indicated one set of low MW intermediate in all oligomer types prepared in AA and C1 and C2 SP, whereas an array of oligomers were displayed in type A1 and A2 SP samples. This might be indicative of an increased sensitivity of these latter two oligomers to denaturing conditions, inducing further aggregation of fragmentation. The size of the low MW bands could not be estimated by using this type of ladder on this system (<41 KDa) (**B**).*

8.5 MTT cell viability after 20 % v/v treatment of a-syn oligomers

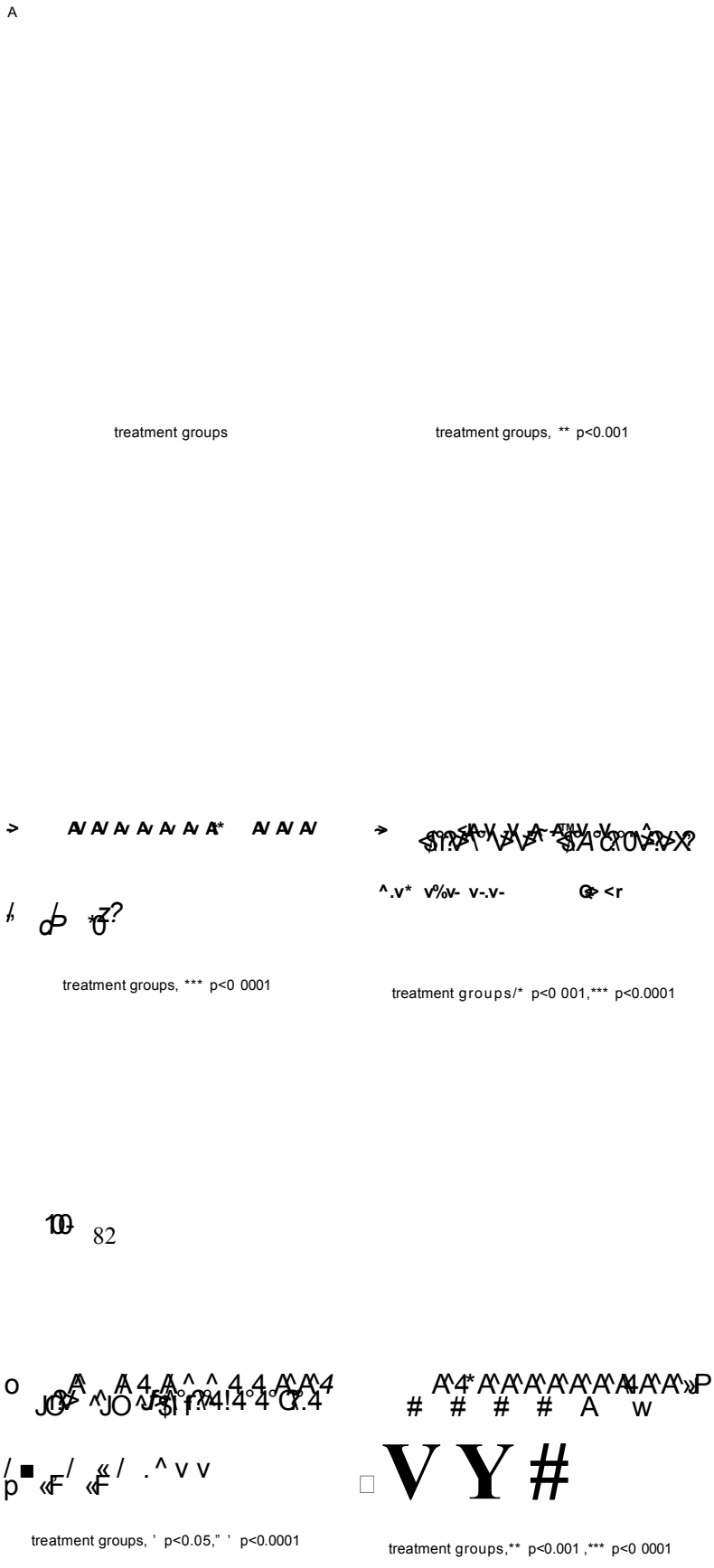

Figure 8.7. *MTT cell viability assay of SH-SY5Y human neuroblastoma cells performed at 1.0x10^5 cells/well seeding density.* ***A*** *shows the data obtained following a 4 hr treatment with 20 % v/v oligomers, their matched vehicle controls and other controls.* ***B*** *represents values obtained after 24 hr exposure of oligomeric treatment in addition to controls at 20 % v/v.* ***C*** *indicates MTT values in % obtained after 48 hr incubation times with alternate oligomeric forms and respective controls at 20 % v/v. All treatments were set up in triplicates three times (n=9) and read at 570 and 690 nm. All readings were averaged, appropriate solvent controls were included and subsequently values have been normalised to untreated cells (100 %). Means are plotted with ±SEM, levels of significance and p values are indicated under each group.*

Figure 8.8. *Immunocytochemistry of a-syn performed with DAB staining (Vecstatin kit) visualised by light microscopy, a-syn is mainly expressed in the cytosol and it is also localised closed to the nuclei. In the cell line transfected with A53T a-syn mutant and expressing the protein stably on the right hand side, the arrow heads point to the increased levels A53T a-syn in the cytoplasm and near the nuclei. In the middle, the endogeneously expressed WT a-syn is shown. On the right, no primary antibody (Sigma, syn 211 antibody) was added and no significant background was seen with secondary antibody only. Staining of nuclei* was *performed using DAPI as displayed by blue colour in the merged images (40X magnification).*

Figure 8.9. *ROS induction and protein oxidation after alternate treatments. SH-SY5Y cells (1x10^5 cells/ well) were treated with 10 % v/v oligomers, vehicle controls or other controls for 8 hr and measurements were taken in triplicates at wavelengths of 485 of excitation and 530 nm of emission (**A**). SH-SY5Y cells overexpressing A53T were exposed to the same treatments for 8 hr and fluorescence signal produced by CMF-DA were recorded and plotted as mean values ±SEM of 3 biological replicates (**B**). Overnight incubation with oligomeric treatment or exposure to controls overnight did not induce production of ROS in SH-SY5Y cells (**C**), nor in SH-SY5Y cells overexpressing α-syn A53T mutant (**D**). Levels of significance are indicated for each group.*

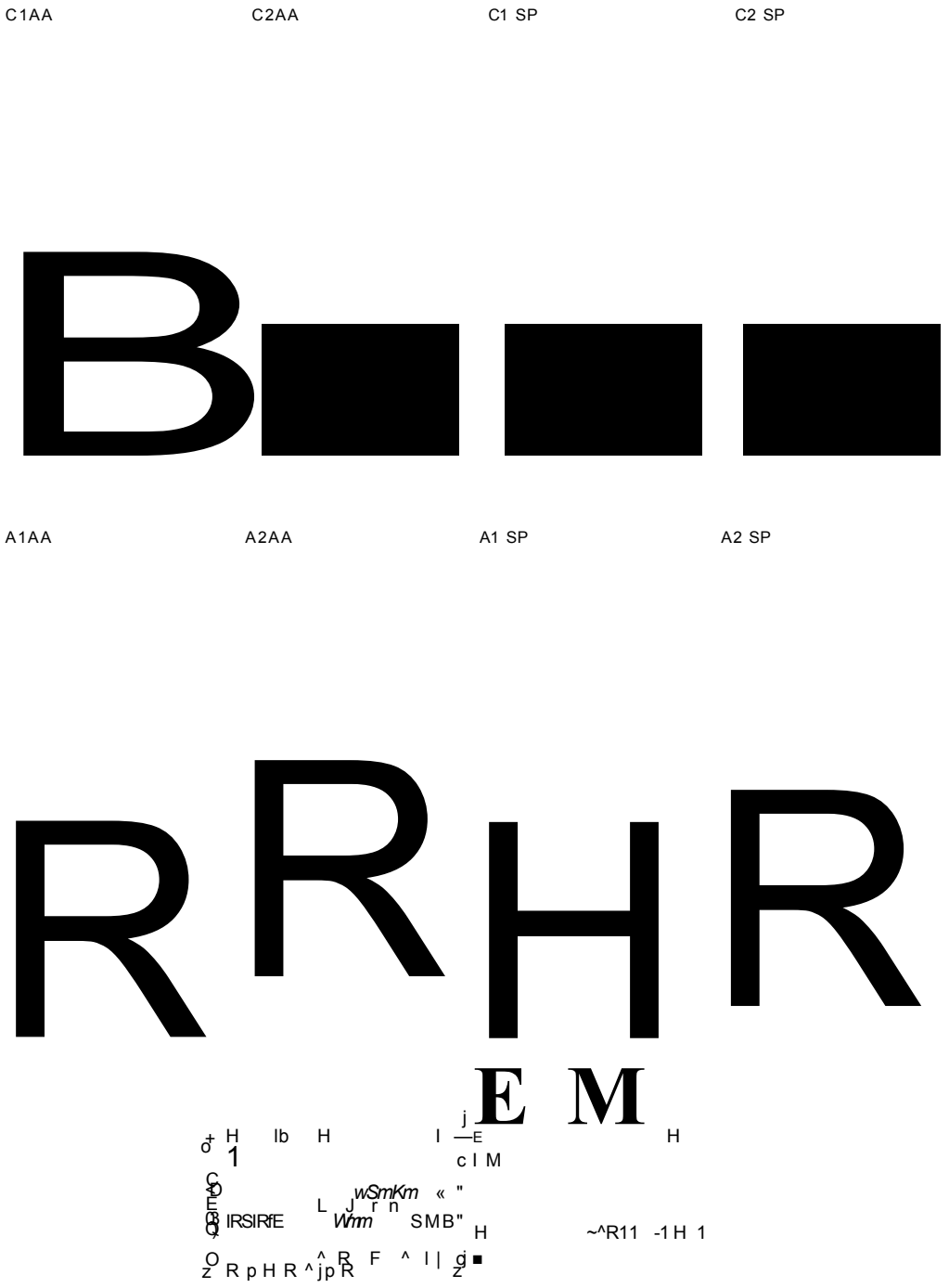

Figure 8.10. *Seeding effect of type C and A oligomers after 8 hr exposure of SH-SY5Y cells. Immunostaining of syn 211 antibody (red colour) after treatment with 10 % v/v a-syn oligomers or matched solvent controls as detected by Alexa 495 goat anti mouse antibody. DAPI is shown by blue counterstain, 40x.The arrows point at cytoplasmic a-syn aggregates formed post-oligomeric treatment.*

Figure 8.10. illustrates that cytosolic a-syn was decreased and an increased punctate formation (white arrows) was observed after treatment with all oligomers except A1 and A2 SP.

8.3 Neurofilament staining of SH-SY5Y cells

Figure 8.11. *Neurofilament staining of SH-SY5Y cells and SH-SY5Y cells overexpressing A53T a-syn at x 100 magnification. Anti-neurofilament antibody (Abeam) was dected by Alexa Fluor 594 conjugated anti-mouse antibody IgG (red colour) and nuclei were counterstained with DAP! (blue colour) in both cells line primary antibody was omitted for control staining.*

8.4 Binding of Cu(II) to a-syn

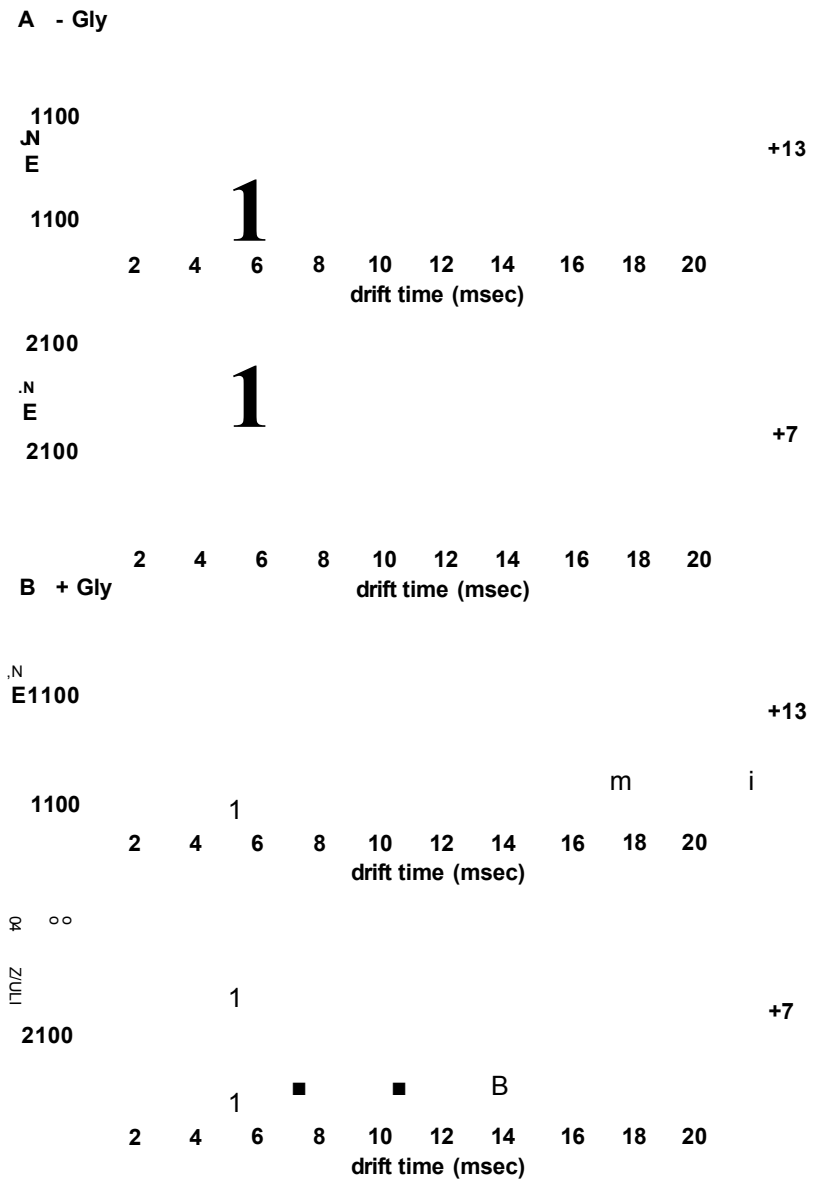

Figure 8.12. *Mobility plots of a-syn either in their apo-form (1:0 protein to metal ratio) or holo-form with up to 2 Cu(II) bound (1:1 protein to metal ratio) at the +13 and +7 charge state ions. Binding studied in the absence (A) or the presence of Ox excess of Gly* ***(B).*** *Instrumental settings were: capillary 1.50 kV, sampling cone 50 V, trap collision energy 4.0 V, Transfer collision energy 10.0 V. source wave velocity 200 m/s, trap wave velocity 311 m/s, IMS wave velocity 800 m/s, transfer wave velocity 200 m/s, backing 3.0 mbar.*

The appearance of new adduct series was evident upon Cu(II) binding as judged by a mass shift, resulting in incresead *m/z* values. The corresponding drift times of these Cu(II)-bound adducts were shortened in case of the +7 charge state ions when compared to the unbound form of the protein, indicating a structural rearrangement. The unbound, extended population of α-syn is indicated by a square with dotted blue line, which almost completely disappeared after co-ordination of Cu(II).

monomers, tetramers from four and so on.

8.6 Calculated Qs of a broad range of proteins

Protein	Mass (Da)	Q (A 2)	SD
folded horse heart myoglobin	17562	1971	267
folded hen egg lysozyme	14305	1469	60
folded bovine ubiquitin	8565	1199	65
folded equine cytochrome c	12355	1622	94
folded ADH monomer	39804	3010.6	74.2
folded ADH tetramer	159216	8497	227.7
folded albumin monomer	66463	4183.7	299.7
folded albumin dimer	132926	7059.3	
folded carbonic anhydrase	29090	2011.6	185.7
folded p2 microglobulin	11860	1990.6	
folded bovine insulin	5734	760	47.5
folded bovine a-lactalbumin	14178	1533.3	81
folded porcine elastase	25907	2133.5	101.5
extended a-syn monomer	14460	2482	159
compact a-syn monomer	14460	1851	276
denatured a-syn monomer	14460	2620	220
a-syn dimer	28920	3375.2	750.6
a-syn trimer	43380	3906.6	231.6
a-syn tetramer	57840	4228.6	225.3
a-syn pentamer	72300	4803	167.2
a-syn hexamer	86760	5553.1	212.4

Table 8.2. Qs *of a range of protein standards over a wide mass range were acquired under native conditions at repeated measurements (except albumin dimer and native /32 microglobulin).* Qs *are expressed as mean and standard deviation is given.*

8.7 ESMMS-MS of Cu(II) induced type A oligomers

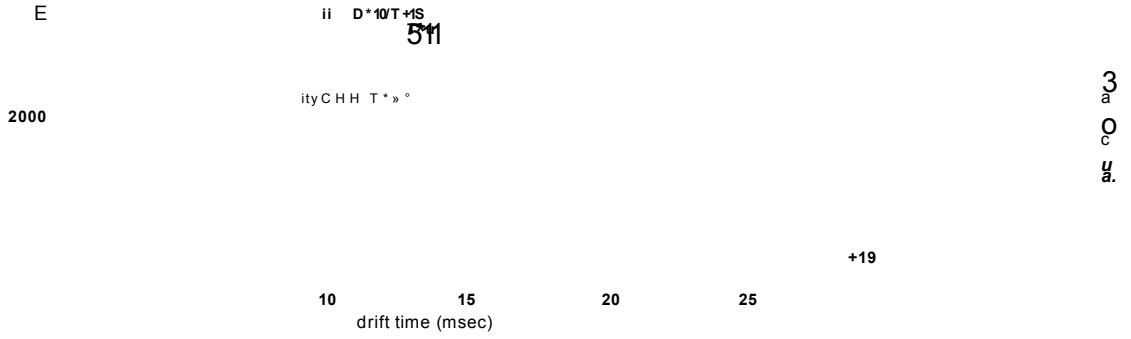

Figure 8.13. *Mobility plot and corresponding mass spectrum of modified type A2 AA oligomer where 10 pM FeCI3 was replaced with CuCI2 in 50 mM AA, pH 7.0 after re-suspension of a freeze-drying step at 24 hr shaking. Instrument settings were: capillary 1.30 kV, source temp 60 °C, cone 30V, trap collision energy 4 V, transfer collision energy 10 V, IMS gas flow 90 mUmin, helium gas flow 180 mUmin, bias 45, source wave velocity 200 m/s, trap wave velocity 311 m/s, IMS wave velocity 800 m/s, transfer wave velocity 200 m/s, backing 3.10 mbar. Monomeric, dimeric (D), and trimeric (T) and a broad range of tetrameric populations (Q) co-existed. Charge states of the oligomers denoted as superscripts in each series on the mobility plot. Monomeric adduct series with one high intensity Cu(II) or another, second Cu(II) with lower intensity are shown in the mass spectrum in a bracket alongside their charge states. The region >2900 was enlarged x54 to view the low abundance oligomeric components.*

8.8 Oxidisation of Met residues following 12 hr incubation with DA

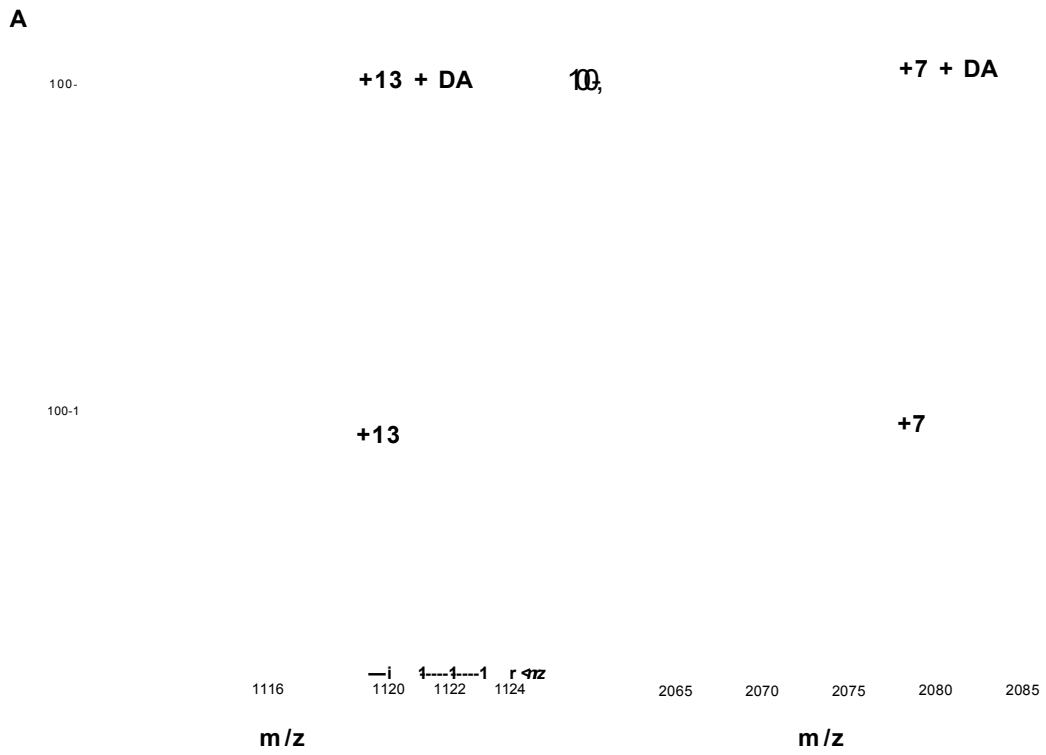

Figure 8.14. *Oxidation of methionine can be observed on long term exposure of a-syn to DA as reported by Leong et al.* (Leong *et al.* 2009b). *Samples ofa-syn-DA at a 1:8 ratio were allowed to incubate at room temperature without agitation for 12 hr. The +13 (A) and +7 (B) charge state ions are shown, arrows indicate a +16 Da increase in mass consistent with the oxidation of the four Met residues. Data was acquired by Dr David P. Smith.*

8.9 Publications

Illes-Toth, E., Smith, D., P.: Conformations and Assembly of Amyloid Oligomers by Electrospray Ionisation- Ion Mobility Spectrometry- Mass Spectrometry. *Curr. Anal. Chem.* 9, 165-180, (2013)

Illes-Toth, E., Dalton, C., F., Smith, D., P.: Binding of dopamine to alpha-synuclein is mediated by specific conformational states- *J Am Soc Mass Spec,* 24, 1346-1354, (2013)

Illes-Toth., E, Ribeiro Ramos., M., Cappai., R., Dalton., C., F., Smith D., P.: Assembly of a-synuclein oligomers with the ability to induce intracellular aggregation proceeds up to a hexameric ring-like structure- in preparation

8.10 Conferences, poster presentations and trainings

BMSS 2013, Eastbourne- poster presentation

BNA 2013, London- poster presentation

BMS ISIG 2013, Warwick- poster presentation

AD/PD 2013, Florence - poster presentation

ASMS, Vancouver 2011- poster presentation

ASMS, Denver 2010- poster presentation

Researchers Who Teach- short course, Sheffield Hallam University, 2013

Fluorescent microscopy and flow cytometry workshop, University of Newcastle, 2011

Mass spectrometry of proteins and peptides- short course, ASMS, Denver, 2010